Solitons in Split Ring Resonator based Metamaterials with Higher Order Nonlinearity

A thesis submitted in fulfilment of the requirement for the degree of

Doctor of Philosophy

By

Neeraj Sharma
(Regn. No.: 901612014)

Under the Supervision of

Dr. Soumendu Jana
(Professor)

Submitted to

THAPAR INSTITUTE
OF ENGINEERING & TECHNOLOGY
(Deemed to be University)

Department of Physics and Material Science

Thapar Institute of Engineering & Technology

Patiala (India)

2024

Declaration

I, Neeraj Sharma, declare that the work presented in this thesis report entitled. **"Solitons in Split Ring Resonator based metamaterials with higher order nonlinearity"** submitted in fulfilment of the requirement for the award of degree of Doctor of Philosophy in the Department of Physics and Material Science, Thapar Institute of Engineering & Technology, Patiala, is an authentic record of my work carried out under the supervision of Dr. Soumendu Jana (Professor, Department of Physics and Material Science, Thapar Institute of Engineering & Technology, Patiala). The matter presented in this thesis has not been submitted in part or whole to any other University or Institute.

Neeraj

Neeraj Sharma

Registration No 901612014.

Date: May 21, 2024

It is certified that the above statement made by the student is correct to the best of my knowledge and belief.

Soumendu Jana

Dr. Soumendu Jana

Professor, DPMS,

TIET, Patiala.

Date: May 21, 2024

ACKNOWLEDGMENTS

First and foremost, I express my sincere gratitude to my supervisor, Dr Soumendu Jana, for his unwavering support, guidance, and mentorship throughout the journey of my Ph.D. his expertise, encouragement, and constructive feedback have been invaluable in shaping the course of this research.

I thank the Head of DPMS, Dr Kulvir Singh, for his support and consistent motivation. I am deeply grateful to my doctoral committee, Dr B.C. Mohanty, Dr Debabrata Deb and Dr Parag Nijhawan, for their insightful comments and valuable suggestions, which have greatly enriched the quality of my thesis. I am very grateful to Dr Manoj Mishra from Somaiya Vidyavihar University, Mumbai, for his valuable support and time-to-time discussions.

I thank my past and present colleagues and friends, Shoaib Noor, Kundan Kumar, Jaspreet Kaur, Aman, Gurpreet Kaur, Anjali Saini, Baldeep Kaur and Gurkirpal Singh Parmar.

Lastly, I want to express my deepest gratitude to my family. Their unwavering love, encouragement, and belief in my abilities have been the cornerstone of my academic pursuits. Their sacrifices and understanding during the highs and lows of this journey have been my pillar of strength.

Neeraj Sharma

Abstract

'Metamaterials' and 'soliton' are the two sought-after topics since the last century. Metamaterials offer some exclusive, apparently unnatural, yet extraordinarily beneficial phenomena. On the other hand, soliton, which is generated using the nonlinearity of the media, comes with a plethora of potential applications besides its strong, wide, and deep theoretical base. This thesis aims to combine these two branches, i.e., metamaterials and nonlinearity-induced soliton in order to reap the benefits of the advantages of both of them. While various types of metamaterials have been explored for soliton generation, and diverse solitons have been identified, limited attention has been paid towards higher-order nonlinearity. Even though the relative value of higher-order nonlinearity might be considerably smaller than the commonly considered lowest-order nonlinearity, its significance lies in the cumulative effects it exerts, especially in certain materials like metamaterials. Furthermore, harnessing higher-order nonlinearity, if appropriately employed, could give rise to intriguing phenomena. The presence of higher-order nonlinearity not only plays a pivotal role in the dynamics and stability of solitons but can also be leveraged for the advancement of smart devices. Precisely, this thesis presents the soliton generation in split ring resonator (SRR) based metamaterials having higher-order nonlinearity. Different types of nonlinearities have been used, namely, cubic-quintic nonlinearity and saturable nonlinearity. The effects of higher-order terms, namely, third-order diffraction, multiphoton absorption, self-steepening, and Raman scattering, have been considered. Soliton has been found in all the cases, however, with delicate stability conditions. Such conditions have been determined and numerically verified. The dynamics of the solitons, both spontaneous and interactive, have been portrayed.

The theoretical investigation on the generation and stabilization of the soliton model is developed using the nonlinear Schrödinger equation or modified nonlinear

Schrödinger equation. And consequently solved by Lagrangian variational method based analytical method as well as split-step Fourier method and Runge–Kutta method based numerical methods.

Stable compound dissipative solitons are found in cubic-quintic nonlinear media with multi-photon absorption and diffusion for a given set of parameters. Since the generation and stabilization conditions have been determined in a generic form, those fit any given material. The interaction dynamics of the dissipative solitons for various initial separations and phases of the participating soliton, ultimately resulting in soliton switching. Notably, it is found that a weak soliton beam has the ability to control a strong soliton beam.

A simple approach has been undertaken to stabilize soliton in a two-dimensional hybrid metamaterial featuring split-ring resonator arrays on a graphene layer. This approach is so fundamental and direct that it can be applied to stabilize solitons in other media, too.

Soliton is formed in SRR-based nonlinear metamaterials, wherein higher-order effects, namely, third-order diffraction, self-steepening and Raman scattering, are prominent. Both self-steepening and Raman scattering cause a transverse shift of the pulse; however, the former causes a greater shift. These soliton pulses are robust against perturbation; only the transverse shift decreases marginally with increasing perturbation. The interaction dynamics demonstrate the typical periodic oscillations along with some deformation due to self-steepening and Raman scattering.

Breather-like diffraction-managed soliton solitons are found in a periodic array of metamaterials having alternate positive and negative diffraction. The initial beam energy required for the generation of diffraction-managed soliton is determined across diverse metamaterial array configurations. The approach enables the production of high-energy beams through the utilization of diffraction-managed metamaterial arrays. The stability zones for diffraction-managed solitons are identified.

Most of the solitons presented in this thesis are robust against the randomness of the system parameters up to a certain extent. The findings of the thesis can be used as a guideline for further experimental observation of solitons and soliton-based devices in different types of metamaterials.

Contents

List of Figures

List of Tables

Chapter 1

Introduction

Localized structures of various kinds have attracted significant attention for centuries due to their natural occurrence and intriguing features that are of fundamental research interest as well as technological applications [1–3]. Localized structures are familiar in various disciplines; for example, in nature (e.g., patterns in shallow water waves [4], isolated roll-cloud [5], sand dunes [6], Tsunami [7, 8]), mechanical systems (e.g., vertically vibrating patterns in granular media [9], coupled pendulum-chain [10], kink in coupled pendulum lattice [11]), optics (e.g., patterns in the transverse plane of optical resonator [12, 13]), chemical systems (e.g., Belousov–Zhabotinsky pattern in 2D chemical reaction [14], in oscillatory chemical reactions [15]) and biological system (e.g., lichen growth patterns [16, 17]).

In this context, the solitons are one of the most important localized structures that arise due to the self-confinement of a beam or pulse by virtue of the nonlinearity of the medium. Soliton is generated due to the perfect counterbalance between the dispersion- or diffraction-induced broadening and nonlinearity-induced contraction. Obviously, the presence of nonlinearity in the medium is essential for the origin of the solitons. Solitons maintain or periodically repeat their shape and size during propagation and show particle nature, i.e., retain the localized nature even after collision with another soliton [18–20]. After the interaction, the soliton reappears without losing its shape or self-repeating behaviour. The interactions between solitons are one of the most fascinating features of solitons [20, 21].

Soliton has been observed in a wide variety of systems, e.g., optics [22], optical fibre [23, 24], waveguides [25, 26], condensed matter [27], plasma wave [28], electric devices [29], metamaterials [30, 31], chemical systems [32, 33], biological systems [34, 35], neuroscience [36, 37], fluids [38], granular media [39, 40], string theory [41, 42] and beyond. In fact, solitons have been developed in almost all disciplines of science and engineering, including social, behavioural science and even in nature [43, 44]. The present research status has been elevated so high that it would not be an overstatement to say that “if there is a wave, there might be a soliton.” The solitary waves have been detected in the magnetosheath of Mars between 1000 km and 3500 km above the martian surface by studying bipolar waves using nonlinear fluid theory and simulations with data from the Langmuir Probe and Waves (LPW) instrument of the Mars Atmosphere and Volatile Evolution (MAVEN) spacecraft [45].

1.1 History and Development of Soliton

Soliton was first noticed by John Scott Russell long back in 1834 in Union Canal in Scotland [46]. Russell, a civil engineer and naval architect, was observing the motion of a boat dragged by horses in the canal. When the boat stopped, the heap of water moving in front of the prow of the ship continued to move in the form of a wave after sustaining an initial turbulence. He followed the wave on horseback and surprisingly noticed that the wave travelled a couple of miles, keeping the same shape before dying down gradually. Later on, he methodically experimented with this phenomenon and reported it as a "wave of translation", which caught the attention of the renowned scientists Henry Bazin (1862 experiments [47, 48]) and Lord Rayleigh who published a paper in Philosophical Magazine in 1876 to support John Scott Russell's experimental observation with his mathematical theory [49]. Lord Rayleigh mentioned Scott Russell's name and also admitted that the first theoretical treatment was by Joseph Valentin Boussinesq in 1871 [50]. The phenomenon of solitary waves had previously been reported in 1826 by Giorgio Bidone in Turin [51, 52], but Bidone's work seems to have gone unnoticed.

Even Russell's work had to await proper recognition for several decades until Korteweg and de Vries brought research attention to it by introducing a partial differential equation to study the one-dimensional solitary wave in 1895. The equation is known as the Korteweg-de Vries equation and is given as $\partial_t u + \partial_x^3 u + 6u\partial_x u = 0$. Korteweg-de Vries equation grabbed significant research interest [53]. Many years later, in 1965, the name "soliton" was coined by Zabsky and Kruskal, who were studying the propagation of nonlinear dispersive media using the Korteweg-de Vries (KdV) equation [20]. In 1967 inverse scattering method was introduced by Clifford *et al.* to solve the KdV equation [54]. In theoretical research, the integrability of systems is very important. Self-similar or self-localized solutions of integrable systems are considered as solitons, while those for nonintegrable systems are referred as solitary waves. Now-a-days, however, both the solitons and the solitary waves are generally considered solitons.

The robust structural behaviour of solitons has led to their widespread implementation across numerous scientific fields. Solitons play a crucial role in fiber optics communication systems, allowing for the efficient transmission of data over long distances [55]. As these waves can withstand dispersion and maintain their shape, the signal integrity is preserved, and the need for intricate signal regeneration processes can be reduced [56]. Solitons have proven valuable in the study of condensed matter [27]. In this discipline, they are used to examine the properties of materials, including the behaviour of electrons in superconductors and the dynamics of magnetic domains [57]. Solitons provide a one-of-a-kind method for examining the transport and interaction of elementary excitations in complex systems, thereby shedding light on fundamental phenomena and potential future technological applications [58]. The extraordinary self-confinement characteristics of solitons can also benefit electric devices [29]. Soliton-based transmission lines have the potential to surmount signal degradation and interference limitations, thereby enhancing the performance and dependability of electronic devices [59]. Solitons have also been utilized in the study of fluid dynamics, where their ability to maintain their shape and stability even in the presence of disturbances has proven to be especially useful [60]. Solitons provide a robust framework for analyzing the behaviour of complex fluid systems [61], from modelling oceanic waves to comprehending atmospheric phenomena. Solitons also contribute to our comprehension of wave propagation in plasmas [62], which has implications for controlled nuclear fusion and astrophysical processes.

Table 1.1: Timeline of soliton development.

1834	First observation of solitary wave by John Scott Russell[46]. 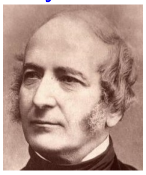 [a].
1895	Korteweg–De Vries proposed solitary wave equation (KdV) [63]: $\partial_t u + \partial_x^3 u + 6u\partial_x u = 0$.
1939	Solitary wave is found in solid state material [64].
1960	Solitary wave is found in plasma [65].
1965	"Soliton" term is coined [20].
1967	Inverse scattering transform is introduced to solve KdV equation [54].
1967	Interaction of two solitons is reported (in nonlinear spring-mass system) [66].
1973	Soliton in optical fiber is proposed theoretically [67].
1974	First experiment on optical soliton [68].
1978	Soliton is found in biological system [69].
1980	Experimental observation of soliton in optical fiber [70].
1984	Soliton Laser is reported [71].
1998	Soliton is found in Josephson junctions [72].
1999	spatiotemporal solitons generated experimentally [73].
2002	Cavity soliton experimentally demonstrated[74].
2013	Multimode fiber solitons demonstrated [75].

[a] Image source: https://commons.wikimedia.org/wiki/File:Russell_J_Scott.jpg

1.2 Soliton in Metamaterial

Among the wide variety of soliton-hosting materials and systems, metamaterials are probably the most unique candidates. Metamaterials are artificially engineered materials whose properties can be tailored as per the requirement [76]. They can possess properties different from ordinary/naturally occurring materials (that's why they are called 'meta', i.e., extraordinary), for example, negative electric permittivity and magnetic permeability, which leads to negative refractive index [77]. The materials having a negative refractive index are also known as left-handed materials (LHM), while the traditional materials having a positive refractive index are called right-handed materials (RHM). Metamaterials consist of an array of micro or nano-order periodic metallic structures that have a different response to the electromagnetic (EM) field than that of an RHM, say, photonic crystals [78, 79]. In fact, the response of metamaterials to the EM field has been a topic of great interest since the beginning. The idea of metamaterials was introduced in the discussion on the electrodynamics of substances with simultaneously negative values of electric permittivity (ϵ) and magnetic permeability (μ) by Veselago *et al.* in 1968 [80]. The metamaterials can be embedded in the dielectric to enhance the EM response. (More details of metamaterials are discussed in the Chapter 2.)

The microscopic structure of the metamaterials modifies the macroscopic properties of the material. The EM wave is found to travel along the surface of a metallic micro-structure known as a surface plasmon (SP). SP is trapped along the surface of the conductors due to the resonance between the wave and the free electrons of the conductors [81]. One such commonly used microstructure is the split ring resonator (SRR). SRR can be considered as an LCR circuit due to the inductance of the ring, the capacitance of the split, and the resistance of connected SRRs [82]. In 1996, the motion of low-frequency SP in metallic microstructures was studied by J.B. Pendry *et al.* [83]. They found that the plasmon has an impact on the properties of metal, e.g., ϵ will be negative below the plasma frequency, which is an interesting result and leads to some untraditional phenomenon, for example, the metallic microstructure of the thin wire array in GHz region was found to exhibit properties analogous to the properties of solid metal in the UV region [83]. Again, in 2000, J.B. Pendery came up with another idea of making a perfect lens with metamaterials [84]. In the same year, Smith *et al.* presented a pioneering work on negative permeability using SRR arrays [85]. They designed and fabricated the SRR arrays that created a magnetic resonance at microwave frequencies. They observed negative permeability using the SRR array. In 2001, P. Markas and C.M. Soukoulis studied metamaterials numerically by removing a split ring from the array to analyze the effect on transmission [86]. They found that only the amplitude of transmission is decreased, which is due to the negative effective permeability of the structure. Also, at resonance, the structure possesses negative permeability and negative susceptibility.

In 2003, Zharov *et al.* demonstrated the nonlinear properties of metamaterial embedded into nonlinear dielectric by showing hysteresis-type dependence of magnetic permeability on the field intensity [87]. Because of intensity dependence, metamaterials can be switched from LHM to RHM and vice versa. The nonlinearity in metamaterials arises due to two factors: the intensity-dependent dielectric permeability of the dielectric in which the SRR is embedded and the response of the SRR resonator, as the capacitance and inductance of SRR depend upon the local field strength [87]. In 2004, Ilya V. Shadrivov *et al.* analyzed the nonlinear guided wave in a metamaterial waveguide surrounded by Kerr-like nonlinear dielectric [88]. Such waveguides can support both fast and slow symmetric as well as antisymmetric nonlinear modes. Their study showed hysteresis-type nonlinearity and novel bright and dark solitons. N. Lazarides *et al.* considered a one-dimensional model formed by a discrete array of SRRs, where rings can interact with each other [89]. The nonlinearity of the medium results in self-focusing, which further combines with the discreteness of the SRR array, resulting in the generation of discrete breather excitations. A similar kind of discrete lattice studied by Giri *et al.* using nonlinear Klein-Gordon equation also results in bright and dark breather soliton [90]. Mandal *et al.* found dark and bright breathers in periodic metamaterial using Klein-Gordon equation [91]. Bright, dark, or grey types of soliton and soliton breather modes are created in a one-dimensional chain of optically linear SRRs with a barrier made of optically nonlinear SRRs [92]. The SRR gaps are filled with Kerr nonlinear dielectric media. The soliton modes emerge spontaneously at a lower critical nonlinearity of the barrier media or result from the breakup of a barrier mode as the barrier media become more nonlinear in the linear media limit [93]. GHz EM wave propagation within the resonant region of a negative index metamaterial may produce both bright and dark optical solitons in the low-frequency response. The bright soliton, characterized by its fast mode, exhibits modulation instability, whereas the dark soliton, a slow mode, remains modulationally stable [94].

Metamaterials are composite materials consisting of a periodic metal lattice, which creates dispersion. This dispersion can be counterbalanced by the Kerr nonlinearity [95, 96]. The periodic structure leads to periodic variation of the dispersion, which eventually takes part in the formation of Gap solitons [25, 97]. Gap solitons arise by balancing the dispersion-induced broadening with the help of nonlinearity-induced contraction, similar to the case of a "regular" soliton. However, in the case of gap soliton, the dispersion is periodic in nature. Such periodic dispersion relation for the EM field is divided into bands separated by gaps. The propagation of EM fields through the gaps is forbidden. However, a high-power nonlinear (e.g., Kerr nonlinear) field having a frequency located inside a gap may locally tune the photonic band gap, which in turn allows the generation and propagation of a localized EM field inside the band gap; hence, the name gap soliton has been coined. A system hosting gap solitons can be represented by nonlinear Schrödinger equation (NLSE), like the case of a regular soliton. Also, gap soliton can be found in the Klein-Gordon (KG) equation with dispersion and Kerr nonlinear term [95, 96]. Cui *et al.* studied the diatomic chain model and found a gap in frequency between acoustic and optical branches [98]. The gap is proportional to the difference between the two types of SRR. In the linear case, wave propagation of a certain wavelength is forbidden due to damping, but by introducing nonlinearity, the wave can be propagated. There are two acoustic modes, i.e., an acoustic lower cut-off and acoustic upper cut-off, which result in gap soliton and kink soliton, respectively. Cui *et al.* found gap soliton in chains of SRR dimers, a pair of coupled SRRs of different sizes [99]. The soliton frequency that lies in the gap of the linear spectrum is damped. The gap solitons exist in a periodic nonlinear media due to periodic variation in media [100].

Shadrivov *et al.* studied the spatial solitons in nonlinear composite structure metamaterial and found transverse electric (TE) and transverse magnetic (TM) mode polarized bright and dark spatial soliton [101]. They demonstrate the single and multihump spatial solitons due to hysteresis-type dependence on intensity and magnetic permeability in SRR-based metamaterials. Boardman *et al.* found spatial soliton in the transmission line that mimics the behaviour of split-ring and wire metamaterials, where the gain is introduced using negative conductance diodes [102]. Using the self-focusing by Kerr nonlinearity of dielectric, Davoyan *et al.* reported the formation of spatial plasmon-polariton solitons along the interface of a metal and dielectric [103]. Bartal *et al.* found subwavelength soliton in metal rod embedded in the dielectric slab by counterbalancing of surface plasmon broadening with self-focusing nonlinearity [104]. Lazarides *et al.* reported dark and bright soliton in isotropic, homogeneous SRR metamaterial using coupled NLSE that arises from Maxwell's equations [105]. A similar physical system is solved by Marklund *et al.* by using the Wigner–Moyal equation, and bright as well as dark soliton have been found [106]. Bright-bright and dark-dark vector solitons of Manakov type are found in metamaterials by Tsitsas *et al.* who modelled EM wave propagation in metamaterials is modelled by two coupled Schrödinger equations and solved by the inverse scattering transformation [107]. The quasi-discrete bright envelope microwave solitons are studied by Veldes *et al.* by considering an SRR coplanar waveguide using an equivalent electric circuit [108]. Rosanov *et al.* demonstrated that weekly coupled SRRs support a new class of topological type of knotted solitons [109]. Yang *et al.* analyze the bright, dark, and grey solitons and quasi-solitons for a wider parameter range using the Drude model [110].

Soliton in metamaterials with higher-order nonlinear effects have been reported regularly. Daoui *et al.* [111] and Triki *et al.*[112] studied optical metamaterials with self-steepening nonlinearity using NLSE. While the earlier group found the propagation of chirped bright and double-kinked quasi-solitons, the later group came up with singular solitons. Further, Triki *et al.* carried out a similar study in nonlinear metamaterials using NLSE with pseudo-quintic nonlinearity and the self-steepening effect to find a chirped dark soliton [113]. The effect of self-steepening is studied on kink and anti-kink chirped soliton propagation using NLSE [114]. Porfyrakis *et al.* studied a periodic metamaterial with cubic nonlinearity using both the nonlinear KG equation and NLSE [115]. The frequency gap caused by linear dispersion attenuates the wave; yet, in the presence of nonlinearity, the propagation of bright and dark gap solitons is found. Zhu *et al.* studied negative refractive index materials with self-steepening and magnetoopic effects using NLSE by applying the F-function method [116]. Jacobian elliptic sine and cosine function and bright soliton solution are found. Ali *et al.* found dissipative soliton in metamaterial with third and fourth-order dispersion and quintic nonlinearity by solving perturbed NLSE using Lagrangian variational method [117]. Abbagari *et al.* [118] and Islam *et al.* [119] found bright and dark soliton in nonlinear metamaterial by solving NLSE using a novel generalized extended direct algebraic method and modified extended direct algebraic method respectively. Mathanaranjan *et al.* found bright, dark, and singular soliton in metamaterials with third and fourth-order dispersions and cubic-quintic nonlinearity [120].

1.3 Motivation

Ample work has been done on the exploration of soliton in metamaterials. Different types of metamaterials have been explored for the existence of soliton, and various types of solitons have been found. However, only limited works are done for higher-order nonlinearity, e.g., quintic nonlinearity. The consideration of higher-order nonlinearity is essential. The reason is two-fold. Firstly, although the relative value of the higher order nonlinearity (namely, quintic nonlinearity) is much smaller than the cubic nonlinearity, it is prominent in some systems, including metamaterials. Moreover, the presence of higher-order nonlinearity, if properly utilized, may lead to intriguing phenomena. Both the dynamics and stability of the soliton can be significantly controlled by the higher-order nonlinearity. These can be utilized for the development of smart devices. The aforementioned points are the major motivations behind this thesis. Another important motivation of the current work comes from the expectation of fascinating phenomena by combining the unique features of metamaterial and nonlinear dynamics. Both the 'metamaterial' and 'nonlinearity' have their scientific charms, so much so that they come under the most sought-after topics of the present times. This thesis attempts to combine these two prominent topics and explore what benefits can be reaped by combining the two. Therefore, we consider a system of nonlinear metamaterials and propose to study the generation and dynamics of localized structures, particularly soliton, in such a system. However, a mere study on the generation of soliton might not be sufficient; one needs to check its sustainability, too. Therefore, we further propose to study the stability analysis of soliton in metamaterials with higher-order nonlinearity to know the basic properties of the localized structure and their preferred operating zones. In summary, in view of the aforementioned research gap and motivation, we set the following objectives for our thesis work.

1.4 Objectives

The main objectives of our theoretical investigation are as follows.

1. To explore the soliton existence in split ring resonator based metamaterials with higher order nonlinearity.

2. To study the dynamics of solitons in split ring resonator based metamaterials with higher order nonlinearity.

3. To study the soliton stability and identify the parametric zone where the solitons are stable.

1.5 Methodology

Soliton propagation in metamaterials can theoretically be presented by a NLSE or perturbed NLSE [118, 121], KG equation [95, 122] or complex Ginzburg-Landau equation (CGLE) [123]. These equations are generally non-integrable, complicated and require particular methods to solve. There are two types of methods to solve these equations: Analytical and Numerical methods. Further, there are two types of analytical methods: exact analytical methods and approximate analytical methods. The commonly used methods under both categories are shown in table 1.2.

Analytical Methods		**Numerical Methods**
Exact Methods	Approximate Methods	
• Inverse scattering method [124] • Darboux transformation method [127] • Lax pair [130] • AKNS Method [133] • Integral Solutions [135] • Conformal Mapping [137] • Separation of Variables [139]	• Lagrangian Variational method [125] • Perturbation Method [128] • Series Expansion [131]	• Split step Fourier method [126] • Methods of Moment [129] • Finite Difference Method [132] • Finite Element Method [134] • Finite Volume Method [136] • Transmission Line Matrix [138]

Table 1.2: Analytical and numerical methods.

Probably, the most significant exact analytical procedure comes in the form of the inverse scattering method. In the inverse scattering, the initial value problem transforms into a linear integral equation, where time is only an implicit variable [124]. The Lax pair method involves replacing a nonlinear partial differential equation with a pair of linear differential equations [130]. In the Darboux transformation Method, the previously known solutions are employed to generate novel solutions to partial differential equations [127].

However, many nonlinear equations can not be solved by exact analytical methods. In such cases, approximate analytical methods can be adopted. One of the most effective approximate analytical methods is the Lagrangian variational method (LVM). First, the Lagrangian density corresponding to a nonlinear equation is developed using the Eular-Lagrangian equation. An ansatz or trial function is considered and employed on Lagrangian density to find the evolution equation corresponding to each system parameter (method discussed in detail in section 1.5.1). The success of the method depends on the proper choice of the trial function. The method is simple to apply and gives a qualitative and as well as quantitative picture of the system dynamics. The moment method is another approach to determining the conservative entities as well as the dynamics of a nonlinear system. In this method, the governing equation undergoes a standard algebraic manipulation that eventually gives rise to the conservative entities of the system. These entities can predict the evolution dynamics of the system. Using the moment method, the unknown solution is expanded into a known sum of solutions of the differential equation and must satisfy the boundary conditions [129].

Another genre of method for solving nonlinear differential equations is the numerical method. Several such methods are available; amongst them, the finite difference time domain (FDTD) method [132] and the split-step Fourier method (SSFM) are the most popular ones. In the FDTD method, the differential equations are replaced by finite difference equations. The problem is discretized in small steps, and the solution at each point is calculated. The method is applied in both space and time domains [132]. In the finite element method, the complex domain of the problem is broken down into small subdomains called elements, and then a solution of a differential equation is approximated at each element [134]. The other efficient numerical method is the SSFM [126], in which the nonlinear equation is written into linear and nonlinear parts, those are subsequently solved separately using Fourier transformation. In the current thesis, we adopted LVM as the analytical tool (followed by the Runge-Kutta 45 method, the numerical solver of the ordinary differential or partial differential equation) and SSFM as the main numerical tool to solve the governing equation. The details of these two methods are given below.

1.5.1 Lagrangian Variational Method

The LVM is an analytical tool that acts as a probe to get information about the dynamics of a nonlinear system, like waves, pulses, etc [140]. The method gives not only qualitative understanding but also quantitative information about the system. The method applied in numerous fields, e.g.,optics [141], plasmonics [142], communication [143], material studied [144], molecular dynamics [145], biological processes [146], weather forecasting [147] and aerodynamics [148], and so on.

To start, we take the governing equation of the system, say an NLSE with a dispersive, a nonlinearity and a dissipative term given as:

$$i\frac{\partial Q}{\partial z}+\frac{1}{2}\frac{\partial^2 Q}{\partial t^2}+|Q|^2 Q=-i|Q|^2 Q. \tag{1.1}$$

Here, Q is an EM field amplitude, z and t are normalized space and time coordinates. In equation 1.1, the first term represents the evolution of the field Q, the second term represents dispersion, the third term represents cubic nonlinearity, and the fourth term represents two-photon absorption (TPA), i.e., dissipation. Equation 1.1 represents a pulse propagation. Notably, for a propagating beam the dispersion term ($\frac{\partial^2 Q}{\partial t^2}$) will be replaced by transverse Laplacian (i.e., $\frac{\partial^2 Q}{\partial x^2}+\frac{\partial^2 Q}{\partial y^2}$), that represent diffraction. Equation 1.1 consists of two parts, i.e., conservative (left-hand side) and dissipative parts (right-hand side).

$$\underbrace{i\frac{\partial Q}{\partial z}+\frac{1}{2}\frac{\partial^2 Q}{\partial t^2}+|Q|^2 Q}_{\text{conservative part}}=-\underbrace{i|Q|^2 Q}_{\text{dissipative part}}. \tag{1.2}$$

The conservative part of the system can be solved using the Euler–Lagrange equation. It will give a minimum functional, i.e., Lagrangian density. The Lagrangian density is achieved in a way that when it is substituted back in the Euler–Lagrange equation, the original NLSE (i.e., eqn 1.1) will appear again. The dissipative term is solved by constructing a Rayleigh's dissipative function (RDF).

The Lagrangian density for NLSE (eqn 1.1) can be found as:

$$\mathcal{L} = i\left(Q\frac{\partial Q^*}{\partial z} - Q^*\frac{\partial Q}{\partial z}\right) + \left|\frac{\partial Q}{\partial t}\right|^2 - |Q|^4 . \tag{1.3}$$

The RDF can be calculated as:

$$\mathcal{R} = i\,|Q|^2\left(Q\frac{\partial Q^*}{\partial z} - Q^*\frac{\partial Q}{\partial z}\right). \tag{1.4}$$

Next, we choose a suitable trial function of the following form:

$$Q = A(z)\exp\left(-\frac{t^2}{w(z)^2} + it^2c(z) + i\phi(z)\right). \tag{1.5}$$

Where $w(z)$, $c(z)$ and $\phi(z)$ are the width, chirp and phase of the beam, respectively. The success of the LVM depends on the choice of the trial function; the closer the trial function is to the exact solution of the governing equation, the better the output. Now, if one knows the exact solution, then why one needs LVM? Actually, for non-integrable or complicated NLSE, the use of LVM is justified. In such cases, we consider the nearest integrable form of the non-integrable NLSE and use the solution of that integrable NLSE as a trial function of the given non-integrable or complicated NLSE. Moreover, another form of trial function can be chosen or check whether that form is supported by the system. Now, substituting the trial function in Lagrangian density (eqn 1.3), we get reduced Lagrangian density and reduced RDF density as:

$$\mathcal{L}_r = \frac{2A(z)^2e^{-\frac{2t^2}{w(z)^2}}\left(w(z)^4\left(t^2c'(z) + \phi'(z)\right) + 2t^2c(z)^2w(z)^4 + 2t^2\right)}{w(z)^4} - A(z)^4e^{-\frac{4t^2}{w(z)^2}} \tag{1.6}$$

and

$$\mathcal{R}_r = 2A(z)^4e^{-\frac{4t^2}{w(z)^2}}\left(t^2c'(z) + \phi'(z)\right) \tag{1.7}$$

To find the total Lagrangian density and total RDF, we have to integrate the reduced Lagrangian and reduced RDF as:

$$\langle\mathcal{L}\rangle = \int_{-\infty}^{\infty}\mathcal{L}_r\ dt \tag{1.8}$$

$$\langle\mathcal{R}\rangle = \int_{-\infty}^{\infty}\mathcal{R}_r\ dt \tag{1.9}$$

to get

$$\langle\mathcal{L}\rangle = \frac{1}{4}\sqrt{\pi}A(z)^2\sqrt{\frac{1}{w(z)^2}}\Big(\sqrt{2}\left(w(z)^4\left(c'(z)+2c(z)^2\right)+4w(z)^2\phi'(z)+2\right) -2A(z)^2w(z)^2\Big) \tag{1.10}$$

and

$$\langle\mathcal{R}\rangle = \frac{\sqrt{\pi}A(z)^4\left(w(z)^2c'(z)+8\phi'(z)\right)}{8\sqrt{\frac{1}{w(z)^2}}} \tag{1.11}$$

Here, again, we adopt the Euler–Lagrange equation for the variation of $\langle L\rangle$ (and $\langle R\rangle$).

$$\frac{d}{dz}\left(\frac{\partial\langle\mathcal{L}\rangle}{\partial q_j^*}\right) - \frac{\partial\langle\mathcal{L}\rangle}{\partial q_j} + \frac{\partial\langle\mathcal{R}\rangle}{\partial q_j^*} = 0. \tag{1.12}$$

where, $q_j^* = \frac{\partial q_j}{\partial z}$, and q_j is $A(t)$, $w(t)$, $c(t)$ and $\phi(t)$. On substituting $\langle L\rangle$ and $\langle R\rangle$ (eqn 1.10 and eqn 1.11) in the Euler-Lagrange equation (eqn 1.12) we get one equation for each variable of q_j. Further solving those equations, we get rate equations or evolution equations corresponding to each parameter as follows:

$$\frac{\partial A}{\partial z} = -\frac{5A^3}{8\sqrt{2}} - Ac \tag{1.13}$$

$$\frac{\partial w}{\partial z} = \frac{1}{8}w\left(\sqrt{2}A^2+16c\right) \tag{1.14}$$

$$\frac{\partial c}{\partial z} = -\frac{A^2}{\sqrt{2}w^2} - 2c^2 + \frac{2}{w^4} \tag{1.15}$$

$$\frac{\partial \phi}{\partial z} = \frac{5A^2}{4\sqrt{2}} - \frac{1}{w^2} \tag{1.16}$$

These evolution equations can be utilized to study the propagation dynamics of the pulse (or beam) parameters. In particular, equations (1.13-1.16) are solved using the RK-45 method (as portrayed in the next subsection). Furthermore, these evolution equations can be used to determine the stability and modulation instability, etc. As we are finding stable wave propagation, we can equate the rate of change to zero (i.e., $\frac{\partial q_j}{\partial z} = 0$) and can find the steady-state values of system parameters. Also, these evolution equations can be used to find stability criteria through Lyapunov stability analysis [149, 150]

For a system that has only conservative parts, the initial pulse (or beam) (E_0) power can be found using the Eular-lagrangian equation (eqn 1.12) for $q_j = \phi$. In that case $\frac{\partial \langle \mathcal{L} \rangle}{\partial \phi} = 0$, that means $\frac{\partial \langle \mathcal{L} \rangle}{\partial \left(\frac{\partial \phi}{\partial z}\right)}$ will be constant, and this constant quantity will be E_0. For the conservative counterpart of equation 1.1, we got:

$$E_0 = \sqrt{2\pi} A^2 w. \tag{1.17}$$

The LVM is an approximate method, yet widely used. The rationale for deploying this method is manyfold. The LVM, while used for studying wave propagation dynamics and soliton generation, gives rise to the evolution information of every individual parameter of the system. It may be noted that the numerical methods, although essentially useful, give rise to the output profile holistically and one needs to run a special routine to calculate the evolution portrait of the individual parameters of the system. Moreover, the evolution equations can be utilized (e.g., in Lyapunov stability criteria) to determine the stability region of the propagating beam. Furthermore, for the numerical simulations, instead of picking random values or wild guessing, the initial values for the parameters of the system can be picked from the afore said stability region. LVM is also more useful in some aspects in comparison to the "exact" analytical methods. In complicated systems, for which the "exact" solution does not exist or is very complicated, the LVM can be used successfully. Even LVM can be used to reveal the propagation scenario, taking a profile of the non-exact solution of the system.

1.5.2 Runge–Kutta 45 method

The Runge-Kutta method is a numerical integration technique commonly used to solve ordinary differential equations [151]. It provides an iterative and accurate methodology to approximate their solutions. The main idea is to break down the ODE into smaller parts and update the solution at each step using a weighted average of derivatives derived at various points within the steps. The fourth-order Runge-Kutta (RK4) method, in particular, is commonly used due to its balance of computational efficiency and accuracy [152]. RK 45 method was given by Fehlberg in 1969 [153]. The RK45 method is the 4th order range kutta method with an error estimator of order 5. Matlab has an integration solver suite '`ode`'. To solve equations using RK45, the suite `ode45` is used. For the understanding of the method, we take differential equations 1.13, 1.14, 1.15 and 1.16.

- In Matlab, the equation that needs to be solved is defined as a function

```
function dydz =f(z,Y)
dydz=[-5Y(1).^3/(8*sqrt(2))-Y(1).*Y(3);Y(2)./8...
(sqrt(2)*Y(1).^2+16*Y(3));-Y(1).^2/(sqrt(2)*Y(2))...
-2*Y(3).^2+2/Y(2).^4;(5*Y(1).^2/(4*sqrt(2)))-...
1/Y(2).^2];
```

  Here, we define the function "`f`" that represents equations (1.13-1.16.)

- Then, the function "`f`" is solved as follows:

```
[t,Y] = ode45(@f,[0 100],[1,1,1,1]);
```

  The function ode45 solver is applied on function `f`, solving for interval 0 to 100 (i.e., `[0,100]`) with an initial condition $y(0) = 1$ (i.e., `[1,1,1,1]`). The solution or answer is presented pictorially.

```
plot(z,Y(:,1),t,abs(:,2),t,Y(:,3),t,Y(:,4));
xlabel('z');
ylabel('A,w,c,\phi');
```

  The figure is plotted between t and y (i.e., `plot(t,Y(:,1))`).

In addition to ode45, Matlab has the ode23 solver to solve nonstiff differential equations.

1.5.3 Split Step Fourier Method

SSFM is a numerical method for solving nonlinear partial differential equations, e.g., the NLSE and complex Ginzburg Landau equations. The SSFM method is relatively fast and does not suffer stability issues [154]. This method solves the system in small steps over its entire length. The effects of dispersion and nonlinearity are taken separately, i.e., when the effect of dispersion is considered, the nonlinearity is considered zero and vice-versa.

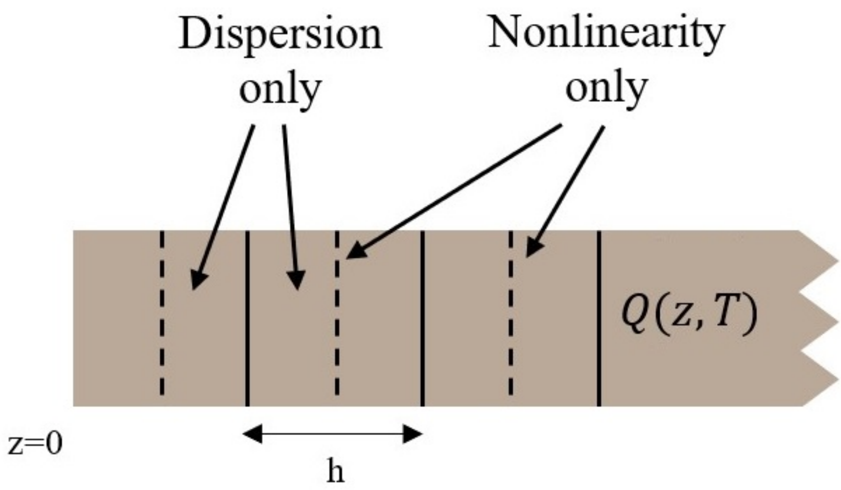

Figure 1.1: The schematic of Split Step Fourier Method.

To start, we have to take the governing equation of the system. We considered an NLSE of a very simple form to show the method:

$$i\frac{\partial Q}{\partial z} + \frac{\beta_2}{2}\frac{\partial^2 Q}{\partial t^2} + |Q|^2 Q = 0. \tag{1.18}$$

The first term of the NLSE is the evolution term, the second term is the dispersion term, and the third term is the Kerr nonlinear term.

The NLSE can be rewritten as:

$$\frac{\partial Q}{\partial z} = -\frac{i\beta_2}{2}\frac{\partial^2 Q}{\partial t^2} + i\,|Q|^2 Q \tag{1.19}$$

or:

$$\frac{\partial Q}{\partial z} = \left(\underbrace{-\frac{i\beta_2}{2}\frac{\partial^2}{\partial t^2}}_{\text{linear part}} + \underbrace{i\left|Q\right|^2}_{\text{nonlinear part}} \right) Q \tag{1.20}$$

Step 1 Separation of the dispersion (linear) and nonlinear parts:

Equation 1.20 be written as a combination of linear and nonlinear parts:

$$\frac{\partial Q}{\partial z} = (\hat{D} + \hat{N})Q, \tag{1.21}$$

where dispersion and nonlinear operaters are given as, $\hat{D} = -\frac{i\beta_2}{2}\frac{\partial^2}{\partial t^2}$ and $\hat{N} = i\left|Q\right|^2$ respectively.

Equation 1.21 is solved by taking step size h and taking nonlinearity and dispersion independently:

For calculating the nonlinear part, we take the dispersion part equal to zero (i.e., $\hat{D} = 0$). On solving equation 1.21 (with $\hat{D} = 0$) we get:

$$Q(z+h,t) = exp(h\hat{N})Q(z,t); \tag{1.22}$$

Now, for solving the dispersion part, we take a nonlinear part equal to zero (i.e., $\hat{N} = 0$). On solving equation 1.21 (with $\hat{N} = 0$) we get:

$$Q(z+h,t) = exp(h\hat{D})Q(z,t). \tag{1.23}$$

Now combining both the equations 1.22 and 1.23, we get:

$$Q(z+h,t) \approx exp(h\hat{D})exp(h\hat{N})Q(z,t).$$

Step 2 Calculation of dispersion term:

The dispersion can be calculated using the Fourier transformation:

$$exp(h\hat{D})Q(z,t) = \mathscr{F}^{-1}exp[h\hat{D}(i\omega)]\mathscr{F}Q(z,t) \tag{1.24}$$

Here, $\frac{\partial}{\partial t}$ is replaced by $i\omega$ in the diffraction operator, which is the frequency in the Fourier domain.

Step 3 Calculation of nonlinear part:

The nonlinear part has no explicit temporal dependence and can be solved directly in the time domain.

Step 4 Repetition of steps 3 and 4 for each step length 'h' over the entire system length.

The Matlab code of SSFM for the above steps is as follows:

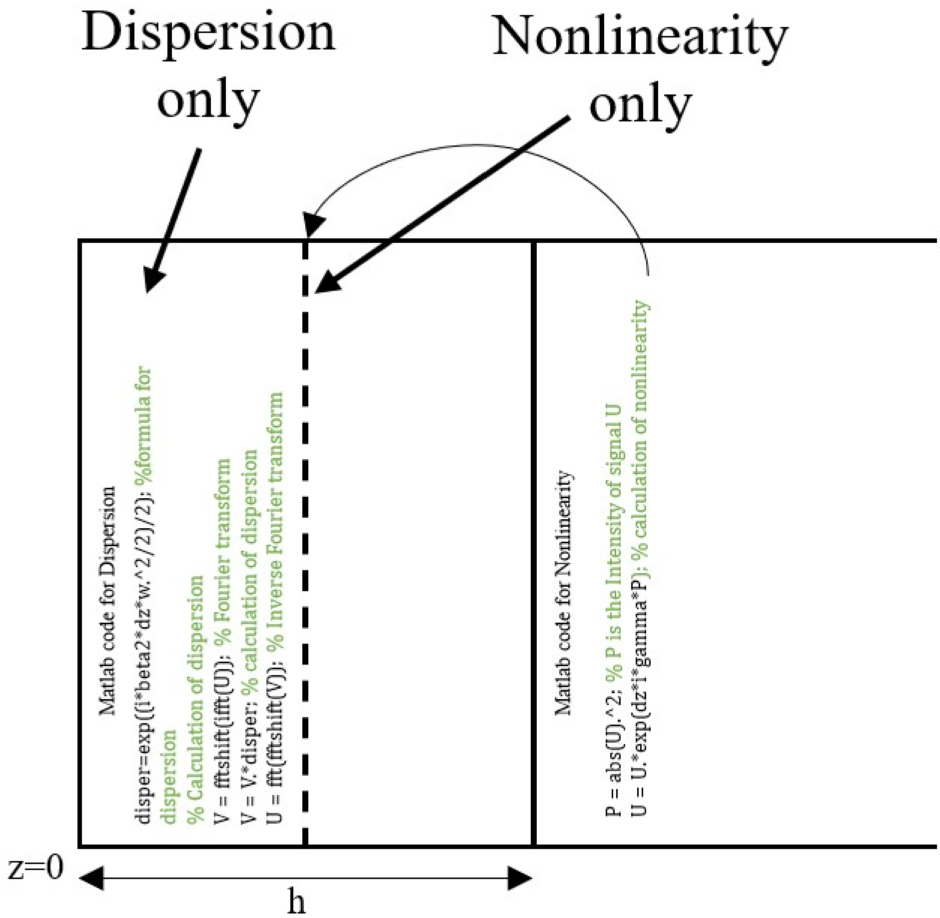

Figure 1.2: The schematic of Matlab code for Split Step Fourier method (The figure is for visual presentation; for details, see the following sample code).

The calculations for dispersion and nonlinearity are performed as shown in Figure 1.2. First, the dispersion is calculated for the first half-step length ($h/2$) of dispersion; then nonlinearity is calculated for the full step length (h) and included at $h/2$, and then again dispersion is calculated for the second half-step length ($h/2$).

Some parts of a simple code are as follows:

Defining step size:

```
coef_dz=1.e-3;   % a fraction useful to set spatial steps
```

Calculation of the nonlinear and linear lengths:

```
L_NL=1/(gamma*peako); %nonlinear length
L_D=largo*largo/abs(gvd); linear length
zstep=coef_dz*Lmin;   % step size in the axial z
   direction
npt=round(L/zstep);   % no. of steps in the z-direction
zstep=L/npt;  % re-adjusting the step for the whole
   number of no. of steps
```

Calculation of dispersion:

```
disper=exp((i*beta2*dz*w.^2/2)/2); %formula for
   dispersion
% Calculation of dispersion
V = fftshift(ifft(U)); % Fourier transform
V = V.*disper; % calculation of dispersion
U = fft(fftshift(V)); % Inverse Fourier transform
```

Here, the formula for dispersion is used as given in Ref [155]. The dispersion is calculated for step length h. Fourier transformation is performed to calculate dispersion in the frequency domain. Thereafter, the inverse Fourier transformation is applied to get it back in the time domain.

Calculation of Nonlinearity:

```
% Calculation of full nonlinearity
P = abs(U).^2; % P is the Intensity of signal U
U = U.*exp(dz*i*gamma*P); % calculation of nonlinearity
```

Here, the calculation of nonlinearity is performed for step length h.

The above routine is repeated for the entire length of the system.

Chapter 2

Elements of Nonlinearity, Soliton and Metamaterials

Solitons in metamaterials represent an extraordinary combination of wave physics and engineered materials with unique properties. Using the intriguing properties of solitons, scientists are on the verge of revolutionising numerous scientific and technological disciplines. With ongoing research advancements in metamaterial design, the possibilities for controlling and leveraging solitons are limitless, paving the way for applications and innovations that have never been seen before. In this chapter, we discuss the basics of the solitons and metamaterials in detail, as they are two major concepts in the current thesis. We start from 'nonlinearity' as it is the essential requirement for soliton formation.

2.1 Nonlinear Phenomena

A nonlinear system is characterized by its deviation from the superposition principle, where the output of the system exhibits a nonlinear response with respect to the input. For example, in a harmonic oscillator spring with force constant k oscillating in x direction, the force is directly proportional to the amplitude in the linear regime, expressed as $F(x) = -kx$. However, the introduction of additional energy will cause the system to enter into the area with different force laws, $F(x) = -kx - k_1 z^2 - k_2 z^3 - k_3 z^4 \ldots$, which is nonlinear in 'x'. The introduction of nonlinearity fundamentally alters the system's behaviour. In a nonlinear process, the input changes the process itself. This section discusses the origin of nonlinearity and some prominent nonlinear phenomena that have been used in the thesis.

2.1.1 Origin on nonlinearity

There are different types of nonlinear media, and so is their origin. We describe one of the commonest origins of nonlinearity, the electron cloud formation. Dielectric materials are non-conductive materials that exhibit a polarization response when subjected to an electric field. The polarization of dielectric materials arises due to the displacement of charges within the material in response to the applied external electric field. For example, when a dielectric medium is illuminated or kept under an EM wave, the charges within the material rearrange themselves due to the applied electric field of the EM wave, creating a polarization response, which can be described by the polarization vector $\mathbf{P}$ (bold mathematical letter represent a vector quantity). For low intensity, the polarization vector is directly proportional to the applied field; $\mathbf{P} \propto \mathbf{E}$ or $\mathbf{P} = \epsilon\chi\mathbf{E}$, where ϵ is the permittivity of the dielectric material, and χ is dielectric susceptibility. The refractive index of the material can be determined as $n = \sqrt{\epsilon_r} = \sqrt{1 + \chi/\epsilon_0} = \sqrt{1 + \chi'} = \sqrt{1 + \chi}$ (for brevity we removed the prime over χ). Here, $\epsilon_r = \epsilon/\epsilon_0$ is the relative permittivity of the material. This refractive index will be linear and function of frequency of the field only. In the presence of a strong electric field (e.g., when illuminated by intense Laser radiation), the polarization response of a dielectric material depends on different powers of $\mathbf{E}$, thus becoming nonlinear. In this case, the polarization vector $\mathbf{P}$ can be written as a power series expansion in terms of the applied electric field $\mathbf{E}$ as:

$$\mathbf{P} = \epsilon \left[\chi^{(1)}\mathbf{E} + \chi^{(2)}\mathbf{E}^2 + \chi^{(3)}\mathbf{E}^3 + \dots\right], \tag{2.1}$$

where $\chi^{(1)}$ is the first-order linear susceptibility, $\chi^{(2)}$ is the second-order nonlinear susceptibility, $\chi^{(3)}$ is the third-order nonlinear susceptibility of the material, and so on. So, for this case, ϵ_r will not only be the function of χ but also depend on E and its different powers. The refractive index will now depend on 'E' as:

$$n = \sqrt{\epsilon_r} = \sqrt{1 + \epsilon\big(\chi^{(1)} + \chi^{(2)}E + \chi^{(3)}E^2 + \dots\big)} \; .$$

If we consider up to $\chi^{(2)}$, the refractive index is amplitude (E) dependent, which is referred to as Pockel's effect. If we consider up to $\chi^{(3)}$ or above, the refractive index (n) will be intensity ($|E|^2$) dependent (Kerr Nonlinearity). Such nonlinear refractive index leads to different nonlinear phenomena. It may be noted here that χs are actually complex entities whose real parts contribute to the nonlinear refractive indices, while the imaginary parts give rise to the multiphoton absorption. Now, depending upon the order of χ, different nonlinearities will be generated. $\chi^{(2)}$ materials correspond to quadratic nonlinearity. This is the simplest nonlinearity found in non-centro-symmetric materials, e.g., potassium titanyl phosphate (KTP) [156], potassium dihydrogen phosphate (KDP) [157], β-barium borate (BBO) [158], lithium tantalate ($LiTaO_3$) [159], lithium niobate ($LiNbO_3$) [160] and ammonium dihydrogen phosphate ($NH_4H_2PO_4$, ADP) [161]. The quadratic nonlinearity leads to some of the iconic nonlinear phenomena, like second harmonic generation [162], sum frequency generation [163], difference frequency generation [164], parametric oscillation [165], four-wave mixing [166]. Centro-symmetric materials lack quadratic nonlinearity and, correspondingly, the Pockel effect [167]. For them, the simplest form of nonlinearity is the cubic or Kerr nonlinearity that corresponds to $\chi^{(3)}$ materials. Such $\chi^{(3)}$ material by virtue of intensity-dependent refractive index (Kerr nonlinearity) may create self-focusing, third-order interactions, third harmonic generation, nonlinear optical mixing processes of higher order, etc. For centro-symmetric materials, the next higher-order nonlinearity is quintic nonlinearity (corresponds to $\chi^{(5)}$). Combining self-focusing Kerr nonlinearity and self-defocusing quintic nonlinearity ultimately leads to a saturable nonlinearity. It is noteworthy that $\chi^{(2)} >> \chi^{(3)} >> \chi^{(5)}$. A typical set of values for dielectric material is given $\chi^{(2)} \approx 1.9 \times 10^{-12} m/V$, $\chi^{(3)} \approx 3.78 \times 10^{-24} m^2/V^2$. It can be noted that there are other mechanisms for generating nonlinearity. It varies from system to system, but the basic theme is the response should be nonlinearly dependent on the applied field.

The following sub-sections briefly describe only those nonlinear phenomena used frequently throughout the thesis.

2.1.2 Kerr or cubic nonlinearity

The Kerr effect is a phenomenon in nonlinear optics that occurs when a high-intensity light travels through materials having third-order nonlinearity [168, 169]. Kerr effect causes the change in the refractive index of the medium, which is proportional to the square of the amplitude or intensity of the applied field:

$$\tilde{n}(\omega, \mid E \mid^2) = n_0(\omega) + n_2 \mid E \mid^2 = n_0(\omega) + n_2 I, \tag{2.2}$$

where $\tilde{n}$ is the modified refractive index, $n_0(\omega)$ is the linear refractive index, and n_2 ($n_2 = \frac{3\mathrm{Re}[\chi^{(3)}]}{4n}$) is the Kerr (cubic) nonlinear refractive index, Kerr nonlinearity is important for several nonlinear effects, namely, self-focusing and self-phase modulation. Actually, χ is a complex quantity. The real part of the susceptibility is responsible for the nonlinear refractive index, while the imaginary part leads to multiphoton absorption. Here, $\chi^{(3)}$ can be written as:

$$\chi^{(3)} = \underbrace{Re(\chi^{(3)})}_{\text{cubic nonlinearity}} + \underbrace{Im(\chi^{(3)})}_{\text{two-photon absorption}} \tag{2.3}$$

The real part corresponds to the cubic nonlinearity, and the imaginary part leads to two-photon absorption. The typical values of $\mathrm{Re}(\chi^{(3)})$ for Silicon is 0.45×10^{-18} m^2/V^2 (for $\lambda = 1.54 \mu m$), GaAs is 0.6×10^{-18} m^2/V^2 (for $\lambda = 1.54 \mu m$) and SiO_2/Si-nc is 2.1×10^{-18} m^2/V^2 (for $\lambda = 1.55 \mu m$) [170, 171].

2.1.3 Quintic nonlinearity

Similar to $\chi^{(3)}$ the $\chi^{(5)}$ is also a complex quantity. The quintic nonlinearity is related to the real part of the fifth-order nonlinear susceptibility (i.e., Re($\chi^{(5)}$) [169, 172]. The typical values of Re($\chi^{(5)}$) for SiO_2 is 4.2×10^{-38} m^4/V^4 , GaAs is 0.25×10^{-26} m^4/V^4 and As_2Se_3 is 1.9×10^{-35} m^4/V^4 [173]. Quintic nonlinearity is much weaker compared to cubic nonlinearity. A positive (focusing) quintic nonlinearity marginally increases being added with focusing Kerr nonlinearity, the total value of nonlinearity in the medium. However, a negative quintic nonlinearity causes the beam defocusing, whatever small, and eventually leads to the saturation of the nonlinearity.

$$\chi^{(5)} = \underbrace{Re(\chi^{(5)})}_{\text{quintic nonlinearity}} + \underbrace{Im(\chi^{(5)})}_{\text{three photon absorption}} \tag{2.4}$$

2.1.4 Saturable nonlinearity

Beyond a certain intensity, the nonlinearity does not increase further. Saturable nonlinearity is obtained when the nonlinearity gets saturated at high intensity [174]. Mathematically, the saturation nonlinear refractive index related to intensity can be defined as $n_{eff}(I) = n_2/(I + I/I_S)$; here, I_S is saturation intensity [175, 176]. Cubic-quintic nonlinearity is also a form of saturable nonlinearity if approximated.

2.1.5 Self-focusing

When an intense EM beam passes through a Kerr nonlinear medium, a lensing effect takes place due to the intensity-dependent refractive index n_2 (described in equation 2.2). The refractive index becomes larger where the intensity of the beam is higher (for example, a Gaussian beam profile has the largest refractive index its the centre). This creates a lensing effect which leads to the focusing of the beam, as shown in Figure 2.1. Further, the self-focusing of the beam can counterbalance the self-diffraction of the beam, which may lead to stable wave propagation in a

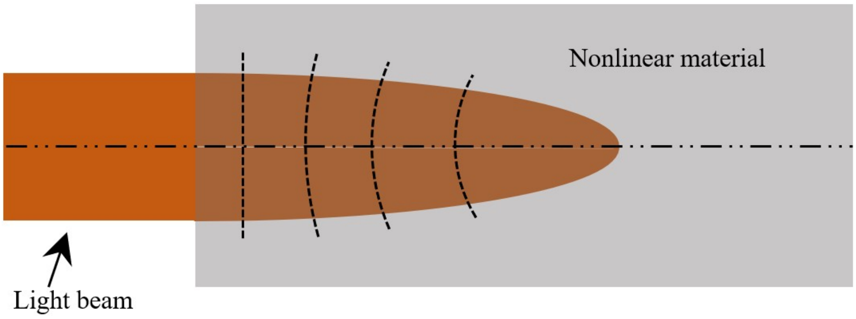

Figure 2.1: Focusing due to third order or cubic or Kerr nonlinearity

nonlinear medium. The self-focusing phenomenon has applications in microscopy, high-resolution imaging, laser technology, etc.

2.1.6 Self-phase modulation

In light-matter interaction at high intensity, the Kerr effect occurs, causing a change in the refractive index of the medium. For a pulse (temporal domain), the refractive index varies with time, which causes a change in the pulse's phase profile. The impact on the pulse phase caused by its own intensity profile is called self-phase modulation (SPM). The nonlinearity of the media (say cubic/ Kerr nonlinearity) will cause a nonlinear phase shift (ϕ_{NL}) due to the SPM. This creates a chirping, i.e., a shift ($\delta\omega(T)$) of the instantaneous frequency of the pulse from its central frequency:

$$\delta\omega(T) = -\frac{\partial \phi_{NL}}{\partial T} = -\left(\frac{L_{eff}}{L_{NL}}\right)\frac{\partial}{\partial T}|U(0,T)|^2 \tag{2.5}$$

L_{eff} is the effective length and L_{NL} is the nonlinear length. $U(0,T)$ is the initial pulse profile.

For a Gaussian pulse, the chirp is

$$\delta\omega(T) = \frac{2}{T_0}\frac{L_{eff}}{L_{NL}}\left(\frac{T}{T_0}\right)exp\left[-\left(\frac{T}{T_0}\right)^2\right] \tag{2.6}$$

The equation indicates that the leading edge of the pulse will be down-chirped or red-shifted, while the trailing edge will be up-chirped or blue-shifted.

2.1.7 Two-photon absorption

Two-photon absorption (TPA) is a nonlinear optical process involving the simultaneous absorption of two photons to excite a molecule from its ground state to an excited state. The schematic of TPA is shown in Figure 2.2(a). The TPA is induced due to the imaginary part of cubic susceptibility, i.e., $\mathrm{Im}(\chi^{(3)})$. TPA has applications in microscopy [177], bioimaging [178], microfabrication [179], optical-power limiting [180] etc.

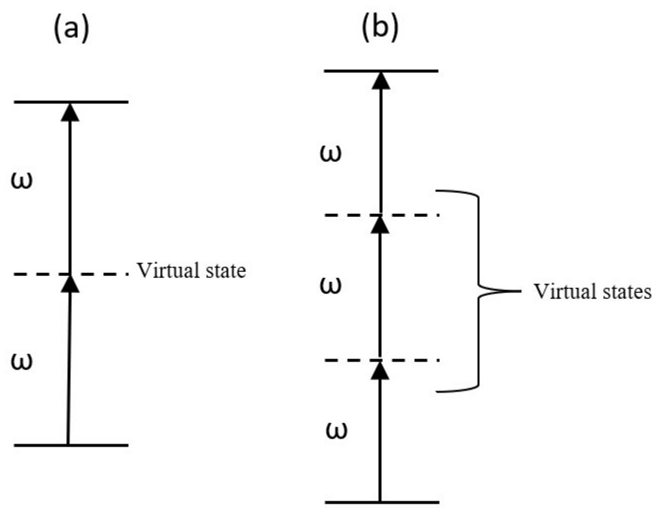

Figure 2.2: Schemetic of (a) two-photon absorption (b) three-photon absorption.

2.1.8 Three photon absorption

Three-photon absorption (3PA) is a nonlinear optical process involving the simultaneous absorption of three photons to excite a molecule from its ground state to an excited state. The schematic of 3PA is shown in Figure 2.2(b). The 3PA is induced due to the imaginary part of quintic susceptibility, i.e., $\mathrm{Im}(\chi^{(5)})$. TPA also has many applications, e.g., fluorescence microscopy [181], near-infrared temperature sensing [182] and optical-power limiting [183] and so on.

2.1.9 Self steepening

When the pulse has high intensity at the highest peak compared to the rest of the pulse, due to the intensity-dependent refractive index, the leading edge of the pulse profile experiences a higher refractive index than the trailing edge. Consequently, the leading edge undergoes a greater phase shift than the trailing edge, causing the pulse to 'steepen' overtime [184, 185]. This steepening of the pulse by its own intensity profile is called self-steepening.

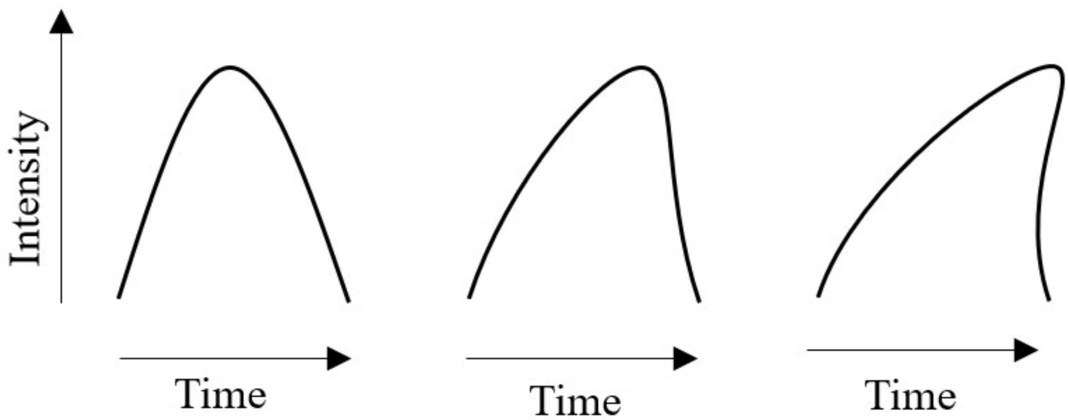

Figure 2.3: Schemeatic of self-steepening, pulse undergoing steepening under the influence of intensity-dependent refractive index.

2.1.10 Stimulated Raman scattering

There are two types of Raman scattering: stimulated Raman scattering (SRS) and intrapulse Raman scattering (IRS). SRS is a non-linear phenomenon in which incident photons interact with a material, resulting in an exchange of energy between the photons and the vibrational modes of the molecules in the material [186, 187]. SRS create a frequency modification, referred to as the Raman shift, that aligns with the characteristic vibrational frequencies of the material. The scattering process involves the stimulation of a molecule by an incident pump photon, causing it to reach a virtual energy level. Subsequently, the molecule emits a Stokes-shifted photon when it reverts back to its original ground state. The energy disparity between the pump and Stokes photons is equivalent to the energy of the molecular vibration. SRS has applications in spectroscopy and Laser. When the scattering occurs within the system due to an intense electric field inducing molecular vibration in the material is called intrapulse Raman scattering [56, 188]. This will lead to self-frequency shift and soliton decay. In IRS, Raman scattering occurs within the temporal structure of a single optical pulse. The intense electric field of the pulse itself induces molecular vibrations in the material, leading to inelastic scattering and the generation of new frequency components within the pulse [189].

2.2 Soliton: Classifications and Mechanism

Soliton can be classified on the basis of physics, topology, shape, governing mathematical equations, the domain of confinement, conservation of energy, etc. [190, 191]. On the basis of physics, there are two kinds of solitons, i.e., classical and quantum [190]. The classical soliton is the solution of classical field theory [192], while the quantum soliton is the solution of quantum field theory [193]; both solitons show stability during propagation and collision [194]. On the basis of topology, a soliton is categorized as non-topological and topological soliton [191, 195]. The boundary conditions at infinity for nontopological solitons and vacuum state (ground state) are the same, e.g., KdV solution, while for topological soliton, the vacuum is degenerate, boundary conditions at infinity are different from the physical ground state, such solitons arise in sine-Gordon theory [196]. On the basis of shape, there are numerous types of solitons, for example, bell soliton, kink soliton, breather soliton [197, 198], etc. The bell soliton is the solution of the KdV equation having a bell shape and found at low frequencies. The kink soliton is the solution of the sine-Gordon (SG) equation and is a topological soliton, e.g., a Bloch wall between two magnetic domains in a ferromagnet. The Bloch wall is a transition region between the up and down spin state in the adjacent domain. The other type of soliton is the breather soliton [199], which is localized and oscillatory in nature.

On the basis of the governing nonlinear equation, the following are some kinds of solitons: 1) the KdV soliton, 2) the Sine-Gordon soliton, and 3) the envelope soliton [200]. KdV solitons are pulse solitons, the amplitude of which increases as the velocity increases, while the sine-Gordon soliton is a topological soliton; the amplitude is independent of velocity. Envelop soliton is called a nonlinear Schrödinger soliton (NLS), as it is similar to the Schrödinger equation of quantum mechanics.

An important type of solitons is optical solitons, which are pulse or beam having robust structure due to counterbalance of nonlinearity with dispersion or diffraction or both [201]. Depending on confinement, there are three types: spatial soliton, temporal soliton, and spatiotemporal soliton.

2.2.1 Spatial soliton

Optical beam has a natural tendency to diffract during propagation in a homogeneous medium, due to its small initial beam cross section. If the beam propagates through a nonlinear media, the intensity-dependent nonlinear refractive index, $n(I) = n_0 + n_2 I$ (where n is the linear refractive index, n_2 is the Kerr nonlinear refractive index and I is intensity) may create a self-focusing effect. For example, a bell-shaped beam, say, Gaussian, creates a refractive index profile, which is the replica of its own intensity profile, i.e., the refractive index becomes highest at the beam axis. So, the velocity of the wavefront at the axial region is smaller than the off-axial region. As a result, the wavefront gradually becomes more concave. Thus, a lensing effect or self-focusing occurs. When self-diffraction-induced broadening (of beam diameter) and self-focusing-induced contraction become equal, the self-trapped beam originates and propagates through the medium as a spatial soliton (Figure 2.4) [202–204]. The stabilization mechanism of the spatial soliton is

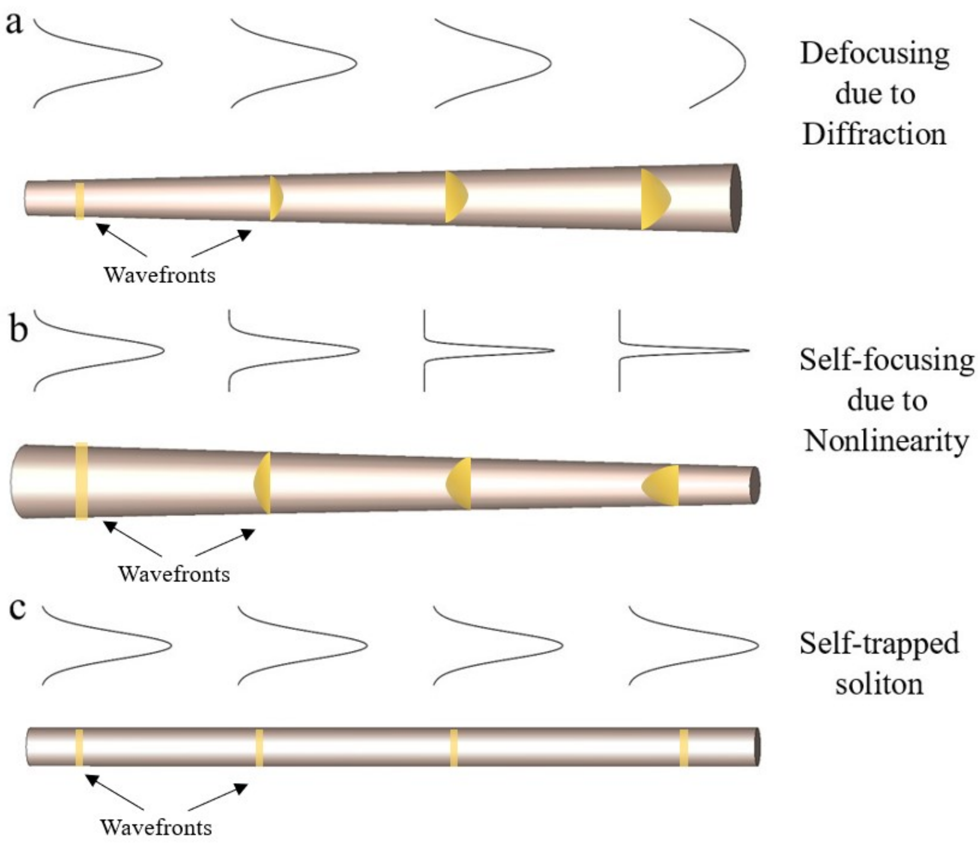

Figure 2.4: Schematic of spatial soliton by counterbalancing diffraction and self-focusing.

intriguing. The critical power for self-focusing (P_c) is characterized as the maximum power contained in a laser beam or pulse that achieves a delicate equilibrium between self-focusing and diffraction influences. Above this critical power threshold, the beam experiences collapse, halted only when an additional nonlinear effect, such as multiphoton absorption or photoionization, intervenes, while below the critical power, the beam diverges due to diffraction. The P_c is inversely proportional to the beam width. Now a beam of power $P < P_c$ will tend to diffract, and consequently, the P_c will be reduced. At some point, the P_c will go below the P, resulting in the self-focusing of the beam. Thereafter, as the self-focusing starts narrowing the beam, the P_c increases and, at some point, goes above P_c, which stops further focusing and starts self-diffraction. These chain processes eventually arrest the collapse and expansion of the soliton beam.

2.2.2 Temporal soliton

A pulse is the result of a number of wavelets of different frequencies. These frequency components travel with different velocities in a dispersive medium, resulting in what is called group velocity dispersion (GVD). Their phase $\phi(z,T)$, (where, T is time measured from a frame of reference attached with the pulse propagating along z direction with a group velocity v_g, i.e., $T = t - z/v_g$) changes across the pulse. Since the phase is time-dependent, the instantaneous frequency across the pulse also changes. The shift of the instantaneous frequency from the central frequency of the pulse is given by

$$\delta\omega(T) = -\frac{\partial\phi}{\partial T} = \frac{sgn(\beta_2)(z/L_D)}{1+(z/L_D)^2}\frac{T}{T_0^2} \tag{2.7}$$

. Here β_2 is the GDV parameter. For normal dispersive media $\beta_2 > 0$; the leading edge ($t < z/v_g$, i.e., T is negative) of the pulse shows the negative shift of frequency or down chirp or red shift. While the trailing edge ($t > z/v_g$, i.e., T is positive) will experience an up chirp or blue shift. On the contrary, for anomalous dispersive media $\beta_2 < 0$; the leading edge of the pulse will be blue-shifted, while the trailing edge will be red-shifted. The SPM-induced chirp is opposite in nature to that of anomalous dispersion-induced chirp. So, if tuned properly, they can counterbalance each other so that the GVD-induced pulse broadening can be arrested by the SPM-induced contraction (Figure 2.5). Such a stable structure in the temporal (spectral) domain, if created, is called a temporal soliton [205]. Now, the nonlinearity of the media will generate an SPM in the pulse.

2.2.3 Spatiotemporal Soliton

As the name implies, spatiotemporal solitons are the solitons confined in both space and time domains. When both diffraction and GVD of a beam are counterbalanced by self-focusing and SPM, respectively, during propagation in a nonlinear medium. The resultant stable structure is called a spatiotemporal soliton [206]. All the afore-

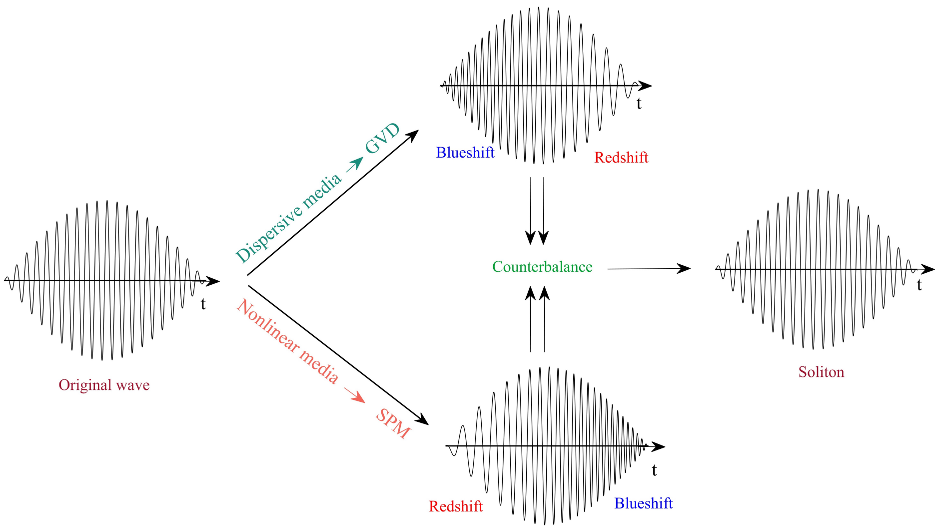

Figure 2.5: Schematic of temporal soliton by counterbalancing GVD and SPM

mentioned solitons, as far as energy conservation is concerned, are again divided into two types of solitons: conservative soliton and dissipative soliton. Conservative solitons arise in a system in which energy mass is conserved. In contrast, dissipative solitons are found in dissipative systems, wherein the system loses or gains energy over time. Dissipative systems are open or porous systems; energy and/or particles can enter or exit the system through its boundaries [207]. In such a system, the soliton can not arise only due to the counterbalance of dispersion (diffraction)-induced linear spreading with nonlinearity-induced contraction, but an additional loss-gain balance is very much essential [208]. The soliton gets stabilized at a point, which is "far from equilibrium".

2.3 Metamaterials

Broadly speaking, metamaterials are man-made materials with unique properties not found in natural materials. They consist of periodic structures smaller than the wavelength of the concerned wave for which it is designed, allowing them to manipulate the wave (say, EM radiation) in ways that were not generally possible. One of the most exciting properties of metamaterials is their negative index of refraction, which means they can refract light in the opposite direction, unlike conventional materials. This property has inspired the development of invisibility cloaks, which use metamaterials to hide objects by bending surrounding light. In addition to invisibility cloaks, metamaterials have also been used to create metalens that can capture images at resolutions beyond the diffraction limit of conventional lenses. Metamaterials have numerous applications due to their quality of structure-dependent properties. They show potential technological applications, ranging from optics and telecommunications to energy harvesting and medical imaging. They can be used to create antennas that are smaller and more efficient than their traditional counterparts and to develop new types of lasers, optical switches, and other photonic devices [209]. Apart from optical metamaterials, there are different types of metamaterials that have applications in various fields. Acoustic metamaterials are designed to manipulate sound waves in specific ways. They can be used to create sound barriers, sound lenses, and other acoustic devices [210]. Metamaterials are also designed to control heat flow, which can be used for better insulating or conducting heat [211]. Metamaterials can also be designed to achieve particular mechanical properties, e.g., shock absorption, protective gear, etc. [212].

2.3.1 Brief history of Metamaterials

The evolution of technology brings us to an era where properties are not just dependent on the natural state of the materials; rather, the response can be modified using an artificial substructure in a material. Metamaterials are such types of materials. However, modification of the properties of materials is not a new concept; the famous Lycurgus cup made of ruby glass with embedded gold nanoparticles [213] was found in the fourth century AD. The colour of the cup depends on whether the light passes through the cup or is reflected from the cup [214]. The cup appears green in the case of reflection and red in the case of transmission of light. In the modern era, the study on metamaterials was carried out for radar systems from the 1940s to 1970s. These systems are then known as “artificial dielectrics” and are subwavelength metal particles periodically distributed in dielectric [215]. Winston Kock, an engineer at Bell Laboratories, was one of the first pioneers of artificial dielectrics [216, 217]. Kock proposed the lens structure of a parallel metal plate or a metallic sphere array embedded in a dielectric matrix to find low-loss, lightweight, and inexpensive lens structures for radio waves.

However, the desired magnetic response is not easy to achieve in materials, as the magnetic field component of the EM field is weakly coupled than the electric field component [218, 219]. To enhance the magnetic response, metallic structures that have a higher magnetic response due to their shape are proposed. The effective permeability of the material was modified using an SRR by Pendry in 1999 [220]. Hardy carried out similar work in 1981 by using a hollow metallic cylinder that has a linear cut and a magnetic resonance near 1GHz [221].

The interaction between EM fields and metaatoms (i.e., building blocks of metamaterial) is complicated at the scale of inhomogeneities; however, the wave feels like a homogeneous medium macroscopically. The EM response of metamaterials to external fields can be homogenized, and effective parameters such as permittivity, permeability, refractive index, and impedance can be used to describe the response. Furthermore, the system can be described by the NLSE using the aforementioned parameters.

2.3.2 Idea of Metamaterials

Resonant metamaterials are engineered in such a way that they can resonate with the incident field at desired frequency [222]. Having a repeated building block with a periodicity order of one-tenth of the operating wavelength, the material behaves as a homogeneous medium for the incident field. The non-resonant metamaterials are made to change the properties of the medium without having resonance with the incident field; the order of periodicity of the building block is smaller than the order of the operating wavelength [223, 224]. While the resonant metamaterials have building blocks of the order of operating wavelength. The idea of resonant metamaterials came into existence when V.G. Veselago in 1968 discussed the electrodynamics of substances with a simultaneously negative value of ϵ (electric permittivity) and μ (magnetic permeability) [80]. When ϵ and μ are simultaneously negative, the properties of the substance will contradict some fundamental laws of nature. According to Maxwell's equations $\vec{k} \times \vec{E} = \omega\mu\vec{H}$, $\vec{k} \times \vec{H} = -\omega\epsilon\vec{E}$, where E and H are electric field and magnetic fields, $\vec{k}$ is a wave vector defined as $\vec{k} = \vec{\omega}\sqrt{\mu\epsilon}$. The vectors $\vec{E}$, $\vec{H}$ and $\vec{k}$ make a right-handed set of vectors. For traditional materials, both ϵ and μ are positive. Such materials are called right-handed materials (LHM). For some metamaterials, ϵ and μ are negative; hence the set of $\vec{E}$, $\vec{H}$ and $\vec{k}$ will be the left-handed set of vectors* [77, 225]. These materials are termed as left-handed materials (LHM). Moreover, by having simultaneously negative ϵ and μ, the refractive index of left-handed materials also becomes negative [226, 227]. Due to this property, the perfect lens can be produced [84, 228], whose resolving power will depend on the nature of the material instead of the wavelength of propagating light.

2.3.3 classification of metamaterial on basis of μ and ϵ

The metamaterial response is mainly determined by the parameters μ and ϵ. On the basis of the sign of each parameter, there can be four types of metamaterials:

(a) **Double Positive (DPS) Materials:** In Figure 2.6, the ϵ and μ are plotted along the x-axis and y-axis, respectively. The first quadrant occupies the materials having μ and ϵ, both positive and are called double positive (DPS) materials, which are conventional materials, e.g., dielectric. In these materials, vectors $\vec{E}$, $\vec{H}$ and $\vec{k}$ makes a right handed set.

(b) **Epsilon Negative (ENG) Materials:** The second quadrant possesses the

*taking $-1 = e^{-\frac{\pi}{2}}$, $\vec{k} = \vec{\omega}\sqrt{e^{-\frac{\pi}{2}}\mu e^{-\frac{\pi}{2}}\epsilon} = \vec{\omega}\sqrt{e^{\pi}\mu\epsilon} = -\omega\epsilon\vec{E}$

materials having negative ϵ and are called epsilon negative (ENG) materials, e.g., electric plasma.

(c) **Double Negative (DNG) Materials:** The third quadrant possesses materials having both μ and ϵ negative, called double negative (DNG) materials. These materials have a negative refractive characteristic. In these materials, vectors $\vec{E}$, $\vec{H}$ and $\vec{k}$ make a left-handed set, so these materials are also called left-handed materials.

(d) **Mu Negative(MNG) Materials:** The fourth quadrant possesses materials having only μ negative and called mu negative(MNG) materials, e.g., magnetic plasma.

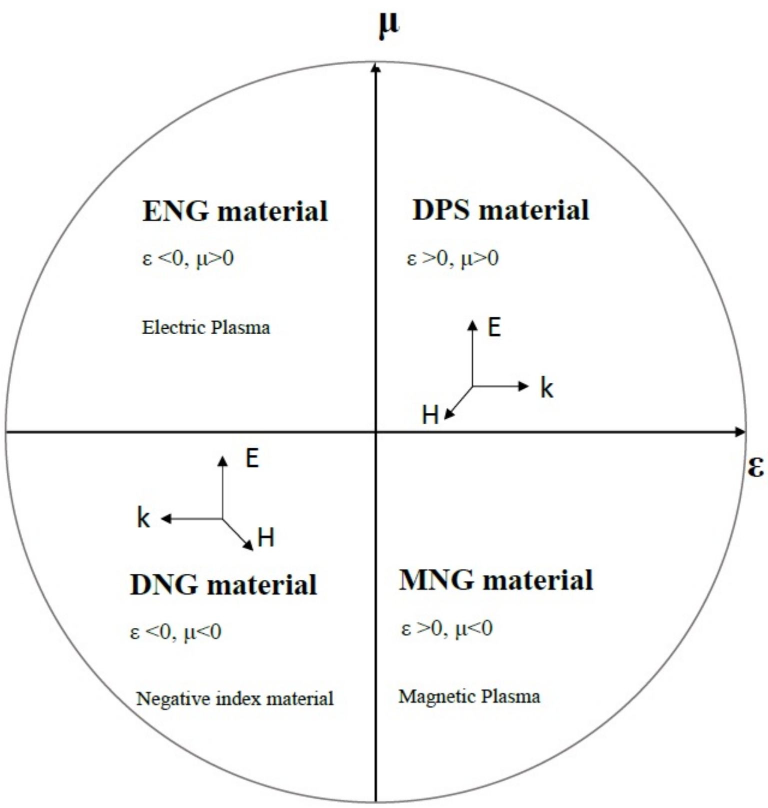

Figure 2.6: Classification of metamaterials on the basis of sign of μ and ϵ

Another way of categorising the Metamaterials are

1. Electromagnetic metamaterials

2. Magnetic metamaterials
3. Electric metamaterials
4. Graphene metamaterials

2.3.4 Metamaterials on the basis of structure

There are many types of metamaterials as per their structure.

1. **Split-ring resonators (SRR) based metamaterials:** SRR are metallic rings with a split. They are designed to resonate at lower frequencies and are used to achieve a negative refractive index [225]. The metamaterials are fabricated by arranging the SRR in a 2D/3D array.

2. **Wire media:** Metallic wires are embedded in dielectric to achieve electric resonance in the desired frequency range and used to select or pass a particular frequency [229].

3. **Dielectric resonators:** These are the structures made of non-conductive materials in different shapes to manipulate the response of EM waves [230].

4. **Plasmonic structures:** Plasmonic structures use the interactions between EM waves and electrons in metals to manipulate light at the nanoscale [231]. They can be used to create ultra-thin lenses, sensors, and other optical devices.

2.3.5 Metamaterials using SRR

The SRR is introduced to seek a high magnetic response. SRR is a tiny metallic ring with a split in between. When a time-changing EM field passes through the metallic ring, according to Faraday's law, a rotating current will be produced, which opposes the incident field [232]. On the split of the ring, there induces a charge on both edges of the split. The opposite charge on the edges of the split, which, as a result, acts as a parallel plate capacitor [233], as shown in Figure 2.7. Thus, SRR acts as an L-C oscillatory circuit containing a capacitor of capacitance C and an inductor of inductance L. [219, 234, 235]. The SRR has a structure-dependent response; thus, by

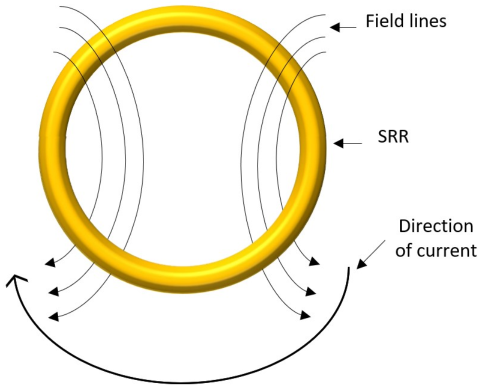

Figure 2.7: Inductance and capacitance in SRR

changing the structure, we can tune the frequency response. Since, the capacitance is produced by a split of the ring and the gap between the two rings, the inductance will increase. By increasing the number of splits, the resonant frequency increases, while adding additional rings will reduce the resonant frequency. [236]. There are many types of SRR structures that have been studied, e.g., circular, twisted ring (stereometamaterials), omega-shaped, S-shaped, etc.

2.3.6 Different Orientation & Geometry of SRR

The EM response in SRR is subjected to the orientation of SRR with respect to the incident field. The placement of the plane and cut of the ring plays a crucial role in interacting with the incident field. In order to have magnetic resonance, the magnetic field must be perpendicular to the SRR. In the case of the parallel magnetic field, no current will be induced in SRR. The perpendicular direction of the magnetic field limits the EM beam propagation direction parallel to SRR. For electric response, the electric field must be parallel to the gap of SRR [237]. As shown in Figure 2.8 configuration, (a) will have electric response only, (b) will have both electric and magnetic response, and (c) will have magnetic response only. SRR are

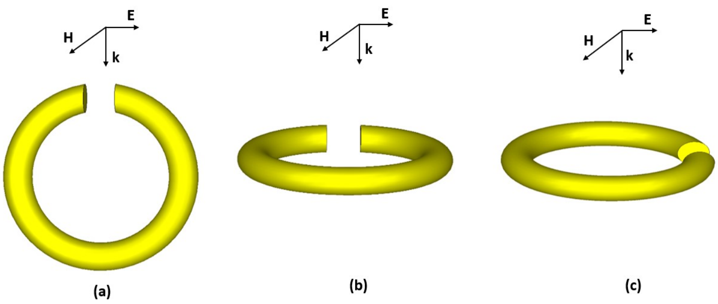

Figure 2.8: different orientation of SRR with respect to incident EM field.

generally circular (Figure 2.9(a)) or rectangular rings (Figure 2.9(b)) [220]. In order to enhance the capacitance and inductance, a ring is inserted inside another ring or placed one ring on the other in different orientations [238]. The SRR structures having one ring inside another are called nested structures, as shown in Figure 2.9(c). On the other hand, placing one SRR on another has an influence on the all-

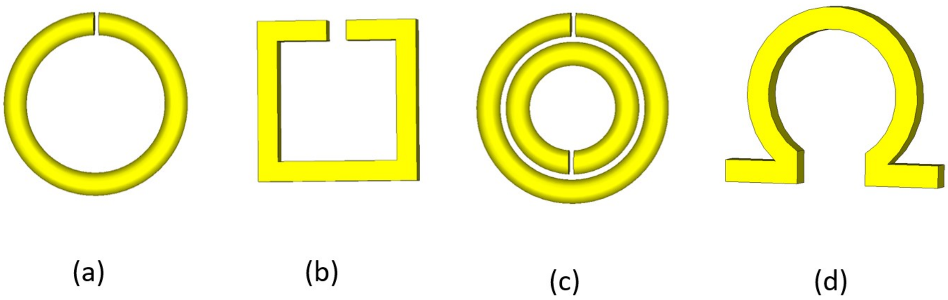

Figure 2.9: (a) Circular SRR, (b) rectangular SRR, (c) Nested SRR, and (d) omega shaped SRR

over response of the structure. Many arrangements can be used, e.g., the SRR can be placed at any angle (Figure 2.10(a)) and are called stereometamaterials [239]. Also, one arrangement can be repeated with different orientations, as shown in Figure 2.10(b) the one arrangement of stereometamaterial repeated with a twist, e.g., a unit cell is formed by setting the pairs of four split rings 0°, 90°, 180° and 270°. These structures are called twisted SRR or chiral metamaterials [240]. Adding a tail

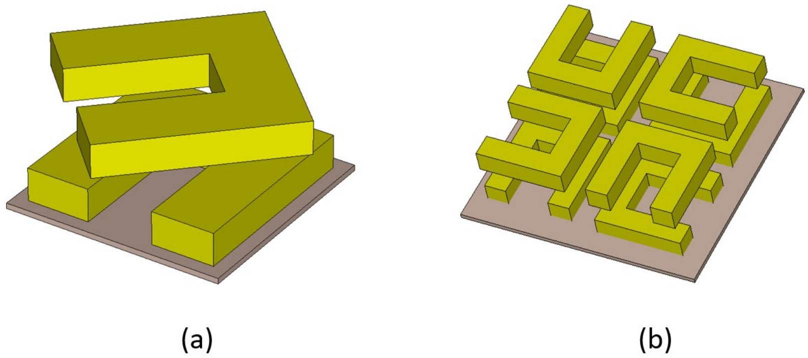

Figure 2.10: (a) One SRR placed on another with a different orientation (stereometamaterial). (b) One stereo-metamaterial rotates at 0°, 90°, 180° and 270° orientation to form a unit cell (twisted SRR)

to the gap in the SRR gives another kind of shape, that is, the Omega (Ω) shape (Figure 2.9d). As we increase the tail, the resonance frequency decreases. When an incident electric field is perpendicular to the Omega tail, the resonant frequency is high compared to when an electric field is parallel to the Omega tail [241].

2.3.7 Importance of SRR-based metamaterials

SRR-based metamaterials have huge significance as they show unconventional phenomena. The reason for the importance of SRR-based metamaterials in research is their negative values of permittivity and permeability, leading to phenomena that are not observed in naturally occurring materials. The simultaneous negative values of permittivity and permeability give the negative value of the refractive index that gives rise to the invisibility cloak [242] and perfect lens [84]. As metamaterial stops the transmission at its natural frequency, it can be used to make stopband filters [243]. EM waves can be confined by using the SRR, as they are impermeable to frequencies near their natural frequency [244]. Dielectric constant can be found in any organic material by replacing it with dielectric.

2.4 Nonlinearity in Metamaterials

Nonlinearity in metamaterials is a complex field that involves various mechanisms. There are diverse strategies and mechanisms for generating nonlinearity in metamaterials, reflecting the rich and evolving landscape of this field. Below are the mechanisms that elaborate on how nonlinearity is generated or incorporated in metamaterials.

1. **Nonlinear Electromagnetic Response:** Nonlinearity can arise from the interaction of intense EM fields with the metamaterial structure itself. This can lead to self-focusing, self-phase modulation, and other nonlinear optical effects [87]. In the current thesis, this mechanism has been commonly used.

2. **Nonlinear Optical Effects:** Nonlinear optical effects in metamaterials can be achieved or enhanced by incorporating nonlinear optical materials. These materials exhibit a nonlinear response to intense EM fields, resulting in nonlinear phenomena such as harmonic generation and parametric amplification [245]. Metamaterials have been designed to leverage these properties for applications, e.g., frequency mixing and nonlinear signal processing, coherent single-photon waveguide transport in a linear two-atom System.

3. **Tunable Resonances:** Metamaterials often rely on resonant structures that can be tuned electronically or even mechanically. This tunability allows for nonlinear responses as the metamaterial's properties change with incident frequencies or intensities. Such tunable metamaterials can be used in nonlinear wave manipulation and signal processing [246, 247].

4. **Nonlinear Magnetic Response:** Some metamaterials employ magnetic elements with nonlinear magnetization properties. These elements induce nonlinear effects through their magnetic response. Such nonlinearity finds applications in nonlinear magneto-optics and magnetic metamaterials [89, 248].

5. **Electro-optic and Magneto-optic Nonlinearity:** Incorporating materials with electro-optic or magneto-optic properties allows for nonlinear responses to applied electric or magnetic fields. These properties can be utilized in metamaterials for terahertz and microwave applications [249, 250].

6. **Integrating Phase Transition Materials:** Phase-transition materials integrated into metamaterial structures can introduce nonlinearity through abrupt changes in properties at specific conditions [251]. These transitions can be exploited in unique and fascinating applications like thermal cloaks.

2.4.1 Soliton in metamaterial based on SRR

A large variety of solitons can be found in SRR based metamaterial. The soliton is achieved by counterbalancing the nonlinear and linear phenomenon in metamaterials [252]. The field intensity of EM wave in SRR shows the hysteresis-type dependence with magnetic permeability [87], which is a nonlinear phenomenon. This nonlinear response of metamaterials allows the material to change from left-handed to right-handed and vice versa. Due to nonlinearity, the self-focusing effect will be induced in metamaterial, which may be utilized for maintaining the shape and size of the wave while propagation. With the knowledge of the basics of nonlinear phenomena, soliton and metamaterial given in this chapter, we now proceed with the investigation to fulfil our research objectives that have been mentioned in chapter 1. Chapter 3 presents the soliton generation, dynamics and stability analysis in an SRR-based metamaterial with cubic-quintic nonlinearity, diffusion and multiphoton absorption. Chapter 4 presents soliton generation and emphasis on the stability of soliton in a graphene-embedded SRR-based metamaterial that behaves as a saturable nonlinear medium due to the presence of graphene. Higher-order linear and nonlinear effects, namely, third-order dispersion, self-steepening, and Raman scattering, modify the soliton generation criterion as well as soliton dynamics. Chapter 5 presents an investigation into that. A different type of soliton, namely, the diffraction-managed soliton, has been presented in chapter 6. That includes generation, dynamics and stability of the soliton. Chapter 7, which is the concluding chapter, suggests some potential applications of the result obtained in the thesis and elaborates on the future scope.

Chapter 3

Generation and Dynamics of Soliton in a SRR Based Metamaterial with Higher Order Nonlinearity, Multi-photon Absorption and Diffusion

As per the objectives, we first explore soliton in SRR-based metamaterials with higher order nonlinearity and subsequently study the soliton dynamics. This chapter presents an investigation of compound dissipative soliton (DS) formation in such metamaterial having higher-order nonlinearity, diffusion and multi-photon absorption. The effect of diffusion and multi-photon absorption on the propagation dynamics of DS is studied. The interaction dynamics of DS are investigated for different initial separations and phases of the participating soliton, which eventually leads to soliton switching. The phase-controlled switching is demonstrated. Interestingly, a weak soliton beam is found to control a strong soliton beam. This chapter corresponds to the first two objectives of this thesis.

3.1 Introduction

'Soliton' and 'left-handed materials' (LHM) are two widely sought-after research topics of the past century that rely on refractive index as their central idea. While the optical 'soliton' can be originated by the virtue of nonlinear refractive index [27, 29, 56], the LHM refers to a special class of metamaterials that possesses 'negative' refractive index [84]. It is the intensity-dependent nonlinear refractive index of the materials that provides the key mechanism for the self-localization of soliton. Actually, the nonlinear refractive index constitutes the backbone of all nonlinear optics. However, only positive-refractive-index medium (whether linear or nonlinear) was known until the inception of LHM in 1968 by Veselago [80] and later on by Pendry [220]. Since the refractive index is the central element of both 'soliton' and 'metamaterials', it is no wonder the LHM immediately attracted huge research attention across the subjects, including soliton research. When placed in an EM field, the gap or cut of the SRR acts as a capacitor, and the ring acts as an inductor according to the Faraday law [253]. The long array of SRR fabricated on a dielectric has a finite resistance. Therefore, the SRR array acts as an LCR circuit and can resonate with the incident EM field [232]. The resonance frequency depends on the shape and size of the rings [254]. At resonance, both the electric permittivity (ϵ) and the magnetic permeability (μ) are negative, which lead to negative refractive index [77, 222, 225].

The SRR-based LHM may behave like a cubic or Kerr nonlinear media if the SRR array is arranged on a suitable nonlinear dielectric medium [87]. In this type of nonlinear metamaterial, the hysteresis-type dependence between magnetic permeability and field intensity may convert the material property from left-handed to right-handed and back. The tiny SRRs act as metamolecules in the dielectric, and as a whole, the system behaves like a composite material. This composite metamaterial (SRR and dielectric) is mainly governed by the surface plasmon, which is generated at the metal-dielectric interface. The localized surface plasmon resonance provides the key mechanism of the large range of applications of metamaterials [81]. In fact, the propagation of EM waves through metamaterials is of primary interest. This makes the soliton formation in metamaterial a pretty appealing research topic. The existence of different types of solitons are reported in SRR-based metamaterials: discrete breather soliton [89, 255], bright-dark soliton [107], gap soliton [95, 96] and spatiotemporal soliton [256, 257]. An incident EM wave may lead to the formation of compound soliton (due to both the electric and magnetic field of the em wave) in the metamaterial. Generally, for in-plane SRR configuration, the magnetic nonlinearity of metamaterial is controlled by the electric field nonlinearity. But a vertical SRR can enable the magnetic field nonlinearity with the "equal right" [258]. Discrete breather solitons are found in metamaterial by virtue of the combination of nonlinearity with the discreteness of SRR array [89]. Subwavelength discrete solitons are found due to balancing the tunnelling of surface plasmon modes by nonlinearity-induced self-trapping [30]. Gap solitons are found in a similar combination of nonlinearity with discreteness in the chain of SRR dimer (i.e., a pair of coupled SRRs of different sizes)[98, 99]. For theoretical modelling, the coupled NLSE is used to generate Manakov-type bright-bright and dark-dark vector solitons found in metamaterials [107]. Bright, dark and grey soliton (or quasi-solitons) can be generated for a wider parametric range using the Drude model [110].

The nonlinearity of SRR-based metamaterials can be enhanced by placing them on a GaAs layer [259]. This structure results in a saturable nonlinearity. The field gets enhanced due to impact ionization, which results in decreasing oscillation strength of SRR [260]. The polarity of permittivity can be controlled by varying the field strength. The saturable nonlinearity can be approximated to a cubic-quintic nonlinearity. However, the currently available literature reporting soliton generation in SRR-based metamaterials with higher-order nonlinearity is not adequate because most of them deal with only cubic nonlinearity. In this chapter, we investigate the soliton generation in an SRR-based cubic-quintic nonlinear metamaterial and study their dynamics with such higher-order nonlinearities. TPA and 3PA effects become important, and we include them in our model. Now, in any spatially extended system, diffusion plays a significant role due to ever-increasing entropy. A spatially symmetric or asymmetric diffusive metamaterials can be used in various fields to capture a better scenario. However, soliton in metamaterials with diffusion has not been explored widely [261]. We therefore, include the diffusion effect in our model. So, collectively, our objective is to study the generation and dynamics of soliton, which will be precisely a dissipative soliton, in a cubic-quintic metamaterial with multi-photon absorption and diffusion. The arrangement of the next part of this chapter is as follows: Section 2 describes the mathematical modelling, followed by a numerical study of the excitation of the DS. Section 3 describes the interaction dynamics of the DS, while section 4 contains a brief conclusion.

3.2 Mathematical Modelling and Generation of Soliton

We consider an LHM that comprises a one-dimensional array of SRR on a nonlinear dielectric substrate. SRR can be fabricated on the substrate by electron beam lithography method [227]. In the composite metamaterial, SRR acts as a meta-atom. The presence of SRR in the composite material changes both the effective permittivity (ϵ_{eff}) and effective permeability (μ_{eff}), as well as the two key material parameters, refractive index and impedance. These four parameters combinedly describe the macroscopic behaviour of the composite metamaterials [215]. The shape and size of the SRR and the metal used in SRR determines the resonance wavelength, from radio frequency and microwavelength to the infrared wavelength and even to visible light wavelength [227]. For the current study, we consider a general model in terms of SRR-dimension and SRR-metal and use normalized values of the system parameters so that the results of the investigation can be interpreted in any of the operating wavelength regions. Essentially, the dimension of the SRR is kept smaller than the operating wavelength of the EM wave so that the SRR-based (composite) metamaterial behaves as a homogeneous, isotropic medium.

Further, we consider the substrate as a cubic-quintic nonlinear medium that turns the composite metamaterial into a cubic-quintic nonlinear metamaterial. In addition, a part of the nonlinearity of the composite metamaterial comes from the lattice of resonator meta-molecule through the SRR capacitance that is dependent on the local electric field strength in the SRR gap [87]. Now, if an EM wave is launched on this nonlinear metamaterial, the higher-order nonlinear effects, namely, TPA and 3PA, become prominent alongside the cubic self-focusing, quintic defocusing and diffusion. Such EM wave propagation in metamaterial can be represented by a pair of coupled higher-order nonlinear Schrödinger equations (HNLSE) of electric and magnetic fields. The coupled HNLSE can be derived from Maxwell's equations, as shown in ref. [105] and in this chapter. Following the same method, we derive the coupled HNLSE for the electric as well as magnetic fields, which are x-polarized and propagating along z direction as follows:

The nonlinear relations for $\vec{D}$ and $\vec{B}$ for SRR based composite metamaterials are given as:

$$\vec{D} = \epsilon_{eff}\vec{E} = \epsilon\vec{E} + \vec{P_{NL}}, \tag{3.1}$$

$$\vec{B} = \mu_{eff}\vec{H} = \mu\vec{H} + \vec{M_{NL}}, \tag{3.2}$$

where, $\vec{E}$ electric and field intensity, $\vec{H}$ magnetic field intensity. $\vec{D}$ is electric flux and $\vec{B}$ is magnetic induction. The ϵ_{eff} and μ_{eff} must be dispersive in order to keep energy density positive [80], and is given as:

$$\epsilon_{eff}(\omega) = \epsilon_0\left(\epsilon_D(|E|^2) - \frac{\omega_p^2}{\omega^2}\right), \tag{3.3}$$

$$\mu_{eff}(\omega) = \mu_0\left(1 - \frac{F\omega^2}{\omega^2 - \omega_{0NL}^2(|H|^2)}\right). \tag{3.4}$$

ω_p, and F are plasmon frequency and filling factor, respectively.

Using nonlinear relation of $\vec{D}$ and $\vec{B}$ (equation 3.1 and 3.2) in Maxwell's equations

[105], we get:

$$\nabla^2\vec{E}-\mu\epsilon\frac{\partial^2\vec{E}}{\partial T^2}-\mu\frac{\partial^2\vec{P}_{NL}}{\partial T^2}-\vec{\nabla}(\nabla.\vec{E})=\frac{\partial}{\partial T}[\vec{\nabla}\mu_{NL}\times\vec{H}]+\frac{\partial}{\partial T}\left[\mu_{NL}\frac{\partial}{\partial T}(\epsilon\vec{E}+\vec{P}_{NL})\right] \quad (3.5)$$

$$\nabla^2\vec{H}-\mu\epsilon\frac{\partial^2\vec{H}}{\partial T^2}-\mu\frac{\partial^2\vec{M}_{NL}}{\partial T^2}-\vec{\nabla}(\nabla.\vec{H})=-\frac{\partial}{\partial T}[\vec{\nabla}\epsilon_{NL}\times\vec{E}]+\frac{\partial}{\partial T}\left[\epsilon_{NL}\frac{\partial}{\partial T}(\mu\vec{H}+\vec{M}_{NL})\right] \quad (3.6)$$

Considering an x-polarized plane wave propagating along the z-axis with frequency ω and wave number k. Also,

$$\vec{E}=\big(E(z,t),0,0\big),\qquad \vec{H}=\big(0,H(z,t),0\big),$$

with

$$E(z,t)=q(z,t)e^{\iota(kz-\omega t)},\quad H(z,t)=p(z,t)e^{\iota(kz-\omega t)},$$

where, $q(z,t)$ and $p(z,t)$ are envelope of $\vec{E}$ and $\vec{H}$ respectively. P_{NL} and M_{NL} are given as $P_{NL}=\epsilon_{NL}E$, $M_{NL}=\mu_{NL}H, \epsilon_{NL}=\alpha|E|^2+\beta|E|^2$, with $\mu_{NL}=\gamma|H|^2+\delta|H|^2$. The value of ϵ_{NL} and μ_{NL} here is different from reference [80], as the values are taken up to the fifth (quintic) order.

$$\epsilon_{NL}=\alpha|E|^2+\beta|E|^4,\qquad \mu_{NL}=\gamma|H|^2+\delta|H|^4. \quad (3.7)$$

We introduce slow variables as $\xi=\varepsilon(z-\omega' t)$, $\tau=\varepsilon^2\tau$ (since the envelopes of E and H change slowly in z and t). Here, $\omega'=\frac{\partial\omega}{\partial k}$ is group velocity.

and assuming $\quad \alpha=\hat{\alpha}\varepsilon^2,\quad \beta=\hat{\beta}\varepsilon^2,\quad \gamma=\hat{\gamma}\varepsilon^2,\quad \delta=\hat{\delta}\varepsilon^2$

q and p can be written as asymptotic expansion in terms of ε,

$$q(\xi,\tau)=q_0(\xi,\tau)+\varepsilon q_1(\xi,\tau)+\varepsilon^2q_2(\xi,\tau).....,\quad (3.8)$$

$$p(\xi,\tau)=p_0(\xi,\tau)+\varepsilon p_1(\xi,\tau)+\varepsilon^2p_2(\xi,\tau)..... \quad (3.9)$$

Collecting the coefficients of $O(\varepsilon^2)$, we get:

$$i\frac{\partial q_0}{\partial\tau}+\frac{c^2}{2\omega}\frac{\partial^2q_0}{\partial\xi^2}+\frac{\hat{\alpha}\mu c^2}{2\omega}|q_0|^2q_0+\frac{\hat{\gamma}\epsilon c^2}{2\omega}|p_0|^2q_0+\frac{\hat{\beta}\mu c^2}{2\omega}|q_0|^4q_0+\frac{\hat{\delta}\epsilon c^2}{2\omega}|p_0|^4q_0=0 \quad (3.10)$$

$$i\frac{\partial p_0}{\partial\tau}+\frac{c^2}{2\omega}\frac{\partial^2p_0}{\partial\xi^2}+\frac{\hat{\gamma}\mu c^2}{2\omega}|p_0|^2p_0+\frac{\hat{\alpha}\epsilon c^2}{2\omega}|q_0|^2p_0+\frac{\hat{\delta}\mu c^2}{2\omega}|p_0|^4p_0+\frac{\hat{\beta}\epsilon c^2}{2\omega x}|q_0|^4p_0=0 \quad (3.11)$$

Further, taking $\xi=X$, $\quad\tau=\frac{c^2}{2\omega}T$, $\quad q_0=Q$ and $p_0=P$, we get

$$i\frac{\partial Q}{\partial T}+\frac{\partial^2Q}{\partial X}+\hat{\alpha}\mu|Q|^2Q+\hat{\gamma}\epsilon|P|^2Q+\hat{\beta}\mu|Q|^4Q+\hat{\delta}\epsilon|P|^4Q=0 \quad (3.12)$$

$$i\frac{\partial P}{\partial T}+\frac{\partial^2P}{\partial X}+\hat{\gamma}\mu|P|^2P+\hat{\alpha}\epsilon|Q|^2P+\hat{\delta}\mu|P|^4P+\hat{\beta}\epsilon|Q|^4P=0. \quad (3.13)$$

Now, the coefficients of the terms, except the first ones, of the above equations are taken as complex. In equation 3.12, the coefficient of $\frac{\partial^2 Q}{\partial X}$ is taken as $(1 + id)$, where the real and imaginary parts are self-diffraction and diffusion coefficients, respectively. $\hat{\alpha}\mu$ is replaced by $(\sigma_1 + i\sigma_2)$, where the real and imaginary parts are Kerr nonlinearity and TPA coefficients respectively. Similarly, $\hat{\gamma}\epsilon$ is replaced by $(\sigma_1' + i\sigma_2')$, where the real and imaginary parts are respectively the Kerr nonlinearity and TPA but due to the other field. Likewise, $\hat{\beta}\mu$ is replaced by $(\sigma_3 + i\sigma_4)$: the real and imaginary parts are quintic nonlinearity and 3PA respectively. Also, $\hat{\delta}\epsilon$ is replaced by $(\sigma_3' + i\sigma_4')$, where the real and imaginary parts represent quintic nonlinearity and 3PA due to the other field respectively. An external net gain term $i\Delta g$ is added to compensate the losses. We also take similar complex coefficients for equation 3.13. Finally, the modified coupled cubic-quintic perturbed nonlinear Schrödinger equations (CQPNLSE) read as follows:

$$
\begin{aligned}
i\frac{\partial Q}{\partial T} + \frac{\partial^2 Q}{\partial X^2} + \sigma_1 \mid Q \mid^2 Q - \sigma_3 \mid Q \mid^4 Q + \sigma_1' \mid P \mid^2 Q - \sigma_3' \mid P \mid^4 Q = i\Delta g Q + id\frac{\partial^2 Q}{\partial X^2} \\
+ i\sigma_2 \mid Q \mid^2 Q + i\sigma_4 \mid Q \mid^4 Q + i\sigma_2' \mid P \mid^2 Q + i\sigma_4' \mid P \mid^4 Q \qquad (3.14) \\
i\frac{\partial P}{\partial T} + \frac{\partial^2 P}{\partial X^2} + \sigma_1 \mid P \mid^2 P - \sigma_3 \mid P \mid^4 P + \sigma_1' \mid Q \mid^2 P - \sigma_3' \mid Q \mid^4 P = i\Delta g P + id\frac{\partial^2 P}{\partial X^2} \\
+ i\sigma_2 \mid P \mid^2 P + i\sigma_2' \mid Q \mid^2 P + i\sigma_4 \mid P \mid^4 P + i\sigma_4' \mid Q \mid^4 P \qquad (3.15)
\end{aligned}
$$

So, in summary, Q and P are the normalized electric field and magnetic field, respectively, and T is the normalized retarded time [105]. X is the slow space variable moving at the linear group velocity. σ_1 and σ_1' are the Kerr nonlinearity coefficients, σ_2, σ_2' are the coefficient of TPA, σ_3, σ_3' are the coefficient of quantic nonlinearity and σ_4, σ_4' are the coefficient of 3PA. Δg is the net gain coefficient and d is the diffusion coefficient. Equations 3.14 and 3.15 can be considered as a set of perturbed NLSE. In both equations, the first term represents the evolution of the field; the second term represents self-diffraction; the third term represents Kerr nonlinearity-induced self-focusing, and the fourth term is quintic nonlinearity-induced self-defocusing.

The fifth and sixth terms are similar to the third and fourth terms but induced by the other field. The first terms in the right-hand side of equations 3.14 and 3.15 are the gain terms, and the second terms are the diffusion terms. The third and fourth terms are TPA and 3PA, respectively, while the fifth and sixth terms are TPA and 3PA terms, respectively and are induced by the other field. In the nonlinear metamaterial, the interplay of the diffraction and nonlinear terms eventually may lead to soliton formation provided the loss of the system due to TPA, 3PA or any other kind of linear or nonlinear loss terms is overcome by an external gain. Such solitons are termed as "dissipative" solitons (DS). Generation of DS corresponds to a stable point that is "far from equilibrium", which can be maintained by supplying a continuous gain into the dissipative system. We explore bright DS in our proposed model of metamaterial with profiles as $Q = Q_0 Sech(x)^{1+i\beta} e^{-i\omega T}$ and $P = P_0 Sech(x)^{1+i\beta} e^{-i\omega T}$, where Q_0 and P_0 are the maximum amplitudes of the normalized electric and magnetic fields respectively, with β as the chirping parameter. CQPNLSE can be solved by approximate analytical methods (e.g., variational method, moment method) or using a direct numerical approach based on SSFM or FDTD method. We choose the numerical path and prefer SSFM over FDTD as the former is a faster routine and suffers from less instability [154].

The role of the system parameters on DSs is of primary interest. We generate DS for a range of values of the system parameters. To mention, d_1 from 0.005 to 0.015, σ_2 from 0.005 to 0.02, σ_3 from 0.0008 to 0.0012 and σ_4 from 0.007 to 0.03. However, in this chapter, we present the results for the typical values of those parameters (unless mentioned otherwise): $d_1 = 0.01$, $\sigma_2 = 0.01$, $\sigma_3 = 0.001$ and $\sigma_4 = 0.01$. We explore the effect of TPA, which is usually detrimental to the propagation of the DS. It can be noted that TPA in metamaterial is very less probable to occur. However, recently TPA of 40 % efficiency has been reported in a Sagnac-style interferometer by injecting N=2 NOON state [262]. The possibility of TPA and 3PA depends on the wavelength of the EM wave. Here, we consider the TPA parameter (σ_2') small and the 3PA parameter (σ_4') is further smaller. The evolution of the EM field in the presence of TPA shows the decay of the field. A proper choice of gain may lead to DS formation with a slightly oscillating peak Figure 3.1). An increase in TPA needs greater gain (Δg) to generate the soliton (Figure 3.2). However, the fluctuation of peak height will increase in case of higher TPA. Similar DS can be obtained with a magnetic field also. Figure 3.3 shows the peak intensity profiles of the soliton at different strengths of TPA. The electric field as well as magnetic field soliton can constitute a compound soliton.

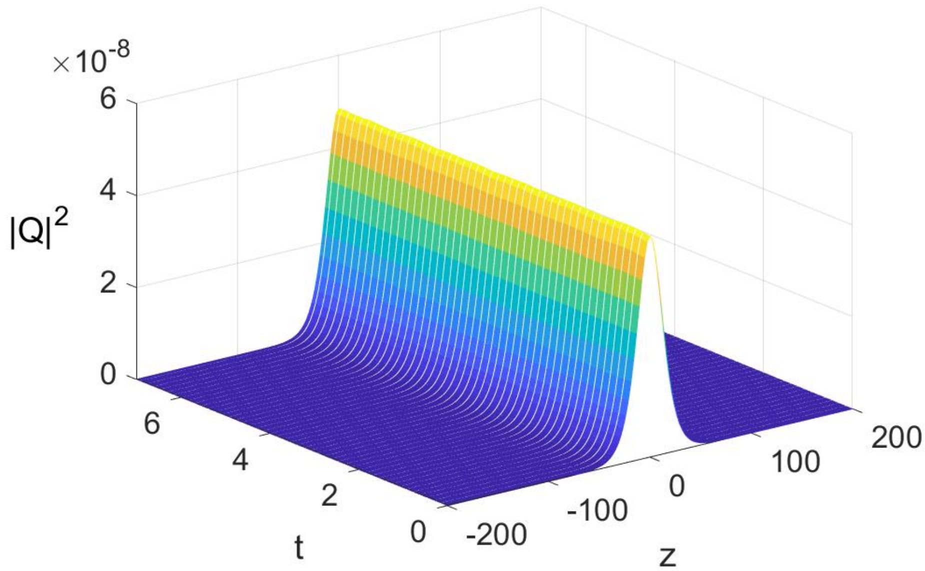

Figure 3.1: Typical profile of DS with electric soliton field Q for TPA coefficient $\sigma_2 = 0.005$. Other parameters are $d_1 = 0.01$, $\sigma_3 = \sigma_3' = 0.001$, $\sigma_4 = \sigma_4' = 0.01$.

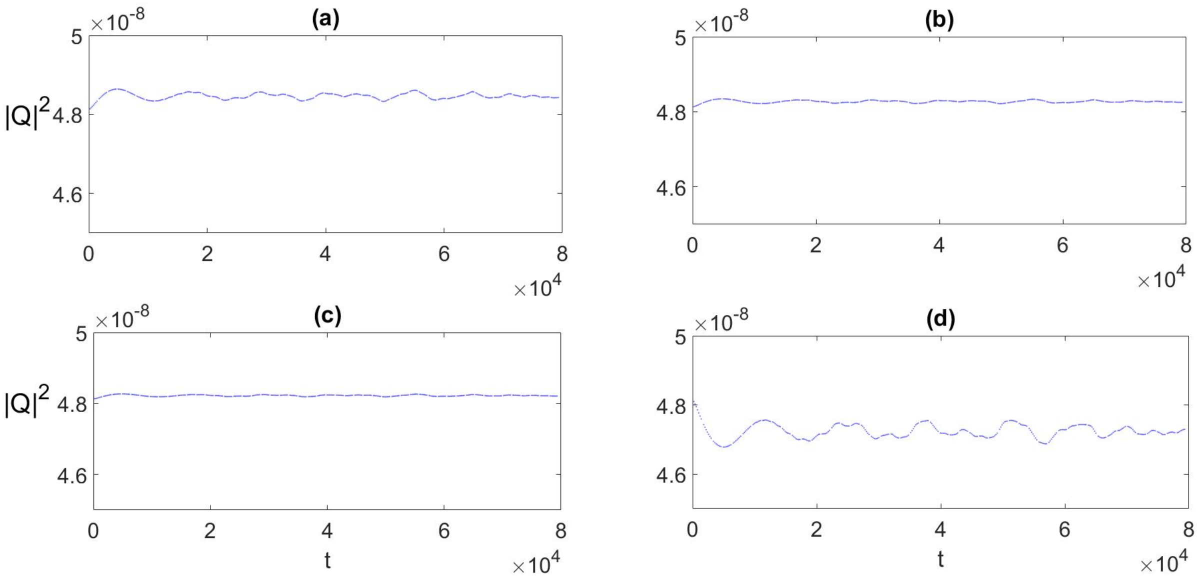

Figure 3.2: The evolution of peak intensities of the electric field $|Q|^2$ at different strength of TPA, (a) σ_2=0.005, (b) σ_2=0.009, (c) σ_2=0.01 and (d) σ_2=0.03. Other parameters are the same as mentioned in Figure 3.1.The horizontal and vertical axes represent the time axis and $|P|^2$, respectively, for all panels. (*Also, in the following figures, the omitted labels can be read in similar manner.)*

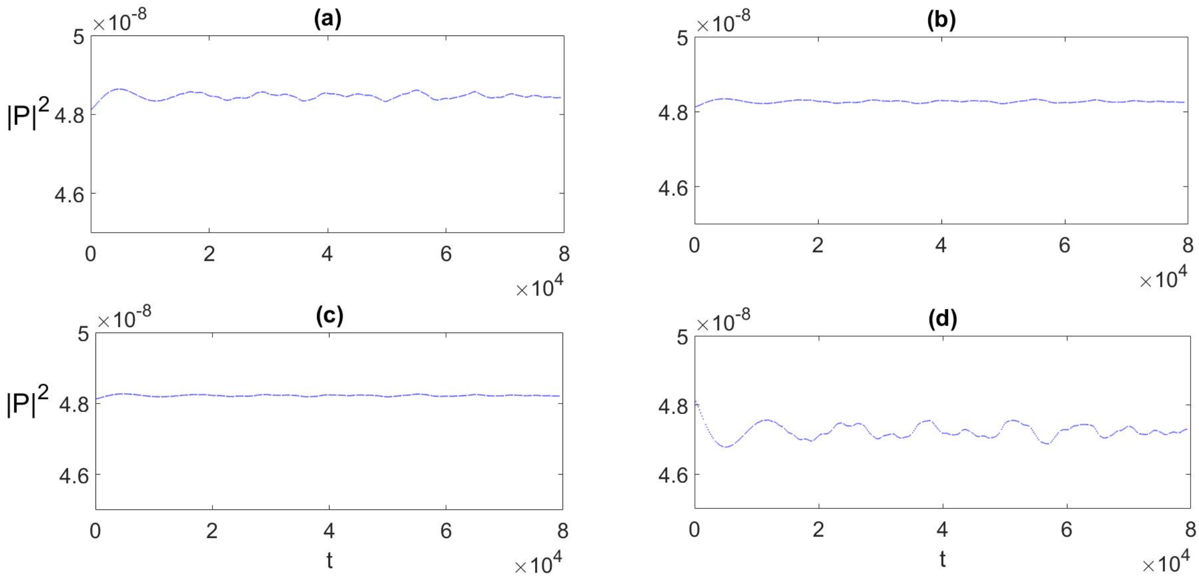

Figure 3.3: The evolution of peak amplitude of the magnetic soliton field P at different strength of TPA, (a) σ_2=0.005, (b) σ_2=0.009, (c) σ_2=0.01 and (d) σ_2=0.03.The average Δg values lies around 2.072×10^{-6}. Other parameters are the same as Figure 3.1.

Now, keeping the amplitude of the magnetic field constant, if the amplitude of the electric field is varied, a phase difference is observed to be developed between the fields. This may lead to the separation of the electric field DS and magnetic field DS (Figure 3.4). The separation is more prominent for a stronger electric field. A breather like field dynamics is observed (not so prominent in fig 3.4 unless magnified) in both the branches of DS.

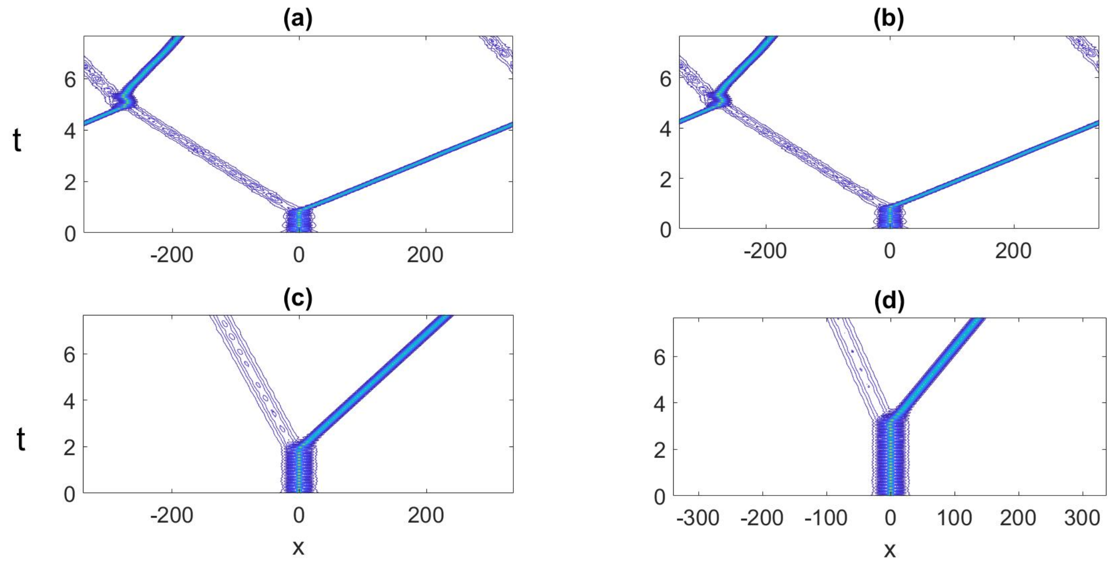

Figure 3.4: Evolution of the EM field for unequal initial electric and magnetic fields. In all plots $| P |^2 = 1.5$ and $| Q |^2$ varies as (a) $| Q |^2$=1 , (b) $| Q |^2$=0.8, (c) $| Q |^2$=0.75 and (d) $| Q |^2$=0.70.

In order to explore the features of the higher-order solitons, we found second-order DS have less stability, while further higher-order solitons are too unstable. We found the contribution of the 3PA is very small, which may be due to the low possibility of 3PA to occur. The diffusive metamaterials are studied using their spatial inversion symmetry and line inversion asymmetry [261]. The spatial asymmetric metamaterial can have large asymmetric diffusion. In the present case, we consider a spatial asymmetric diffusion. We find that the DS can be stabilized with a diffusion up to 4×10^{-5} times of the self-diffraction. Beyond that, the DS gets distorted.

3.3 Soliton Interaction Dynamics and Switching

The fundamental aspect of soliton can be revealed by their interactional behaviour, which is presented in this section. The basic motto for studying interaction is to reinforce the "soliton" nature of the generated DS and to demonstrate the all-optical controlling of the DS and, hence, to explore the possibility of useful dynamics, if any. For the said purpose, we consider the electric fields of the two interacting DS given by the following general form:

$$\begin{aligned} i\frac{\partial Q_i}{\partial T} + \frac{\partial^2 Q_i}{\partial X^2} + \sigma_1 \mid Q_i \mid^2 Q_i - \sigma_3 \mid Q_i \mid^4 Q_i + \sigma_1' \mid Q_{3-i} \mid^2 Q_i - \sigma_3' \mid Q_{3-i} \mid^4 Q_i = i\Delta g Q_i \\ + id\frac{\partial^2 Q_i}{\partial X^2} + i\sigma_2 \mid Q_i \mid^2 Q_i + i\sigma_4 \mid Q_i \mid^4 Q_i + i\sigma_2' \mid Q_{3-i} \mid^2 Q_i + i\sigma_4' \mid Q_{3-i} \mid^4 Q_i. \end{aligned} \quad (3.16)$$

Here, Q_i represents the amplitude of electric fields as $i = 1, 2$. All other terms are similar to those described in the previous section. The two DSs interact with each other for an initial normalized separation of 80 or less.

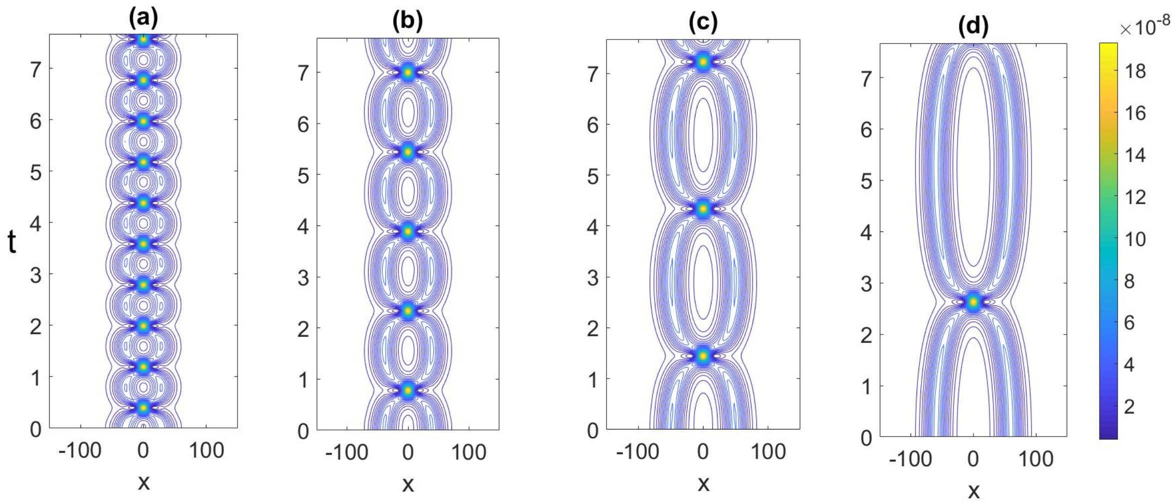

Figure 3.5: Interaction between two DSs at different separations: (a) 40, (b) 45, (c) 50 and (d) 60. Other parameters are the same as mentioned in the figure. 3.1

The interaction of two solitons for different separations between them is shown in Figure 3.5. The initially separated solitons come closer, collide and get separated then collide again. The periodic collision continues (Figure 3.5). As the separation between solitons increases, the number of collisions decreases. This happens because the induction between the solitons becomes weak for larger separation of solitons. The spatial power spectra corresponding to Figure 3.5 are shown in Figure 3.6. Both the cases of figures 3.5 and 3.6 support the formation of periodically colliding DSs. In order to identify the relation between the rate of collision and separation between DSs, the variation of the 'time for the first collision' is plotted with respect to the initial separation between DSs Figure 3.7). The 'time for the first collision' is observed to increase nonlinearly with the increase in separation, and consequently, the number of interactions decreases (Figure 3.7). Not only the separation between the interacting solitons but also the phase difference significantly modifies the interaction dynamics.

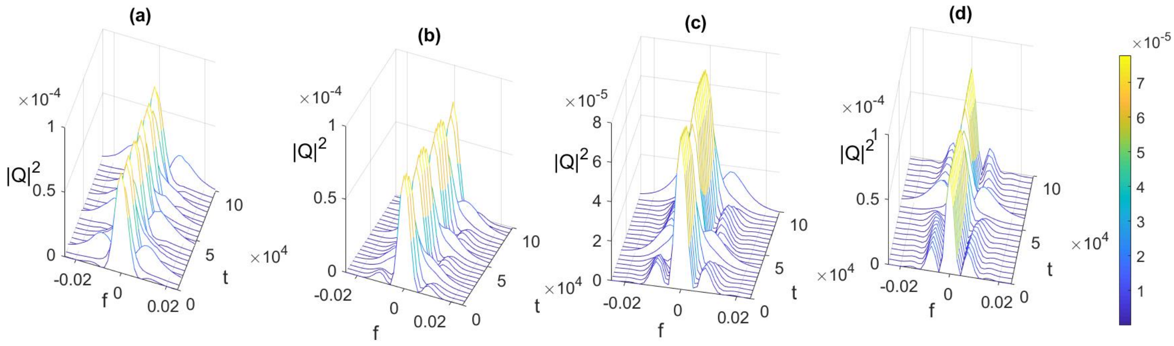

Figure 3.6: The spatial power spectra corresponding to fig 3.5. Here f is the spatial frequency

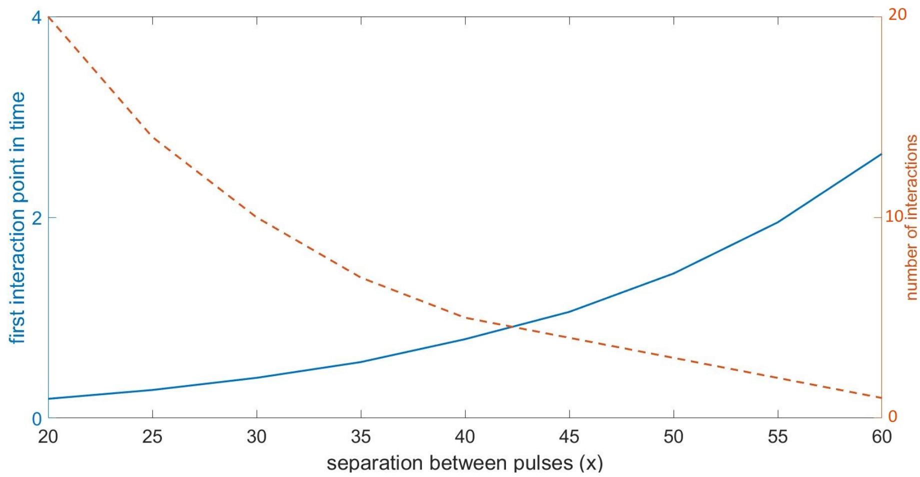

Figure 3.7: Left scale (solid line): The variation of 'time of first collision' with the separation between DSs. Right Scale (dashed line): The variation of the number of interactions with the separation between DSs.

An initial phase difference between the interacting DSs breaks the interaction symmetry and leads to the transfer of energy from one DS to another (Figure 3.8).

The corresponding spatial power spectra also show the energy transfer (Figure 3.9). As the initial phase difference between interacting DSs increases, the DSs go to less ordered states, and the symmetric breather state disappears eventually. However, a phase difference of π can create symmetric interactions (fig 3.10). With decreasing separation, the rate of interaction increases (fig 3.10(a,b)). A separation as small as 10 units may yield a very clumsy interaction scenario (fig 3.10(C)). Interestingly, although both 0 and π phase differences lead to symmetric interactions, the nature of interactions are different (one may compare Figure 3.5 and 3.10). A mirror image-like interaction dynamics is observed for a particular choice of a set of initial phase differences. For instance, in Figure 3.11 (a),(b) an initial phase difference of 0.2π and 1.8π (or -0.2π) create interaction profiles that are mirror images of each other. The corresponding spatial power spectra portrayed in Figure 3.11 (c),(d) validate the same.

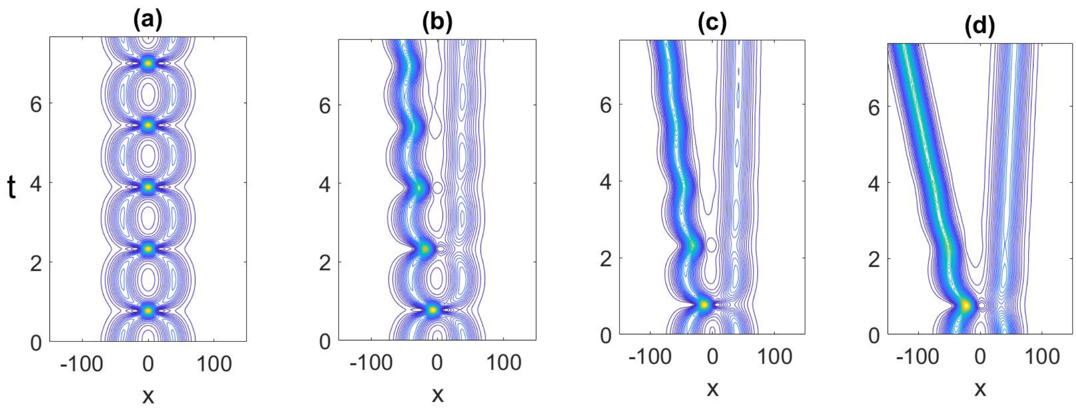

Figure 3.8: Interaction of two DSs at different phase difference $\Delta\phi$ between them, (a) $\Delta\phi = 0$, (b) $\Delta\phi = 0.05\pi$, (c) $\Delta\phi = 0.1\pi$ and (d) $\Delta\phi = 0.2\pi$. Two *in-phase* DSs interact symmetrically (a), while a phase difference makes the interaction asymmetric (b-d). Other parameters are the same as mentioned in Figure 3.1.

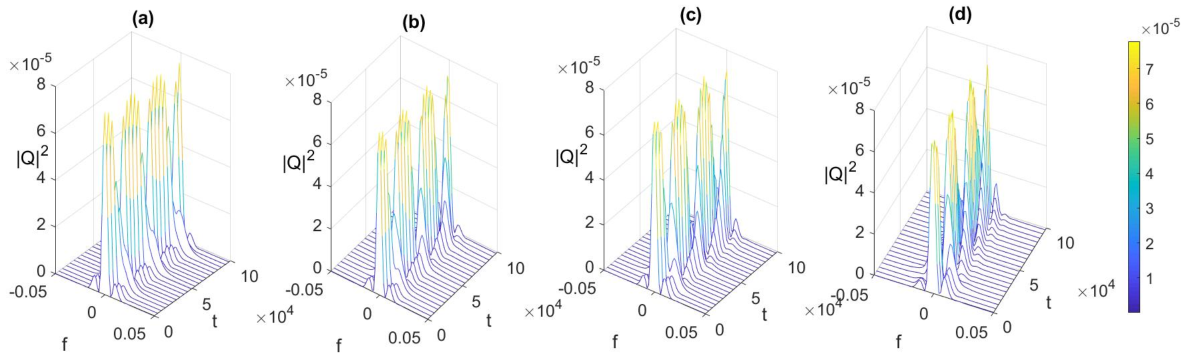

Figure 3.9: Spatial power spectra corresponding to fig 3.8.

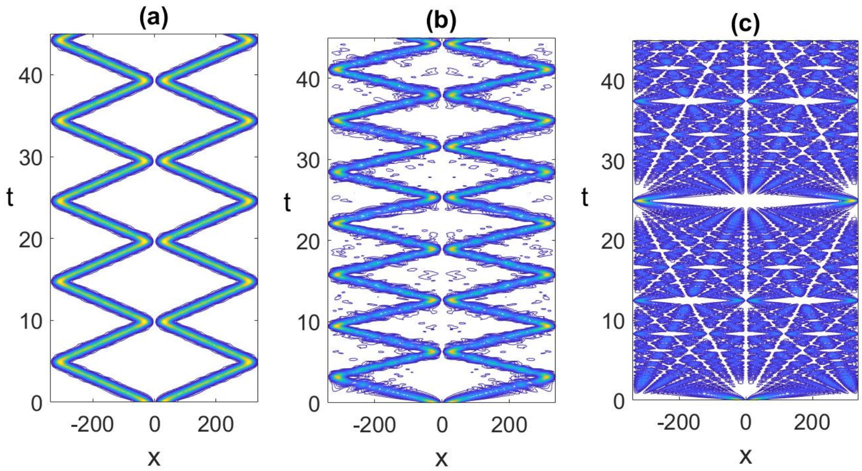

Figure 3.10: Interaction of two DSs at a phase difference of π, for initial separations equal to (a) 30, (b) 20 and (c) 10.

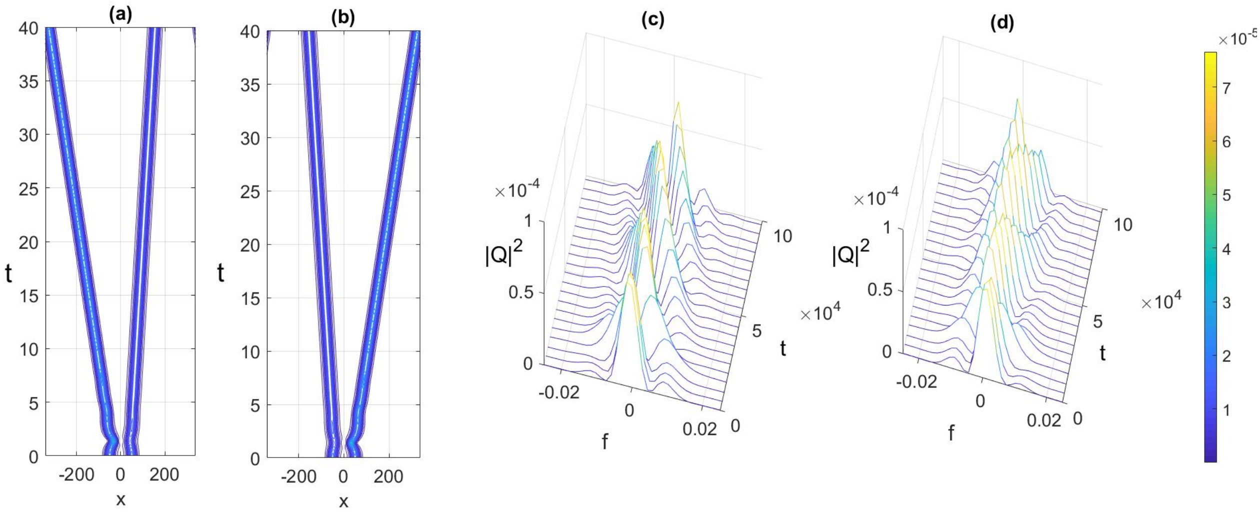

Figure 3.11: Interaction dynamics of two DSs for phase difference $\Delta\phi$ between them: (a) $\Delta\phi = 0.2\pi$ and (b) $\Delta\phi = 1.8\pi$ (or -0.2π). The corresponding spatial power spectra are plotted in (c) and (d).

In fact, such mirror image-like interaction dynamics are found for a large range of phase differences (Figure 3.12 and 3.13). For such interaction, the deviation (δx) of the two DSs from the centre point is plotted with respect to the phase difference in Figure 3.14. This shows that both the DSs have symmetrical behaviour.

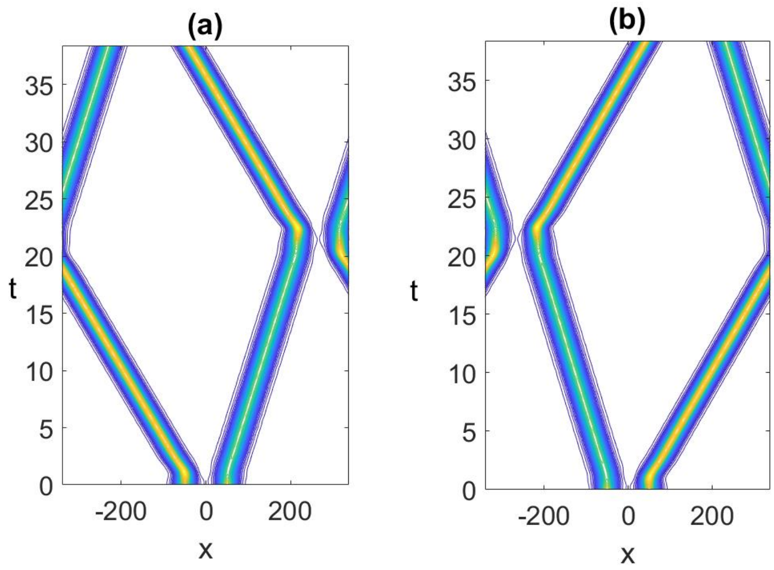

Figure 3.12: Interaction dynamics of two DSs at initial phase difference $\Delta\phi$ between two DSs: (a) $\Delta\phi$=0.5π and (b) $\Delta\phi$=1.5π or (-0.5π).

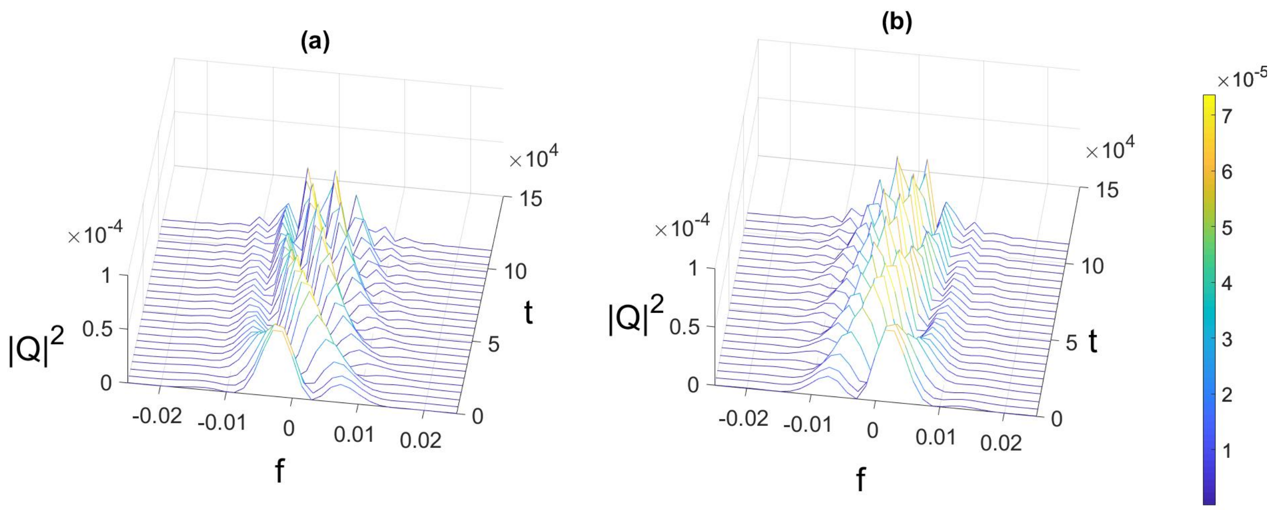

Figure 3.13: The spatial power spectra corresponding to Figure 3.12.

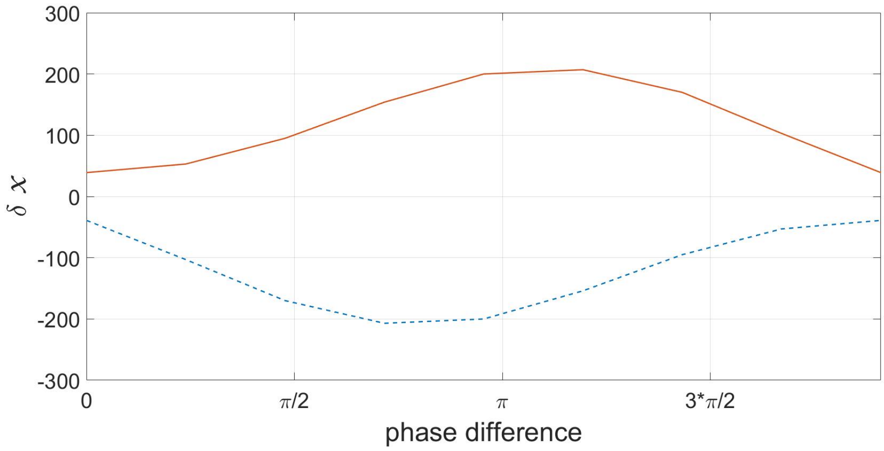

Figure 3.14: Phase induced deviation δx of two DSs, from the central point. The solid line (red) represents the right-hand side DS while the dashed one (blue) represents the left-hand side DS

We now study the interaction of two DSs of unequal intensities. The interaction center of DS shifts towards the higher amplitude DS (Figure 3.25). The corresponding spatial power spectra are given as Figure 3.26. For second-order DS, the number of interactions is found to increase with decreasing separation between DSs (Figure 3.27). However, the second-order interactions are found to be less stable.

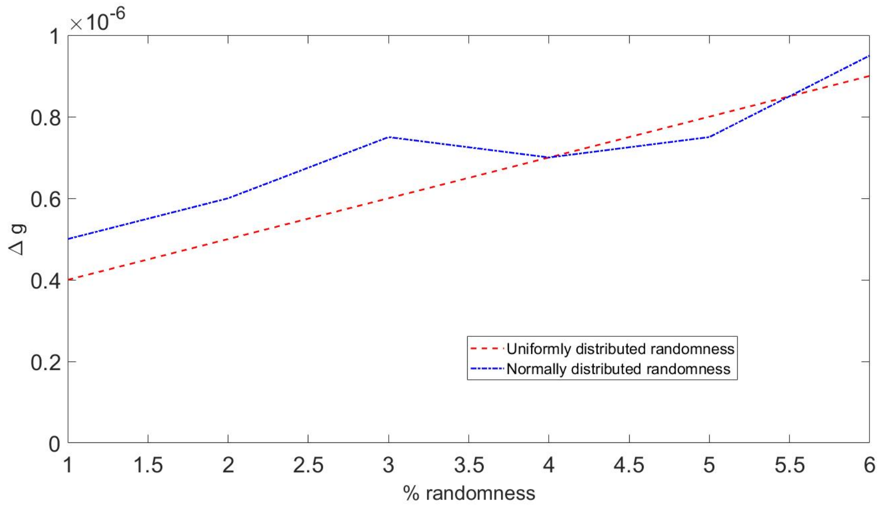

Figure 3.15: Variation of linear gain Δg required for soliton formation with the increase in randomness in self-diffraction induced broadening. Solid line is for *normally distributed* randomness, while the dashed line corresponds to the *uniformly distributed* randomness.

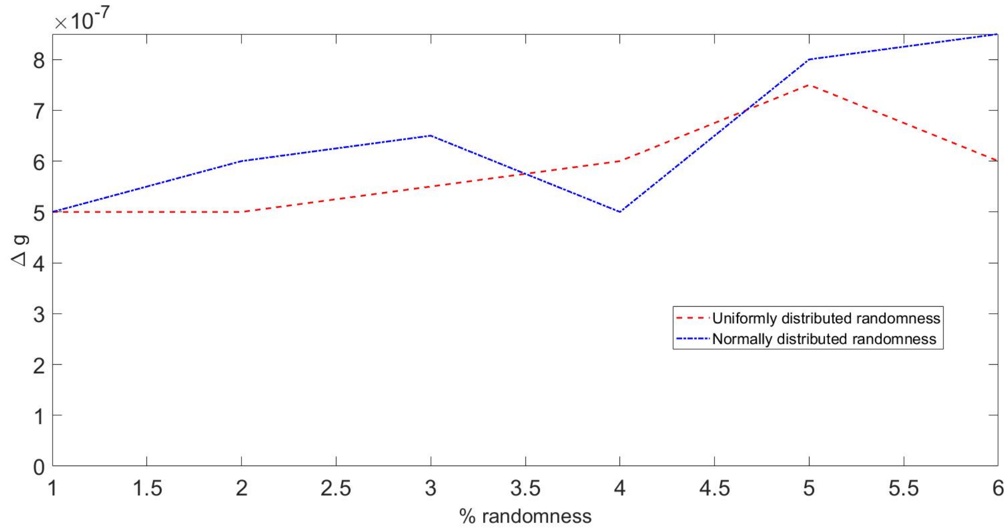

Figure 3.16: Variation of linear gain Δg required for soliton formation with the increase in randomness in self-diffraction induced broadening and diffusion terms. The solid line is for *normally distributed* randomness, while the dashed line corresponds to the *uniformly distributed* randomness.

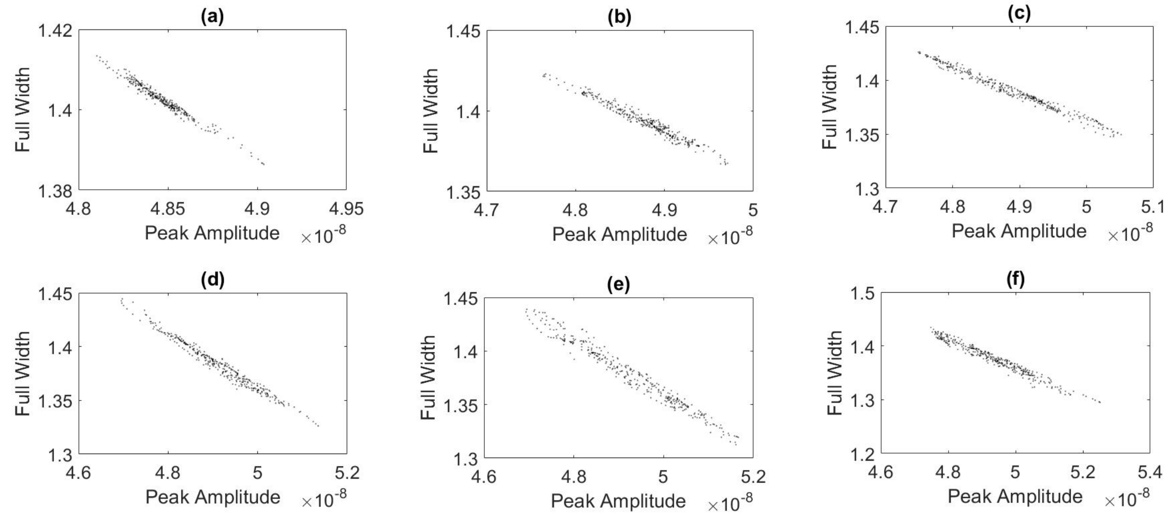

Figure 3.17: Phase plots for different percentages of *uniformly distributed* randomness in self-diffraction induced broadening (corresponding to Figure 3.15) (a) 1%, (b) 2%, (c) 3%, (d) 4%, (e) 5% and (f) 6%.

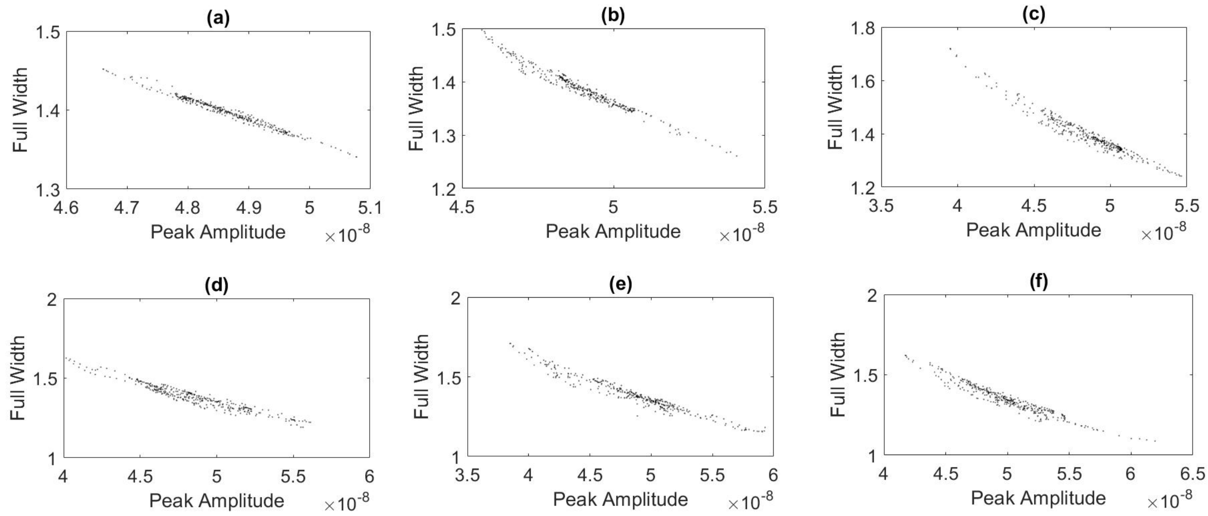

Figure 3.18: Phase plots for different percentages of *normally distributed* randomness in self-diffraction induced broadening (corresponding to Figure 3.15) (a) 1%, (b) 2%, (c) 3%, (d) 4%, (e) 5% and (f) 6%.

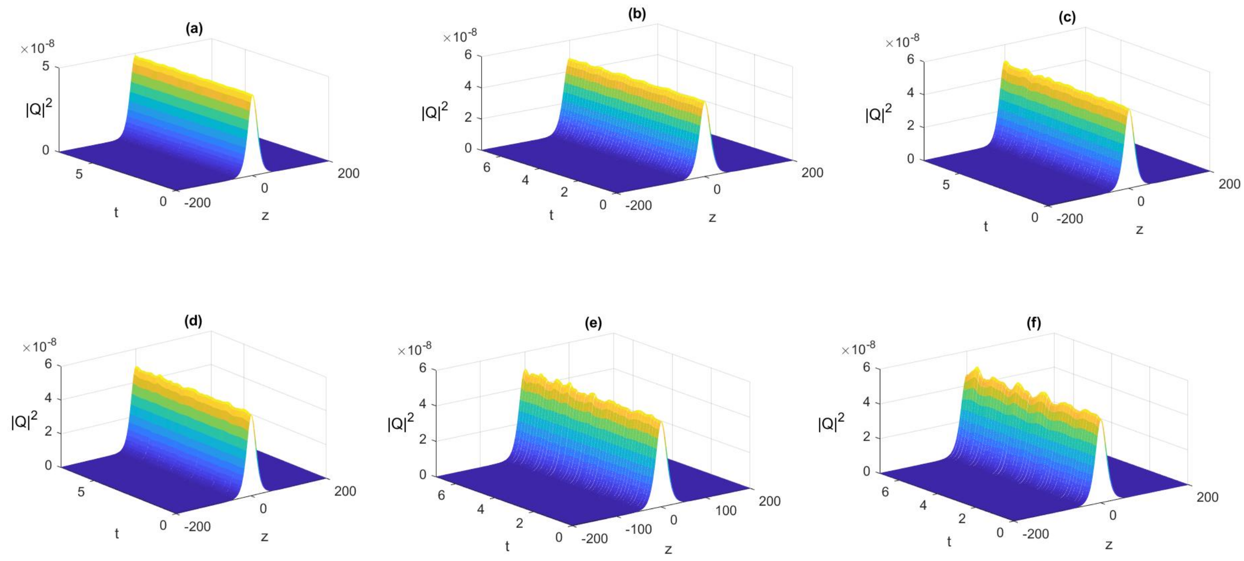

Figure 3.19: Soliton profiles in the presence of different amounts of *uniformly distributed* randomness self-diffraction. The values of randomness in self-diffraction are (a) 1%, (b) 2% ,(c) 3% ,(d) 4% (e) 5% and (f) 6%. Required gains are 0.040×10^{-3}, 0.050×10^{-3}, 0.060×10^{-3}, 0.070×10^{-3}, 0.080×10^{-3} and 0.090×10^{-3} respectively.

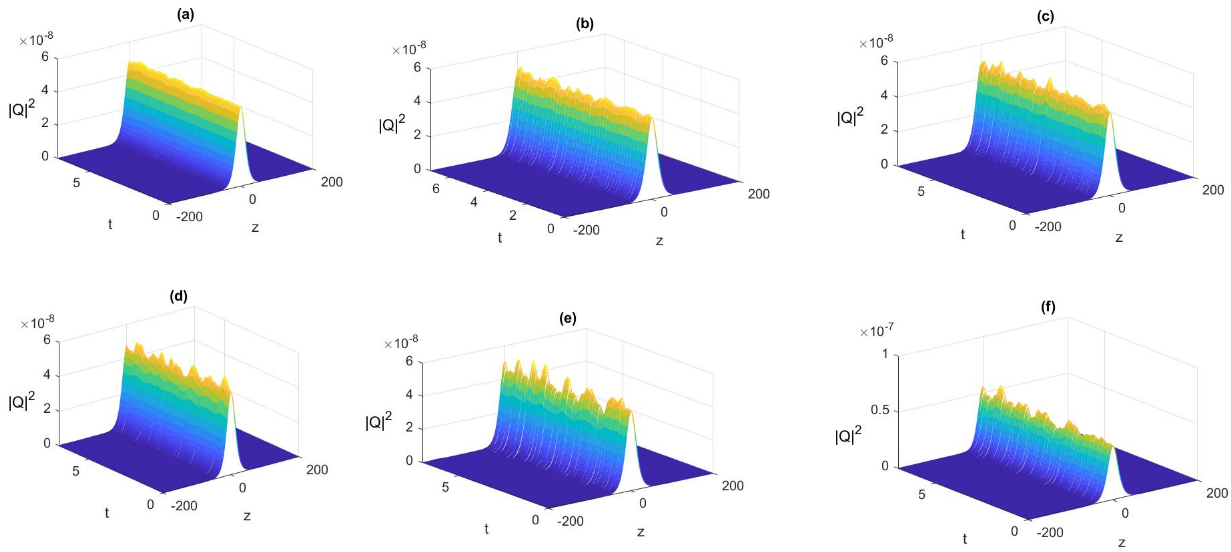

Figure 3.20: Soliton profiles in the presence of different amounts of *normally distributed* randomness in self-diffraction induced broadening compensated by linear gain. (a) 1%, (b) 2% ,(c) 3% ,(d) 4% (e) 5% and (f) 6%. Required gains are 0.050×10^{-3}, 0.060×10^{-3}, 0.075×10^{-3}, 0.070×10^{-3}, 0.075×10^{-3} and 0.095×10^{-3} respectively.

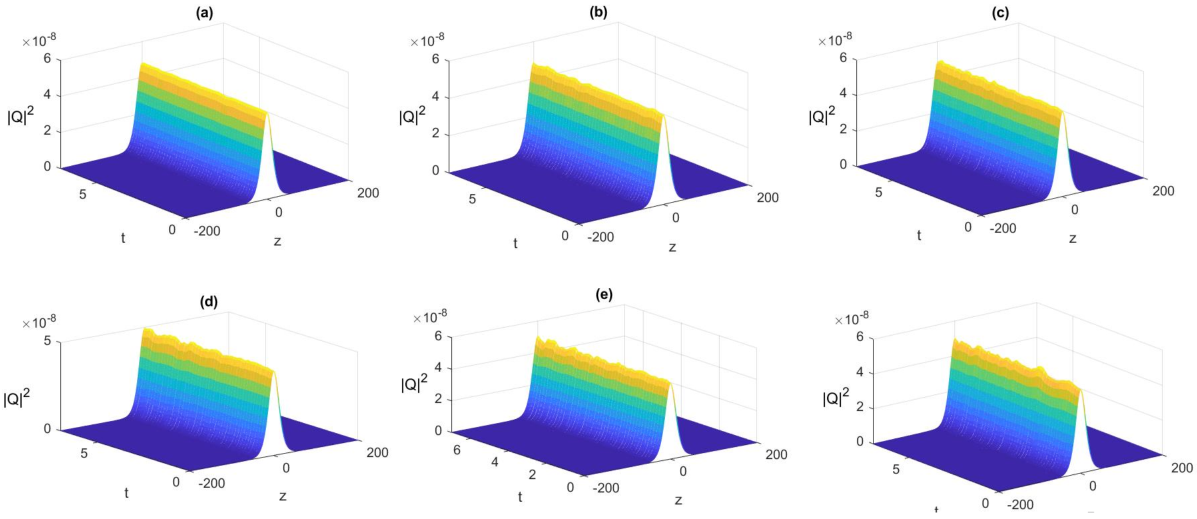

Figure 3.21: Soliton profiles in the presence of different amounts of *uniformly distributed* randomness in self-diffraction induced broadening and diffusion compensated by linear gain. (a) 1%, (b) 2% ,(c) 3% ,(d) 4% (e) 5% and (f) 6%. Required gains are 0.050×10^{-3}, 0.050×10^{-3}, 0.055×10^{-3}, 0.060×10^{-3}, 0.075×10^{-3} and 0.060×10^{-3} respectively.

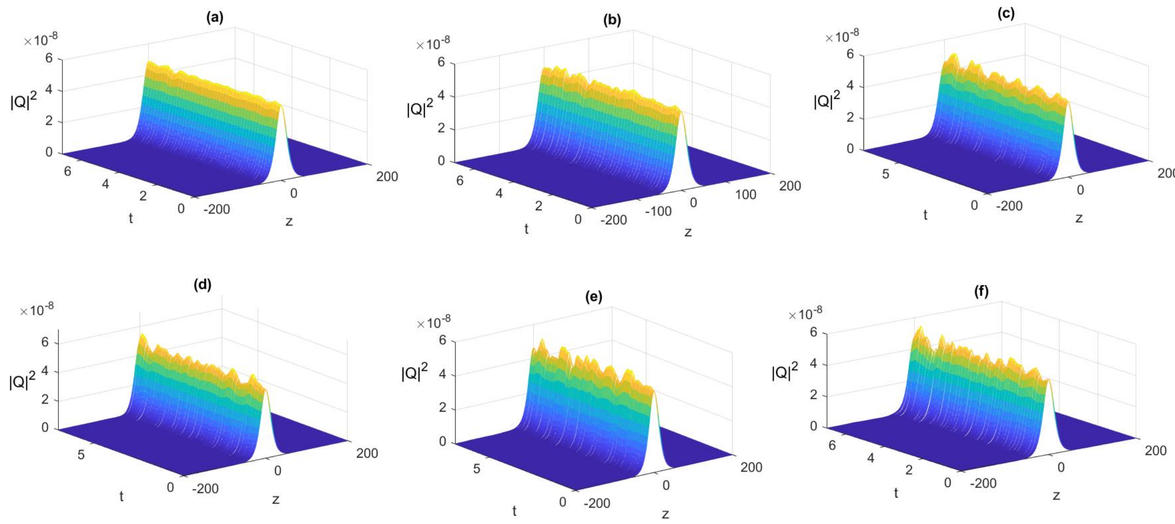

Figure 3.22: Soliton profiles in the presence of different amounts of *normally distributed* randomness in self-diffraction induced broadening and diffusion compensated by linear gain. (a) 1%, (b) 2% ,(c) 3% ,(d) 4% (e) 5% and (f) 6%. Required gains are 0.050×10^{-3}, 0.060×10^{-3}, 0.065×10^{-3}, 0.050×10^{-3}, 0.080×10^{-3} and 0.085×10^{-3} respectively.

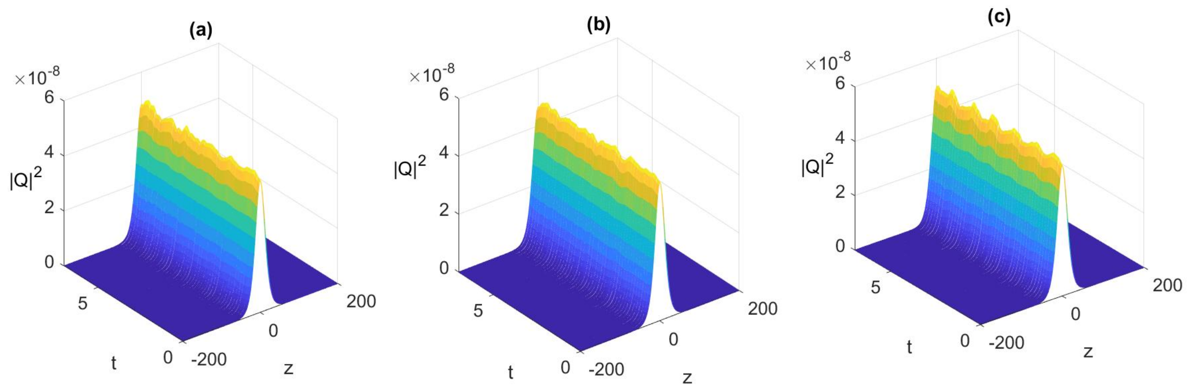

Figure 3.23: Soliton profiles in presence of 3% *uniformly distributed* randomness. (a) for TPA+3PA, (b) only TPA and (c) only 3PA.

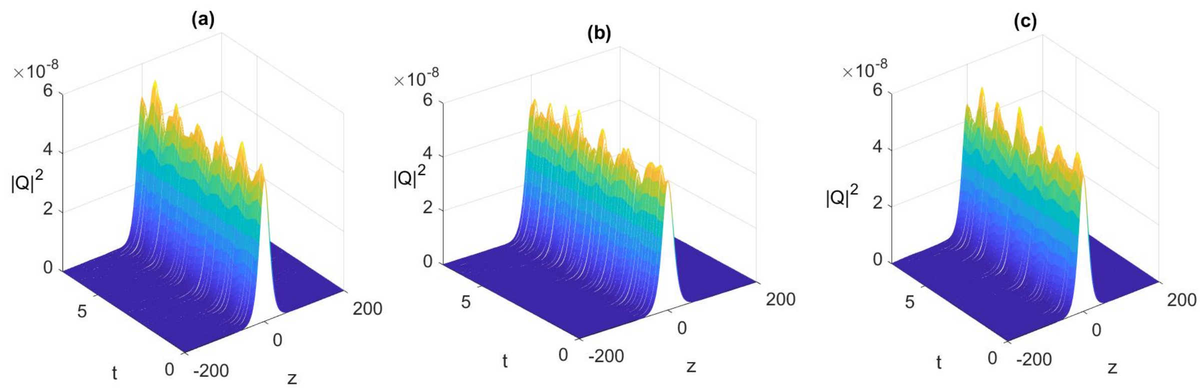

Figure 3.24: Soliton profiles in presence of 3% *normally distributed* randomness. (a) for TPA+3PA, (b) only TPA and (c) only 3PA.

3.4 Robustness of the DS

Till now, we have discussed DSs formation in perfect SRR-based metamaterials. However, a practical system suffers from irregularities in the spacing of SRR, different sizes of SRR or other irregularities in the composite media [263]. These may lead to randomness in the diffraction-induced broadening (i.e., in the second terms in the *left* hand side of equations 1 & 2) and diffusion (i.e., in the second terms in the *right* hand side of equations 1 & 2). These DSs are found to be robust enough to sustain such randomness. With increasing random diffraction, a higher gain is required to stabilize the DSs. However, the random diffraction has little effect on the *time the for first* interaction of DSs. Two types of randomness can be there: *uniformly distributed* randomness and *normally distributed* randomness. We find that a higher Δg is required at higher randomness of self-diffraction for both the types of aforesaid randomness (Figure 3.15). Similar behaviour is observed for randomness in both self-diffraction and diffusion (Figure 3.16). The phase plot of DSs at different percentages of *uniformly distributed* randomness in self-diffraction is given in Figure 3.17. Up to a certain limit of randomness, the DSs remain confined. Similar confinement is achieved for randomness in both self-diffraction and diffusion (Figure 3.18). Soliton profiles become stable or almost stable for both types of randomness in self-diffraction and diffusion (Figures 3.19-3.22) provided that a proper Δg is given into the system. In addition to self-diffraction and diffusion, randomness may appear in TPA, 3PA or both. We found stable DSs with all these cases (Figures 3.23 & 3.24).

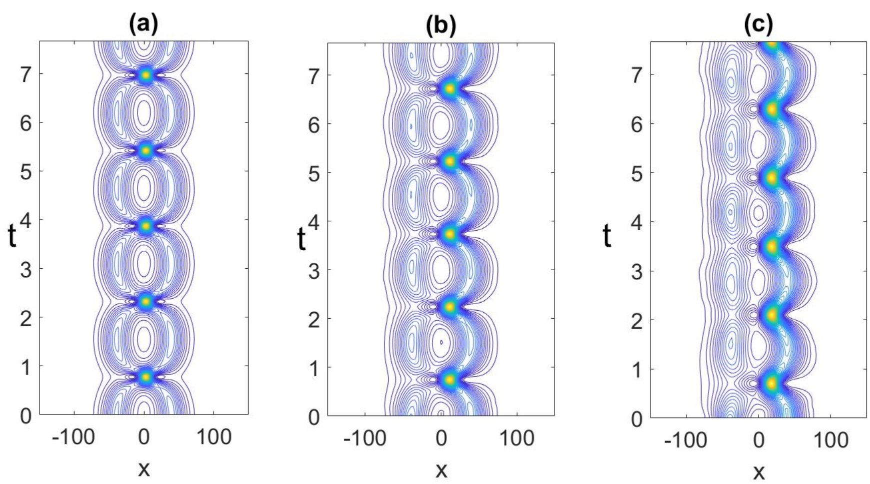

Figure 3.25: Interaction dynamics of two DSs of different amplitudes. The amplitude ratio is (a) 0.99, (b) 0.95 and (c) 0.90.

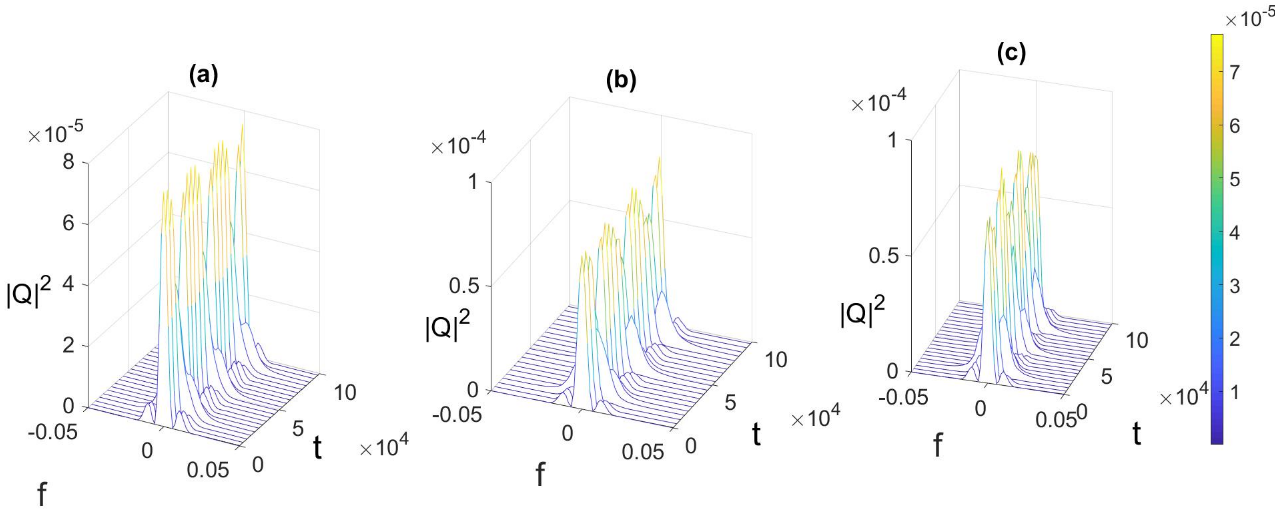

Figure 3.26: The spatial power spectra corresponding to Figure 3.25.

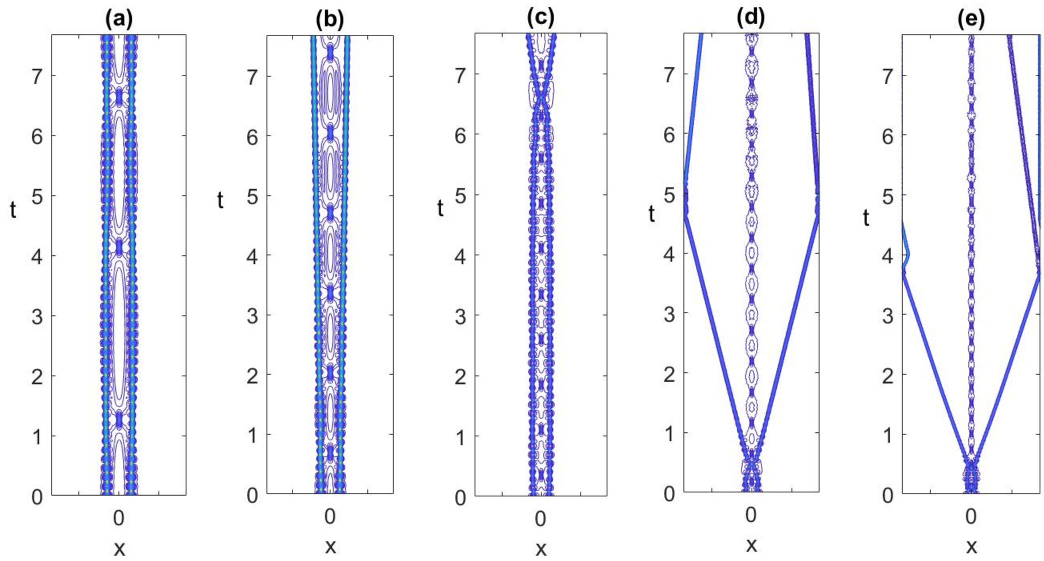

Figure 3.27: Interaction of second order DSs at initial separations equal to (a) 60, (b) 50, (c) 40, (d) 30 and (e) 20. Other parameters are the same as mentioned in Figure 3.1.

3.5 Conclusion

Compound DSs are generated and stabilized in the SRR-based metamaterial with cubic-quintic nonlinearity, multi-photon absorption and diffusion. The findings of this investigation validate the two basic aspects of any soliton, firstly, the evolution of self-similar wave profile and secondly, the "immunity" against interaction. The interaction of DSs can be controlled by tuning their separation and relative phase. A smaller separation between the DSs and the increase in self-diffraction may lead to early interaction. The introduction of a phase difference or variation in the amplitude of any of the DS may break the symmetry of interaction. Switching can be obtained by tuning the phase difference between the DSs. Interestingly, a weak DS is found to control a strong one. The result obtained in this study is somewhat familiar in optics but may be lesser known in SRR-based metamaterial. The findings can be used to design metamaterial-based devices that rely on higher-order nonlinearity and multiphoton absorption. It may also help in identifying and optimizing the operating region of metamaterial-based devices. To validate the results, an experimental setup can be designed using an SRR-based nonlinear metamaterial, an EM signal source and a suitable detector. The source and the detector can be chosen as per the application. For instance, to generate a DS in optical wavelength, laser light can be used in conjugation with a polarizer. A spectrometer or a CCD camera corresponding to the operating wavelength can be employed as a detector. The numerical procedures used in this investigation can be utilized for calibrating such devices. Since this model includes diffusion, one can further plan to use it for sensing and related purposes in chemical mixing, thermal management, electronics, material processing, etc., wherein diffusion has a critical role. Also, the inclusion of multi-photon absorption in the model makes it a potential candidate for the application of TPA-assisted medical imaging.

More investigations can be done in future by combining nonlinearity with metamaterials, e.g., to identify the role of various saturable absorbers. Graphene saturable absorber and graphene flakes saturable absorber on the compound soliton generation and dynamics can be considered in that context. In fact, the investigation presented in the next chapter utilizes the Graphene saturable absorber. Intriguing soliton dynamics, like soliton switching and multistability behaviour, can be demonstrated using the present model. Even there are possibilities to utilize the current model and method further to investigate rogue waves in nonlinear metamaterials with higher-order nonlinearity.

Chapter 4

Generation and Stabilization of Solitons in Graphene-embedded Metamaterials

If generating solitons in metamaterials is the primary goal, then achieving their stability is the ultimate challenge. Propagation of localized EM waves, more precisely solitons, generally encounters difficulties due to challenges like strong dispersion from resonant responses and high losses. Addressing these issues, this chapter discusses a strategy to transform propagating EM waves into stable soliton waves capable of sustaining dispersion and mitigating losses. The approach is demonstrated theoretically using a two-dimensional hybrid metamaterial featuring SRR arrays on a graphene layer. A specific parametric range is identified, enabling the propagation of EM waves in the form of dissipative solitons. This methodology can be applied to diverse metamaterials and metasurfaces, which are represented by coupled rate equations. This chapter corresponds to the first and majorly the third objectives of the thesis.

4.1 Introduction

The investigation into the transmission of EM waves through 2D materials remains a significant and expansive research area over an extended period, owing to its diverse range of applications. In this context, there has been significant research focus on the utilization of SRR-based metamaterials, along with single and multi-layer graphene, which have garnered substantial attention and demonstrated notable technological applications [264–269]. SRR responds to the incident EM field by virtue of their configurable physical dimensions, therefore making the response tunable. A major challenge for EM wave propagation through a metamaterial is the dispersion due to resonance and high loss [270]. This can be overcome by converting an EM wave into a soliton, in particular, a dissipative soliton (DS) (since the loss is present in the system). The inclusion of nonlinearity makes SRR a promising host for the solitons [271]. In a dissipative system, the counterbalance between the inherent broadening (self-diffraction in the spatial domain and group velocity dispersion in the temporal domain) and nonlinearity-induced contraction (self-focusing in the spatial domain and self-phase modulation in the temporal domain) is not sufficient for self-trapping; rather an additional balance between the system loss and an external gain is essential for the stabilization of the soliton [272]. Since generated in a lossy or dissipative system, these solitons are termed DS and require a continuous supply of external energy to sustain [273, 274]. They are formed at a position 'far from equilibrium' [275, 276]. Both the dark and bright solitons are found in SRR-based metamaterial using coupled Schrödinger equations [264, 277]. One- and two-dimensional transmission of EM waves are studied through a finite slab of a dielectric material with negative refraction. When the dielectric slab exhibits an intensity-dependent nonlinear response, the study reveals the transmission of waves influenced by nonlinearity through an otherwise opaque slab, concurrently leading to the generation of spatiotemporal solitons [265]. Although not precisely solitons, electric and magnetic excitations arise from resonances in both electric and magnetic fields, specifically occurring at odd multiples of half-wavelengths. [278]. A one-dimensional array of SRR was found to host the discrete breather structures due to weak coupling with the nearest SRR [266]. In the context of discreteness and nonlinearity, it was observed that a one-dimensional array of SRR can facilitate the existence of gap solitons [279]. Bright soliton can be generated due to nonlinearity and capacitance fluctuations [280].

Graphene is a 2D material that has shocked the spotlight since its experimental fabrication in 2004 [281]. Owing to the nano-size layer and large nonlinearity, graphene comes in handy in many photonics, nano-electronic and nonlinear optical devices [282, 283]. The materials that have thickness-dependent optical properties can be combined with graphene that finds applications in biomedical [284, 285], solid-state [286], electronics [287] and optics [288]. Graphene can be used as a saturable absorber in erbium-doped laser to generate multiple soliton patterns [267]. Due to the wide band saturable absorption of graphene, one can make the DS of erbium-doped laser tunable [268]. When layers of graphene are sandwiched between two layers of a dielectric material, the propagation of discrete plasmons is found [269]. Surface plasmon in one-dimensional domain walls is found in layer-stacking domain walls in bilayer graphene using near-field infrared nanoscopy [289]. Arrays of nanodisks of graphene support the propagation of discrete vector soliton [290]. Graphene monolayers are found to support the propagation of spatial optical soliton by virtue of its nonlinear third-order susceptibility [291]. In recent times, an effort to combine these two major players (i.e., SRR and graphene) to fabricate a hybrid 2D structure is witnessed partly because of the common tendency to insert graphene in all possible structures and chiefly because of the versatile nature of graphene [292–294].

Although soliton dynamics have been studied in different 2D materials separately, significant efforts have been noticed with the recently famous hybrid 2D material that comprises graphene-embedded SRR. In this chapter, we present soliton formation in a graphene-embedded SRR-based metamaterial through an easy analytical-numerical method. Basically, the dynamical equations of the system are set for a steady state condition to get the stability of the system. To demonstrate this, we use a hybrid material as modelled in the reference [295]. This method is too basic to identify the parametric zone for soliton formation in a variety of surfaces and even beyond. In fact, it can be successfully adopted where ever the coupled rate equations are involved.

The system of the current investigation consists of an infinite array of SRR [295] on a suitable substrate. A layer of graphene is placed beneath the SRR arrays (Figure. 4.1(a)) to increase the nonlinearity of the system (considering up to the third-order susceptibility of graphene) [296–298]. The nonlinear response of graphene is enhanced when combined with plasmon, due to the enhancement of the local density of states near metal-dielectric interface [299, 300]. The conductivity of graphene can be tuned by changing the electric field, which further changes the work function of the graphene [301, 302]. This gives the liberty to tune the spectrum of resonance for metamaterial. The electronic structure of multilayer graphene is similar to the isolated single layer graphene [303]. The reflectance of multi-layer graphene falls rapidly due to the direct interband electron transitions [304]. The plasmon propagation occurs in multi-layer graphene due to domain walls [289]. The carrier mobility is greater in monolayer than multi-layer graphene due to the dispersion relation [305]. In the present model we used a monolayer graphene. However one can use multilayer graphene to reduce the cost.

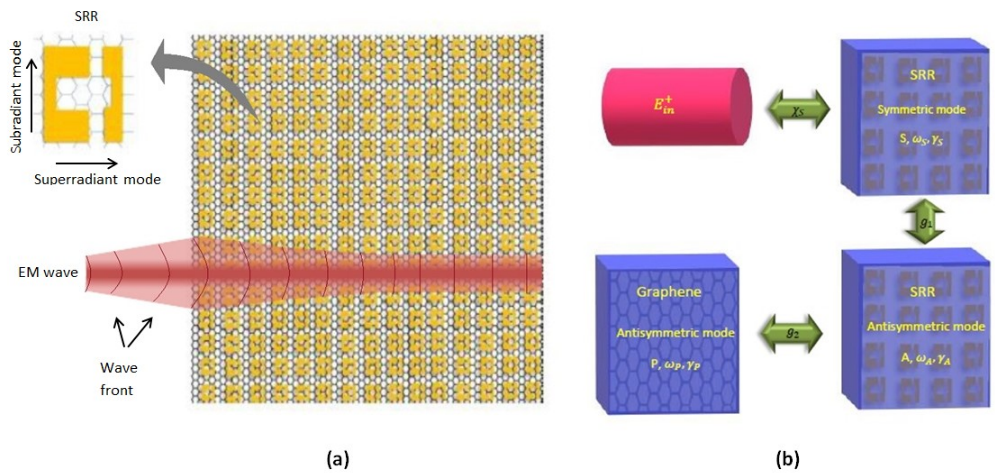

Figure 4.1: (a)Schematic diagram of the graphene embedded SRR based hybrid metamaterial (b) A schematic of interactions of different modes of SRR and graphene. (E_{in}^{+} is amplitude of incoming wave.)

The SRR has two propagating modes along the two arms and these modes arise due to the in-phase and out-of-phase current distribution along the arms (Figure 4.1(a)). One mode is strongly coupled with the incoming field and is reffered as a symmetric mode. This is the superradiant mode. The other is an asymmetric mode referred as subradiant mode [306]. When both modes are coupled together a Fano like asymmetric spectra occurs. The Fano resonance is an asymmetric resonance that arises from two narrow resonances from two different resonators of the system [295, 307, 308]. The graphene layer also holds an asymmetric mode (subradiant modes) that arises due to the out-of-phase dipole oscillation [309–311]. The modes of the graphene and SRR can be presented using complex amplitudes S, A and P, where S is bright symmetric mode due to SRR, A dark asymmetric mode due to SRR and P is dark asymmetric mode due to graphene. The system of equations can be generated starting from each mode as an independent resonator with frequencies ω_S, ω_A and ω_P, radiative decay coefficients γ_S, γ_A and γ_S for S, A and P modes respectively as follows [312]:

$$\dot{S} = (-i\omega_S - \gamma_S)S \tag{4.1}$$

$$\dot{A} = (-i\omega_A - \gamma_A)A \tag{4.2}$$

$$\dot{P} = (-i\omega_P - \gamma_P)P \tag{4.3}$$

The dot represents the time evolution of the modes. The above mentioned rate equations 4.1, 4.2, 4.3 represent the modes of uncoupled SRR and graphene layer. In the present system the subradiant mode of graphene couples with the conventional subradiant mode of SRR metasurface [295] and leads to a strong confinement of light (Figure 4.1(b)). Such a system can be demonstrated using temporal coupled-mode theory [311, 313].A scheme for the coupling of the modes is shown in Figure 4.1(b). The S mode is coupled with incoming flux (E_{in}^+) and the coupling is quantified by interaction strength coefficient χ_S. Mode A and S are coupled with each other by a coupling coefficient g_1 and mode P with A by another coupling coefficient g_2. Thus the coupled modes are defined by the following differential equations [295]:

$$\dot{S} = (-i\omega_S - \gamma_S)S + ig_1A + i\chi_S E_{in}^+ \tag{4.4}$$

$$\dot{A} = (-i\omega_A - \gamma_A)A + ig_1S + ig_2P \tag{4.5}$$

$$\dot{P} = (-i\omega_P - \gamma_P)P + ig_2A \tag{4.6}$$

The system may have other losses. The linear losses have been included in imaginary part of the first term and the coupling coefficients in the RHS of eqn (4.4-4.6). The steady state of S, A, P (namely S_S, A_S, P_S respectively) can be determined as:

$$S_s = \frac{ig_1A_s + i\chi_S E_{in}^+}{i\omega_S + \gamma_S} \tag{4.7}$$

$$A_s = \frac{(i\omega_P + \gamma_P)ig_1\chi_S E_{in}^+}{(i\omega_S + \gamma_S)(i\omega_A + \gamma_A)(i\omega_P + \gamma_P) + g_1^2(i\omega_P + \gamma_P) + g_2^2(i\omega_S + \gamma_S)} \tag{4.8}$$

$$P_s = \frac{ig_2A_S}{i\omega_P + \gamma_P} \tag{4.9}$$

The variation of these steady-state values has been portrayed in Figures 4.2-4.10.

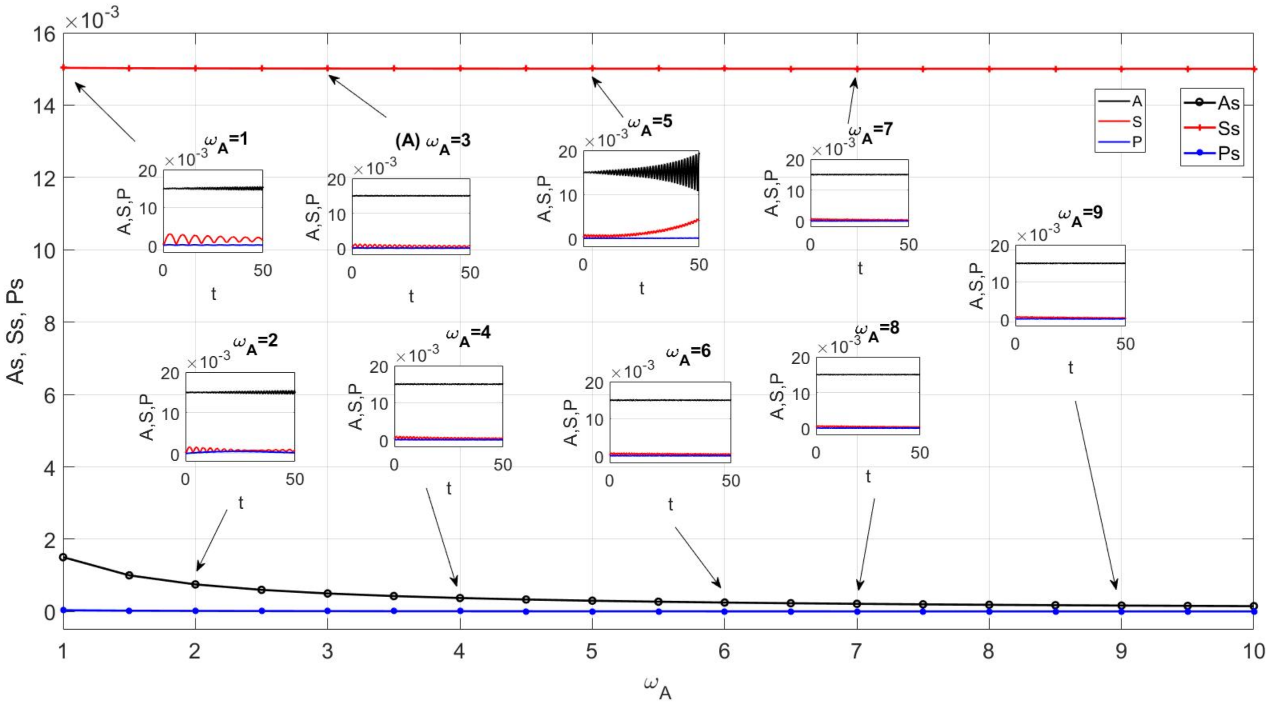

Figure 4.2: Variation of steady state values S_s, A_s, P_s with ω_A. Insets: Evolution dynamics of the S, A and P modes at different ω_A (indicated by arrows) and corresponding steady states (S_S, A_S and P_S). Inset A: This corresponds to the set of parameters and steady-state values commonly used throughout the manuscript.

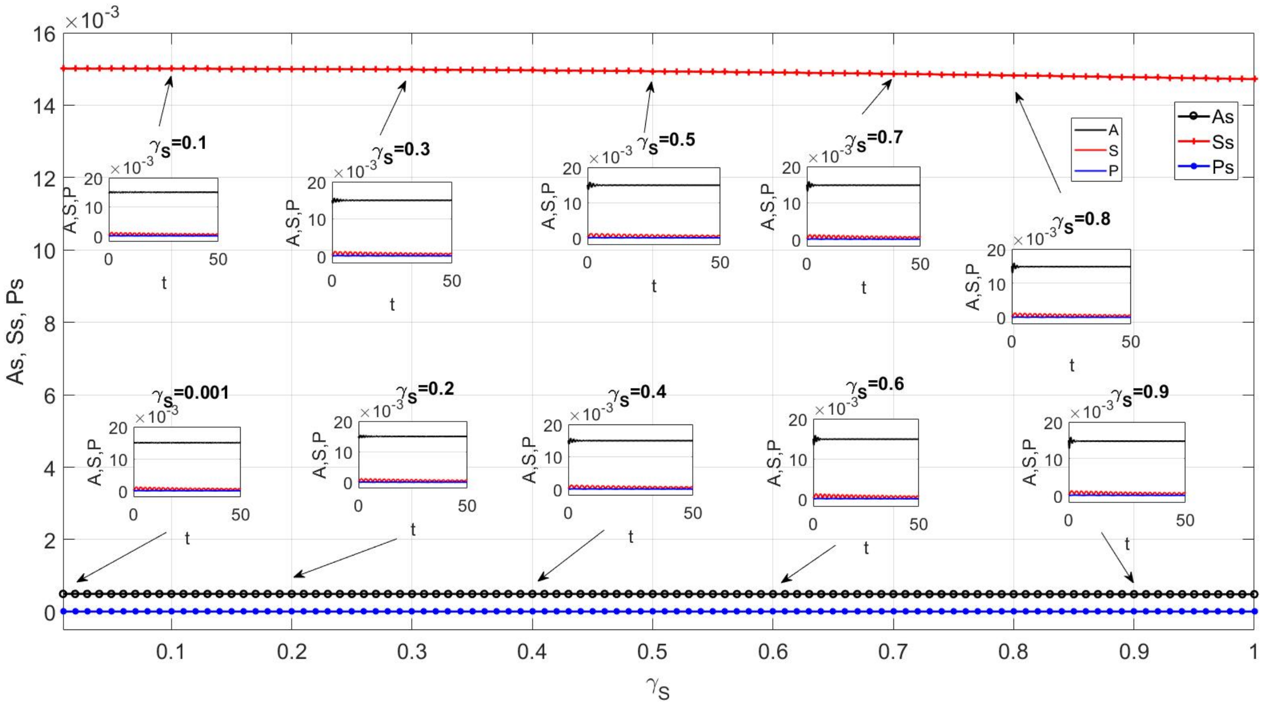

Figure 4.3: Variation of steady state values S_s, A_s, P_s with γ_S. Insets: Evolution of the S, A and P modes at different γ_S.

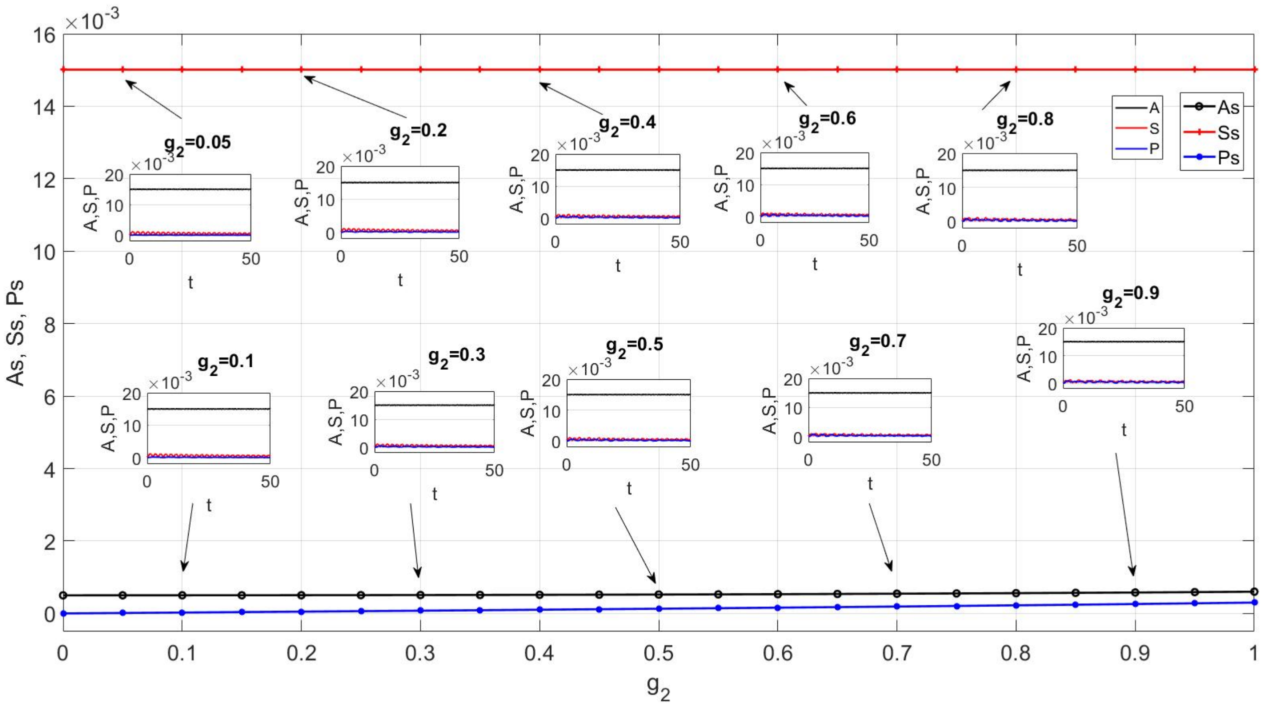

Figure 4.4: Variation of steady state values S_s, A_s, P_s with g_2. Insets: Evolution dynamics of the S, A and P modes at different g_2.

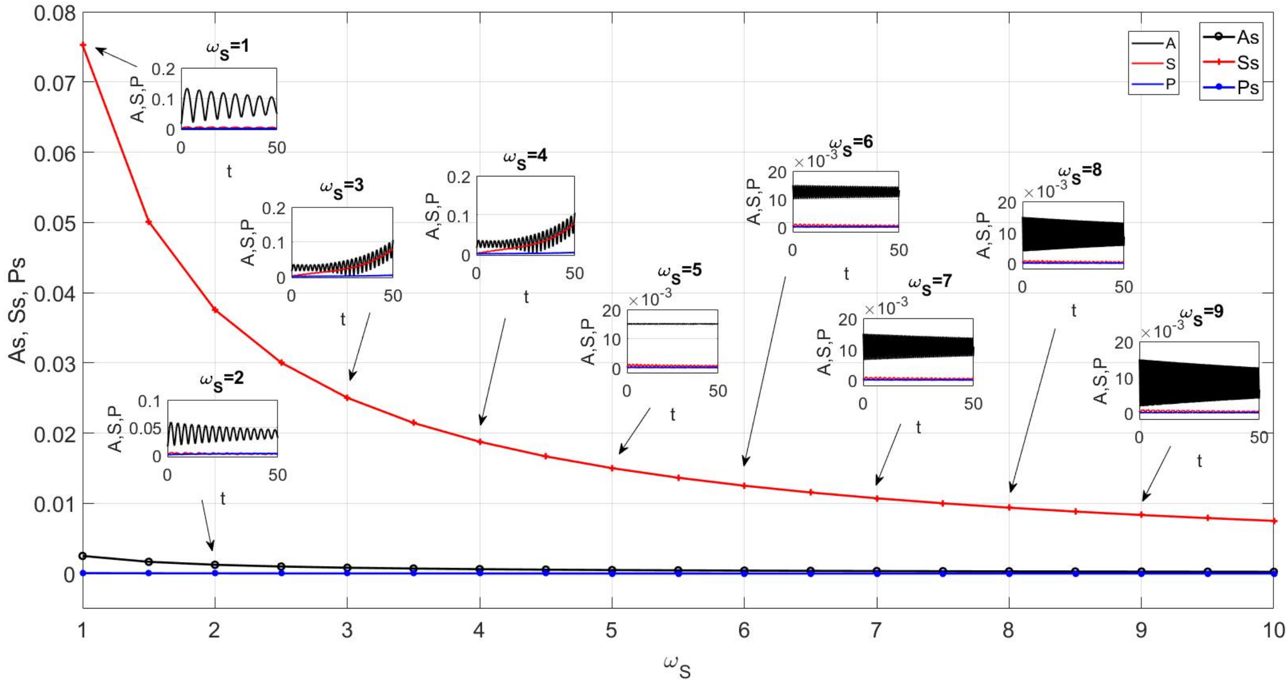

Figure 4.5: Variation of steady state values S_s, A_s, P_s with ω_S. Insets: Evolution dynamics of the S, A and P modes at different ω_S, (indicated by arrows) and corresponding S_S, A_S and P_S.

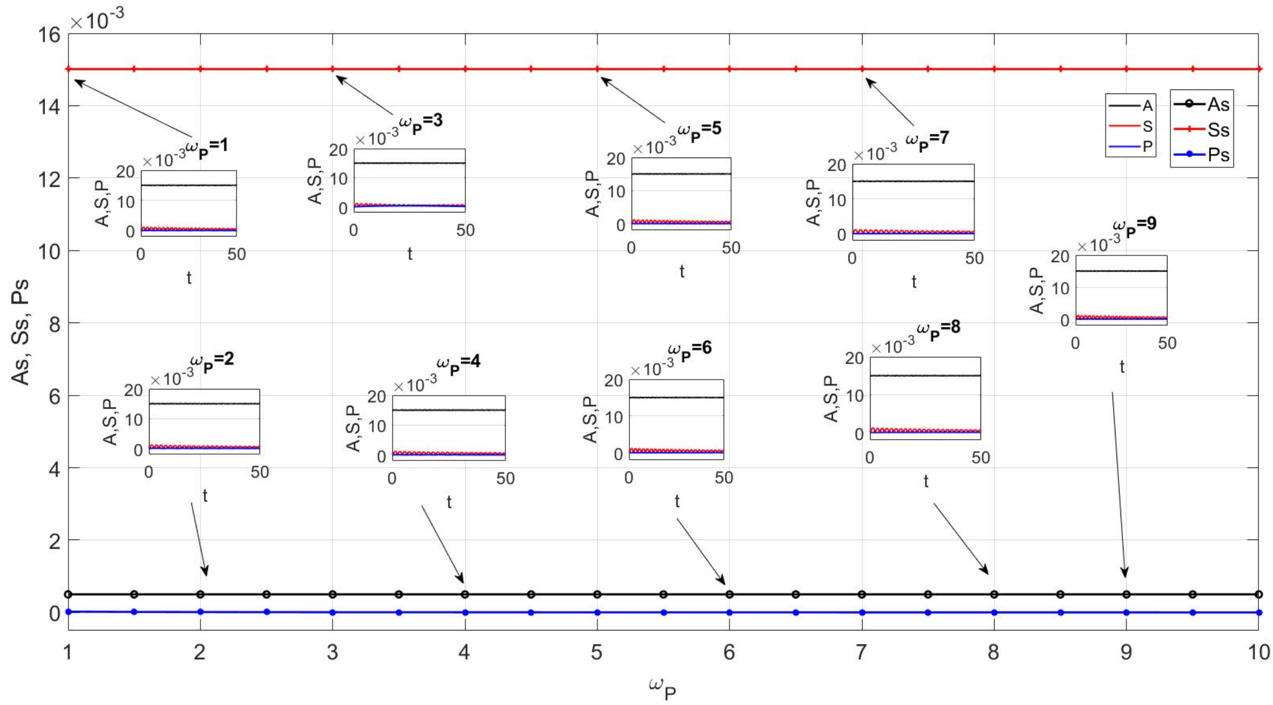

Figure 4.6: Same as Figure 4.5 but with respect to ω_P.

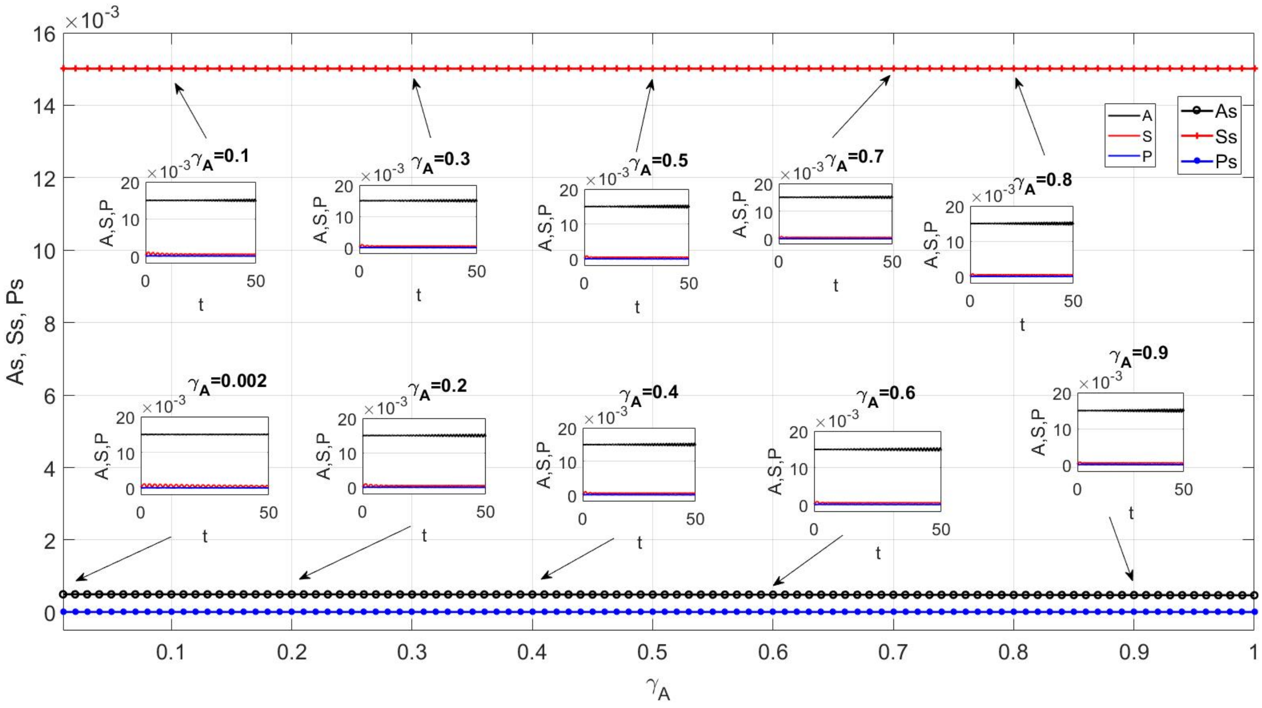

Figure 4.7: Same as Figure 4.3 but with respect to γ_A.

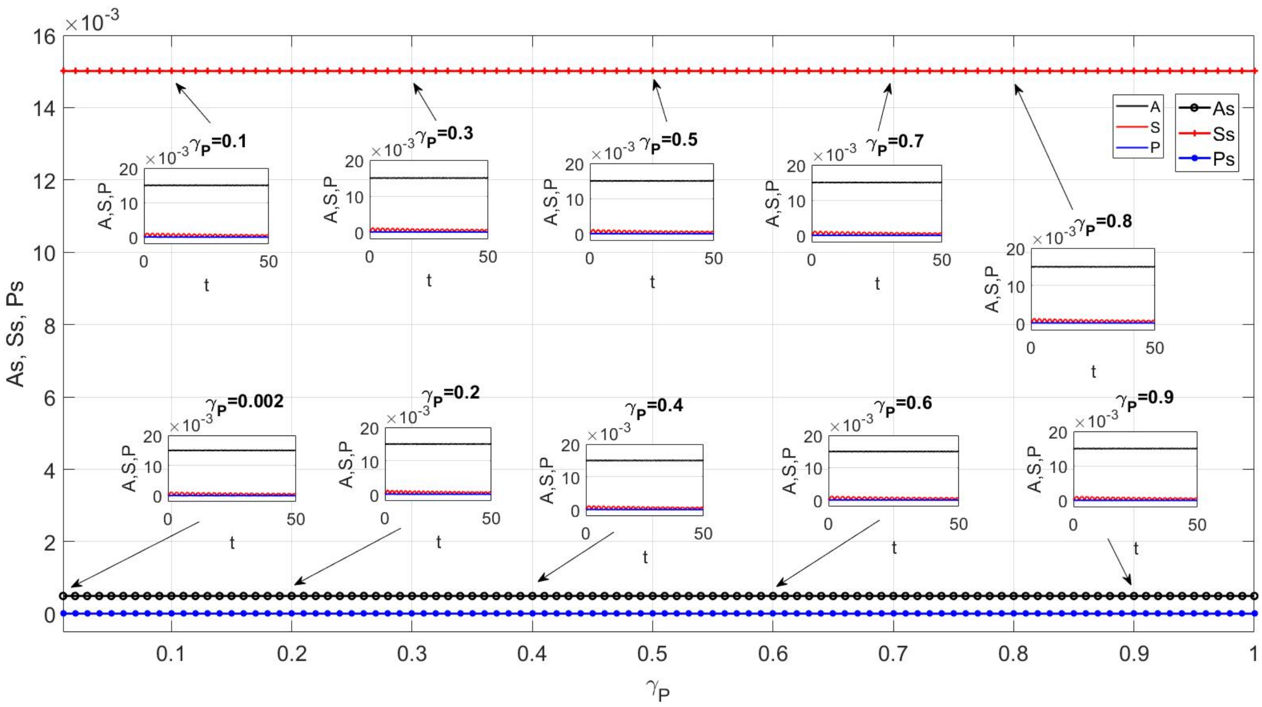

Figure 4.8: Same as Figure 4.3 but with respect to γ_P.

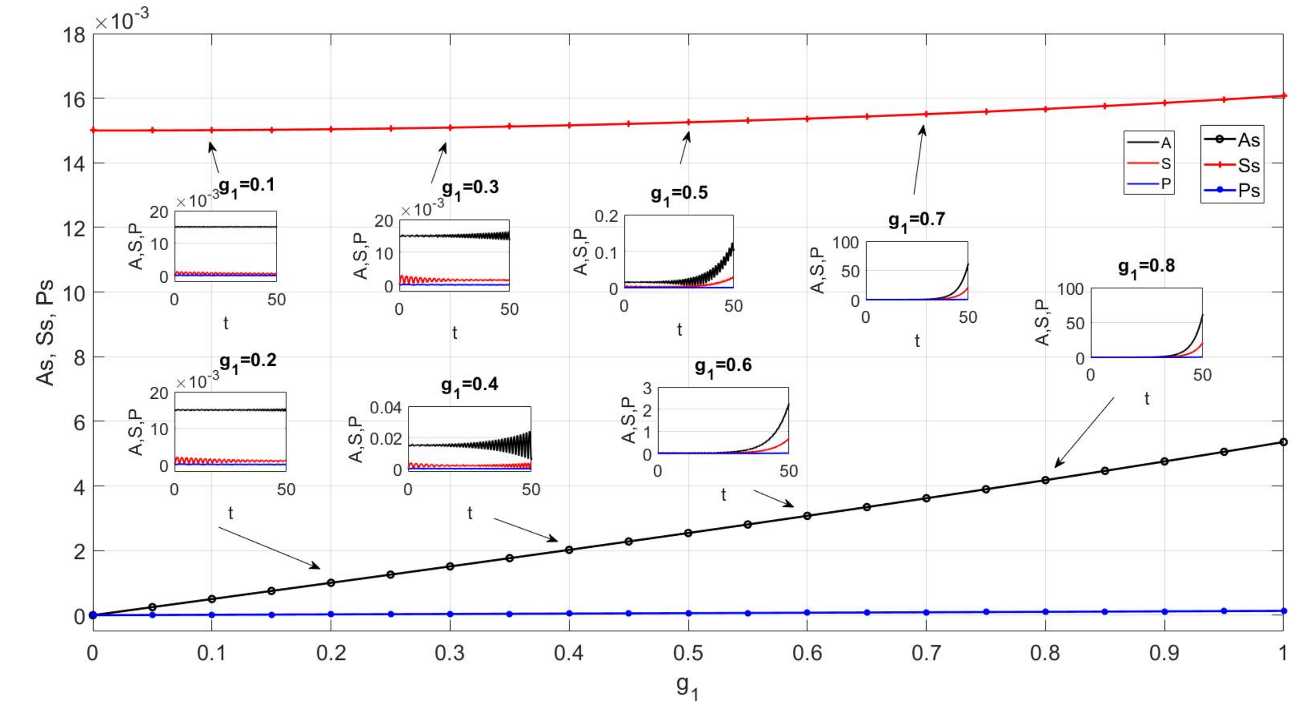

Figure 4.9: Variation of steady state values S_s, A_s, P_s with g_1. Insets: Evolution dynamics of the S, A and P modes at different g_1.

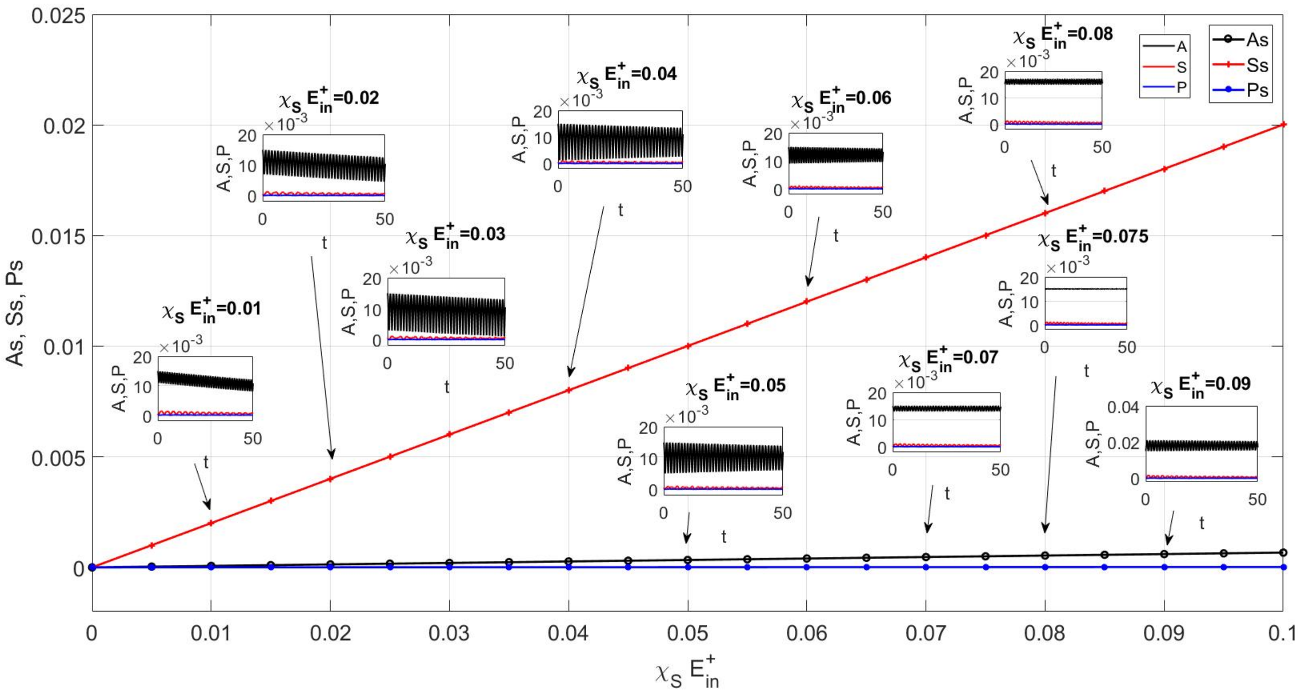

Figure 4.10: Variation of steady state values S_s, A_s, P_s with $\chi_S E_{in}^{+}$. Insets: Evolution dynamics of the S, A and P modes at different $\chi_S E_{in}^{+}$.

4.2 Steady Sate Solution and Solitons

We now explore the possibility of DS formation in the hybrid metamaterial system (equation 4.4-4.6) using the steady state values (S_S, A_S, P_S from eqn 4.7-4.9) as initial condition. Equation 4.4-4.6 has been solved numerically by Runge-Kuta 4-5 method. We found DS for a wide range of system parameters. The DS in the aforementioned system is influenced by the choice of frequencies (ω_S, ω_A, ω_P), radiative decay coefficients (γ_S, γ_A, γ_P), coupling coefficients (g_1, g_2) and coupled flux ($\chi_S E^+_{in}$). Each parameter is explored to identify the range of stable DS propagation. Following the analytical-numerical method described till now, the DS can be achieved for the number of sets of parameters. In this chapter we have used ω_S=5, $\omega_A = 3$, $\omega_P = 2$, $\gamma_S = 1 \times 10^{-2}$, $\gamma_A = 2 \times 10^{-2}$, $\gamma_P = 2 \times 10^{-2}$, $g_1 = 1 \times 10^{-1}$, $g_2 = 0.5 \times 10^{-1}$ and $\chi_S E^+_{in} = 0.75 \times 10^{-1}$ unless mention otherwise. The consolidated results have been presented in Figures (4.2-4.10). Figures (4.3-4.10) show the variations of steady-state values (S_S, A_S, P_S) with the variation of different system parameters and formation of DS at different parametric points. These figures, i.e., (4.2-4.10) have a common format. The variation of the steady state values A_S, S_S and P_S are shown in the main Figures. The insets show the evolution of the modes (S, A, P), which leads to DS in most of the cases. For example, Figure 4.2 shows the variation of S_S, A_S, P_S with respect to ω_A. Now, the insets show the evolution of A, S, P at different values of ω_A (indicated by the arrows). The other parameters are already mentioned above. At lower value of ω_A the numerical values of S_s, A_s, P_s are quite different (particularly S_S). For all values of ω_A except $\omega_A = 5$ we get solitonic evolution of S, A, P modes. Now, for a variation of ω_S the modes S and P has quite similar type of evolution for all values of ω_S, while mode A has large oscillations with increasing frequency along the range of ω_S except near ω_S=5 & 6 where all the modes shows a solitonic behaviour with smaller oscillations (Figure 4.5). For $\omega_S > 5$ the oscillations in mode A increase mode rapidly. For other values of ω_A (i.e., $\omega_A \neq 3$) the DS formation point changes. For the variation of ω_P the A_S, S_S and P_S varies symmetrically (Figure 4.6). The DS achieved for whole range of ω_P (from 1 to 10) with slight oscillation in S mode. Like the resonant frequency the radiative decay coefficient (γ_S, γ_A, γ_P) have great impact on the DS formation. The γ_S show the DS formation for wider range (Figure 4.3). As the value of γ_S increase the A mode has some initial oscillations and then got stabilized. Both γ_A and γ_P shows similar type of wave evolution and has DS for wide range (Figure 4.7 and 4.8). The A mode has slight growth of oscillations with increasing value of γ_A. Like the resonator frequencies and decay coefficients the coupling coefficient (g_1, g_2, χ) have important role in DS formation (Figures 4.4, 4.9, 4.10). For weaker coupling between A and S modes (i.e., lower values of g_1) soliton formation is favourable (Figure 4.9). But a stronger coupling (i.e., intermediate values of g_1) sees large oscillations of DS and further stronger coupling blows-up the DSs.

Quite different DS formation scenario has been witnessed for variation of coupling coefficient g_2 between P and A modes. Here DS are easily formed for stronger coupling strength (Figure 4.4), while large oscillations are witnessed in S larger coupling strength. Notably, DS formation is not favourable at larger values of g_2. We also analyse the mode propagation with $\chi_S E_{in}^+$ (i.e., the incoming flux coupled with S mode). The S_S varies linearly while A_S and P_S varies with little slope along with $\chi_S E_{in}^+$. The A and S modes has high oscillations along $\chi_S E_{in}^+$. Further, a stability analysis can be done by applying the Lyapunov stability analysis method in the system [314–316]. As per Hurwitz's stability criteria, the system is found to be stable as the real part of the eigenvalues of the characteristic equation (of the corresponding Jacobian matrix) is negative. The stability zones are marked for all three sets of γ and ω. (Figure 4.11).

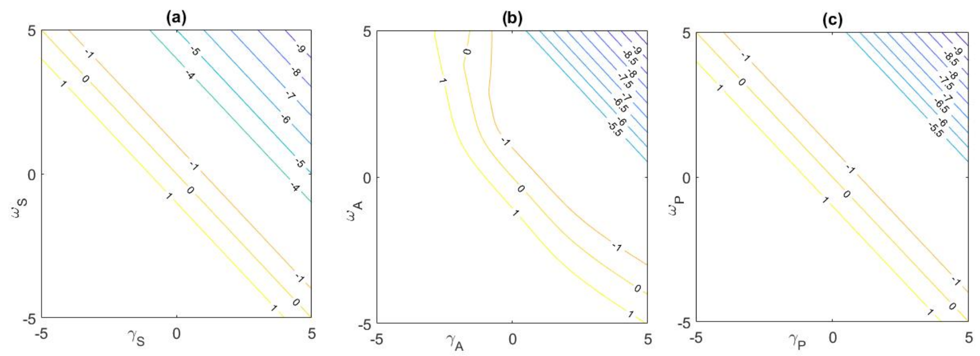

Figure 4.11: Contour plots of eigenvalues corresponding to (a) γ_S and ω_S, (b) γ_A and ω_A , (c) γ_P and ω_P. The system is stable in the negative side, i.e., the right hand side of the 0 line.

The dynamics of the three modes at steady state (that have been depicted in the insets of Figure 4.5-4.10) can be alternatively shown through phase diagram. Typical phase diagram of $(S-A)$, $(S-P)$ and $(A-P)$ are presented in Figure 4.12 a,b and c respectively, wherein the modes show bound oscillations. With evolution the phase diagram show oscillations with repeated of pattern.

Since our main objective is to make the metamaterial "soliton ready" (i.e., the coupled modes to always behave steadily) its an obvious to check the robustness of steady state dynamics.

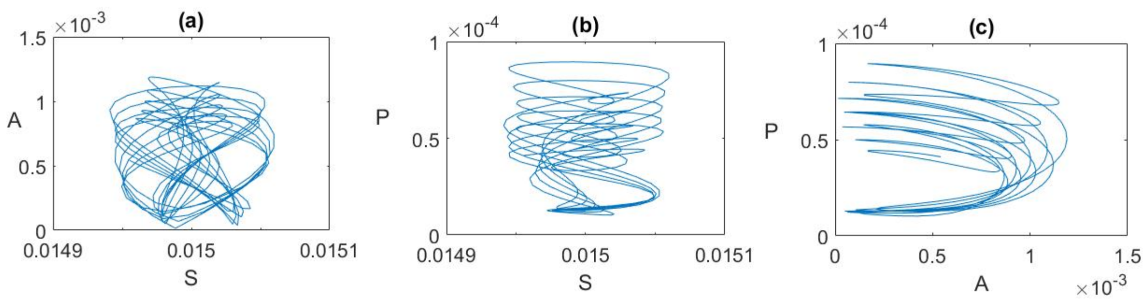

Figure 4.12: Phase diagram for (a) $S-A$ (b) $S-P$ (c) $A-P$. (for ω_S=5, $\omega_A = 3$, $\omega_P = 2$, $\gamma_S = 1 \times 10^{-2}$, $\gamma_A = 2 \times 10^{-2}$, $\gamma_P = 2 \times 10^{-2}$, $g_1 = 1 \times 10^{-1}$, $g_2 = 0.5 \times 10^{-1}$ and $\chi_S E_{in}^{+} = 0.75 \times 10^{-1}$)

Perturbation analysis through a standard numerical method (i.e., $S_S + \delta S_S$) shows the system is robust against perturbations as high as 10% (Figure 4.14). Beside checking the robustness of the solitonic modes against perturbation we also tested the tolerance of the DS against the randomness of the system parameters. The reason behind is, for any system there will be some intrinsic irregularity, whatever small. The system we consider may be fabricated by nanosphere lithography [317]. Although, modern lithography, leaves less chance for error, still one can expect some randomness in terms of the spacing of the SRR, their individual structure etc. Even randomness may arise in the coupling of SRR with the graphene layer. All these may lead to the randomness in the resonant frequencies ($\omega_A,\ \omega_P,\ \omega_S$), decay coefficients ($\gamma_A,\ \gamma_P,\ \gamma_S$) and coupling coefficients ($g_1,\ g_2, \chi$). It is found that the parametric zone that corresponds to stable soliton is so accurately calculated that even randomness as high as 5% can allow stable DS formation, Figure 4.13 portrays it through different phase-diagrams for randomness in resonate frequencies. The same are depicted in Figure 4.15 and 4.16 for randomness in decay coefficients and coupling coefficients respectively. Although, the S mode is more sensitive to randomness in $\chi_S E_{in}^{+}$, Figure 4.16(g) and (h) show different kind of plots due to large oscillations in S mode.

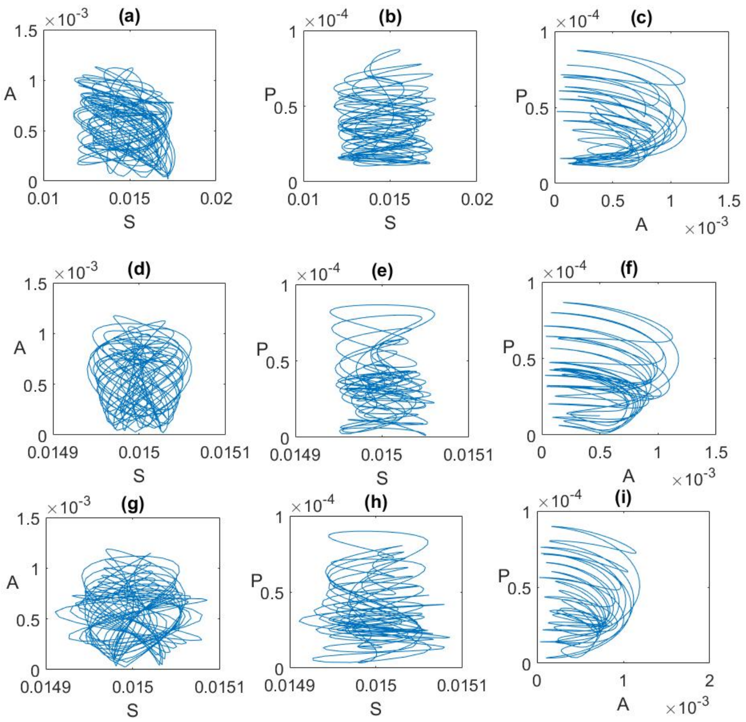

Figure 4.13: The phase plots for 5% randomness in (a),(b),(c) ω_A, (d),(e),(f) ω_P and (g),(h),(i) ω_S.

The method illustrated so far can be further improved by introducing the interaction of the individual meta elements of the metamaterial surface by adopting the coupled mode theory (CMT) [318] CMT gives rise to the spatial distribution of the far-field using the following mathematical scheme [282, 318]. The metasurface is considered to consist of M number of coupled resonators which are well isolated, lossless and each of them supports a single resonance. The resonators interact with the wave that comprises N number of plane-wave channels. CMT gives rise to a set of coupled rate equations for the complex amplitudes of the resonators as a function of incoming wave ($N \times 1$ matrix), coupling coefficients ($M \times N$ matrix) of the incident wave ($N \times 1$ matrix), coupling coefficients of ($M \times N$ matrix) of each resonator to the plane waves of each channel, radiative decay rate of the resonators ($M \times N$ matrix) far-field coupling of the resonator ($M \times N$ matrix), resonance frequencies of resonators ($M \times N$ matrix); coupling between the resonators through evanescent fields ($M \times N$ matrix). The rate equations of the complex amplitudes of the resonators and the incoming wave are then used to find the outgoing wave in conjugation with the background reflection and transmission coefficient ($M \times N$ matrix). Finally, the far-field wave is obtained by the knowledge of the outgoing wave and propagation phase of the waves of each channel. For different substrate, the coupled mode equations are modified as given in the supporting information of ref [282, 318]. Furthermore, the stability criteria can be determined in this case of CMT by adopting the method already described in this paper.

For many practical purpose, a curved metasurface may provide more flexibility in operation [319, 320]. A metasurface is equivalent to spatial sheet discontinuities for electric fields [319]. A bianisotropic surface susceptibility tensor that can be used to model the same [319, 320]. Such tensor is comprised of the average and difference fields on the two sides of the metasurface calculated by means of the electric and magnetic surface polarization densities. For a curved metasurface, the bianisotropic surface susceptibility tensor is modified. Also, the scattered as well as absorbed fields are modified. Numerical techniques (e.g., Finite-difference time-domain method, finite element method. method of moments) in conjugation with the generalized sheet transition boundary condition can be applied to investigate the dynamics of such curved metasurface.

4.3 Conclusion

DSs are formed using three modes, namely: bright symmetric mode, dark asymmetric mode due to SRR and dark asymmetric mode due to graphene in graphene-embedded SRR-based hybrid metamaterial. The stability zones are highlighted. Soliton behaviour has been explored for wide parametric regions. This simple methodology for identifying the solitonic propagation region of EM waves can be applied to a wide variety of metamaterials and beyond. The result of this investigation may be validated through experiments. Further, the results can be used as a guideline for the preparation of a chart of ranges of system parameters that promise stable soliton. The applications of SRR as a negative refractive index material, smarter tools (e.g., a perfect lens), and material having thickness-dependent optical properties can now be combined with those of graphene in biomedical, solid state, electronics and optics. This investigation can be extended to multi-layer graphene, which might be a cheaper substitution for the monolayer one. Since the graphene layer is used, all the advantages of graphene (e.g., electrically controlled GATING) can be utilized while designing applications.

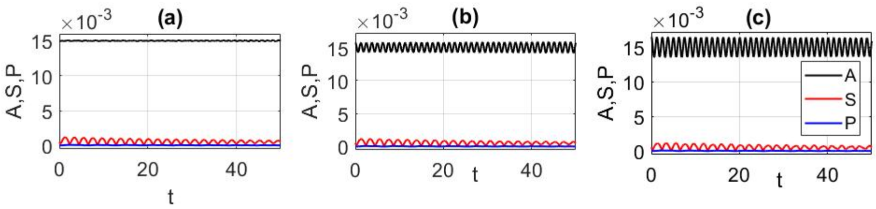

Figure 4.14: The evolution of the three modes (A, S, P) under the influence of (a) no perturbation (b) 5% perturbation, (c) 10% perturbation.

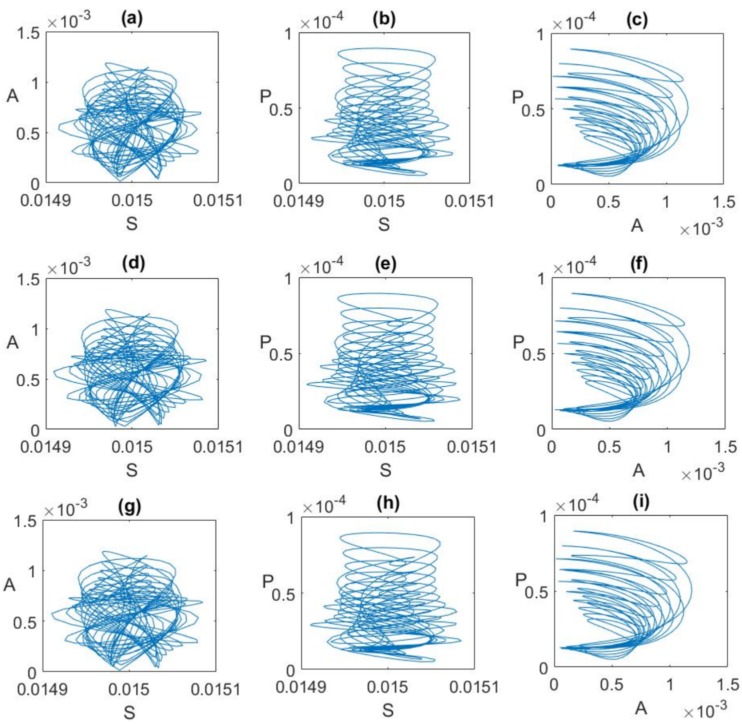

Figure 4.15: The phase plots for 5% randomness in (a),(b),(c) γ_A, (d),(e),(f) γ_P and (g),(h),(i) γ_S.

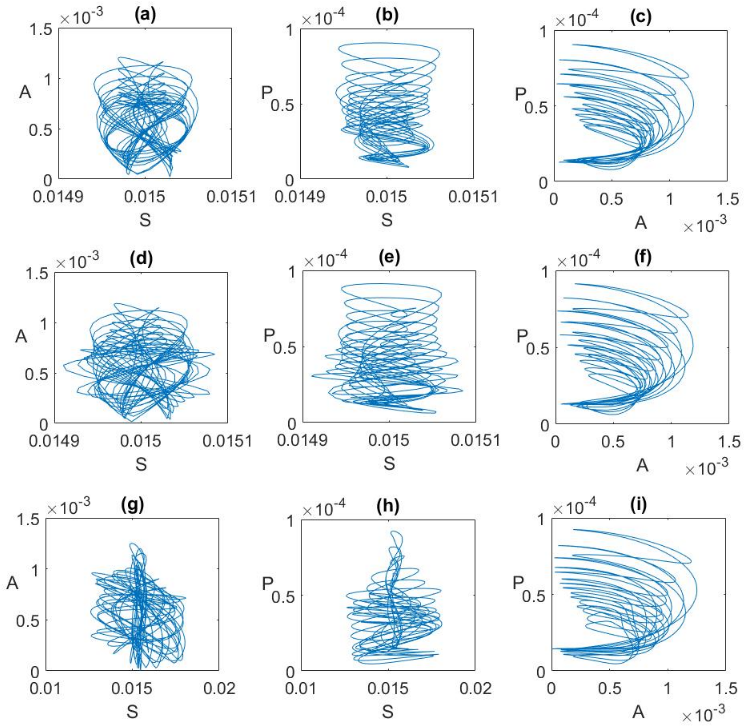

Figure 4.16: The phase plots for 5% randomness in (a),(b),(c) g_1, (d),(e),(f) g_2 and (g),(h),(i) $\chi_S E_{in}^{+}$.

Chapter 5

Soliton Generation and Dynamics in Metamaterial with Higher Order Nonlinear Effects

Previous chapters dealt with soliton formation and soliton dynamics in an SRR-based metamaterial having Kerr (cubic), cubic-quintic, and graphene-embedded nonlinear media. This chapter presents soliton formation in SRR-based nonlinear metamaterials, wherein higher-order effects, namely, third-order diffraction, self-steepening and Raman scattering, are prominent. Both self-steepening and Raman scattering cause a transverse shift of the pulse; however, self-steepening causes a competitively greater shift. These soliton pulses are robust against perturbation; only the transverse shift decreases marginally with increasing perturbation. The interaction dynamics of the generated solitons have been demonstrated. The typical periodic oscillations are observed along with some deformation due to self-steepening and Raman scattering; also, the phase difference between the interacting solitons significantly modifies the interaction dynamics. The whole investigation has been done theoretically by solving a perturbed NLSE following the LVM (analytical) as well as the SSFM (numerical). This chapter corresponds to all the objectives.

5.1 Intoduction

Two processes, self-steepening and Raman scattering, stand out in the field of nonlinear optics—where light interacts with materials in ways that go beyond typical linear optics for their significant influence on pulse propagation [321–323]. Despite their individuality, these effects frequently combine in materials, leading to a complex interaction that dramatically changes how optical pulses behave. Self-steepening is a well-known nonlinear phenomenon that has also gained significant attention in the realm of metamaterials, causing possibilities for manipulating EM waves and modifying the performance of various devices. Basically, self-steepening refers to the nonlinear process where the leading edge of a pulse or wave becomes steeper as it propagates through a medium. The reason behind this is that the pulse has high intensity at peak and hence a high refractive index at peak compared to the trailing edge; as a result, the wave gets steeped. The steepening occurs as long as the dispersion limit is allowed above that; the wave gets fragmented [184]. In metamaterials, self-steepening arises from the interplay of material nonlinearities, such as Kerr, cubic-quintic and saturable nonlinearities. Experimental studies have demonstrated self-steepening in various types of metamaterials, including plasmonic metamaterials, photonic crystals, and acoustic metamaterials. Various techniques, such as ultrafast optics and terahertz spectroscopy, have been employed to observe and quantify the self-steepening effect.

Raman scattering, a nonlinear optical process, involves inelastic scattering of photons by vibrational modes of molecules [324]. In metamaterials, the interaction between incident light and vibrational modes is further modulated by the engineered properties of the material. Theoretical models, such as the Raman scattering tensor [325] and effective medium theories [326], have been instrumental in understanding the intricate interplay between metamaterial structures and Raman scattering processes. Researchers have conducted experiments to investigate Raman scattering in various types of metamaterials, including plasmonic, photonic, and acoustic metamaterials. Techniques such as Raman spectroscopy and surface-enhanced Raman scattering (SERS) have been employed to study and manipulate the Raman signals in these engineered materials. The experimental findings have unveiled novel phenomena, including enhanced Raman signals and the development of metamaterial-based sensors.

Soliton generation in metamaterials with higher-order nonlinear effects has been reported regularly. xu *at el.* studied the soliton under higher order effects, namely, third order dispersion (TOD), Self-steepening, and stimulated Raman scattering in mono-mode optical fibers [327]. The system is solved using the Hirota equation and using Darboux transformation, and the exact N-soliton solution is obtained. Chen *et al.* studied the interaction of periodic optical solitons in an optical fiber having fifth-order dispersion, self-steepening effect and Raman effect using NLSE. The GVD and TOD were found to have an effect on soliton interaction and period of soliton [328]. Yi *et al.* studied soliton in an optical fiber having third-order dispersion and steepening term using a perturbed NLSE [329]. The system is solved analytically, and the dynamics and interaction have been studied. The interaction was found to be significantly impacted by TOD and steepening terms. Chen *et al.* studied three-dimensional quantum systems having dispersion up to fourth-order and higher-order scattering described by NLSE [330]. The system is solved analytically, the bright soliton is found. The higher-order effects found to support the bright soliton behaviour. Vithya *et al.* studied inhomogeneous optical fiber having fifth-order dispersion using NLSE [331]. The system is solved using the Darboux transformation method by constructing the solution using the Lax pair method, and soliton propagation is found in the system. GVD and fifth-order dispersion were found to control the width, amplitude and phase shift of soliton dynamics. Wang *et al.* studied the propagation of ultrashort pulse in an optical fiber having higher-order nonlinearity, fourth-order dispersion and self-steepening using higher order nonlinear Schörindger equation (HONLSE) [332]. They discuss the criteria for the transformation from breathers to solitons with distinct configurations and the interaction between solitons and breathers. Arshad *et al.* studied soliton in an optical fiber having cubic-quintic nonlinearity, third- and fourth-order dispersion and self-steepening using NLSE [333]. The propagation and condition for formation of bright, dark and periodic solitons are found for the system. Yang *et al.* studied optical fiber having TOD, self-steepening and delayed nonlinear response using HONLSE [334]. They found propagation and parametric conditions for dark solitons and studied interactions between solitons. Guo *et al.* studied the propagation of ultrashort optical pulse using HONLSE in an optical fiber having fourth-order dispersion, cubic–quintic nonlinearity, self-steepening and self-frequency shift [335]. The system is solved by using Darboux transformation, and the propagation of breather solitons is found. The two types of interactions, i.e., elastic and mutual attraction and repulsion, are found.

The same types of studies under higher-order effects are also reported in metamaterials. Ali *et al.* studied SRR-based metamaterials having cubic-quintic nonlinearity, TOD, FOD and self-steepening using a modified NLSE [117]. The system is solved by applying LVM, and the dynamics of stable soliton propagation are studied. Hosseini *et al.* studied the nonlinear metamaterials having pseudo-quintic nonlinearity and the self-steepening effect using NLSE [114]. The propagation of kink and anti-kink chirped soliton are reported. Zhu *et al.* studied the nonlinear metamaterials having third- and fourth-order dispersion, cubic-quintic nonlinearity and self-steepening using NLSE [336]. The system is solved by finding Jacobian elliptic function solutions using the mapping method. The propagation of bright or dark solitons is found. Min *et al.* studied the nonlinear metamaterials having cubic-quintic nonlinearity, FOD and self-steepening using an NLSE. Using ansatz method, exact dipole solitary wave solutions are found [337]. Further, using the Drude model, the region for the existence of dipole solitary waves is found. Xiang et al. studied the metamaterials having TOD, self-steepening and Raman effect using a NLSE. They demonstrated Raman soliton self-frequency shift (SSFS) can be controlled by using linear and nonlinear EM properties and self-steepening.

Although a good number of reports are available, the effects of higher-order nonlinear terms on soliton generation and dynamics need to be investigated for various circumstances and system parameters to reveal more insight. Thus, we investigate the soliton generation and dynamics in SRR-based metamaterials with an emphasis on higher-order effects, namely, Raman scattering, self-steepening and TOD. Incorporating TOD is essential due to its significance in handling ultrashort pulses. Although higher-order effects are commonly examined in the study of solitons in various media, including metamaterials, our motive is to 'kind of' reinvestigate it to uncover the generation conditions and dynamics specific to our model and our set of system parameters.

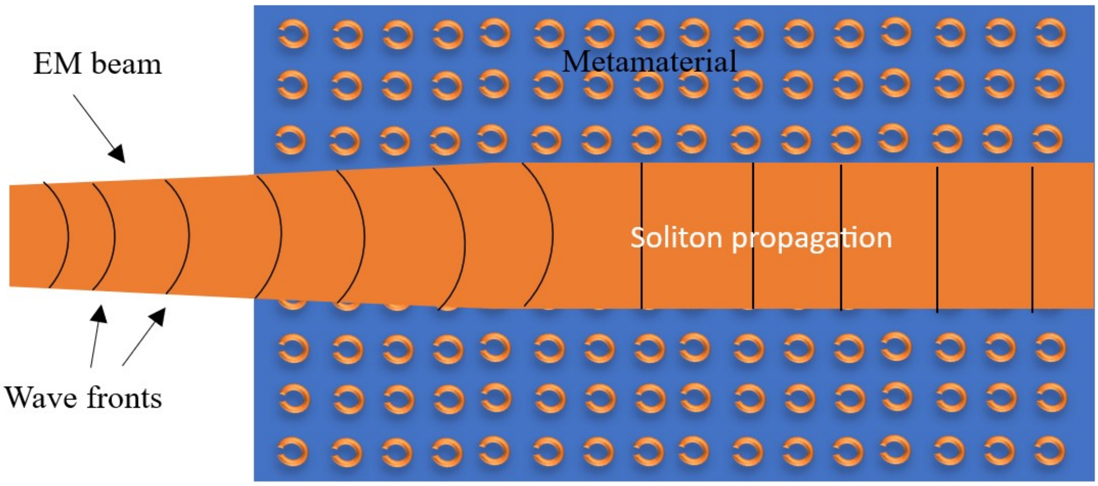

Figure 5.1: Schemetic figure of soliton propagation in Metamaterials.

5.2 Mathematical model

We consider the propagation of an ultrashort pulse in a media that consists of SRR-based metamaterial embedded in a nonlinear dielectric (Figure 5.1). Such a composite system can be fabricated by creating a two-dimensional array of SRR on a nonlinear dielectric media. The dimension of the SRR is smaller than the wavelength of the EM wave passing through the composite material so that the material will behave like an average media. We take into account the higher-order nonlinearity inherent in the media, specifically a 'local' type of nonlinearity. The inclusion of saturable nonlinearity allows for the consideration of higher-order effects, which can be approximated as cubic-quintic nonlinearity in our model. The present system utilizes a combination of self-focusing cubic and self-defocusing quintic nonlinearity, resulting in a form of competing nonlinearity. Mathematically, the ultrafast EM pulse propagation through such nonlinear metamaterial with higher order dispersion and nonlinear effects, namely, self-steepening and Raman scattering, can be given by the following modified nonlinear Schrödinger equation (MNLSE) [117, 338]:

$$i\frac{\partial Q}{\partial z} - \frac{\beta_2}{2}\frac{\partial^2 Q}{\partial t^2} - i\frac{\beta_3}{6}\frac{\partial^3 Q}{\partial t^3} + \sigma_1 \mid Q \mid^2 Q + \sigma_2 \mid Q \mid^4 Q + iS_1\frac{\partial \mid Q \mid^2 Q}{\partial t} - T_r Q\frac{\partial \mid Q \mid^2}{\partial t} = 0 \tag{5.1}$$

Here, Q is a normalised EM field amplitude, z is a normalised displacement, and t is a normalised or co-varying time. β_2 is the well-known second-order dispersion or GVD parameter. β_3 is the coefficient of TOD. σ_1 and σ_2 are the coefficients of cubic and quintic nonlinearity, respectively. S_1 is the coefficient of self-steepening, while T_r is the coefficients of Raman scattering.

Such MNLSE can be solved both analytically and numerically. For the current investigation we first adopt LVM to derive the evolution of the EM pulse parameters as well as to generate the phase diagrams of the propagating pulse. Thereafter, SSFM based numerical study has been undertaken to reveal more vivid pictures of pulse dynamics and pulse interactions.

Following the regular steps of the LVM, the Lagrangian density (for the conservative part of the MNLSE) and Rayleigh dissipative function (for the dissipative part of the MNLSE) can be calculated as [339]:

$$\mathcal{L} = \frac{i}{2}\left(Q\frac{\partial Q^*}{\partial z} - Q^*\frac{\partial Q}{\partial z}\right) - \frac{\beta_2}{2}\left|\frac{\partial Q}{\partial t}\right|^2 - \frac{\sigma_1}{2}|Q|^4 - \frac{\sigma_2}{3}|Q|^6, \tag{5.2}$$

$$\begin{aligned}\mathcal{R} = & -i\frac{\beta_3}{6}\left(\frac{\partial^3 Q}{\partial t^3}\frac{\partial Q^*}{\partial z} - \frac{\partial^3 Q^*}{\partial t^3}\frac{\partial Q}{\partial z}\right) - T_r\frac{\partial |Q|^2}{\partial t}\left(Q\frac{\partial Q^*}{\partial z} + Q^*\frac{\partial Q}{\partial z}\right) \\ & + iS_1\left(\frac{\partial |Q|^2 Q}{\partial t}\frac{\partial Q^*}{\partial z} - \frac{\partial |Q|^2 Q^*}{\partial t}\frac{\partial Q}{\partial z}\right).\end{aligned} \tag{5.3}$$

We consider the following Gaussian profile of the propagating EM pulse:

$$\begin{aligned}Q = & \sqrt{\frac{E_0}{\sqrt{\pi}w(z)}}exp\left(-\frac{(t-t_0(z))^2}{2w(z)}\right) \times \\ & exp\left[-i\left(\frac{c(z)(t-t_0(z))^2}{2w(z)} + \Omega(z)(t-t_0(z)) - \phi(z)\right)\right],\end{aligned} \tag{5.4}$$

where, $w(z)$ is the width of the pulse, $c(z)$ is the phase front curvature, $t_0(z)$ is the pulse centre, $\Omega(z)$ is frequency and $\phi(z)$ is the phase of the pulse. Equation 5.4 has been taken as the trial function for LVM. On substituting the trial function (equation 5.4) in the Lagrangian density (equation 5.2) and in the Rayleigh dissipative function density (equation 5.3) we get reduced Lagrangian density ($\mathcal{L}_R$) and reduced Rayleigh dissipative function density ($\mathcal{R}_R$) as follows:

$$\begin{aligned}\mathcal{L}_R = & -\frac{E_0 e^{-\frac{4(t-t_0(z))^2}{w(z)^2}}}{6\pi^2 w(z)^5}\Bigg[-6\pi^{3/2}t_0(z)e^{\frac{3(t-t_0(z))^2}{w(z)^2}}\left(\beta_2 t + tw(z)^2\frac{\partial c(z)}{\partial z} + w(z)^4\frac{\partial \Omega(z)}{\partial z}\right) \\ & +3\pi^{3/2}t_0(z)^2 e^{\frac{3(t-t_0(z))^2}{w(z)^2}}\left(\beta_2 + w(z)^2\frac{\partial c(z)}{\partial z}\right) + 6\pi^{3/2}c(z)w(z)(t-t_0(z))e^{\frac{3(t-t_0(z))^2}{w(z)^2}} \times \\ & \left(\beta_2\Omega(z)w(z) + (t_0(z)-t)\frac{\partial w(z)}{\partial z} - w(z)\frac{\partial t_0(z)}{\partial z}\right) + 3\pi^{3/2}\beta_2 c(z)^2(t-t_0(z))^2 e^{\frac{3(t-t_0(z))^2}{w(z)^2}} \\ & +3\pi^{3/2}\beta_2\Omega(z)^2 w(z)^4 e^{\frac{3(t-t_0(z))^2}{w(z)^2}} + 3\pi^{3/2}\beta_2 t^2 e^{\frac{3(t-t_0(z))^2}{w(z)^2}} + 3\pi^{3/2}t^2 w(z)^2\frac{\partial c(z)}{\partial z}e^{\frac{3(t-t_0(z))^2}{w(z)^2}} \\ & +2E_0^3\sigma_2 w(z) + 3\pi E_0\sigma_1 w(z)^3 e^{\frac{2(t-t_0(z))^2}{w(z)^2}} + 6\pi^{3/2}tw(z)^4\frac{\partial \Omega(z)}{\partial z}e^{\frac{3(t-t_0(z))^2}{w(z)^2}} - 6\pi^{3/2}\Omega(z) \times \\ & w(z)^4\frac{\partial t_0(z)}{\partial z}e^{\frac{3(t-t_0(z))^2}{w(z)^2}} + 6\pi^{3/2}w(z)^4\frac{\partial \phi(z)}{\partial z}e^{\frac{3(t-t_0(z))^2}{w(z)^2}}\Bigg].\end{aligned} \tag{5.5}$$

$$
\begin{aligned}
\mathcal{R}_R \;=\;& \frac{e^{-\frac{2(t-t_0(z))^2}{w(z)^2}}}{12\pi w(z)^{10}}\Bigg[i\sqrt{\pi}\beta_3 e^{\frac{(t-t_0(z))^2}{w(z)^2}}\Bigg(E_0\Bigg(i\Big(c(z)(t-t_0(z))+\Omega(z)w(z)^2+i(t-t_0(z))\Big)^3\\
&+3(c(z)+i)w(z)^2\Big(c(z)(t-t_0(z))+\Omega(z)w(z)^2+i(t-t_0(z))\Big)\Bigg)\Bigg(iw(z)(t-t_0(z))\times\\
&\left(\frac{\partial c(z)}{\partial z}(t-t_0(z))-2(c(z)-i)\frac{\partial t_0(z)}{\partial z}\right)-2i(c(z)-i)(t-t_0(z))^2\frac{\partial w(z)}{\partial z}+2iw(z)^3\times\\
&\left(\frac{\partial \Omega(z)}{\partial z}(t-t_0(z))-\Omega(z)\frac{\partial t_0(z)}{\partial z}+\frac{\partial \phi(z)}{\partial z}\right)+w(z)^2\frac{\partial w(z)}{\partial z}\Bigg)-E_0\Bigg(\Big(ic(z)(t-t_0(z))\\
&+i\Omega(z)w(z)^2+t-t_0(z)\Big)^3+3(c(z)-i)w(z)^2\Big(c(z)(t-t_0(z))+\Omega(z)w(z)^2-it\\
&+it_0(z)\Big)\Bigg)\Bigg(-iw(z)(t-t_0(z))\left(\frac{\partial c(z)}{\partial z}(t-t_0(z))-2(c(z)+i)\frac{\partial t_0(z)}{\partial z}\right)+2i(c(z)\\
&+i)(t-t_0(z))^2\frac{\partial w(z)}{\partial z}-2iw(z)^3\left(\frac{\partial \Omega(z)}{\partial z}(t-t_0(z))-\Omega(z)\frac{\partial t_0(z)}{\partial z}+\frac{\partial \phi(z)}{\partial z}\right)+w(z)^2\times\\
&\frac{\partial w(z)}{\partial z}\Bigg)\Bigg)-12E_0^2S_1w(z)^3\Bigg(w(z)(t-t_0(z))^2\left(4c(z)\frac{\partial t_0(z)}{\partial z}-3\frac{\partial c(z)}{\partial z}(t-t_0(z))\right)\\
&+w(z)^2(t-t_0(z))\frac{\partial w(z)}{\partial z}(c(z)+2\Omega(z)(t_0(z)-t))+4c(z)(t-t_0(z))^3\frac{\partial w(z)}{\partial z}\\
&-2w(z)^3(t-t_0(z))\left(3\frac{\partial \Omega(z)}{\partial z}(t-t_0(z))-2\Omega(z)\frac{\partial t_0(z)}{\partial z}+3\frac{\partial \phi(z)}{\partial z}\right)+\Omega(z)w(z)^4\times\\
&\frac{\partial w(z)}{\partial z}\Bigg)+24E_0^2T_Rw(z)^3(t-t_0(z))\Bigg(2w(z)(t-t_0(z))\frac{\partial t_0(z)}{\partial z}+2(t-t_0(z))^2\frac{\partial w(z)}{\partial z}\\
&-w(z)^2\frac{\partial w(z)}{\partial z}\Bigg)\Bigg].
\end{aligned}\tag{5.6}
$$

On integrating the reduced Lagrangian density and reduced Rayleigh dissipative function density with respect to the time, we get the total Lagrangian ($\langle L\rangle$) and total Rayleigh dissipative function ($\langle R\rangle$), respectively:

$$
\begin{aligned}
\langle L\rangle \;=\;& \int_{-\infty}^{\infty}\mathcal{L}_R\,dt=-\frac{E_0}{12\pi^{3/2}w(z)^3}\Bigg[2E_0^3\sigma_2+3\pi\sqrt{2}E_0\sigma_1w(z)^2+3\pi^{3/2}w(z)\Bigg(\beta_2\big(c(z)^2+\\
&2\Omega(z)^2w(z)^2+1\big)\Bigg)+w(z)\Bigg(w(z)\Big(\frac{\partial c(z)}{\partial z}-4\Omega(z)\frac{\partial t_0(z)}{\partial z}+4\frac{\partial \phi(z)}{\partial z}\Big)\Big)-2c(z)\frac{\partial w(z)}{\partial z}\Bigg),
\end{aligned}\tag{5.7}
$$

$$
\begin{aligned}
\langle R\rangle \;=\;& \int_{-\infty}^{\infty}\mathcal{R}_R=-\frac{E_0}{4\pi w(z)^3}\Bigg[\pi\beta_3\Bigg(w(z)\Big(c(z)^2\frac{\partial \Omega(z)}{\partial z}+2c(z)c(z)\Omega(z)+2\Omega(z)^2w(z)^2\frac{\partial \Omega(z)}{\partial z}+\\
&+\frac{\partial \Omega(z)}{\partial z}\Big)-2(c(z)^2+1)\Omega(z)\frac{\partial w(z)}{\partial z}\Bigg)+\sqrt{2\pi}E_0\Bigg(-2S_1c(z)\frac{\partial t_0(z)}{\partial z}+S_1w(z)\Big(3w(z)\frac{\partial \Omega(z)}{\partial z}\\
&-\Omega(z)\frac{\partial w(z)}{\partial z}\Big)+2T_r\frac{\partial t_0(z)}{\partial z}\Bigg)\Bigg].
\end{aligned}\tag{5.8}
$$

The Euler-Lagrangian equation compatible for this dissipative system is given by:

$$
\frac{d}{dz}\left(\frac{\partial\langle L\rangle}{\partial\left(\frac{\partial q_j}{\partial z}\right)}\right)-\frac{\partial\langle L\rangle}{\partial q_j}+\frac{\partial\langle R\rangle}{\partial\left(\frac{\partial q_j}{\partial z}\right)}=0,\tag{5.9}
$$

where, q_j is $w(t)$, $t_0(z)$, $\Omega(z)$, $c(z)$ and $\phi(t)$.

On substituting the total Lagrangian (equation 5.7) and total Rayleigh function (equation 5.8) in Euler-Lagrangian equation (equation 5.9) we get a set of five equations. Solving those five equations, we get the following rate equations of the system parameters:

$$\frac{\partial w(z)}{\partial z} = \frac{\beta_2 c(z)}{w(z)} \tag{5.10}$$

$$\frac{\partial t_0(z)}{\partial z} = \frac{1}{4\pi w(z)^2}\left(w(z)\left(4\pi\beta_2\Omega(z)w(z)+3\sqrt{2\pi}E_0S_1\right)+\pi\beta_3\left(c(z)^2+2\Omega(z)^2w(z)^2+1\right)\right) \tag{5.11}$$

$$\frac{\partial c(z)}{\partial z} = \frac{\left(c(z)^2+1\right)\left(\beta_2+\beta_3\Omega(z)\right)}{w(z)^2}+\frac{E_0^3\sigma_2}{\pi^{3/2}w(z)^3}+\frac{E_0\left(\sigma_1+\Omega(z)S_1\right)}{\sqrt{2\pi}w(z)} \tag{5.12}$$

$$\frac{\partial \Omega(z)}{\partial z} = \frac{E_0(c(z)S-T_r)}{\sqrt{2\pi}w(z)^3} \tag{5.13}$$

It can be noted that the evolution equations are coupled.

5.3 Result and discussion

This section presents the generation of soliton through analytical methods (LVM & RK45) as well as a direct numerical method (SSFM). Thereafter, it describes the interaction dynamics of the generated solitons.

5.3.1 Generation of soliton

In order to find a soliton, we first consider the steady-state situation of the rate equation or evolution equations (equations 5.10-5.13) by setting $\frac{\partial q_j}{\partial z}=0$. The resultant coupled algebraic equations can be solved to find the steady-state values of the pulse parameters, which will be subsequently used for solving the coupled evolution equations by the Range-Kutta 45 method. At steady state, we get constant pulse width (w), chirp (c) and frequency (Ω) while propagating through the metamaterial (Figure 5.2a). This can be verified by solving the main governing equation, i.e., the MNLSE (equation 5.1) directly using a numerical method. Hence, we adopt the SSFM to find the pulse intensity profile during propagation for different levels of quintic nonlinearity (Figures 5.2b-d). The horizontal lines corresponding to w, c, Ω in Figure 5.2a and the steady intensity profiles (with slightly oscillating peak profiles) in Figures 5.2(b-d) indicate the generation of soliton in the metamaterial. The above result is for an ideal system wherein dispersion and nonlinearity coefficients are constant. However, in a practical system or experimental setup, the system parameters might fluctuate. For example, the orientation of the SRR may be random (by whatever small amount), the size of the SRR may be different (although small), and the dielectric media may be slightly inhomogeneous. All these will add a random dispersion in the system. We introduced random perturbation in both second and third-order dispersion; even then, we were able to generate soliton (Figure 5.3). Similarly, introducing the random perturbation in self-steepening, Raman scattering, we succeed to generate solitonic pulses. The corresponding phase plots of the solitons are presented in Figure 5.4. The phase plots of the pulse (Figure 5.4) are like straight lines that indicate the bound oscillation (of very small amplitude) of the pulse parameters.

In order to identify the effect of the higher-order nonlinear effects, we vary the self-steepening coefficient (Figure 5.5), which results in shifting of the pulse towards larger time values, i.e., retardation of the pulse. This is prominent at normalized self-steepening parameters as high as 0.1 (Figure 5.5c). Further, the transverse shift (retardation) of the pulse increases with the increase in quintic nonlinearity (Figure 5.5d). A similar study but with Raman scattering shows the transverse shift (retardation) of the pulse at greater T_r (Figure 5.6a-c) as well as greater quintic nonlinearity (Figure 5.6d). A comparison between Figures 5.5d & 5.6d reveals that for a given percentage of change, self-steepening creates greater shift (retardation) of the pulse. This is true even if perturbation high as 6% is present or introduced in the system (Figure 5.7)

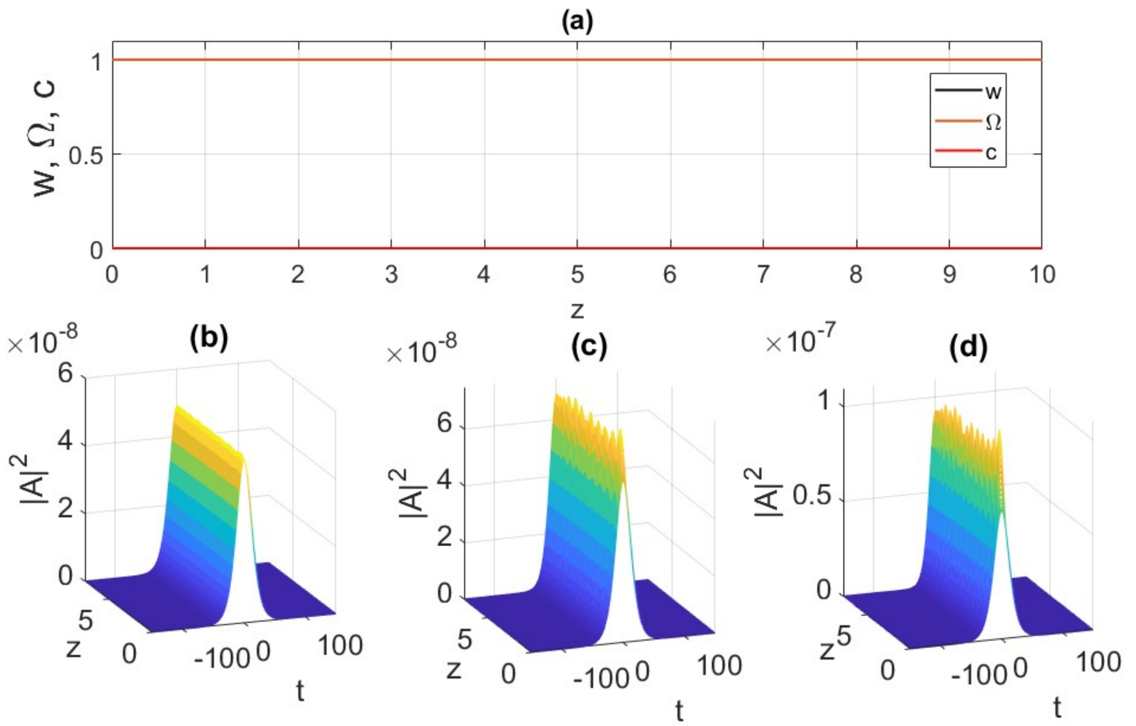

Figure 5.2: (a)The stable propagation for w, Ω and c (line for Ω is overlapping on line for w). Intensity profile for the different values of σ_2 (b) σ_2=0.001, (c) σ_2=0.01 and (d) σ_2=0.1.

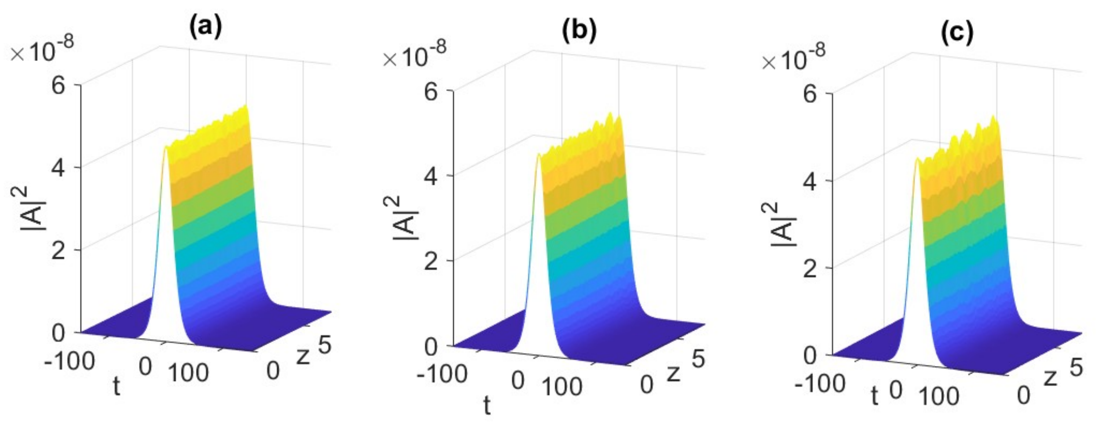

Figure 5.3: The intensity profile for perturbation in dispersion (a) 2% (b) 4% (c) 6%

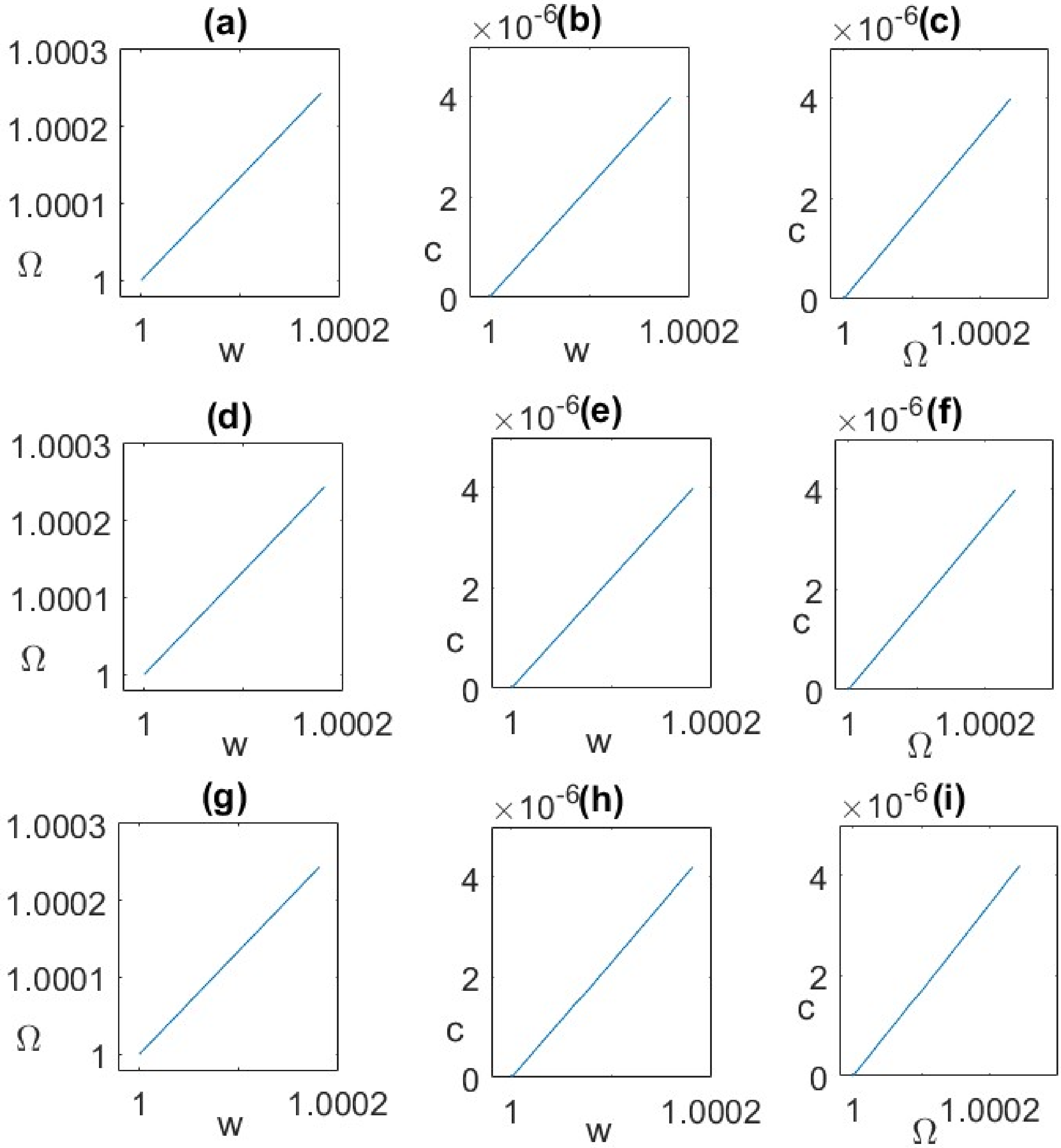

Figure 5.4: The phase plots for 6% randomness in (a-c) quintic nonlinearity (first column), (d-f) self-steepening (second column), and (g-i) Raman scattering (third column).

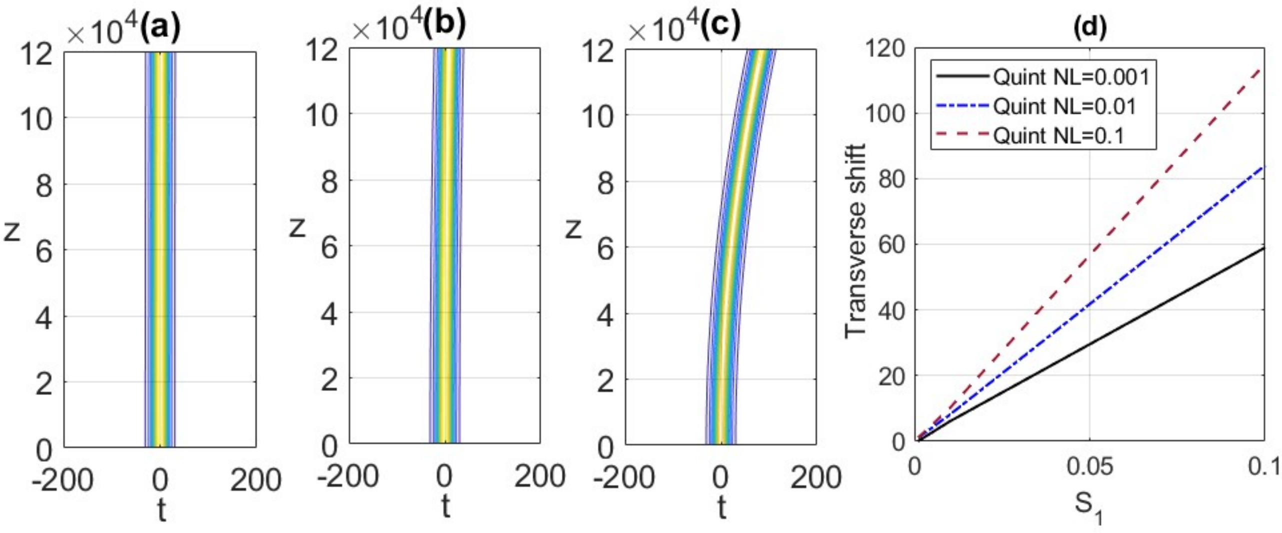

Figure 5.5: The propagation of EM pulse for the different values of S_1, (a) S_1=0.001, (b) S_1=0.01, (c) S_1=0.1. (d) The variation of the transverse shift of the pulse with respect to self-steepening with different quintic nonlinearity.

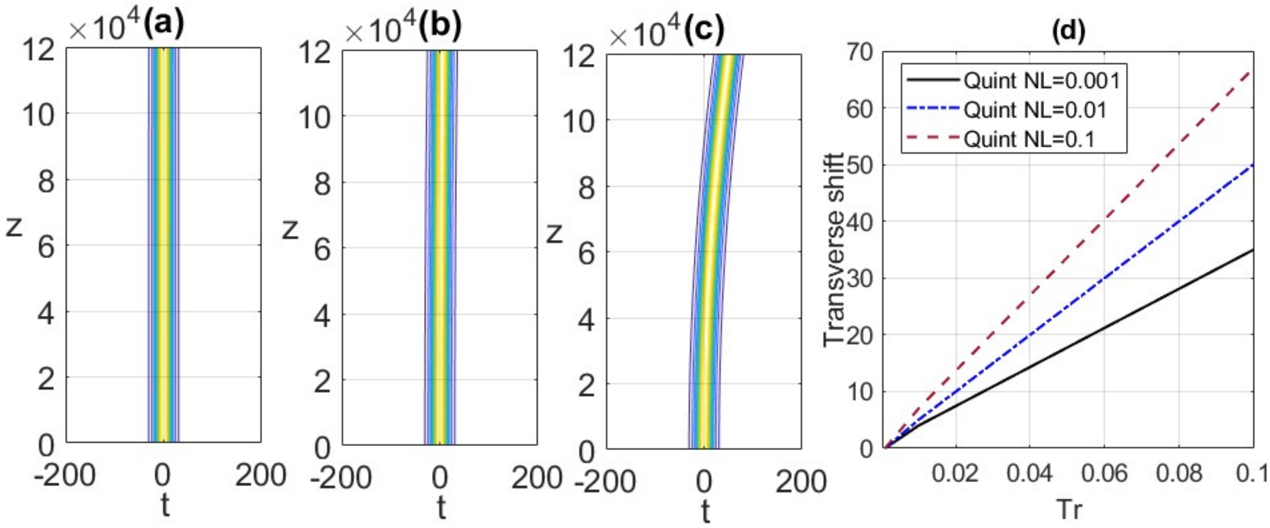

Figure 5.6: The propagation of pulse the different values of T_R, (a) T_R=0.001, (b) T_R=0.01, (c) T_R=0.1. (d) The variation of the transverse shift with respect to T_R for different quintic nonlinearity.

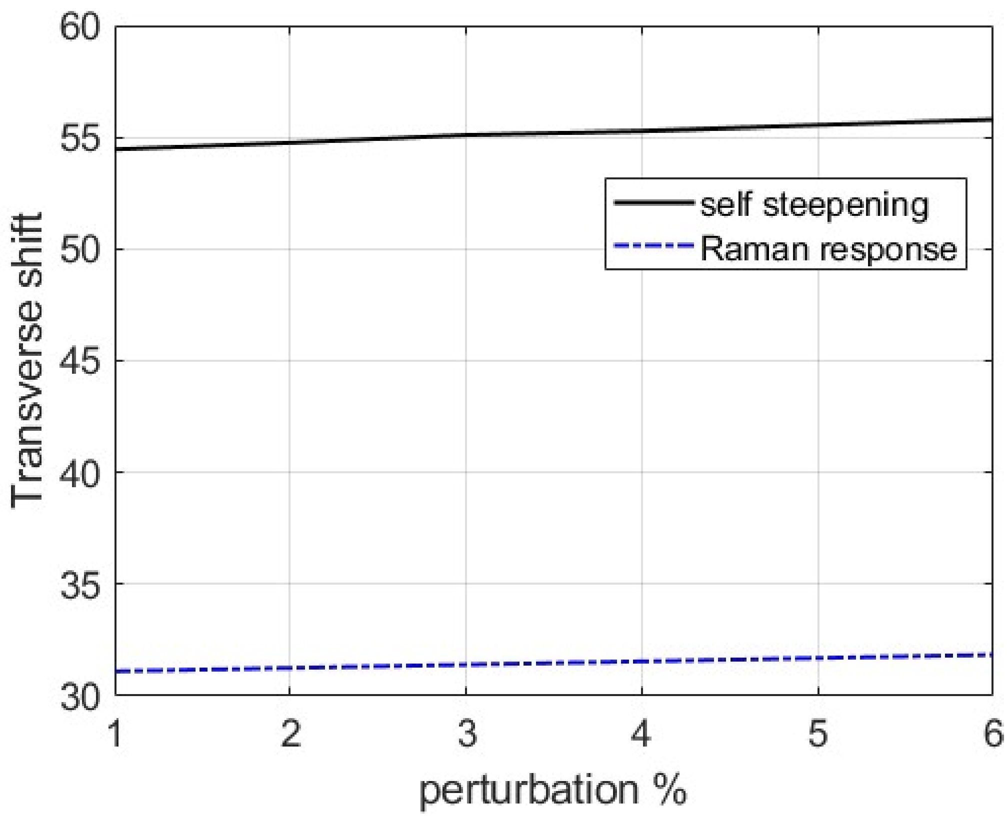

Figure 5.7: The variation of transverse shift due to perturbation; in S_1 is given by black line, in T_R is given by blue dash line.

5.3.2 Interaction dynamics

It is of fundamental interest to determine the interaction dynamics of the soliton pulses at different values of the pulse parameters. Generally, two interacting pulses periodically attract-repulse or in other words unite-separate during propagation (Figure 5.8). The nature or profile of the interaction is similar for a wide range of quintic nonlinearity. However, the soliton peak intensity increases with the increase in quintic nonlinearity. To reveal the effect of self-steepening on interaction dynamics, we draw contour plots of interaction for a wide range of self-steepening (Figure 5.9). The increase in self-steepening disturbs the periodic attraction-repulsion of the pulse, and at higher self-steepening, the pulse interaction ceases. A similar study with varying Raman scattering exhibits more or less similar results (Figure 5.10).

Here, it may be noted that the transverse shift (retardation) of one of the interacting pulses (Figure 5.10c) is much greater that of the case of the single pulse (Figure 5.5c). This can be utilized to fabricate an all-optical switching device wherein a pulse can control another pulse.

Besides the nonlinear effects, the separation as well as phase difference between the pulse obviously play an important role in interaction dynamics. As pulse separation increases, the periodic collision between them becomes, no surprise, less frequent (Figure 5.11). For a separation as large as 100 (normalized unit), no interaction takes place. When a phase difference is introduced between interacting pulses, the periodic collision gets disturbed. In fact, the interaction profile is very sensitive to phase difference (Figure 5.12).

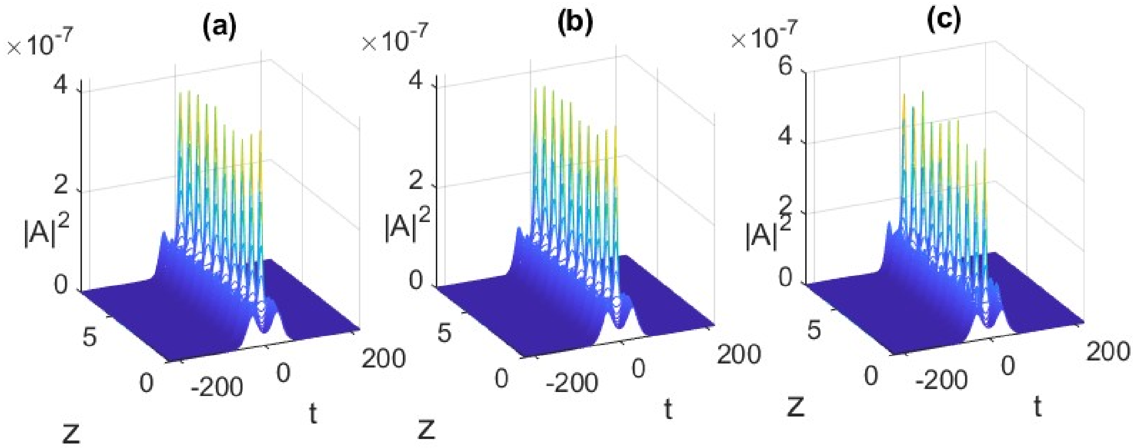

Figure 5.8: The pulse interaction the different values of σ_2, (a) σ_2=0.001, (b) σ_2=0.01 and (c) σ_2=0.1.

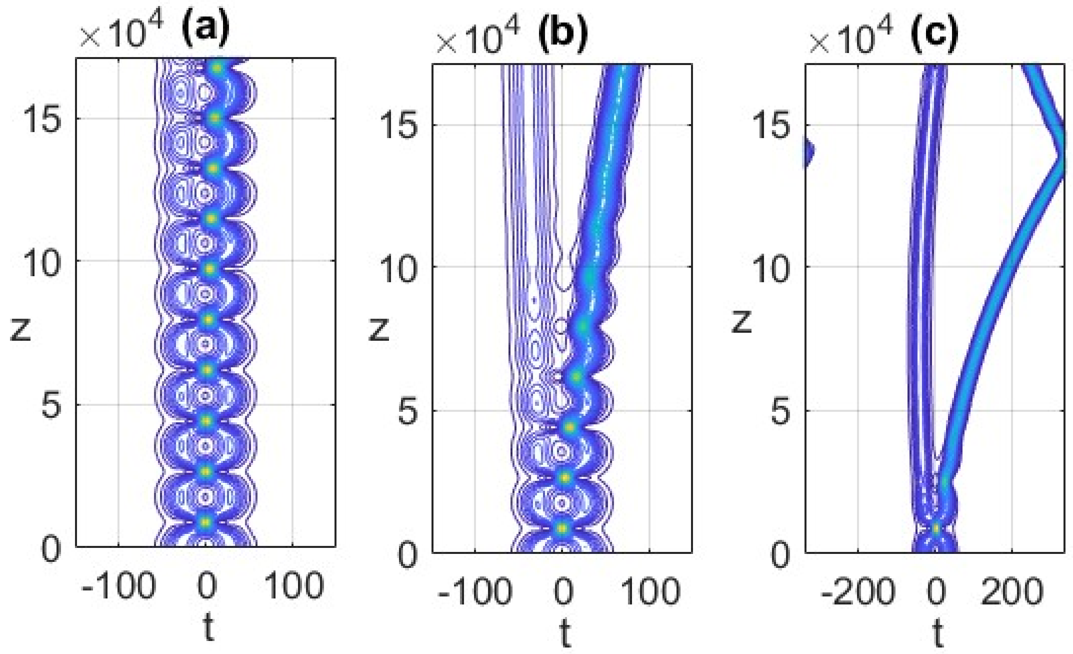

Figure 5.9: The pulse interaction with the different values of S_1, (a) S_1=0.001, (b) S_1=0.01 and (c) S_1=0.1.

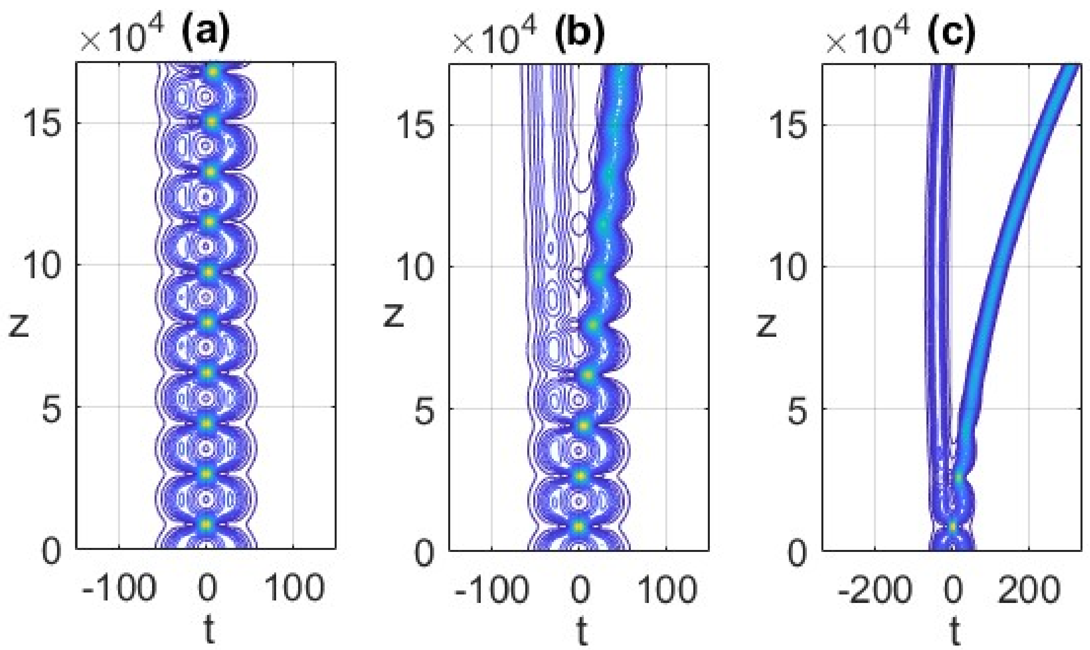

Figure 5.10: The pulse interaction the different values of T_R, (a) T_R=0.001, (b) T_R=0.01 and (c) T_R=0.1.

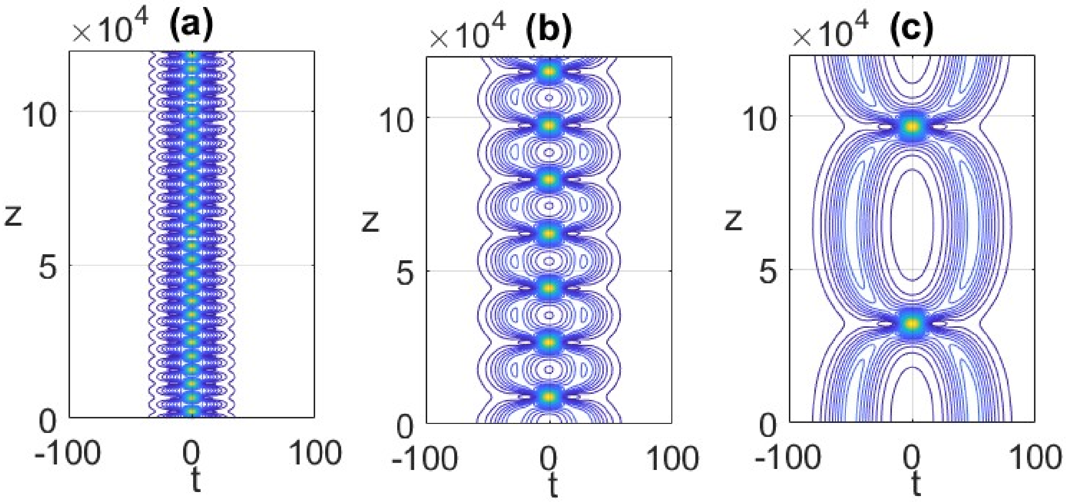

Figure 5.11: The pulse interaction with the increase in separation in interacting pulses (a) 10, (b) 30 and (c) 50.

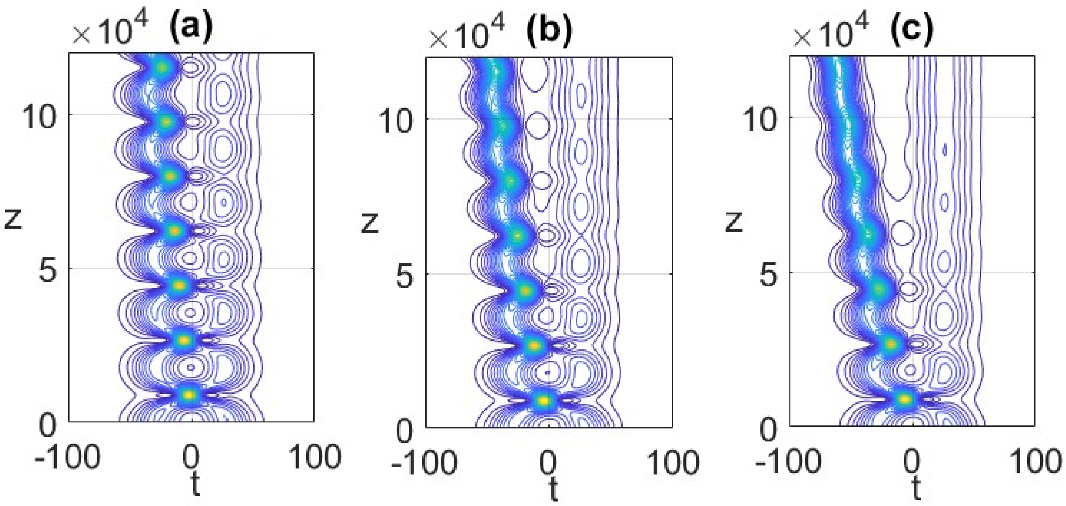

Figure 5.12: The pulse interaction for different values of the phase difference of interacting pulses (a) 5°, (b) 10° and (c) 15°.

5.4 Conclusion

The propagation of EM pulse through an SRR-based metamaterial with higher-order nonlinear terms can create soliton, which is robust against perturbation up to a certain extent. The self-steepening, as well as Raman scattering, can cause retardation of the pulse, which is more prominent at greater quintic nonlinearity. Also, self-steepening creates comparatively more retardation of the pulse than that of Raman scattering. The interaction of two pulses in higher-order nonlinear media shows the typical attraction-repulsion or union-separation. However, it gets disturbed at higher values of both self-steepening and Raman scattering. The pulse separation and phase difference between interacting pulses significantly modify the interaction dynamics. This can be utilized for the fabrication of all-optical switching or all-optical monitoring devices. These results can be a guideline for the experimental realization of soliton in higher-order nonlinear media and the study of the interaction dynamics.

Chapter 6

Diffraction-Managed Soliton in SRR Based Metamaterial

The previous chapters dealt with metamaterial having constant diffraction. This chapter considers a periodic array of metamaterials having alternate positive and negative diffraction and studies the propagation dynamics of EM waves through it and the subsequent formation of breather-like solitons. The system is governed by an NLSE and analysed using analytical and numerical methods, employing the LVM and the SSFM, respectively. The diffraction-managed breather soliton is produced in the system. The study determines the initial beam energy required for the generation of diffraction-managed solitons across diverse metamaterial-array configurations. Notably, the present approach enables the production of high-energy beams through the utilization of diffraction-managed metamaterial arrays. Furthermore, the stability zones for diffraction-managed solitons are identified, offering insights into the intricate stability dynamics within this soliton framework. This chapter corresponds to all the three objectives of the thesis work.

6.1 Introduction

Fundamental solitons maintain their shape and intensity profile over long distances [340–342], while higher-order solitons periodically repeat their shape and size. Generally, constant diffraction has been used for the generation of soliton. A unique class of spacial soliton can be generated by placing alternate positive and negative dispersion media. A detailed dispersion-management technique can be found in ref [22], wherein the diffraction properties of the waveguide arrays yield reduced diffraction, cancelled diffraction and even reversed diffraction. The array will create alternate defocusing and focusing of the propagating beam and eventually entrap the broadening of the propagating beam. Such a localized beam is called a dispersion-managed soliton [343, 344]. Such dispersion-managed soliton looks like a breather and usually takes less energy for formation compared to a constant dispersion media [345]. Since its inception in 1995, a good volume of work has been reported. Similar to dispersion management, diffraction management in a medium, i.e., a media comprising alternate positive and negative diffraction layers or, in other words, alternate defocusing and focusing layers, may lead to the formation of soliton. Such soliton can be referred as diffraction-managed soliton and has attracted research attention for a little longer than the past two decades [346].

Diffraction-managed solitons have been designed to overcome diffraction limitations in nonlinear media [347]. Discret diffraction-managed spatial solitons have been studied in nonlinear waveguide arrays [348, 349]. This variation acts as a periodic potential that helps to confine the beam and prevent it from spreading out due to diffraction. The soliton produced in a diffraction-managed system propagates with periodic oscillations of width (i.e., squeeze and expansion) like the dispersion-managed breather soliton. Diffraction-managed solitons have several advantages over regular spatial solitons. For example, increased stability, longer propagation distances, and reduced sensitivity to noise and imperfections or irregularities in the medium [350]. They are also highly controllable and tunable by adjusting the parameters of the periodic potential [102]. Diffraction-managed solitons have many potential applications in nonlinear optics, including optical communication [348], data processing [351] and imaging [352]. They can be used to develop all-optical switches [353]. Although dispersion-managed soliton and diffraction-managed soliton look similar, there are significant differences. Dispersion is a material property, but diffraction arises from geometrical structure.

Diffraction-managed media can be created using metamaterials, too. The negative refractive index metamaterials were found to exhibit negative diffraction or anomalous diffraction, which leads to focusing of the beam. On the other hand, the positive index materials exhibit positive diffraction, resulting in defocusing. Kockaert *et al.* conducted a thorough analysis and presented an exhaustive mathematical framework that demonstrates that the coefficient of diffraction has a negative correlation with the refractive index [354]. An inverse proportionality relationship can be observed between the coefficient of diffraction and the refractive index. The negative diffraction property was found to be dependent on the metamaterial's specific structural and design parameters. Zhang *et al.* showed a similar analysis for dispersive Kerr metamaterial and showed that the negative diffraction is possessed by metamaterial [355]. Mattheakis *et al.* investigated the properties of metal-dielectric metamaterials with the epsilon-near-zero (ENZ) effect [356]. Negative diffraction (or anomalous) was observed to be a distinctive characteristic of these particles.

Owing to the structural dependent properties of metamaterials, various types of metamaterials have been designed, e.g., dispersion-managed metamaterial[120, 357] and diffraction-managed metamaterial [102, 358–360]. Boardman *et al.* reported nonlinear layered media by making the diffraction coefficient as a function of the propagation distance to manage the diffraction by placing the RHM slab followed by LHM slab [361]. The diffraction in RHM is counterbalanced by using LHM.
The higher-order diffraction in metamaterial is influenced by the unit period, which is the spacing between meta-unit structures. The third-order diffraction is seen to have a dependence on the interspacing of unit cells of the metamaterial [362]. Also, the interspacing of the meta-unit cells can change the overall behaviour of metamaterial, such as response frequency and coupling among adjacent unit cells. A large volume of research has been done on spatial soliton in the metamaterial [101, 360].

However, investigation on diffraction-managed soliton in metamaterial is not that frequently available. Therefore, we investigate the diffraction-managed soliton in a system consisting of slabs of metamaterial with the periodically arranged RHM and LHM as shown in Figure 6.1(a). We are using SRR-based metamaterials. The dimensions of the SRR are comparable to the operating wavelength in order to have an interaction between the beam and the metamaterials. The RHM creates normal diffraction, i.e., positive diffraction, which will lead to self-defocusing, while LHM shows anomalous diffraction, i.e., negative diffraction, which is responsible for self-focusing. The array of alternate defocusing and focusing media generates a diffraction-managed system that can form a diffraction map of zero, positive and negative average diffraction depending on the relative diffraction values of LHM and RHM. Figure 6.1(c) illustrates one such diffraction-managed map with zero average diffraction; such a diffraction map helps in realizing stable wave propagation. That comprises an alternate contraction and expansion of the beam (Figure 6.1(b)) like a breather structure.

The layout of the chapter is as follows: In section 6.2, the theoretical model is discussed using the LVM. The generation of soliton is discussed in section 6.3. Section 6.4 describes the interaction of diffraction-managed soliton. Section 6.5 presents stability analysis of the soliton, which is followed by a conclusion in section 6.6.

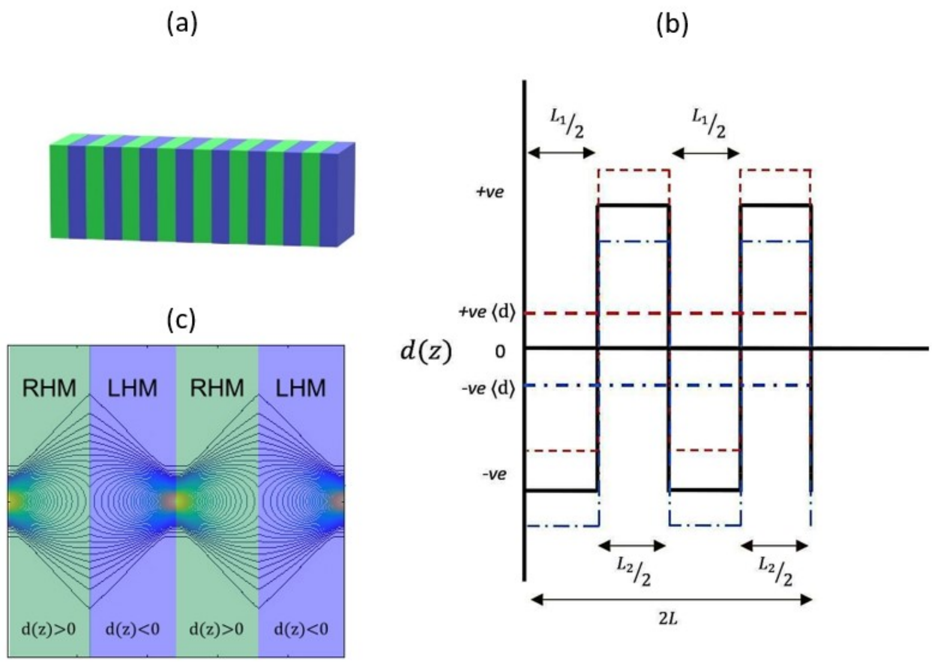

Figure 6.1: (a) Array of metamaterial consisting of alternate slabs of LHM and RHM, (b) Diffraction map for zero average diffraction (solid line, black colour), positive average diffraction (dashed line, red colour) and negative average diffraction (dash-dotted line, blue colour), and (c) Breather soliton in periodic metamaterial of LHM and RHM

6.2 Theoretical Modeling

Our theoretical model consists of a diffraction-managed cubic-quintic nonlinear media. The EM wave propagation in such a diffraction-managed system can be described theoretically by a NLSE of the following type [105, 363]:

$$i\frac{\partial Q}{\partial t} + d(z)\frac{\partial^2 Q}{\partial x^2} + \sigma_1 \mid Q \mid^2 Q - \sigma_3 \mid Q \mid^4 Q = 0. \tag{6.1}$$

Here, Q is the normalized electric field and $\mid Q \mid^2$ is the electric field intensity of the EM beam, t is the normalized retarded time. x is the slow space variable transverse to propagation. σ_1 is the Kerr nonlinearity coefficient and σ_3 is the quantic nonlinearity coefficient. Both σ_1, and σ_3 are positive. $d(z)$ is the diffraction coefficient given by the diffraction map as follows:

$$d(z) = \begin{cases} -d_1 + \langle d \rangle & \text{for } 0 < z \leq \frac{L_1}{2} \\ +d_2 + \langle d \rangle & \text{for } \frac{L_2}{2} < z \leq \frac{L_1}{2} + \frac{L_2}{2} \\ -d_1 + \langle d \rangle & \text{for } \frac{L_1}{2} + \frac{L_2}{2} < z \leq L_1 + \frac{L_2}{2} \end{cases} \tag{6.2}$$

where,

$$\langle d \rangle = \frac{d_1 + d_2}{2}, \tag{6.3}$$

$L_1/2$ is the length of RHM (equivalent to a dielectric media), and $L_2/2$ is the length of LHM. The first term of equation 6.1 represents the evolution of the electric field of the EM wave propagating through the diffraction-managed system. The second term represents diffraction, the third term represents Kerr nonlinearity-induced self-focusing, and the fourth term is quintic nonlinearity-induced self-defocusing. The combination of the third and fourth terms gives rise to a competing nonlinearity and even saturable nonlinearity.

To solve the equation 6.1, we apply the well-known LVM as follows [125]. The Lagrangian density $\mathcal{L}$ corresponding to equation 6.1 is given by:

$$\mathcal{L} = \frac{i}{2}\left(Q\frac{\partial Q^*}{\partial t} - Q^*\frac{\partial Q}{\partial t}\right) + d\left|\frac{\partial Q}{\partial x}\right|^2 - \frac{\sigma_1}{2}|Q|^4 + \frac{\sigma_3}{3}|Q|^6. \tag{6.4}$$

The following secant hyperbolic ($Sech$) solution is considered as a trial function

$$Q = A(t)Sech\left(\frac{x}{w(t)}\right)\exp\left(ix^2\mu(t) + i\phi(t)\right), \tag{6.5}$$

where, $A(t)$ is amplitude, $w(t)$ is width, $\mu(t)$ is chirp and $\phi(t)$ is the phase of the EM wave. The reduced Lagrangian (L) can be calculated by putting equation 6.5 in equation 6.4. We determine,

$$L = \frac{A^2 sech^2\left(\frac{x}{w}\right)}{6w^2}\left[6d\tanh^2\left(\frac{x}{w}\right) - 3\sigma_1 A^2 w^2 sech^2\left(\frac{x}{w}\right) + 2\sigma_3 A^4 w^2 sech^4\left(\frac{x}{w}\right) \right.$$
$$\left. +6w^2\left(4dx^2\mu^2 + x^2\frac{\partial \mu}{\partial t} + \frac{\partial \phi}{\partial t}\right) + 6d\tanh^2\left(\frac{x}{w}\right)\right] \tag{6.6}$$

The total Lagrangian ($\langle L \rangle$) can be found by integrating L over the available space as:

$$\langle L \rangle = \int_{-\infty}^{\infty} L \, dx, \tag{6.7}$$

$$\langle L\rangle = \frac{A^2}{6}\left[\pi^2 w^3\frac{\partial\mu}{\partial t} + 12w\frac{\partial\phi}{\partial t}\right] + \frac{2dA^2}{3w}\left[1+\pi^2 w^4\mu^2\right] - \frac{2}{3}\sigma_1 A^4 w + \frac{16}{45}\sigma_3 A^6 w, \quad (6.8)$$

Now $\langle L\rangle$ is varied with respect to the wave parameters using the following Euler-Lagrange equation:

$$\frac{d}{dt}\left(\frac{\partial\langle L\rangle}{\partial\left(\frac{\partial q_j}{\partial t}\right)}\right) - \frac{\partial\langle L\rangle}{\partial q_j} = 0, \quad (6.9)$$

where, q_j is $A(t)$, $w(t)$, $\mu(t)$ and $\phi(t)$. The variation with respect to $\phi(t)$ yields $2A^2w = Constant = E_0(say)$. E_0 is the initial beam energy. Similarly, variations with respect to $A(t)$, $w(t)$, $\mu(t)$ give rise to the following set of coupled ordinary differential equations, which describe the evolution of the system parameters:

$$\frac{\partial A}{\partial t} = -2Ad\mu, \quad (6.10)$$

$$\frac{\partial w}{\partial t} = 4d\mu w, \quad (6.11)$$

$$\frac{\partial\mu}{\partial t} = -\frac{1}{15\pi^2 w^4}\left(60\pi^2 d\mu^2 w^4 - 60d - 8E_0^2\sigma_3 + 15E_0\sigma_1 w\right). \quad (6.12)$$

One can determine the steady state values of $A(t)$, $w(t)$and $\mu(t)$ by setting the left-hand sides of the above evolution equations equal to zero. Such steady-state values are used as initial conditions in the Range-Kutta method for numerical determination of the evolution of $A(t)$, $w(t)$and $\mu(t)$. Also, these equations can determine the phase dynamics of the diffraction-managed soliton.

6.3 Generation of diffraction managed soliton

The dynamics of the beam in metamaterials are studied by employing both analytical and numerical methods. Analytical LVM is used to solve the system to find the evolution equation of the system parameters (in the previous section) and determine the phase trajectories (in the later part of this section). Before further discussion on the analytical investigation, the SSFM is applied to see the solitons profile vividly. In particular, the 3D soliton profile, corresponding contour plots, and interaction dynamics are determined by SSFM. For a suitable range of parameters, we obtain soliton with periodic oscillations of width and amplitude. This is the typical breather characteristic diffraction-managed soliton. One set of examples of such numerically obtained diffraction-managed soliton is depicted in Figure 6.2. For positive average diffraction ($\langle d \rangle > 0$), the diffraction-managed soliton amplitude is higher than that of with negative $\langle d \rangle$ (Figure 6.2 d & e). A zero $\langle d \rangle$ yields an intermediate soliton peak height (Figure 6.2f). The peak heights periodically change (Figure 6.2 d-f), and periodic oscillation of their widths (Figure 6.2 a-c) make them an ideal diffraction-managed breather soliton.

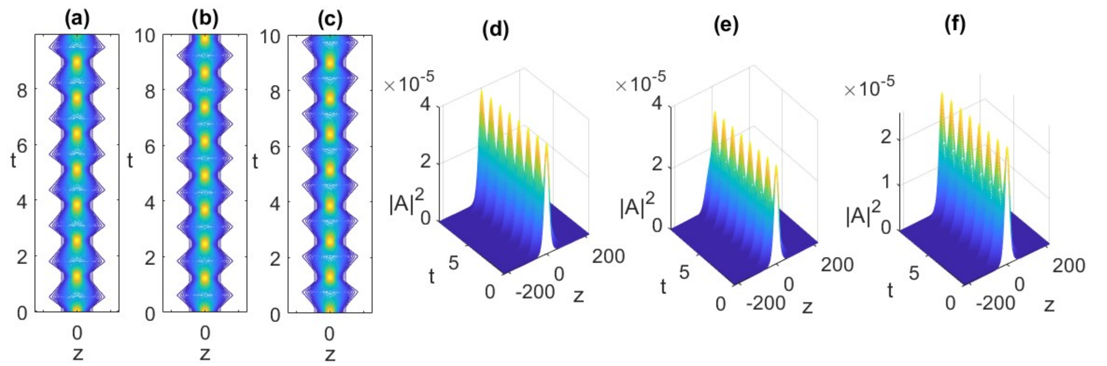

Figure 6.2: The typical diffraction-managed soliton formation contour plots for (a) positive $\langle d \rangle$; LHM is 1.2, and RHM is 0.8, (b) negative $\langle d \rangle$; LHM is 0.8, and RHM is 1.2, and the intensity profile of soliton for diffraction coefficient (c) zero $\langle d \rangle$. (d), (e) and (f) are the intensity profiles corresponding to (a), (b), and (c), respectively.

In some metamaterial, the third-order diffraction (TOD) and fourth-order diffraction (FOD) may be significant [364]. For such a system, the NLSE must be modified. The modified NLSE (MNLSE) will read as follows:

$$i\frac{\partial Q}{\partial t} + d(z)\frac{\partial^2 Q}{\partial x^2} + d_3(z)\frac{\partial^3 Q}{\partial x^3} + d_4(z)\frac{\partial^4 Q}{\partial x^4} + \sigma_1 \mid Q \mid^2 Q - \sigma_3 \mid Q \mid^4 Q = 0 \quad (6.13)$$

Here, d_3 and d_4 are the coefficients of TOD and FOD, respectively. The value of parameters are (unless mentioned otherwise) $d_1 = 1$, $d_2 = 9$, $\sigma_1 = 8.44$ and $\sigma_2 = 8.44 \times 10^{-2}$. Diffraction-managed breather solitons are found for such higher-order diffraction (Figure 6.3–6.8). As the TOD coefficient increases, the periodic oscillation of width doesn't vary that much, but an asymmetry in the transverse profile appears. This is true for $\langle d \rangle = 0$ (Figure 6.3), positive (Figure 6.4) and negative (Figure 6.5). However, the effect of FOD on soliton formation seems marginal for all $\langle d \rangle$, namely $\langle d \rangle = 0$ (Figure 6.6), positive (Figure 6.7) and negative (Figure 6.8).

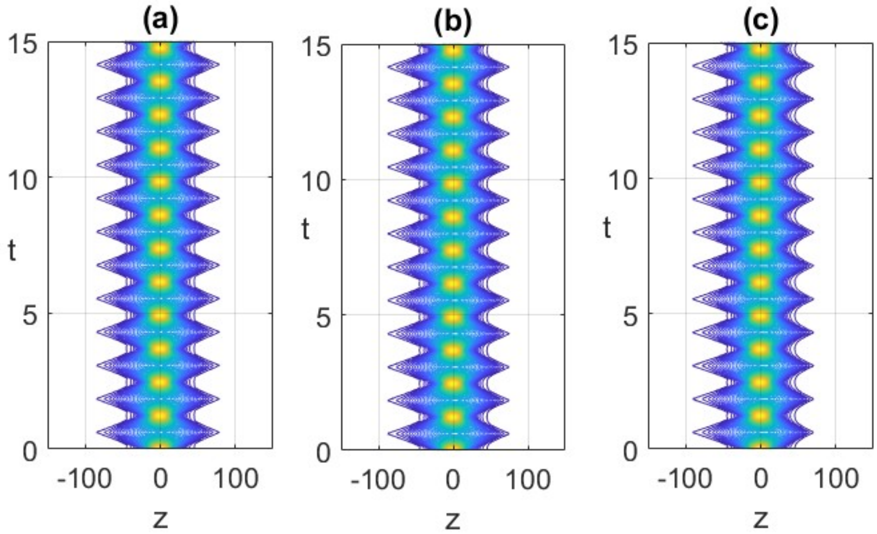

Figure 6.3: Contour plots of propagation of soliton for TOD coefficient (a) 1, (b) 2, and (c) 3. Here $\langle d \rangle = 0$.

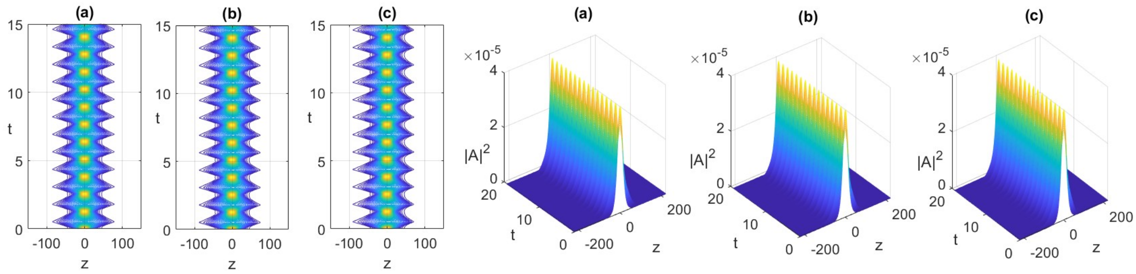

(i) (ii)

Figure 6.4: (i) Contour plots for the propagation of soliton for positive $\langle d \rangle$; LHM is 1.2 times, and RHM is 0.8, and TOD coefficient (a) 1, (b) 2, and (c) 3. (ii) Intensity profile corresponding to Figure 6.4i

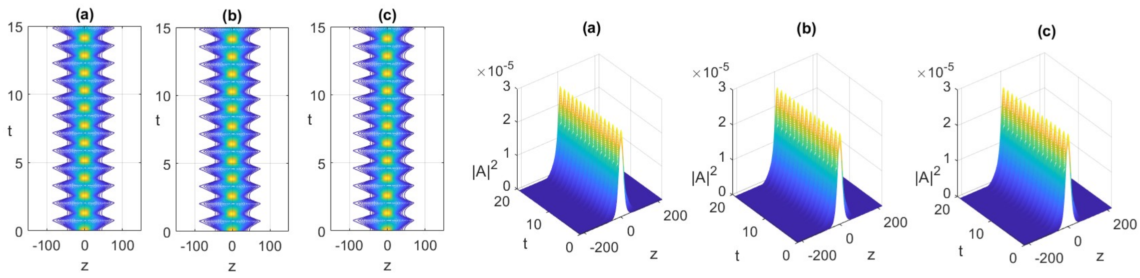

(i) (ii)

Figure 6.5: (I) Contour plots for the propagation of soliton for negative $\langle d \rangle$; LHM is 0.8, and RHM is 1.2, and TOD coefficient (a) 1, (b) 2, and (c) 3. (ii) Intensity profile corresponding to Figure 6.5i

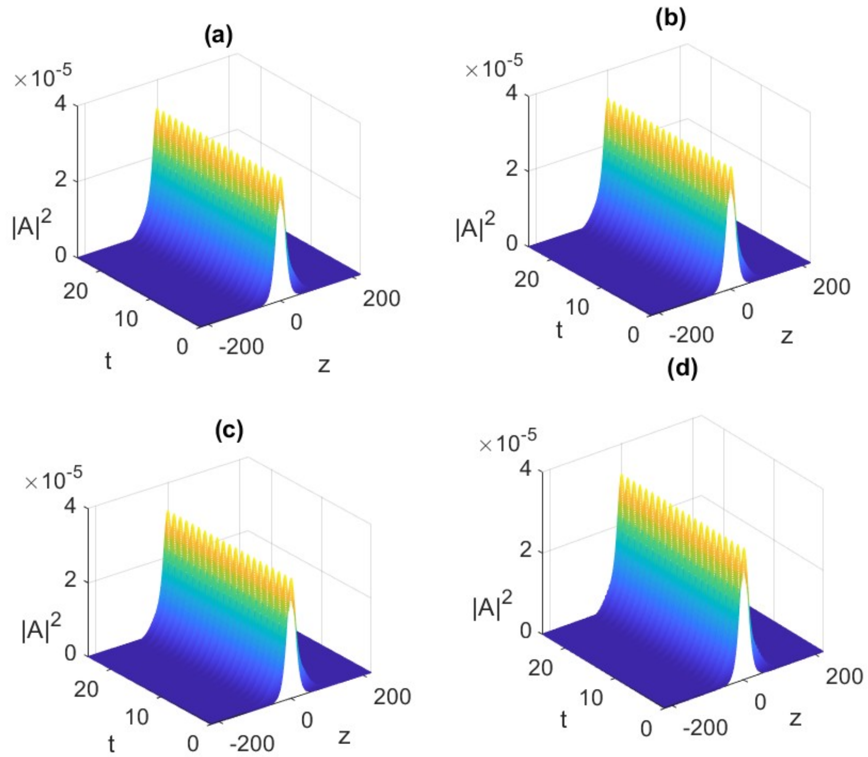

Figure 6.6: Intensity profiles of soliton for FOD coefficient (a) 9, (b) 10, (c) 11, and (d) 12. Here $\langle d \rangle = 0$.

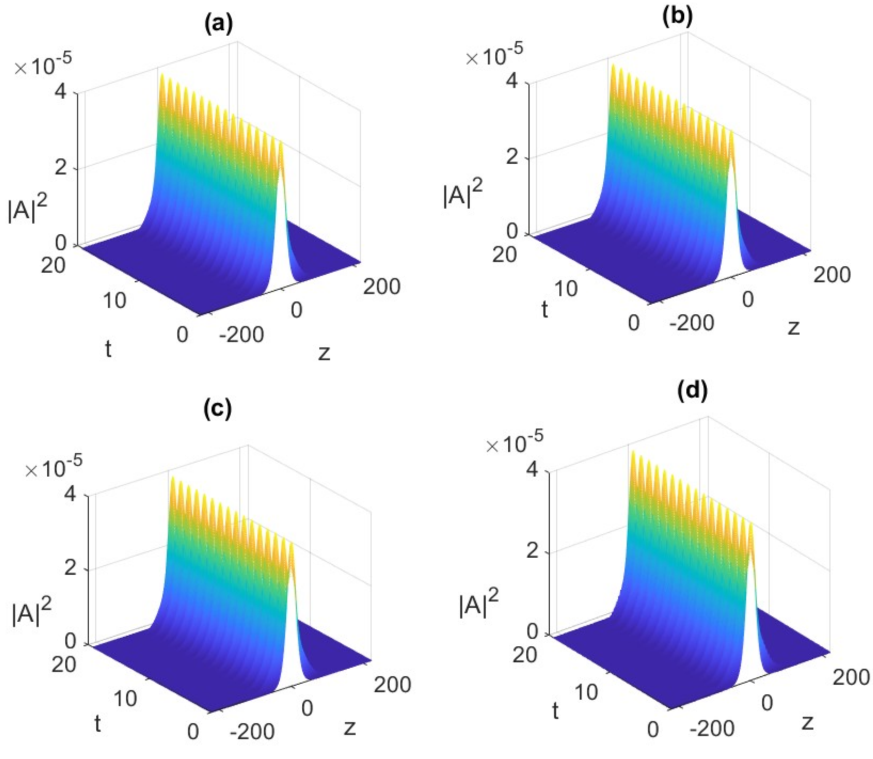

Figure 6.7: Intensity profiles of soliton for positive $\langle d \rangle$; LHM is 1.2, and RHM is 0.8, having FOD coefficient (a) 9, (b) 10, (c) 11 and (d) 12.

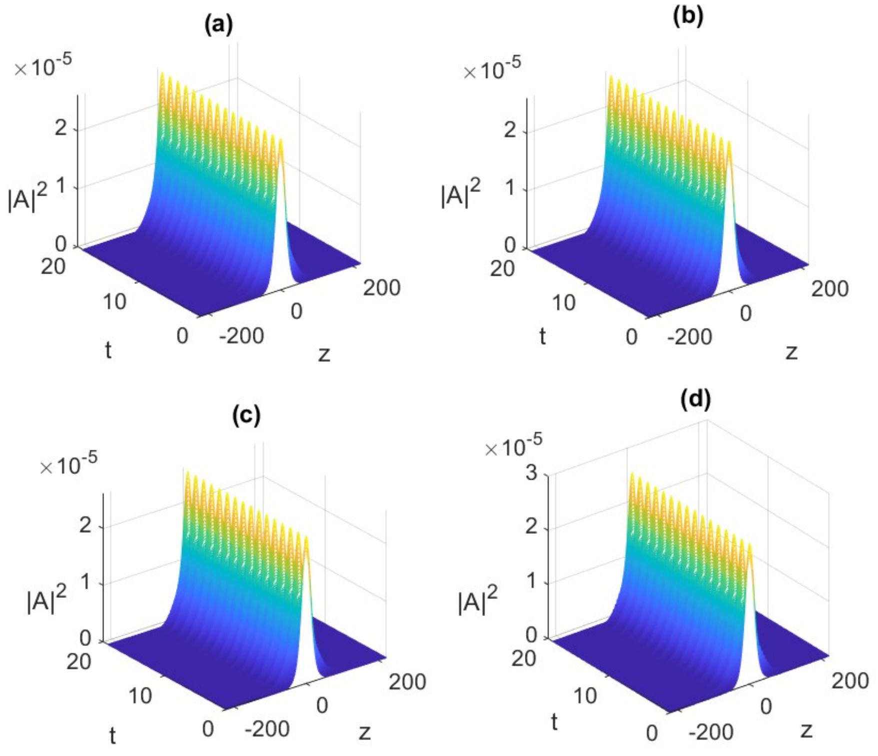

Figure 6.8: Intensity profiles of soliton for negative $\langle d \rangle$; LHM is 0.8, and RHM is 1.2, having FOD coefficient (a) 9, (b) 10, (c) 11 and (d) 12.

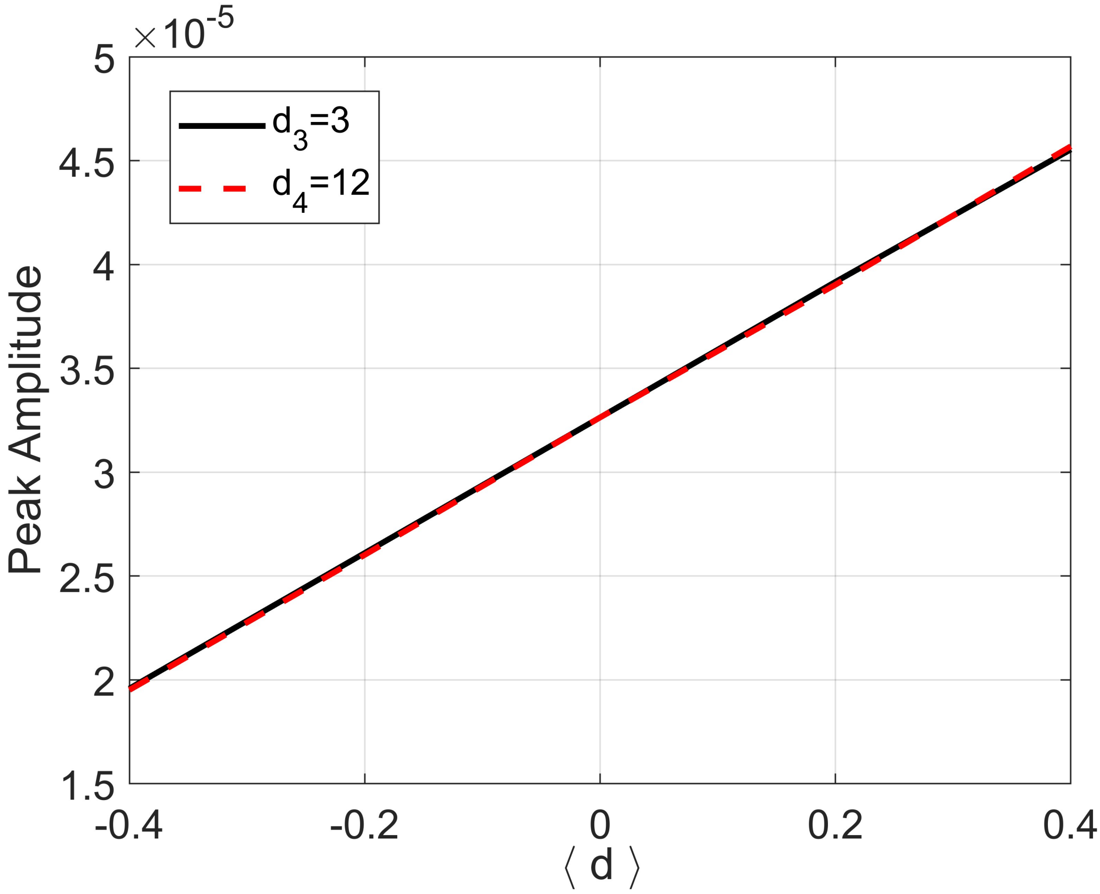

Figure 6.9: Variation of peak hight with increasing $\langle d \rangle$. The black line is for $d_3 = 3$ and $d_4 = 0$, red dashed line is for $d_4 = 12$ and $d_3 = 0$.

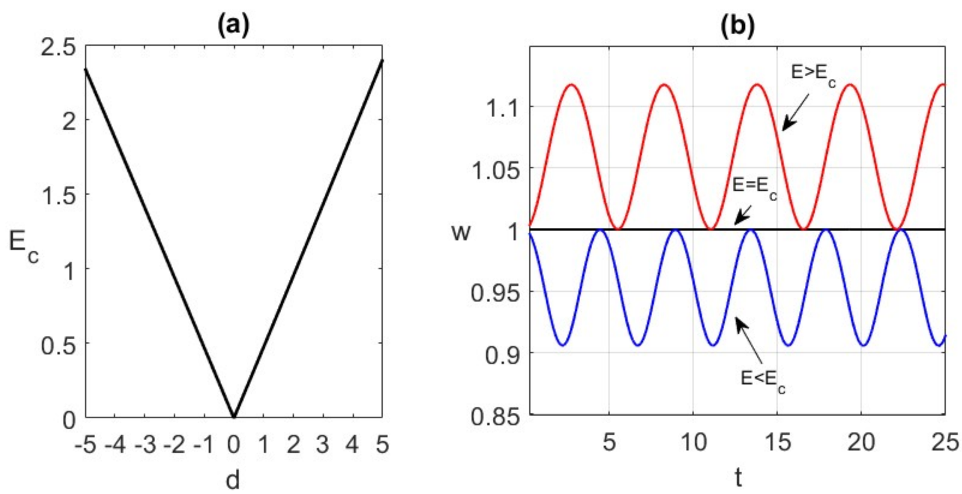

Figure 6.10: (a) The variation of critical energy E_c for different d. (b) Variation of soliton width with propagation for $E < E_c$, $E = E_c$, and $E > Ec$.

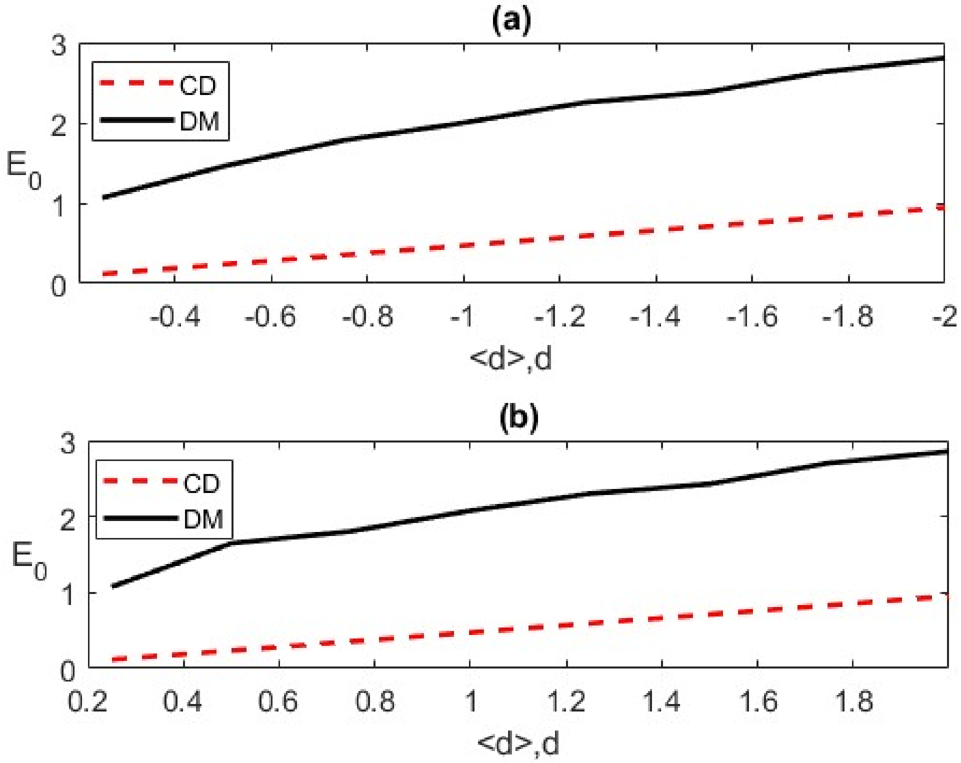

Figure 6.11: Variation of beam energy with (a) variation of negative average diffraction $\langle d\rangle$, d_1 is varied keeping $d_2 = -10$ (b) variation of positive average diffraction $\langle d\rangle$, d_1 is varied keeping $d_2 = 10$. The black line represents the Diffraction management beam, while the red line represents the constant diffraction beam (CD).

To show the influence of TOD and FOD on the soliton peak amplitude, we find and plot the same for different $\langle d\rangle$ (Figure 6.9), once in the presence of TOD only($d_3 = 3,\ d_4 = 0$) and then in the presence of FOD only ($d_4 = 12,\ d_3 = 0$). As such, no significant peak amplitude variation is observed. Therefore, short-range applications TOD and FOD can be neglected.

The critical energy (E_c) to form soliton can be determined from equation 6.12, by putting $\frac{\partial\mu}{\partial t} = 0$. The critical energy comes out to be $E_c = \frac{15w\sigma_1+\sqrt{15}\sqrt{15w^2\sigma_1^2+128d\sigma_3(\pi^2w^4\mu^2-1)}}{16\sigma_3}$. E_c increases monotonically with the increase in 'd', whether normal (positive) or anomalous (negative) (Figure 6.10a). An EM wave with energy exactly equal to E_c will give rise to a soliton of constant width (Figure 6.10(b)), while a wave with energy both less and greater than E_c will exhibit soliton (at a suitable parametric range) with periodically oscillating width.

Further, we compare initial beam energy (E_0) for the diffraction-managed system with a constant dispersion (CD) by plotting E_0 with respect to $\langle d \rangle$ and d (Figure 6.11)

The E_0 required for diffraction-management is higher than that for the CD system and increases more rapidly with d or $\langle d \rangle$ compared to the CD system. It is exactly opposite to the dispersion-managed system as well as the previous report on accessible soliton in a non-local nonlinear media (ref [365]), where E_0 for diffraction-managed soliton is smaller than that of CD soliton. Therefore, in our nonlinear metamaterial, a beam of higher energy (with respect to the CD system) can be produced using diffraction-management, and energy can be controlled using diffraction.

6.4 Soliton Interaction

The solitonic nature of the localized structure can be confirmed only after determining the interaction dynamics to check whether the interacting solitons maintain their shape and size after the collision. Moreover, soliton interaction many times leads to intriguing novel phenomena that can be further used to realize switching, controller, sensor, etc. The soliton interaction profiles show the self-confined 'particle-like' nature for different separation between the interacting solitons (Figure 6.12) and for different value of $\langle d \rangle$ (Figure 6.13). In this case, breather solitons are generated. The interaction gets weaker with an increase in separation. Interactions of soliton with TOD (Figure 6.14−6.16) and FOD (Figure 6.17−6.19) also show the self-confined breather solitons. Also, the TOD and FOD varied simultaneously to reveal the interaction profile as is shown in Figures 6.20 and 6.21. It may be noted the initial values of $\mu,\ w,\ \sigma_1$ and σ_3 were set to $0,\ 1,\ 8.44$ and 8.44×10^{-2} respectively, throughout the study, unless mentioned otherwise.

(a) $\langle d \rangle = -1$			(b) $\langle d \rangle = 1$		
d_1	d_2	E_0	d_1	d_2	E_0
-7	5	2.9866291055	7	-5	1.05057779103
-8	6	4.0400470601	8	-6	1.227237213
-9	7	4.3464335566	9	-7	1.41340419064
-10	8	4.9491193738	10	-8	1.59834161162
-11	9	6.9310915143	11	-9	1.84089057572
-12	10	6.3150217130	12	-10	2.00101010100
-13	11	6.9620865374	13	-11	2.21234048300
-14	12	5.7442150574	14	-12	2.39080693983
-15	13	7.7060105216	15	-13	2.39643923535
-16	14	9.5333700775	16	-14	2.66848822434
-17	15	11.3060061883	17	-15	3.25321247500
-18	16	12.7099837838	18	-16	3.40821565800
-19	17	15.6209829974	19	-17	3.37175399151
-20	18	16.9690012685	20	-18	3.98144443300
-21	19	18.3249334056	21	-19	4.20240913451

Table 6.1: Variation of initial beam energy with the variation of d_1 and d_2, for (a) negative average diffraction $\langle d \rangle = -1$, and (b) positive average diffraction $\langle d \rangle = 1$

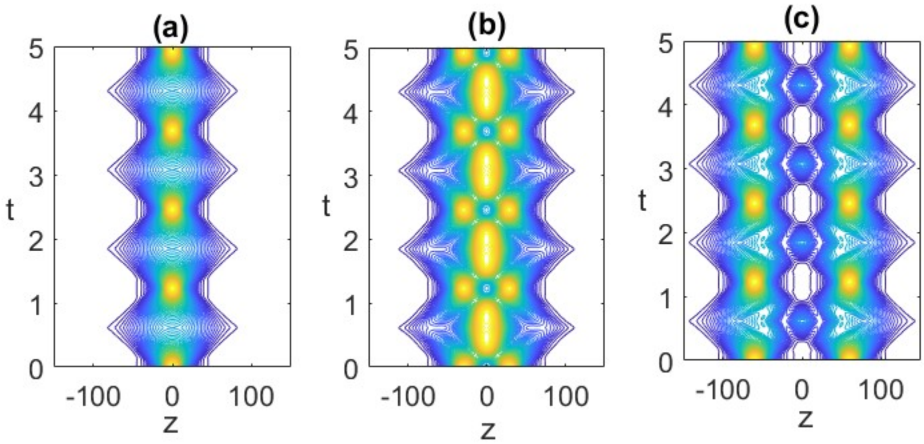

Figure 6.12: Solitons interaction (contour plots) at separation (a) 0, (b) 30 and (c) 60 (normalized units)

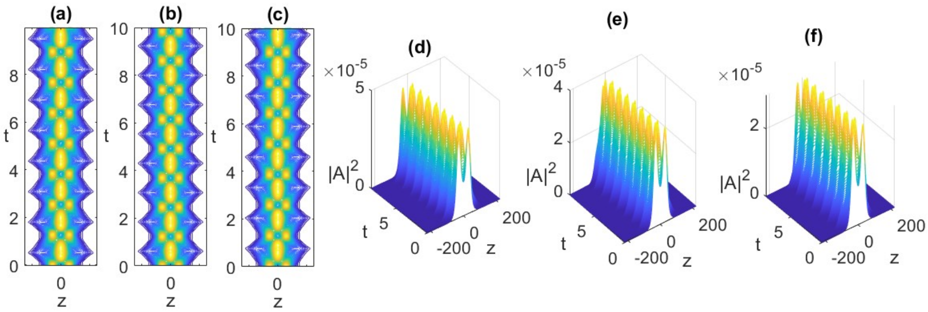

Figure 6.13: Contour plots for the soliton interaction (at a separation of 30 normalized units) (a) positive $\langle d \rangle$; LHM is 1.2 times, and RHM is 0.8, (b) negative $\langle d \rangle$; LHM is 0.8 times, and RHM is 1.2, (c) zero $\langle d \rangle$.

(d), (e) and (f) are the intensity profiles corresponding to (a), (b), and (c), respectively.

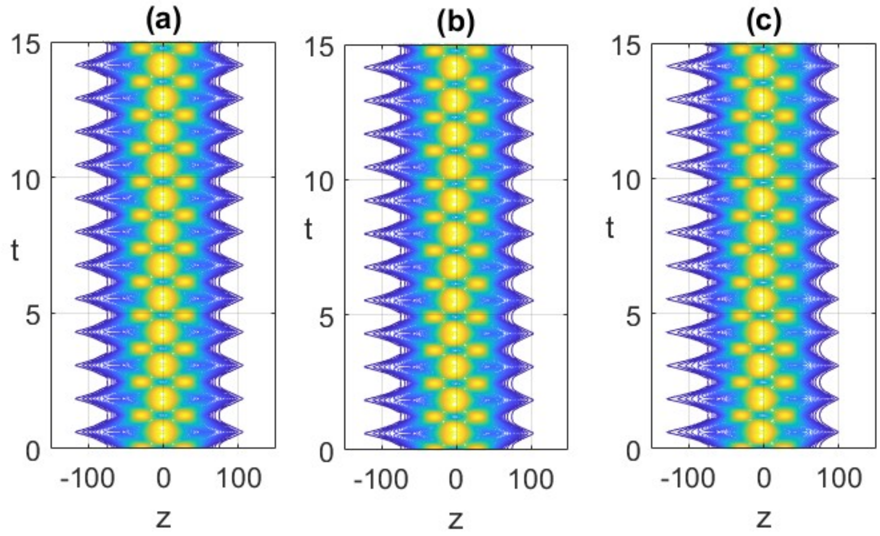

Figure 6.14: Contour plots of interactions of soliton (at a separation of 30 normalized units) for TOD coefficient (a) 1, (b) 2, and (c) 3. Here $\langle d \rangle = 0$.

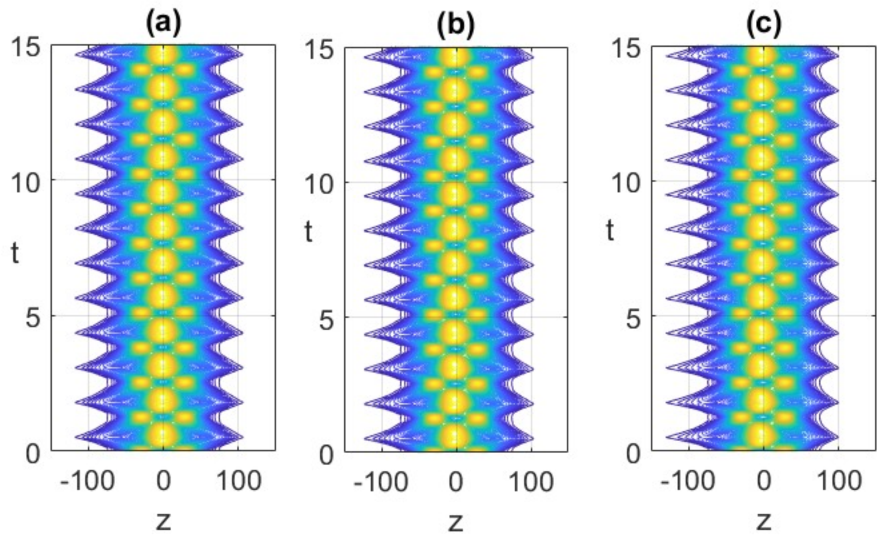

Figure 6.15: Contour plots for interactions of soliton (at a separation of 30 normalized units) for *positive* $\langle d \rangle$; LHM is 1.2, and RHM is 0.8, having TOD coefficient (a) 1, (b) 2, and (c) 3.

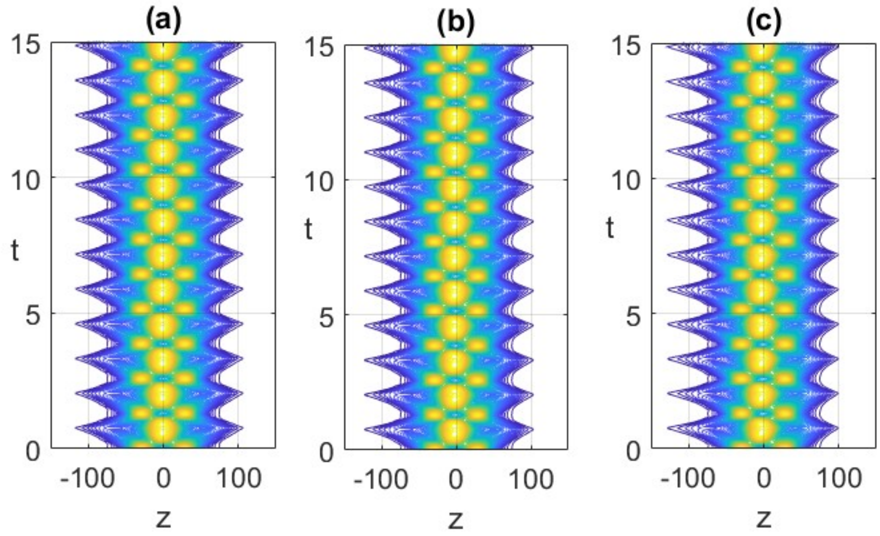

Figure 6.16: Same as Figure 6.15 for *negative* $\langle d \rangle$

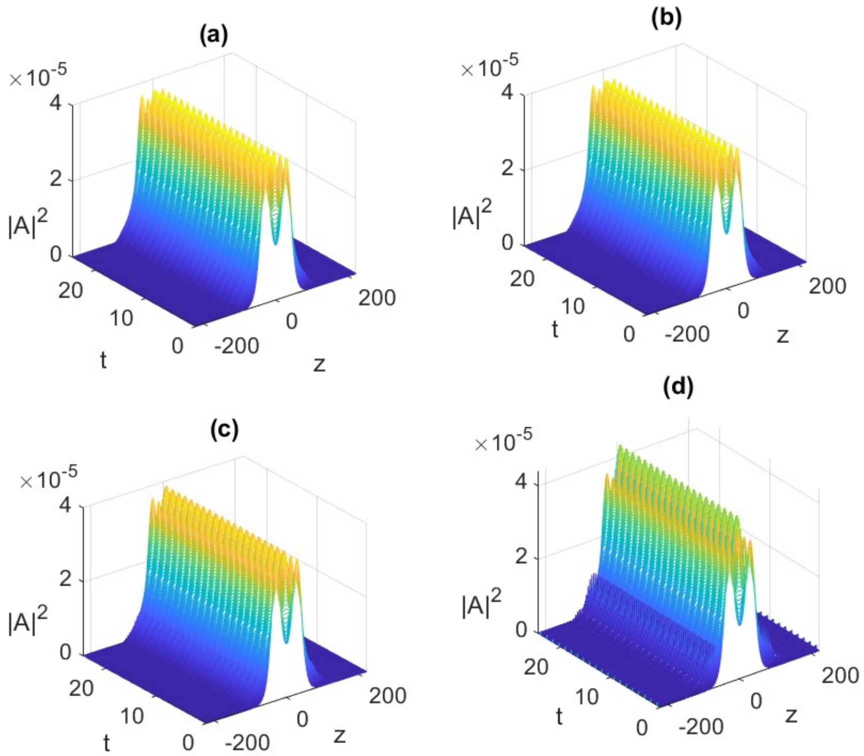

Figure 6.17: Intensity profile for interactions of soliton (at a separation of 30 normalized units) for FOD coefficient (a) 9, (b) 10, (c) 11 and (d) 12. Here $\langle d \rangle = 0$

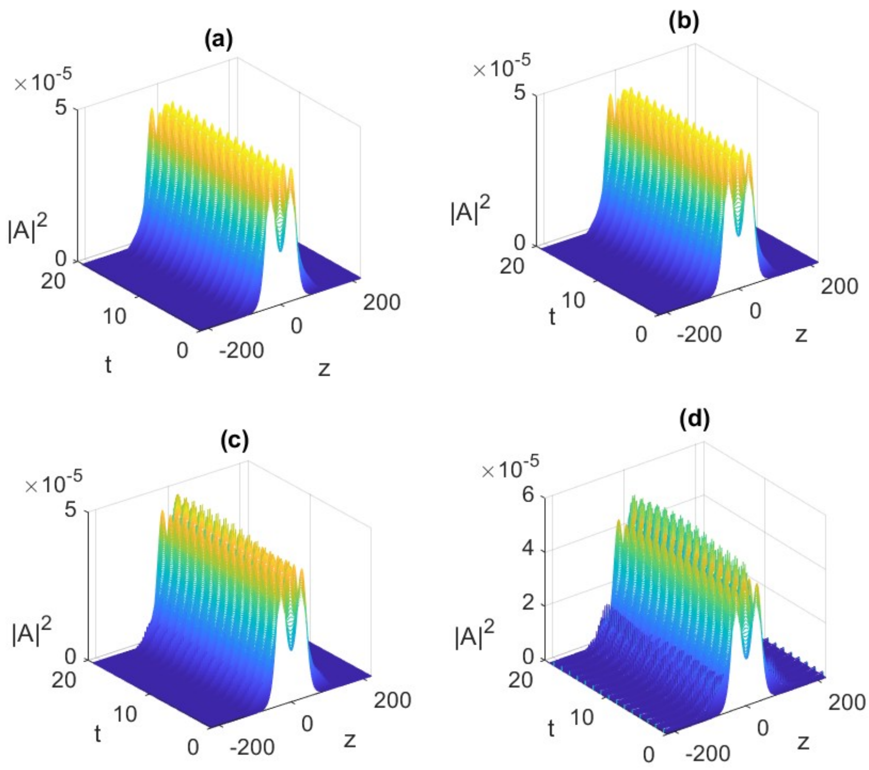

Figure 6.18: Same as Figure 6.17 for positive $\langle d \rangle$.

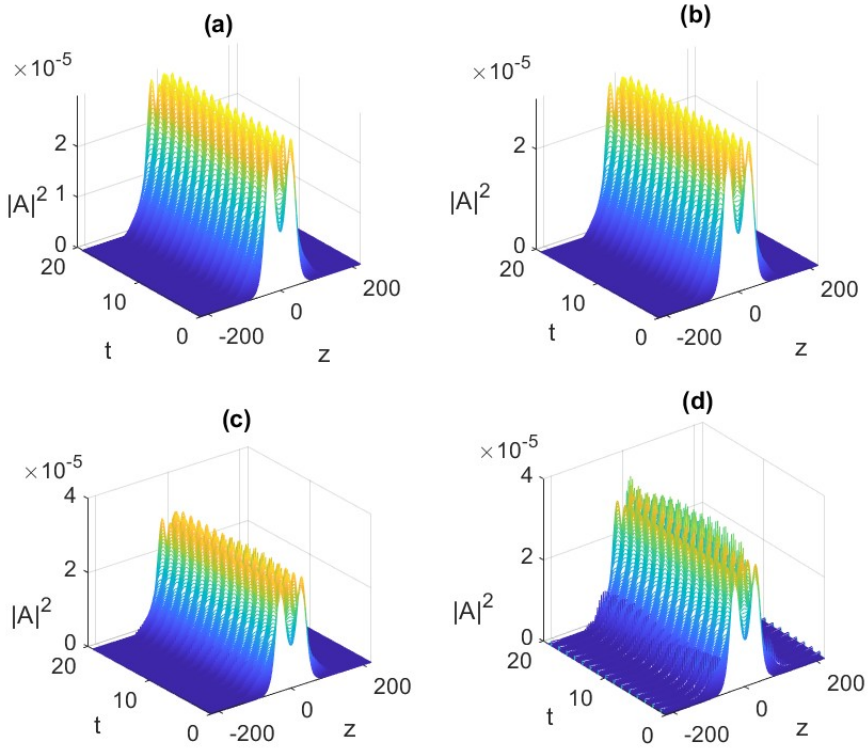

Figure 6.19: Same as Figure 6.17 for negative $\langle d \rangle$.

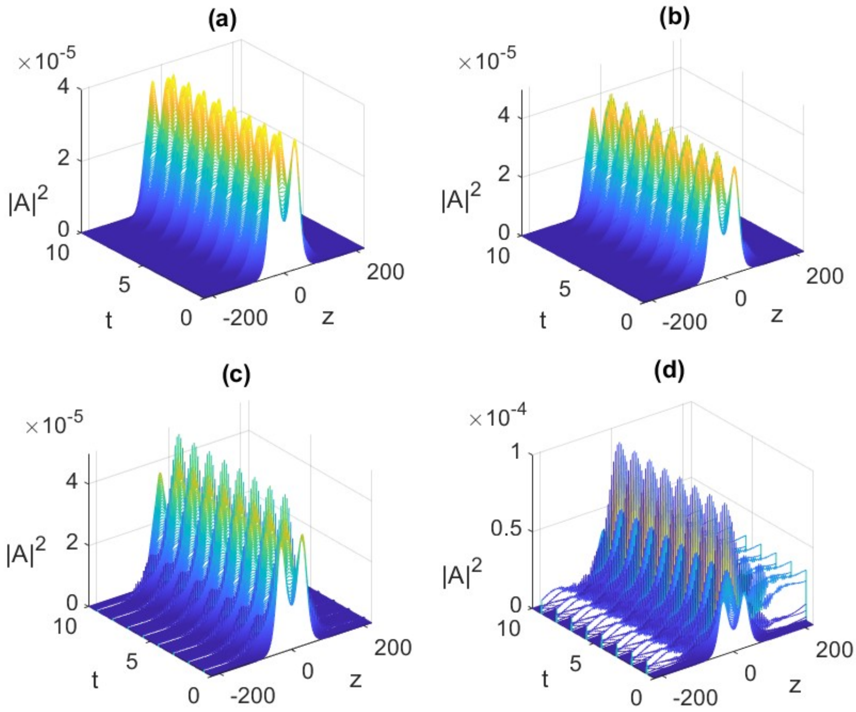

Figure 6.20: The intensity profile for the interaction of beam (at a separation of 30 normalized units) having TOD and FOD. The TOD and FOD coefficients are, respectively, (a) 0.5 and 9, (b) 0.5 and 10, (c) 1 and 9, and (d) 1 and 10.

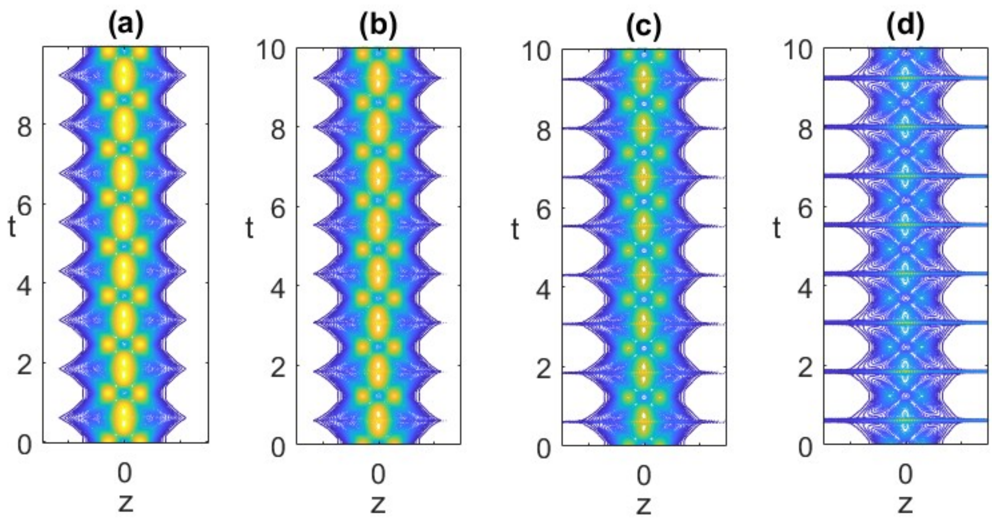

Figure 6.21: The contour plots corresponding to Figure 6.20.

6.5 Stability Analysis

For any dynamic system, and hence for solitons, stability is an essential issue. In this section, we perform stability analysis following two roots: firstly, we use the resultant set of ODEs from LVM, and thereafter, we adopt the perturbation technique, wherein the Eigenvalues play the decisive role. In the first method, to examine the stability of the diffraction-managed solitons and reveal the evolution of beam parameters during propagation, we solve the coupled ODEs of w and μ (equation 6.11 and 6.12) using the Range-Kutta 45 method, with periodic boundary conditions namely $\mu(0) = \mu(L)$ and $w(0) = w(L)$. The evolution of w and μ and the phase diagrams are shown in Figure 6.22. Here $d_1 = 10$ and $d_2 = -8$,i.e., $\langle d\rangle = 1$. The $(w - \mu)$ phase plot (Figure 6.22(a)) is a closed loop indicating a stable soliton propagation. The periodic behaviour of the width is confirmed by Figure 6.22(b). The variation of chirp, however, is not periodic (Figure 6.22(c)). Similar behaviour of w and μ is found for negative $\langle d\rangle$ (Figure 6.23).

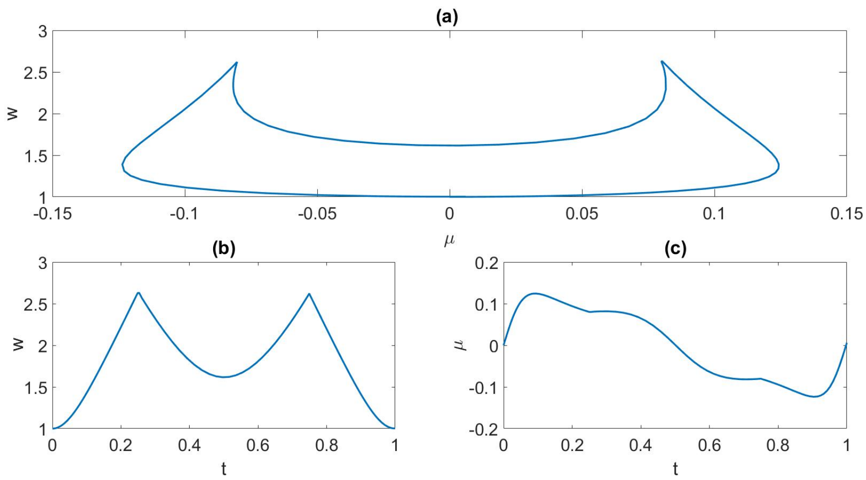

Figure 6.22: (a) Width and chirp $(w - \mu\ )$ phase trajectory. Evolution of (b) width and (c) chirp. Here, $d_1 = 10$, $d_2 = -8$, $\langle d\rangle = 1$.

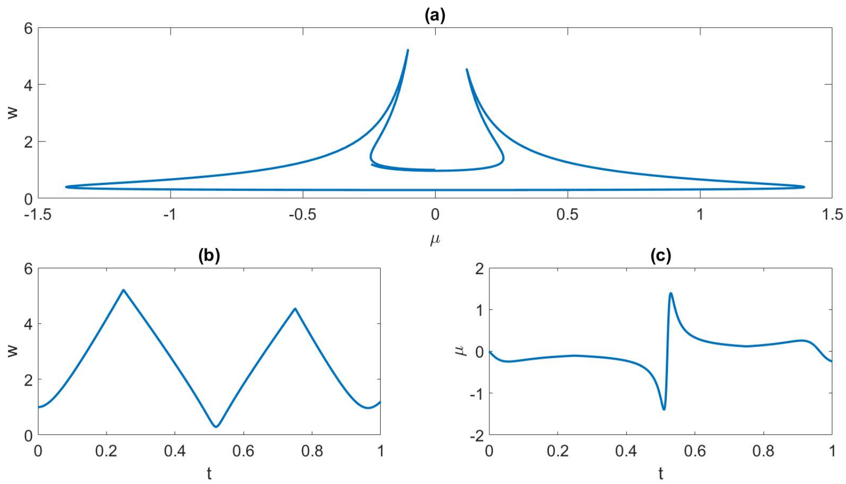

Figure 6.23: (a) width and chirp ($w - \mu$) phase trajectory. Evolution of (b) width and (c) chirp. Here, $d_1 = -10$, $d_2 = 8$, $\langle d \rangle = -1$.

The variation of E_0 with the variation of d_1 and d_2 has been calculated, keeping the $\langle d \rangle$ constant. For negative average diffraction, i.e., $\langle d \rangle = -1$ (Table 6.1(a)), the energy keeps on increasing as the values of d_i ($i = 1, 2$) increase. A similar trend is found for positive average diffraction, i.e., $\langle d \rangle = +1$. The second method of stability analysis has been performed by perturbation method using the equations 6.11 and 6.12. As per the standard procedure, a perturbation (i.e., a slight deviation from the equilibrium point) is added to the equilibrium width (w_0) and equilibrium chirp (μ_0). Putting the new initial values, namely, $w = w_0 + w'$ and $\mu = \mu_0 + \mu'$, (the primed symbols are the perturbation parts) in equations 6.11 and 6.12 and subsequently linearizing we get a set of equations that can be represented as following matrix equation:

$$\frac{d}{dt}\begin{pmatrix} \mu' \\ w' \end{pmatrix} = \begin{pmatrix} -8\mu d & M \\ 4dw & 4\mu d \end{pmatrix}\begin{pmatrix} \mu' \\ w' \end{pmatrix} \tag{6.14}$$

with, $M = \frac{-240\pi^2 d\mu^2 w^3 - 15E_0\sigma_1}{15\pi^2 w^4} - \frac{4\left(-60\pi^2 d\mu^2 w^4 + 60d + 8E_0^2\sigma_3 - 15E_0\sigma_1 w\right)}{15\pi^2 w^5}$.

The 2×2 on the right-hand side of the above equation is called the stability matrix, which can be solved for the characteristics equation (of the eigenvalue λ) as follows:

$$\begin{vmatrix} -8\mu d - \lambda & M \\ 4dw & 4\mu d - \lambda \end{vmatrix} = 0 \tag{6.15}$$

$$\lambda^2 + 4d\mu\lambda - (32d^2\mu^2 + 4dMw) = 0, \tag{6.16}$$

Equation 6.16 is the characteristic equation, which eventually gives rise to a pair of eigenvalues:

$$\lambda_1 = 2\left(-\sqrt{9d^2\mu^2 + dMw} - \mu d\right) \tag{6.17}$$

$$\lambda_2 = 2\left(-\sqrt{9d^2\mu^2 + dMw} + \mu d\right). \tag{6.18}$$

The properties of the eigenvalues determine the nature of the stability of the soliton [366]. The system will be stable if the real part of both the eigenvalues are negative. Figure 6.24 shows the contour plots of the real and imaginary parts of the eigenvalues with the average diffraction and chirp. This can be used to identify the stability zones. The system is stable near the origin $(0, 0)$ and in the lower parts of the first and third quadrants for real λ_1 and λ_2 (first column of Figure 6.24). The real part of λ_2 is zero in the middle and in the lower part of the first and third quadrants, which renders the system neutral. However, λ_1 has negative values in the same region, which implies that the system is stable for that region. The variation of λ_1 and λ_2 with chirp (μ) is given in Figure 6.25. For our particular set of systems parameters and their neighbouring values, no stable and unstable nodes are available. Here, one can see the recent stability analysis results in a nonlocal nonlinear system (ref [365]), wherein stable and unstable nodes are available. Now, whether it is due to the nonlocality of the nonlinearity just for the different sets of parameters is a question of further investigation.

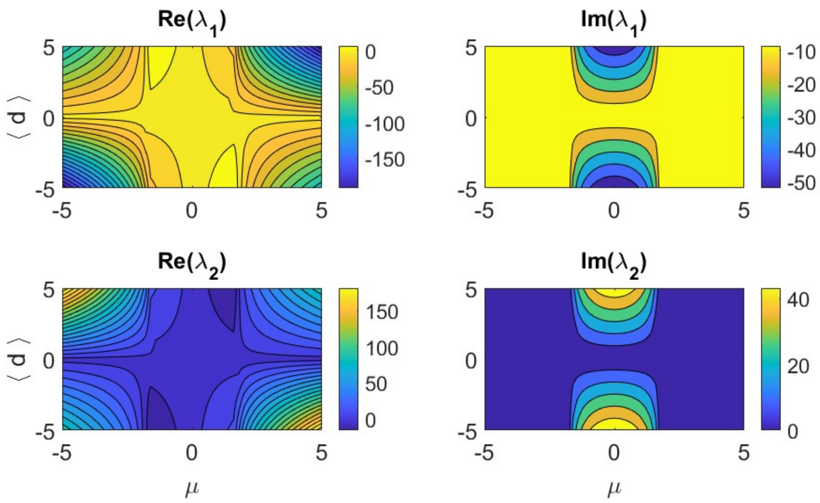

Figure 6.24: Contour plots for real and imaginary parts of the eigenvalues (λ_1 and λ_2) with respect to the chirp (μ) and average diffraction ($\langle d \rangle$).

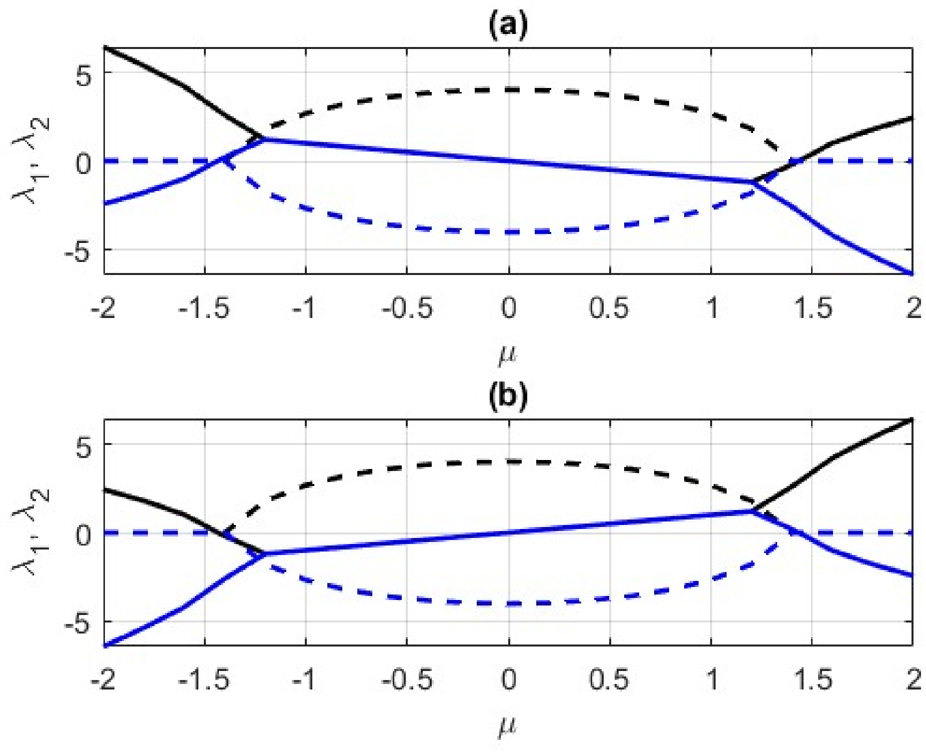

Figure 6.25: Variation of eigenvalue with respect to chirp (μ), (a) for d=0.5, (b) for d=-0.5. The black line is for λ_1, and blue is for λ_2. The solid line is for the real part, and the dashed line is for the imaginary part.

6.6 Conclusion

The breather soliton is generated in a diffraction-managed metamaterial consisting of an array of RHM (positive diffraction) and LHM (negative diffraction) slabs. The system is solved analytically using LVM and numerically using SSFM. The soliton beam energy for the diffraction-managed system is found to be higher than that of the constant diffraction system. Thus, the system can be used to produce a high-energy beam. The soliton dynamics are studied under the effect of TOD and FOD. The beam width gets asymmetric under the FOD effect, while the effect of the FOD is marginal. The soliton interactions are also studied for higher-order diffraction. The stability zones for the system are identified using two different approaches: the phase diagram method and the perturbation method. The results of the current investigation can be used for further theoretical and experimental research on diffraction-managed soliton in metamaterials with higher-order diffraction and nonlinearity.

Chapter 7

Summary, Applications and Future Scope

7.1 Summary and applications

Theoretical investigation presented in this thesis focuses on three main objectives; investigating the existence of solitons in metamaterials based on SRR with higher-order nonlinearity, revealing the dynamics of the generated solitons and analyzing soliton stability as well as identifying the parametric zone of soliton stability. Both analytical and numerical methods are employed to accomplish these objectives. The summary of the findings is as follows: Compound DSs are generated and stabilized within the SRR-based metamaterial featuring cubic-quintic nonlinearity, multi-photon absorption, and diffusion. The outcomes of this investigation confirm the two fundamental aspects of any soliton: the evolution of a self-similar wave profile and preserving the self-similar profile even after interaction with another soliton. The interaction of DSs can be manipulated by adjusting their separation and relative phase, where a smaller separation or an increase in self-diffraction leads to early interaction. Introducing a phase difference or varying the amplitude of any DS symmetry of the interaction profile can be broken. This allows switching phenomena by tuning the phase difference between the DSs. Notably, a weak DS is discovered to exert control over a stronger one, a phenomenon familiar in optics but perhaps less recognized in SRR-based metamaterials. The above findings have practical implications for designing metamaterial-based devices reliant on higher-order nonlinearity and multiphoton absorption. They may also aid in identifying and optimizing the operational region of such devices. Given the inclusion of diffusion in this model, it could be strategically employed for sensing applications in chemical mixing, thermal management, electronics, material processing, etc., where diffusion plays a critical role. Additionally, the incorporation of multi-photon absorption in the model makes it a promising candidate for applications in TPA-assisted medical imaging.

Dissipative solitons are generated in a hybrid metamaterial, wherein graphene is embedded in SRR structures. Solitons arise from three distinct modes: a bright symmetric mode, a dark asymmetric mode induced by the SRR, and another dark asymmetric mode facilitated by graphene. The stability zones of these solitons are determined, and their behaviour is explored across a wide parametric range. This straightforward methodology for identifying the solitonic propagation region of electromagnetic waves is applicable to a diverse array of metamaterials and beyond. Experimental validation of these findings is recommended for future investigation, and the results can serve as a valuable guide for charting the stable soliton ranges based on system parameters. The combination of SRR's negative refractive index properties, capabilities like acting as a perfect lens, and exhibiting thickness-dependent optical properties can now be synergized with graphene's unique attributes in biomedical, solid-state, electronics, and optics applications. This investigation holds potential for extension to multi-layer graphene, offering a cost-effective alternative to monolayer graphene. Leveraging the graphene layer allows for the utilization of all the advantages it brings, such as electrically controlled gating, in the design of various applications.

Solitons are generated in cubic-quintic nonlinear metamaterials based on SRR in the presence of higher-order effects such as third-order diffraction, self-steepening, and Raman scattering. These solitons exhibit robustness against perturbations up to a certain threshold. Both the self-steepening and Raman scattering can cause retardation of the soliton and the pulse retardation becomes more pronounced, particularly with greater quintic nonlinearity. Notably, self-steepening induces relatively more significant retardation compared to Raman scattering. The interaction between two pulses in such higher-order nonlinear media follows the expected attraction-repulsion or union-separation pattern, although disruption occurs at greater values of both self-steepening and Raman scattering. As anticipated, the variations in pulse separation and phase difference between interacting pulses can significantly modify interaction dynamics. This phenomenon can be utilized, in principle, for the creation of all-optical switching or all-optical monitoring devices.

A different type of soliton, namely, the breather soliton, is generated in a diffraction-managed metamaterial consisting of an array of right-handed material, i.e., positive diffraction and left-handed material, i.e., negative diffraction slabs. The energy of the soliton beam in the diffraction-managed system is observed to be higher compared to that in a system with constant diffraction. Consequently, this system holds the potential for generating high-energy beams. The dynamics of the breather soliton are investigated in the presence of third and fourth-order diffraction. Under the influence of third-order diffraction, the beam width profile during propagation becomes asymmetric, while the impact of fourth-order diffraction is marginal. Additionally, soliton interactions are examined for higher-order diffraction. The stability zones of the system are identified using two different approaches: a phase diagram and a perturbation approach. The findings of this study provide valuable insights for further theoretical and experimental exploration of diffraction-managed solitons in metamaterials featuring higher-order diffraction and nonlinearity.

For further validation of the findings and their implementation in device fabrication, experimental configurations can be devised incorporating a suitable nonlinear metamaterial based on SRR, an electromagnetic signal source, and an appropriate detector. The choice of both the source and the detector can be tailored according to the specific application. For instance, in the context of generating a dispersive soliton within the optical wavelength, laser light can be employed in conjunction with a polarizer. A detector, such as a spectrometer or a CCD camera tuned to the operating wavelength, can be integrated into the setup.

7.2 Future Scope

The current investigation presented in the thesis can be further extended to cover wider areas and deeper levels. Different types of nonlinear metamaterial models, including graphene-saturable absorbers, have been used. One can further explore stable soliton generation and dynamics in other variants of saturable nonlinearity models, e.g., graphene flakes of different dimensions, distribution, and different no of graphene layers. In fact, using the methodology presented in the thesis, one can find solitons in metamaterial (and others) with any known type of nonlinearity model. Even if a particular media's nonlinear and dispersion profile is known, our methodology may predict stable solitons in such media. Investigation can be undertaken into spontaneous and as well interaction dynamics in SSR-based metamaterial, wherein the SRRs are irregular in size and unevenly orientated, leading to inhomogeneity of the media. In actual practice, systems will be more or less inhomogeneous. Therefore, the extended investigation can mimic the practical scenario so that experimental work can be facilitated. In the earlier section, we suggested some potential applications of the output of the thesis work. Further investigations can be done to reveal the strengths, weaknesses, opportunities and challenges of the theory to realise the applications.

Bibliography

[1] Orazio Descalzi, Marcel Clerc, Stefania Residori, and Gaetano Assanto. *Localized states in physics: solitons and patterns*. Springer Science & Business Media, 2011.

[2] Dumitru Mihalache. Localized structures in optical and matter-wave media: a selection of recent studies. *Rom. Rep. Phys*, 73(2):403, 2021.

[3] Dumitru Mihalache. Multidimensional localized structures in optics and bose-einstein condensates: A selection of recent studies. *Rom. J. Phys*, 59(3-4):295–312, 2014.

[4] Ryogo Hirota and Junkichi Satsuma. N-soliton solutions of model equations for shallow water waves. *Journal of the Physical Society of Japan*, 40(2):611–612, 1976.

[5] DR Christie, KJ Muirhead, and AL Hales. Intrusive density flows in the lower troposphere: A source of atmospheric solitons. *Journal of Geophysical Research: Oceans*, 84(C8):4959–4970, 1979.

[6] Veit Schwämmle and Hans J Herrmann. Solitary wave behaviour of sand dunes. *Nature*, 426(6967):619–620, 2003.

[7] Adrian Constantin. On the relevance of soliton theory to tsunami modelling. *Wave Motion*, 46(6):420–426, 2009.

[8] Adrian Constantin and David Henry. Solitons and tsunamis. *Zeitschrift für Naturforschung A*, 64(1-2):65–68, 2009.

[9] Paul B Umbanhowar, Francisco Melo, and Harry L Swinney. Localized excitations in a vertically vibrated granular layer. *Nature*, 382(6594):793–796, 1996.

[10] Mariano Cadoni, Roberto De Leo, and Giuseppe Gaeta. Solitons in a double pendulums chain model, and dna roto-torsional dynamics. *Journal of Nonlinear Mathematical Physics*, 14(1):128–146, 2007.

[11] Huang Guoxiang and Xu Zaixin. Kinks and solitons in coupled pendulum lattices. *Chinese Physics Letters*, 9(12):659, 1992.

[12] VB Taranenko, G Slekys, and CO Weiss. Spatial resonator solitons. *Chaos: An Interdisciplinary Journal of Nonlinear Science*, 13(2):777–790, 2003.

[13] Daniel C Cole, Erin S Lamb, Pascal Del'Haye, Scott A Diddams, and Scott B Papp. Soliton crystals in kerr resonators. *Nature Photonics*, 11(10):671–676, 2017.

[14] Vladimir K Vanag. Waves and patterns in reaction–diffusion systems. belousov–zhabotinsky reaction in water-in-oil microemulsions. *Physics-Uspekhi*, 47(9):923, 2004.

[15] Yoshiki Kuramoto and Tomoji Yamada. Pattern formation in oscillatory chemical reactions. *Progress of theoretical physics*, 56(3):724–740, 1976.

[16] James B Benedict. Experiments on lichen growth. i. seasonal patterns and environmental controls. *Arctic and Alpine Research*, 22(3):244–254, 1990.

[17] Claus Bässler, Marc W Cadotte, Burkhard Beudert, Christoph Heibl, Markus Blaschke, Johannes Heribert Bradtka, Thomas Langbehn, Silke Werth, and Jörg Müller. Contrasting patterns of lichen functional diversity and species richness across an elevation gradient. *Ecography*, 39(7):689–698, 2016.

[18] George I Stegeman and Mordechai Segev. Optical spatial solitons and their interactions: universality and diversity. *Science*, 286(5444):1518–1523, 1999.

[19] Robert A Meyers et al. *Encyclopedia of complexity and systems science*, volume 9. Springer New York, 2009.

[20] Norman J Zabusky and Martin D Kruskal. Interaction of" solitons" in a collisionless plasma and the recurrence of initial states. *Physical review letters*, 15(6):240, 1965.

[21] Jing Yang, Zhenghua Huang, Yu Zhu, Qin Zhou, Jitao Li, Yunzhou Sun, Hashim M Alshehri, and Anjan Biswas. Soliton–soliton interaction and its influence on soliton amplitude and period. *Results in Physics*, 30:104831, 2021.

[22] Falk Lederer, George I Stegeman, Demetri N Christodoulides, Gaetano Assanto, Moti Segev, and Yaron Silberberg. Discrete solitons in optics. *Physics Reports*, 463(1-3):1–126, 2008.

[23] Hermann A Haus. Optical fiber solitons, their properties and uses. *Proceedings of the IEEE*, 81(7):970–983, 1993.

[24] Soumendu Jana, Swapan Konar, and Manoj Mishra. Soliton switching in fiber coupler with periodically modulated dispersion, coupling constant dispersion and cubic quintic nonlinearity. *Zeitschrift für Naturforschung A*, 63(3-4):145–151, 2008.

[25] Diana Mandelik, R Morandotti, JS Aitchison, and Yaron Silberberg. Gap solitons in waveguide arrays. *Physical review letters*, 92(9):093904, 2004.

[26] HS Eisenberg, R Morandotti, Yaron Silberberg, JM Arnold, Giovanni Pennelli, and JS Aitchison. Optical discrete solitons in waveguide arrays. i. soliton formation. *JOSA B*, 19(12):2938–2944, 2002.

[27] AR Bishop, JA Krumhansl, and SE Trullinger. Solitons in condensed matter: a paradigm. *Physica D: Nonlinear Phenomena*, 1(1):1–44, 1980.

[28] Tal Carmon, Marin Soljačić, and Mordechai Segev. Pattern formation in a

cavity longer than the coherence length of the light in it. *Physical Review Letters*, 89(18):183902, 2002.

[29] Thomas H Lee. Electrical solitons come of age. *Nature*, 440(7080):36–37, 2006.

[30] Yongmin Liu, Guy Bartal, Dentcho A Genov, and Xiang Zhang. Subwavelength discrete solitons in nonlinear metamaterials. *Physical Review Letters*, 99(15):153901, 2007.

[31] Anjan Biswas, Kaisar R Khan, Mohammad F Mahmood, and Milivoj Belic. Bright and dark solitons in optical metamaterials. *Optik*, 125(13):3299–3302, 2014.

[32] Alan J Heeger, Steven Kivelson, John Robert Schrieffer, and W-P Su. Solitons in conducting polymers. *Reviews of Modern Physics*, 60(3):781, 1988.

[33] Laren M Tolbert. Solitons in a box: the organic chemistry of electrically conducting polyenes. *Accounts of chemical research*, 25(12):561–568, 1992.

[34] Hidekazu Kuwayama and Shuji Ishida. Biological soliton in multicellular movement. *Scientific reports*, 3(1):2272, 2013.

[35] Guo-Ping Zhou. Biological functions of soliton and extra electron motion in dna structure. *Physica Scripta*, 40(5):698, 1989.

[36] Anjan Biswas, Abdul H Kara, Michelle Savescu, Ashfaque H Bokhari, and FD Zaman. Solitons and conservation laws in neurosciences. *International Journal of Biomathematics*, 6(03):1350017, 2013.

[37] Oswaldo González-Gaxiola, Anjan Biswas, Luminita Moraru, and Abdulah A Alghamdi. Solitons in neurosciences by the laplace–adomian decomposition scheme. *Mathematics*, 11(5):1080, 2023.

[38] JF Gregg, I Petej, E Jouguelet, and C Dennis. Spin electronics—a review. *Journal of Physics D: Applied Physics*, 35(18):R121, 2002.

[39] AN Bogdanov and AT Skvortsov. Nonlinear shear waves in granular medium. *SOVIET PHYSICS ACOUSTICS C/C OF AKUSTICHESKII ZHURNAL*, 38:224–224, 1992.

[40] Stéphane Job, Francisco Melo, Adam Sokolow, and Surajit Sen. How hertzian solitary waves interact with boundaries in a 1d granular medium. *Physical review letters*, 94(17):178002, 2005.

[41] Curtis Callan, Jeff Harvey, and Andrew Strominger. Supersymmetric string solitons. *String theory and quantum gravity*, 91:208, 1991.

[42] Donam Youm. Black holes and solitons in string theory. *Physics Reports*, 316(1-3):1–232, 1999.

[43] John R Apel, Lev A Ostrovsky, Yury A Stepanyants, and James F Lynch. Internal solitons in the ocean and their effect on underwater sound. *The Journal of the Acoustical Society of America*, 121(2):695–722, 2007.

[44] Anna Karczewska, Piotr Rozmej, and Eryk Infeld. Shallow-water soliton dynamics beyond the korteweg–de vries equation. *Physical Review E*, 90(1):012907, 2014.

[45] Bharati Kakad, Amar Kakad, Harikrishnan Aravindakshan, and Ioannis Kourakis. Debye-scale solitary structures in the martian magnetosheath. *The Astrophysical Journal*, 934(2):126, 2022.

[46] John Scott Russell. *Report on Waves: Made to the Meetings of the British Association in 1842-43.* Richard and John E. Taylor, London, 1845.

[47] Henry Darcy and Henry Bazin. *Recherches hydrauliques: Recherches expérimentales sur l'écoulement de l'eau dans les canaux découverts. 1ère partie*, volume 1. Impr; Impériale, 1865.

[48] Glenn O Brown, Jürgen D Garbrecht, and Willi H Hager. Henry pg darcy and other pioneers in hydraulics. In *Contributions in celebration of the 200th birthday of Henry Philibert Gaspard Darcy*. American Society of Civil Engineers, 2003.

[49] Lord Rayleigh. On waves. *Phil. Mag.*, 1:257–259, 1876.

[50] Joseph Boussinesq. Théorie de l'intumescence liquide appelée onde solitaire ou de translation se propageant dans un canal rectangulaire. *CR Acad. Sci. Paris*, 72(755-759):1871, 1871.

[51] George Bidone. *Expériences sur le remou et sur la propagation des ondes*. de l'Imprimerie Royale, 1820.

[52] Yoshimi Goda. On the historical development of the mathematical theory of water waves. *35th Summer Training Course Lecture Collection, Japan Society of Civil Engineers Coastal Engineering Committee*, 1999.

[53] Alex Kasman. A brief history of solitons and the kdv equation. *Current Science*, 115(8):1486–1496, 2018.

[54] Clifford S Gardner, John M Greene, Martin D Kruskal, and Robert M Miura. Method for solving the korteweg-devries equation. *Physical review letters*, 19(19):1095, 1967.

[55] Akira Hasegawa. Soliton-based optical communications: An overview. *IEEE Journal of Selected Topics in Quantum Electronics*, 6(6):1161–1172, 2000.

[56] Govind P Agrawal. Nonlinear fiber optics. In *Nonlinear Science at the Dawn of the 21st Century*, pages 195–211. Springer, 2000.

[57] Steven A Kivelson, Daniel S Rokhsar, and James P Sethna. Topology of the resonating valence-bond state: Solitons and high-t c superconductivity. *Physical Review B*, 35(16):8865, 1987.

[58] Carmel Rotschild, Barak Alfassi, Oren Cohen, and Mordechai Segev. Long-range interactions between optical solitons. *Nature Physics*, 2(11):769–774, 2006.

[59] DL Sekulic, MV Sataric, MB Zivanov, and JS Bajic. Soliton-like pulses along electrical nonlinear transmission line. *Elektronika ir Elektrotechnika*, 121(5):53–58, 2012.

[60] JD Gibbon, IN James, and Irene M Moroz. An example of soliton behaviour in a rotating baroclinic fluid. *Proceedings of the Royal Society of London. A. Mathematical and Physical Sciences*, 367(1729):219–237, 1979.

[61] MA Helal. Soliton solution of some nonlinear partial differential equations and its applications in fluid mechanics. *Chaos, Solitons & Fractals*, 13(9):1917–1929, 2002.

[62] Gurbax Singh Lakhina, Satyavir Singh, Rajith Rubia, and Selvaraj Devanandhan. Electrostatic solitary structures in space plasmas: Soliton perspective. *Plasma*, 4(4):681–731, 2021.

[63] Diederik Johannes Korteweg and Gustav De Vries. Xli. on the change of form of long waves advancing in a rectangular canal, and on a new type of long stationary waves. *The London, Edinburgh, and Dublin Philosophical Magazine and Journal of Science*, 39(240):422–443, 1895.

[64] J Frenkel. On the theory of plastic deformation and twinning. *J. Phys.*, 1:137–149, 1939.

[65] Clifford S Gardner and GK Morikawa. Similarity in the asymptotic behavior of collision-free hydromagnetic waves and water waves. Technical report, New York Univ., New York. Inst. of Mathematical Sciences, 1960.

[66] Morikazu Toda. Vibration of a chain with nonlinear interaction. *Journal of the Physical Society of Japan*, 22(2):431–436, 1967.

[67] Akira Hasegawa and Frederick Tappert. Transmission of stationary nonlinear optical pulses in dispersive dielectric fibers. i. anomalous dispersion. *Applied Physics Letters*, 23(3):142–144, 1973.

[68] JE Bjorkholm and AA Ashkin. Cw self-focusing and self-trapping of light in sodium vapor. *Physical Review Letters*, 32(4):129, 1974.

[69] Bertil Hille. Ionic channels in excitable membranes. current problems and biophysical approaches. *Biophysical journal*, 22(2):283–294, 1978.

[70] Linn F Mollenauer, Roger H Stolen, and James P Gordon. Experimental observation of picosecond pulse narrowing and solitons in optical fibers. *Physical Review Letters*, 45(13):1095, 1980.

[71] Linn F Mollenauer and Roger H Stolen. The soliton laser. *Optics letters*, 9(1):13–15, 1984.

[72] AV Ustinov. Solitons in josephson junctions. *Physica D: Nonlinear Phenomena*, 123(1-4):315–329, 1998.

[73] X Liu, LJ Qian, and FW Wise. Generation of optical spatiotemporal solitons. *Physical review letters*, 82(23):4631, 1999.

[74] Stephane Barland, Jorge R Tredicce, Massimo Brambilla, Luigi A Lugiato, Salvador Balle, Massimo Giudici, Tommaso Maggipinto, Lorenzo Spinelli, Giovanna Tissoni, Thomas Knoedl, et al. Cavity solitons as pixels in semiconductor microcavities. *Nature*, 419(6908):699–702, 2002.

[75] William H Renninger and Frank W Wise. Optical solitons in graded-index multimode fibres. *Nature communications*, 4(1):1719, 2013.

[76] Tie Jun Cui, David R Smith, and Ruopeng Liu. *Metamaterials*. Springer, 2010.

[77] David R Smith, John B Pendry, and Mike CK Wiltshire. Metamaterials and negative refractive index. *Science*, 305(5685):788–792, 2004.

[78] Yongmin Liu and Xiang Zhang. Metamaterials: a new frontier of science and technology. *Chemical Society Reviews*, 40(5):2494–2507, 2011.

[79] Seojoo Lee, Soojeong Baek, Teun-Teun Kim, Hyukjoon Cho, Sangha Lee, Ji-Hun Kang, and Bumki Min. Metamaterials for enhanced optical responses and their application to active control of terahertz waves. *Advanced Materials*, 32(35):2000250, 2020.

[80] Viktor G Veselago. Electrodynamics of substances with simultaneously negative ϵ and μ. *Usp. fiz. nauk*, 92(7):517, 1967.

[81] William L Barnes, Alain Dereux, and Thomas W Ebbesen. Surface plasmon subwavelength optics. *nature*, 424(6950):824–830, 2003.

[82] Divya Chaturvedi and Singaravelu Raghavan. Srr-loaded metamaterial-inspired electrically-small monopole antenna. *Progress In Electromagnetics Research C*, 81:11–19, 2018.

[83] John B Pendry, AJ Holden, WJ Stewart, and I Youngs. Extremely low frequency plasmons in metallic mesostructures. *Physical review letters*, 76(25):4773, 1996.

[84] John Brian Pendry. Negative refraction makes a perfect lens. *Physical review letters*, 85(18):3966, 2000.

[85] DR Smith, Willie Padilla, DC Vier, SC Nemat-Nasser, and S Schultz. Negative permeability from split ring resonator arrays. In *The European Conference on Lasers and Electro-Optics*, page JSTuA5. Optica Publishing Group, 2000.

[86] P Markoš and CM Soukoulis. Transmission studies of left-handed materials. *Physical Review B*, 65(3):033401, 2001.

[87] Alexander A Zharov, Ilya V Shadrivov, and Yuri S Kivshar. Nonlinear properties of left-handed metamaterials. *Physical Review Letters*, 91(3):037401, 2003.

[88] Ilya Shadrivov, Andrey Sukhorukov, Yuri Kivshar, et al. Nonlinear guided waves and solitons in left-handed materials. In *Proceedings of the 2004 URSI EMTS International Symposium on Electromagnetic Theory*, pages 742–744. International Union of Radio Science, 2004.

[89] N Lazarides, M Eleftheriou, and GP Tsironis. Discrete breathers in nonlinear magnetic metamaterials. *Physical review letters*, 97(15):157406, 2006.

[90] Pradipta Giri, Kamal Choudhary, Arnab Sen Gupta, AK Bandyopadhyay, and Arthur R McGurn. Klein-gordon equation approach to nonlinear split-ring resonator based metamaterials: One-dimensional systems. *Physical Review B*, 84(15):155429, 2011.

[91] Bijoy Mandal, Sutapa Adhikari, Reshmi Basu, Kamal Choudhary, Subhro Jyoti Mandal, Arindam Biswas, AK Bandyopadhyay, AK Bhattacharjee, and D Mandal. Role of coupling of discrete breathers in split-ring-resonator-based metamaterials. *Physica Scripta*, 86(1):015601, 2012.

[92] Arthur R McGurn. Barrier transmission map of one-dimensional nonlinear split-ring-resonator-based metamaterials: Bright, dark, and gray soliton resonances. *Physical Review B*, 88(15):155110, 2013.

[93] Arthur R McGurn. Transmission in a 1d split-ring resonator metamaterial containing a nonlinear barrier: soliton modes. In *Photonic and Phononic Properties of Engineered Nanostructures IV*, volume 8994, pages 94–106. SPIE, 2014.

[94] UA Mofiz. Optical solitons in negative-index meta-materials. In *2013 2nd International Conference on Advances in Electrical Engineering (ICAEE)*, pages 37–42. IEEE, 2013.

[95] Stefano Longhi. Gap solitons in metamaterials. *Waves in Random and Complex Media*, 15(1):119–126, 2005.

[96] Weina Cui, Yongyuan Zhu, Hongxia Li, and Sumei Liu. Self-induced gap solitons in nonlinear magnetic metamaterials. *Physical Review E*, 80(3):036608, 2009.

[97] C Martijn De Sterke and JE Sipe. Iii gap solitons. *Progess in Optics*, 33:203–260, 1994.

[98] Weina Cui, Yongyuan Zhu, Hongxia Li, and Sumei Liu. Soliton excitations in a one-dimensional nonlinear diatomic chain of split-ring resonators. *Physical Review E*, 81(1):016604, 2010.

[99] Wei-na Cui, Hong-xia Li, Min Sun, and Ling-bing Bu. Gap solitons in a chain of split-ring resonator dimers. *Physics Letters A*, 381(23):1950–1954, 2017.

[100] Daniel B Ostrowsky and Raymond Reinisch. *Guided wave nonlinear Optics*, volume 214. Springer Science & Business Media, 2012.

[101] Ilya V Shadrivov and Yuri S Kivshar. Spatial solitons in nonlinear left-handed metamaterials. *Journal of Optics A: Pure and Applied Optics*, 7(2):S68, 2005.

[102] AD Boardman, N King, RC Mitchell-Thomas, VN Malnev, and YG Rapoport. Gain control and diffraction-managed solitons in metamaterials. *Metamaterials*, 2(2-3):145–154, 2008.

[103] Arthur R Davoyan, Ilya V Shadrivov, and Yuri S Kivshar. Self-focusing and spatial plasmon-polariton solitons. *Optics express*, 17(24):21732–21737, 2009.

[104] Guy Bartal, Yongmin Liu, Dentcho A Genov, and Xiang Zhang. Subwavelength discrete solitons in nonlinear metamaterials. In *Photonic Metamaterials: From Random to Periodic*, page TuB29. Optica Publishing Group, 2007.

[105] N Lazarides and GP Tsironis. Coupled nonlinear schrödinger field equations for electromagnetic wave propagation in nonlinear left-handed materials. *Physical Review E*, 71(3):036614, 2005.

[106] Mattias Marklund, Padma K Shukla, Lennart Stenflo, and Gert Brodin. Solitons and decoherence in left-handed metamaterials. *Physics Letters A*, 341(1-4):231–234, 2005.

[107] NL Tsitsas, N Rompotis, I Kourakis, PG Kevrekidis, and DJ Frantzeskakis. Higher-order effects and ultrashort solitons in left-handed metamaterials. *Physical Review E*, 79(3):037601, 2009.

[108] Giorgios P Veldes, J Cuevas, Panayotis G Kevrekidis, and Dimitri J Frantzeskakis. Quasidiscrete microwave solitons in a split-ring-resonator-based left-handed coplanar waveguide. *Physical Review E*, 83(4):046608, 2011.

[109] Nikolay N Rosanov, Nina V Vysotina, Anatoly N Shatsev, Anton S Desyatnikov, and Yuri S Kivshar. Knotted solitons in nonlinear magnetic metamaterials. *Physical Review Letters*, 108(13):133902, 2012.

[110] Rongcao Yang, Xuemin Min, Jinping Tian, Wenrui Xue, and Wenmei Zhang. New types of exact quasi-soliton solutions in metamaterials. *Physica Scripta*, 91(2):025201, 2016.

[111] Abdel Kader Daoui, Houria Triki, Anjan Biswas, Qin Zhou, Seithuti P Moshokoa, and Milivoj Belic. Chirped bright and double-kinked quasi-solitons in optical metamaterials with self-steepening nonlinearity. *Journal of Modern Optics*, 66(2):192–199, 2019.

[112] Houria Triki, Qin Zhou, Seithuti P Moshokoa, Malik Zaka Ullah, Anjan Biswas, and Milivoj Belic. Novel singular solitons in optical metamaterials for self-steepening effect. *Optik*, 154:545–550, 2018.

[113] Houria Triki, Anjan Biswas, MM Babatin, and Qin Zhou. Chirped dark solitons in optical metamaterials. *Optik*, 158:312–315, 2018.

[114] Kamyar Hosseini, Mohammad Mirzazadeh, Qin Zhou, Yaxian Liu, and Mojtaba Moradi. Analytic study on chirped optical solitons in nonlinear metamaterials with higher order effects. *Laser Physics*, 29(9):095402, 2019.

[115] Polykarpos Porfyrakis, Nikolaos L Tsitsas, and Dimitri J Frantzeskakis. On the formation of gap solitons in nonlinear electromagnetic metamaterials. *Mathematical Methods in the Applied Sciences*, 42(18):7326–7334, 2019.

[116] Hai-Ping Zhu and Ya-Hong Hu. Chirped optical soliton and jacobian elliptic function solutions in a metamaterial waveguide. *Optik*, 224:165459, 2020.

[117] AK Shafeeque Ali, Malik Zaka Ullah, and M Lakshmanan. Impact of higher-order effects on dissipative soliton in metamaterials. *Physics Letters A*, 384(28):126744, 2020.

[118] Souleymanou Abbagari, Alphonse Houwe, Serge P Mukam, Hadi Rezazadeh, Mustafa Inc, Serge Y Doka, and Thomas B Bouetou. Optical solitons to the nonlinear schrödinger equation in metamaterials and modulation instability. *The European Physical Journal Plus*, 136(7):1–22, 2021.

[119] Islam Samir, Niveen Badra, Hamdy M Ahmed, and Ahmed H Arnous. Solitons dynamics in optical metamaterial with quadratic–cubic nonlinearity using modified extended direct algebraic method. *Optik*, 243:166851, 2021.

[120] Thilagarajah Mathanaranjan, Dipankar Kumar, Hadi Rezazadeh, and Lanre

Akinyemi. Optical solitons in metamaterials with third and fourth order dispersions. *Optical and Quantum Electronics*, 54(5):271, 2022.

[121] Boris A Malomed. Bound solitons in coupled nonlinear schrödinger equations. *Physical Review A*, 45(12):R8321, 1992.

[122] T Alagesan, Y Chung, and K Nakkeeran. Soliton solutions of coupled nonlinear klein–gordon equations. *Chaos, Solitons & Fractals*, 21(4):879–882, 2004.

[123] Laure Tiam Megne, Conrad Bertrand Tabi, and Timoléon Crépin Kofane. Modulation instability in nonlinear metamaterials modeled by a cubic-quintic complex ginzburg-landau equation beyond the slowly varying envelope approximation. *Physical Review E*, 102(4):042207, 2020.

[124] Eryk Infeld and George Rowlands. *Nonlinear waves, solitons and chaos*. Cambridge university press, 2000.

[125] Dan Anderson. Variational approach to nonlinear pulse propagation in optical fibers. *Physical review A*, 27(6):3135, 1983.

[126] GM Muslu and HA Erbay. A split-step fourier method for the complex modified korteweg-de vries equation. *Computers & Mathematics with Applications*, 45(1-3):503–514, 2003.

[127] Decio Levi, Orlando Ragnisco, and A Sym. Dressing method vs. classical darboux transformation. *Nuovo Cimento B;(Italy)*, 83(1), 1984.

[128] Govind P Agrawal. Nonlinear fiber optics. In *Nonlinear Science at the Dawn of the 21st Century*, pages 167–169. Springer, 2000.

[129] Hilal M El Misilmani, Karim Y Kabalan, Mohamad Y Abou-Shahine, Mohammed Al-Husseini, et al. A method of moment approach in solving boundary value problems. *Journal of Electromagnetic Analysis and Applications*, 7(03):61, 2015.

[130] Terry Bridgman, Willy Hereman, G Reinout W Quispel, and Peter H van der Kamp. Symbolic computation of lax pairs of partial difference equations using consistency around the cube. *Foundations of Computational Mathematics*, 13:517–544, 2013.

[131] Ali Demir, Sertaç Erman, Berrak Özgür, and Esra Korkmaz. Analysis of fractional partial differential equations by taylor series expansion. *Boundary Value Problems*, 2013:1–12, 2013.

[132] Randall J LeVeque. Finite difference methods for differential equations. *Draft version for use in AMath*, 585(6):112, 1998.

[133] Metin Gürses and Aslı Pekcan. (2+ 1)-dimensional local and nonlocal reductions of the negative akns system: soliton solutions. *Communications in Nonlinear Science and Numerical Simulation*, 71:161–173, 2019.

[134] W Fred Ramirez. *Computational methods for process simulation*. Butterworth-Heinemann, 1997.

[135] GM Mophou and GM N'guérékata. On integral solutions of some nonlocal fractional differential equations with nondense domain. *Nonlinear Analysis: Theory, Methods & Applications*, 71(10):4668–4675, 2009.

[136] Robert Eymard, Thierry Gallouët, and Raphaèle Herbin. Finite volume methods. *Handbook of numerical analysis*, 7:713–1018, 2000.

[137] Paul R Garabedian. A partial differential equation arising in conformal mapping. *Pacific Journal of Mathematics*, 1(4):485 – 524, 1951.

[138] Peter Russer. The transmission line matrix method. *Applied Computational Electromagnetics: State of the Art and Future Trends*, pages 243–269, 2000.

[139] George Cain and Gunter H Meyer. *Separation of variables for partial differential equations: an eigenfunction approach*. CRC Press, 2005.

[140] Ambaresh Sahoo, Samudra Roy, and Govind P Agrawal. Perturbed dissipative solitons: A variational approach. *Physical Review A*, 96(1):013838, 2017.

[141] D Anderson, M Lisak, and A Berntson. A variational approach to nonlinear evolution equations in optics. *Pramana*, 57:917–936, 2001.

[142] Van Hieu Nguyen and Bich Ha Nguyen. Quantum theory of plasmon. *Advances in Natural Sciences: Nanoscience and Nanotechnology*, 5(2):025001, 2014.

[143] Boris A Malomed. Variational methods in nonlinear fiber optics and related fields. *Progress in optics*, 43(71), 2002.

[144] Blaise Bourdin, Gilles A Francfort, and Jean-Jacques Marigo. The variational approach to fracture. *Journal of elasticity*, 91:5–148, 2008.

[145] Feliks Nuske, Bettina G Keller, Guillermo Pérez-Hernández, Antonia SJS Mey, and Frank Noé. Variational approach to molecular kinetics. *Journal of chemical theory and computation*, 10(4):1739–1752, 2014.

[146] Axel Constant, Maxwell JD Ramstead, Samuel PL Veissiere, John O Campbell, and Karl J Friston. A variational approach to niche construction. *Journal of the Royal Society Interface*, 15(141):20170685, 2018.

[147] Matthew Lang and Mathew J Owens. A variational approach to data assimilation in the solar wind. *Space Weather*, 17(1):59–83, 2019.

[148] Jianmin Ma and SM Daggupaty. Using all observed information in a variational approach to measuring z0m and z0t. *Journal of Applied Meteorology and Climatology*, 39(8):1391–1401, 2000.

[149] Baldeep Kaur, Anu Mittal, Soumendu Jana, Soumya Suddha Mallick, and Peter Wypych. Stability and phase space analysis of fluidized-dense phase pneumatic transport system. *Powder Technology*, 330:190–200, 2018.

[150] Seyed Kamaleddin Yadavar Nikravesh. *Nonlinear systems stability analysis: Lyapunov-based approach*. CRC Press, 2018.

[151] John Charles Butcher. A history of runge-kutta methods. *Applied numerical mathematics*, 20(3):247–260, 1996.

[152] George Lindfield and John Penny. *Numerical methods: using MATLAB*. Academic Press, 2018.

[153] Erwin Fehlberg. Low-order classical runge-kutta formulas with stepsize control. *NASA Technical Report R-315*, 1969.

[154] Luke Taylor. A comparison between the split step fourier and finite-difference method in analysing the soliton collision of a type of nonlinear schr\" odinger equation found in the context of optical pulses. *arXiv preprint arXiv:1709.04805*, 2017.

[155] Govind P Agrawal. Nonlinear fiber optics. In *Nonlinear Science at the Dawn of the 21st Century*, pages 51–55. Springer, 2000.

[156] Silvia Carrasco, Hongki Kim, George Stegeman, and Lluis Torner. Self-focusing of light mediated by cubic nonlinearities in potassium titanyl phosphate. In *Nonlinear Guided Waves and Their Applications*, page NLTuD37. Optica Publishing Group, 2002.

[157] Yusuke Tamaki, Minoru Obara, and Katsumi Midorikawa. Second-harmonic generation from intense, 100-fs ti: sapphire laser pulses in potassium dihydrogen phosphate, cesium lithium borate and β-barium metaborate. *Japanese journal of applied physics*, 37(9R):4801, 1998.

[158] Morten Bache, Hairun Guo, Binbin Zhou, and Xianglong Zeng. The anisotropic kerr nonlinear refractive index of the beta-barium borate (β-bab 2 o 4) nonlinear crystal. *Optical Materials Express*, 3(3):357–382, 2013.

[159] Satoshi Ashihara, Jun Nishina, Tsutomu Shimura, Kazuo Kuroda, Tomoya Sugita, Kiminori Mizuuchi, and Kazuhisa Yamamoto. Nonlinear refraction of femtosecond pulses due to quadratic and cubic nonlinearities in periodically poled lithium tantalate. *Optics communications*, 222(1-6):421–427, 2003.

[160] Mario Garcia-Lechuga, Jan Siegel, Javier Hernandez-Rueda, and Javier Solis. Imaging the ultrafast kerr effect, free carrier generation, relaxation and ablation dynamics of lithium niobate irradiated with femtosecond laser pulses. *Journal of Applied Physics*, 116(11), 2014.

[161] MI Baig, Mohd Anis, H Algarni, MD Shirsat, and SS Hussaini. Customizing optical and dielectric traits of ammonium dihydrogen phosphate (adp) crystal exploiting zn2+ ion for photonic device applications. *Chinese Journal of Physics*, 63:70–77, 2020.

[162] David A Kleinman. Theory of second harmonic generation of light. *Physical Review*, 128(4):1761, 1962.

[163] YR Shen. Basic theory of surface sum-frequency generation. *The Journal of Physical Chemistry C*, 116(29):15505–15509, 2012.

[164] Robert W Boyd, Alexander L Gaeta, and Enno Giese. Nonlinear optics. In *Springer Handbook of Atomic, Molecular, and Optical Physics*, pages 1097–1110. Springer, 2008.

[165] TJ Kippenberg, SM Spillane, and KJ Vahala. Kerr-nonlinearity optical parametric oscillation in an ultrahigh-q toroid microcavity. *Physical review letters*, 93(8):083904, 2004.

[166] Lu Deng, Edward W Hagley, J Wen, M Trippenbach, Y Band, Paul S Julienne, JE Simsarian, Kristian Helmerson, SL Rolston, and William D Phillips. Four-wave mixing with matter waves. *Nature*, 398(6724):218–220, 1999.

[167] Geoffrey New. *Introduction to nonlinear optics*. Cambridge University Press, 2011.

[168] Michelle Moreno. Kerr effect. *São Carlos, Brazil: Instituto de Física de São Carlos-Universidade de São Paulo*, 4, 2018.

[169] Soumendu Jana and S Konar. Induced focusing of two laser beams in cubic quintic nonlinear media. *Physica Scripta*, 70(6):354, 2004.

[170] Sara Ferretti and Dario Gerace. Single-photon nonlinear optics with kerr-type nanostructured materials. *Physical Review B*, 85(3):033303, 2012.

[171] Mihaela Dinu, Francesco Quochi, and Hugo Garcia. Third-order nonlinearities in silicon at telecom wavelengths. *Applied physics letters*, 82(18):2954–2956, 2003.

[172] Albert S Reyna, Emeric Bergmann, Pierre-François Brevet, and Cid B de Araújo. Nonlinear polarization instability in cubic-quintic plasmonic nanocomposites. *Optics Express*, 25(18):21049–21067, 2017.

[173] Rohit Mukherjee and S Konar. Effect of quintic nonlinearity on self-phase modulation and modulation instability in multiple coupled quantum wells under electromagnetically induced transparency. *Results in Physics*, 17:103090, 2020.

[174] S Gatz and Joachim Herrmann. Soliton propagation in materials with saturable nonlinearity. *JOSA B*, 8(11):2296–2302, 1991.

[175] Luciene Demenicis, ASL Gomes, DV Petrov, Cid B de Araújo, Celso P de Melo, Clécio G Dos Santos, and Rosa Souto-Maior. Saturation effects in the nonlinear-optical susceptibility of poly (3-hexadecylthiophene). *JOSA B*, 14(3):609–614, 1997.

[176] S Medhekar, Ram Krishna Sarkar, and Punya Prasanna Paltani. Coupled spatial-soliton pairs in saturable nonlinear media. *Optics letters*, 31(1):77–79, 2006.

[177] Peter TC So, Chen Y Dong, Barry R Masters, and Keith M Berland. Two-photon excitation fluorescence microscopy. *Annual review of biomedical engineering*, 2(1):399–429, 2000.

[178] Paige A Shaw, Ewan Forsyth, Fizza Haseeb, Shufan Yang, Mark Bradley, and Maxime Klausen. Two-photon absorption: an open door to the nir-ii biological window? *Frontiers in chemistry*, 10:921354, 2022.

[179] Gilles Lemercier, Jean-Christophe Mulatier, Cécile Martineau, Rémi Anémian, Chantal Andraud, Irène Wang, Olivier Stéphan, Nadia Amari, and Patrice Baldeck. Two-photon absorption: from optical power limiting to 3d microfabrication. *Comptes rendus. Chimie*, 8(8):1308–1316, 2005.

[180] Guangyong Zhuo, Xiaomei Wang, Dong Wang, Chun Wang, Xian Zhao, Zongshu Shao, and Minhua Jiang. Two-photon induced optical-power limiting and upconverted superradiance properties of a new organic dye heaspi. *Optics & Laser Technology*, 33(4):209–212, 2001.

[181] Stefan W Hell, Karsten Bahlmann, Martin Schrader, Aleksi Soini, Henryk M Malak, Ignacy Gryczynski, and Joseph R Lakowicz. Three-photon excitation in fluorescence microscopy. *Journal of biomedical optics*, 1(1):71–74, 1996.

[182] Jan K Zaręba, Marcin Nyk, Jan Janczak, and Marek Samoć. Three-photon absorption of coordination polymer transforms uv-to-vis thermometry into nir-to-vis thermometry. *ACS applied materials & interfaces*, 11(11):10435–10441, 2019.

[183] Duo-Yuan Wang, Chuan-Lang Zhan, Yu Chen, Yun-Jing Li, Zhen-Zhong Lu,

and Yu-Xin Nie. Large optical power limiting induced by three-photon absorption of two stilbazolium-like dyes. *Chemical physics letters*, 369(5-6):621–626, 2003.

[184] F DeMartini, CH Townes, TK Gustafson, and PL Kelley. Self-steepening of light pulses. *Physical Review*, 164(2):312, 1967.

[185] J Vieira, F Fiúza, LO Silva, M Tzoufras, and WB Mori. Onset of self-steepening of intense laser pulses in plasmas. *New Journal of Physics*, 12(4):045025, 2010.

[186] Richard C Prince, Renee R Frontiera, and Eric O Potma. Stimulated raman scattering: from bulk to nano. *Chemical reviews*, 117(7):5070–5094, 2017.

[187] Luigi Sirleto and Maria Antonietta Ferrara. Fiber amplifiers and fiber lasers based on stimulated raman scattering: a review. *Micromachines*, 11(3):247, 2020.

[188] Govind P Agrawal. Effect of intrapulse stimulated raman scattering on soliton-effect pulse compression in optical fibers. *Optics letters*, 15(4):224–226, 1990.

[189] Samudra Roy, Shyamal K Bhadra, and Govind P Agrawal. Perturbation of higher-order solitons by fourth-order dispersion in optical fibers. *Optics Communications*, 282(18):3798–3803, 2009.

[190] H Matsumoto, G Oberlechner, M Umezawa, and H Umezawa. Quantum soliton and classical soliton. *Journal of Mathematical Physics*, 20(10):2088–2096, 1979.

[191] Nicholas Manton and Paul Sutcliffe. *Topological solitons*. Cambridge University Press, 2004.

[192] Tamara I Belova and Aleksandr E Kudryavtsev. Solitons and their interactions in classical field theory. *Physics-Uspekhi*, 40(4):359, 1997.

[193] Gia Dvali, Cesar Gomez, Lukas Gruending, and Tehseen Rug. Towards a quantum theory of solitons. *Nuclear Physics B*, 901:338–353, 2015.

[194] Yousef Yousefi and Khikmat Kh Muminov. A simple classification of solitons. *arXiv preprint arXiv:1206.1294*, 2012.

[195] S Murugesh et al. Knot soliton solutions for the one-dimensional non-linear schr\"{o} dinger equation. *arXiv preprint arXiv:1711.03318*, 2017.

[196] Tsung-Dao Lee and Yang Pang. Nontopological solitons. *Physics Reports*, 221(5-6):251–350, 1992.

[197] Vladimir G Ivancevic and Tijana T Ivancevic. Sine–gordon solitons, kinks and breathers as physical models of nonlinear excitations in living cellular structures. *Journal of Geometry and Symmetry in Physics*, 31:1 – 56, 2013.

[198] Hongcai Ma, Qiaoxin Cheng, and Aiping Deng. Solitons, breathers, and lump solutions to the (2+ 1)-dimensional generalized calogero–bogoyavlenskii–schiff equation. *Complexity*, 2021:1–10, 2021.

[199] Sergej Flach. Discrete breathers in a nutshell. *Nonlinear Theory and Its Applications, IEICE*, 3(1):12–26, 2012.

[200] Geeta Arora, Richa Rani, and Homan Emadifar. Soliton: A dispersion-less solution with existence and its types. *Heliyon*, 2022.

[201] Nail N Akhmediev, Adrian Ankiewicz, et al. *Nonlinear pulses and beams.* Springer, 1997.

[202] Yuri S Kivshar and Govind Agrawal. *Optical solitons: from fibers to photonic crystals.* Academic press, 2003.

[203] Yuri S Kivshar and George I Stegeman. Spatial optical solitons. *Optics and Photonics News*, 13(2):59–63, 2002.

[204] Sarang Medhekar, Ram Krishna Sarkar, and Punya Prasanna Paltani. Soliton pairing of two coaxially co-propagating mutually incoherent 1-d beams in kerr type media. *Optica Applicata*, 37(3):243, 2007.

[205] S Crutcher, A Biswas, MD Aggarwal, and ME Edwards. Oscillatory behavior of spatial solitons in two-dimensional waveguides and stationary temporal power law solitons in optical fibers. *Journal of Electromagnetic Waves and Applications*, 20(6):761–772, 2006.

[206] Lucian-Cornel Crasovan, Boris A Malomed, and Dumitru Mihalache. Spinning solitons in cubic-quintic nonlinear media. *Pramana*, 57(5):1041–1059, 2001.

[207] Neil Akhmediev and Adrian Ankiewicz. Dissipative solitons in the complex ginzburg-landau and swift-hohenberg equations. *Dissipative solitons*, pages 1–17, 2005.

[208] Boris A Malomed. Multidimensional dissipative solitons and solitary vortices. *Chaos, Solitons & Fractals*, 163:112526, 2022.

[209] Ortwin Hess, John B Pendry, Stefan A Maier, Rupert F Oulton, Joachim M Hamm, and Kosmas L Tsakmakidis. Active nanoplasmonic metamaterials. *Nature materials*, 11(7):573–584, 2012.

[210] Steven A Cummer, Johan Christensen, and Andrea Alù. Controlling sound with acoustic metamaterials. *Nature Reviews Materials*, 1(3):1–13, 2016.

[211] Sophia R Sklan and Baowen Li. Thermal metamaterials: functions and prospects. *National Science Review*, 5(2):138–141, 2018.

[212] Katia Bertoldi, Vincenzo Vitelli, Johan Christensen, and Martin Van Hecke. Flexible mechanical metamaterials. *Nature Reviews Materials*, 2(11):1–11, 2017.

[213] David J Barber and Ian C Freestone. An investigation of the origin of the colour of the lycurgus cup by analytical transmission electron microscopy. *Archaeometry*, 32(1):33–45, 1990.

[214] Ulf Leonhardt. Invisibility cup. *Nature photonics*, 1(4):207–208, 2007.

[215] Wenshan Cai and Vladimir M Shalaev. *Optical metamaterials*. Springer, 2010.

[216] Winston E Kock. Metal-lens antennas. *Proceedings of the IRE*, 34(11):828–836, 1946.

[217] Winston E Kock. Metallic delay lenses. *Bell System Technical Journal*, 27(1):58–82, 1948.

[218] Lev Davidovich Landau, John Stewart Bell, MJ Kearsley, LP Pitaevskii, EM Lifshitz, and JB Sykes. *Electrodynamics of continuous media*, volume 8. elsevier, 2013.

[219] Stefan Linden, Christian Enkrich, Martin Wegener, Jiangfeng Zhou, Thomas Koschny, and Costas M Soukoulis. Magnetic response of metamaterials at 100 terahertz. *Science*, 306(5700):1351–1353, 2004.

[220] John B Pendry, Anthony J Holden, David J Robbins, and WJ Stewart. Magnetism from conductors and enhanced nonlinear phenomena. *IEEE transactions on microwave theory and techniques*, 47(11):2075–2084, 1999.

[221] WN Hardy and LA Whitehead. Split-ring resonator for use in magnetic resonance from 200–2000 mhz. *Review of Scientific Instruments*, 52(2):213–216, 1981.

[222] Richard A Shelby, David R Smith, and Seldon Schultz. Experimental verification of a negative index of refraction. *science*, 292(5514):77–79, 2001.

[223] Ruopeng Liu, Qiang Cheng, Jessie Y Chin, Jack J Mock, Tie Jun Cui, and David R Smith. Broadband gradient index microwave quasi-optical elements based on non-resonant metamaterials. *Optics express*, 17(23):21030–21041, 2009.

[224] Mikhail Omelyanovich, Victor Ovchinnikov, and Constantin Simovski. A non-resonant dielectric metamaterial for the enhancement of thin-film solar cells. *Journal of Optics*, 17(2):025102, 2015.

[225] David R Smith, Willie J Padilla, DC Vier, Syrus C Nemat-Nasser, and Seldon Schultz. Composite medium with simultaneously negative permeability and permittivity. *Physical review letters*, 84(18):4184, 2000.

[226] John B Pendry and David R Smith. Reversing light with negative refraction. *Physics today*, 57:37–43, 2004.

[227] Basudev Lahiri. *Split ring resonator (srr) based metamaterials.* PhD thesis, University of Glasgow, 2010.

[228] Atsushi Ishikawa and Takuo Tanaka. Negative magnetic permeability of split ring resonators in the visible light region. *Optics communications*, 258(2):300–305, 2006.

[229] Constantin R Simovski, Pavel A Belov, Alexander V Atrashchenko, and Yuri S Kivshar. Wire metamaterials: physics and applications. *Advanced materials*, 24(31):4229–4248, 2012.

[230] Vladimir R Tuz, Vyacheslav V Khardikov, Anton S Kupriianov, Kateryna L Domina, Su Xu, Hai Wang, and Hong-Bo Sun. High-quality trapped modes in all-dielectric metamaterials. *Optics express*, 26(3):2905–2916, 2018.

[231] Kan Yao and Yongmin Liu. Plasmonic metamaterials. *Nanotechnology Reviews*, 3(2):177–210, 2014.

[232] Jiangfeng Zhou, Thomas Koschny, and Costas M Soukoulis. Magnetic and electric excitations in split ring resonators. *Optics express*, 15(26):17881–17890, 2007.

[233] Sreedevi P Chakyar, Sikha K. Simon, C Bindu, Jolly Andrews, and VP Joseph. Complex permittivity measurement using metamaterial split ring resonators. *Journal of Applied Physics*, 121(5):054101, 2017.

[234] Ricardo Marqués, Francisco Medina, and Rachid Rafii-El-Idrissi. Role of bianisotropy in negative permeability and left-handed metamaterials. *Physical Review B*, 65(14):144440, 2002.

[235] Hongcang Guo, Na Liu, Liwei Fu, Heinz Schweizer, Stefan Kaiser, and Harald Giessen. Thickness dependence of the optical properties of split-ring resonator metamaterials. *physica status solidi (b)*, 244(4):1256–1261, 2007.

[236] A Nutan Reddy and S Raghavan. Split ring resonator and its evolved structures over the past decade: This paper discusses the nuances of the most celebrated composite particle (split-ring resonator) with which novel artificial structured materials (called metamaterials) are built. In *2013 IEEE International Conference ON Emerging Trends in Computing, Communication and Nanotechnology (ICECCN)*, pages 625–629. IEEE, 2013.

[237] N Katsarakis, Th Koschny, M Kafesaki, EN Economou, and CM Soukoulis. Electric coupling to the magnetic resonance of split ring resonators. *Applied physics letters*, 84(15):2943–2945, 2004.

[238] Xun-jun He, Liang Qiu, Yue Wang, Zhao-xin Geng, Jian-min Wang, and Tailong Gui. A compact thin-film sensor based on nested split-ring-resonator (srr) metamaterials for microwave applications. *Journal of Infrared, Millimeter, and Terahertz Waves*, 32:902–913, 2011.

[239] Na Liu, Hui Liu, Shining Zhu, and Harald Giessen. Stereometamaterials. *Nature Photonics*, 3(3):157–162, 2009.

[240] M Decker, R Zhao, CM Soukoulis, Stefan Linden, and M Wegener. Twisted split-ring-resonator photonic metamaterial with huge optical activity. *Optics letters*, 35(10):1593–1595, 2010.

[241] Koray Aydin, Zhaofeng Li, M Hudlička, SA Tretyakov, and Ekmel Ozbay. Transmission characteristics of bianisotropic metamaterials based on omega shaped metallic inclusions. *New Journal of Physics*, 9(9):326, 2007.

[242] David Schurig, Jack J Mock, BJ Justice, Steven A Cummer, John B Pendry, Anthony F Starr, and David R Smith. Metamaterial electromagnetic cloak at microwave frequencies. *Science*, 314(5801):977–980, 2006.

[243] Ignacio Gil, F Martın, Xavier Rottenberg, and Walter De Raedt. Tunable stop-band filter at q-band based on rf-mems metamaterials. *Electronics Letters*, 43(21):1153–1154, 2007.

[244] MS Kushwaha and Bahram Djafari-Rouhani. Theory of confined plasmonic waves in coaxial cylindrical cables fabricated of metamaterials. *JOSA B*, 27(1):148–167, 2010.

[245] Augustine M Urbas, Zubin Jacob, Luca Dal Negro, Nader Engheta, AD Boardman, P Egan, Alexander B Khanikaev, Vinod Menon, Marcello Ferrera, Nathaniel Kinsey, et al. Roadmap on optical metamaterials. *Journal of Optics*, 18(9):093005, 2016.

[246] Yuri S Kivshar. Tunable and nonlinear metamaterials: toward functional metadevices. *Advances in Natural Sciences: Nanoscience and Nanotechnology*, 5(1):013001, 2013.

[247] GR Keiser, K Fan, X Zhang, and RD Averitt. Towards dynamic, tunable, and nonlinear metamaterials via near field interactions: a review. *Journal of Infrared, Millimeter, and Terahertz Waves*, 34:709–723, 2013.

[248] Ilya V Shadrivov, Alexander B Kozyrev, DanielW van der Weide, and Yuri S Kivshar. Nonlinear magnetic metamaterials. *Optics express*, 16(25):20266–20271, 2008.

[249] Jiaye Wu, Ze Tao Xie, Yanhua Sha, HY Fu, and Qian Li. Epsilon-near-zero photonics: infinite potentials. *Photonics Research*, 9(8):1616–1644, 2021.

[250] Xinxiang Niu, Xiaoyong Hu, Saisai Chu, and Qihuang Gong. Epsilon-near-zero photonics: a new platform for integrated devices. *Advanced Optical Materials*, 6(10):1701292, 2018.

[251] Hongwei Liu, Junpeng Lu, and Xiao Renshaw Wang. Metamaterials based on the phase transition of vo2. *Nanotechnology*, 29(2):024002, 2017.

[252] Ioannis Kourakis, N Lazarides, and GP Tsironis. Self-focusing and envelope pulse generation in nonlinear magnetic metamaterials. *Physical Review E*, 75(6):067601, 2007.

[253] Thomas P Weldon, Konrad Miehle, Ryan S Adams, and Kasra Daneshvar. A wideband microwave double-negative metamaterial with non-foster loading. In *2012 Proceedings of IEEE SoutheastCon*, pages 1–5. IEEE, 2012.

[254] J Paul, GJ Sharp, B Lahiri, RM De La Rue, and NP Johnson. Simulation and experimental responses of the asymmetric split ring resonators (a-srrs) for sensing applications in the mid-infrared region. In *2015 9th International Congress on Advanced Electromagnetic Materials in Microwaves and Optics (METAMATERIALS)*, pages 469–471. IEEE, 2015.

[255] Nikos Lazarides, George P Tsironis, and Yuri S Kivshar. Surface breathers in discrete magnetic metamaterials. *Physical Review E*, 77(6):065601, 2008.

[256] Nina A Zharova, Ilya V Shadrivov, Alexander A Zharov, and Yuri S Kivshar. Nonlinear transmission and spatiotemporal solitons in metamaterials with negative refraction. *Optics Express*, 13(4):1291–1298, 2005.

[257] Jinggui Zhang, Shuangchun Wen, Yuanjiang Xiang, Youwen Wang, and Hailu Luo. Spatiotemporal electromagnetic soliton and spatial ring formation in nonlinear metamaterials. *Physical Review A*, 81(2):023829, 2010.

[258] Pin Chieh Wu, Wei-Lun Hsu, Wei Ting Chen, Yao-Wei Huang, Chun Yen Liao, Ai Qun Liu, Nikolay I Zheludev, Greg Sun, and Din Ping Tsai. Plasmon coupling in vertical split-ring resonator metamolecules. *Scientific reports*, 5(1):9726, 2015.

[259] Xiaoguang Zhao, Jingdi Zhang, Kebin Fan, Guangwu Duan, Grace D Metcalfe, Michael Wraback, Xin Zhang, and Richard D Averitt. Nonlinear terahertz metamaterial perfect absorbers using gaas. *Photonics Research*, 4(3):A16–A21, 2016.

[260] Kebin Fan, Harold Y Hwang, Mengkun Liu, Andrew C Strikwerda, Aaron Sternbach, Jingdi Zhang, Xiaoguang Zhao, Xin Zhang, Keith A Nelson, and Richard D Averitt. Nonlinear terahertz metamaterials via field-enhanced carrier dynamics in gaas. *Physical Review Letters*, 110(21):217404, 2013.

[261] Miguel Camacho, Brian Edwards, and Nader Engheta. Achieving asymmetry and trapping in diffusion with spatiotemporal metamaterials. *Nature communications*, 11(1):3733, 2020.

[262] Ashley Lyons, Dikla Oren, Thomas Roger, Vassili Savinov, João Valente, Stefano Vezzoli, Nikolay I Zheludev, Mordechai Segev, and Daniele Faccio. Coher-

ent metamaterial absorption of two-photon states with 40% efficiency. *Physical Review A*, 99(1):011801, 2019.

[263] Takeya Tsurumi. Soliton propagation in nonlinear magnetic metamaterials with microscopic disorder. *Journal of the Physical Society of Japan*, 77(7):074006, 2008.

[264] N Lazarides and GP Tsironis. Coupled nonlinear schrödinger field equations for electromagnetic wave propagation in nonlinear left-handed materials. *Physical Review E*, 71(3):036614, 2005.

[265] Nina A Zharova, Ilya V Shadrivov, Alexander A Zharov, and Yuri S Kivshar. Nonlinear transmission and spatiotemporal solitons in metamaterials with negative refraction. *Optics Express*, 13(4):1291–1298, 2005.

[266] N Lazarides, M Eleftheriou, and GP Tsironis. Discrete breathers in nonlinear magnetic metamaterials. *Physical review letters*, 97(15):157406, 2006.

[267] Yichang Meng, Shumin Zhang, Xingliang Li, Hongfei Li, Juan Du, and Yanping Hao. Multiple-soliton dynamic patterns in a graphene mode-locked fiber laser. *Optics express*, 20(6):6685–6692, 2012.

[268] Han Zhang, Dingyuan Tang, Randall James Knize, Luming Zhao, Qiaoliang Bao, and Kian Ping Loh. Graphene mode locked, wavelength-tunable, dissipative soliton fiber laser. *Applied Physics Letters*, 96(11):111112, 2010.

[269] Yu V Bludov, Daria A Smirnova, Yu S Kivshar, Nuno MR Peres, and Mikhail I Vasilevskiy. Discrete solitons in graphene metamaterials. *Physical Review B*, 91(4):045424, 2015.

[270] Kun Yu, Zhiwei Guo, Haitao Jiang, and Hong Chen. Loss-induced topological transition of dispersion in metamaterials. *Journal of Applied Physics*, 119(20):203102, 2016.

[271] Alexander A Zharov, Ilya V Shadrivov, and Yuri S Kivshar. Nonlinear properties of left-handed metamaterials. *Physical Review Letters*, 91(3):037401, 2003.

[272] Adrian Ankiewicz and Nail Akhmediev. *Dissipative solitons: from optics to biology and medicine*. Springer, 2008.

[273] Gurkirpal Singh Parmar, Soumendu Jana, and Boris A Malomed. Dissipative soliton fiber lasers with higher-order nonlinearity, multiphoton absorption and emission, and random dispersion. *JOSA B*, 34(4):850–860, 2017.

[274] Gurkirpal Singh Parmar, Boris A Malomed, and Soumendu Jana. Interplay of multiphoton absorption, raman scattering, and third-order dispersion in soliton fiber lasers. *JOSA B*, 38(2):342–352, 2021.

[275] Baldeep Kaur and Soumendu Jana. Generation and dynamics of one-and two-dimensional cavity solitons in a vertical-cavity surface-emitting laser with a saturable absorber and frequency-selective feedback. *JOSA B*, 34(7):1374–1385, 2017.

[276] Baldeep Kaur and Soumendu Jana. Cavity soliton molecules and all-optical push-broom effect. *Journal of Lightwave Technology*, 36(12):2463–2470, 2018.

[277] Jaspreet Kaur Nagi and Soumendu Jana. Operating regimes of cavity solitons by virtue of a graphene flake saturable absorber. *Physical Review E*, 104(2):024209, 2021.

[278] Jiangfeng Zhou, Thomas Koschny, and Costas M Soukoulis. Magnetic and electric excitations in split ring resonators. *Optics express*, 15(26):17881–17890, 2007.

[279] Weina Cui, Yongyuan Zhu, Hongxia Li, and Sumei Liu. Self-induced gap soli-

tons in nonlinear magnetic metamaterials. *Physical Review E*, 80(3):036608, 2009.

[280] Takeya Tsurumi. Soliton propagation in nonlinear magnetic metamaterials with microscopic disorder. *Journal of the Physical Society of Japan*, 77(7):074006, 2008.

[281] Haiming Dong, Claudio Conti, Andrea Marini, and Fabio Biancalana. Terahertz relativistic spatial solitons in doped graphene metamaterials. *Journal of Physics B: Atomic, Molecular and Optical Physics*, 46(15):155401, 2013.

[282] Jie Hu, Sankhyabrata Bandyopadhyay, Yu-hui Liu, and Li-yang Shao. A review on metasurface: From principle to smart metadevices. *Frontiers in Physics*, 8:502, 2021.

[283] Alexander E Minovich, Andrey E Miroshnichenko, Anton Y Bykov, Tatiana V Murzina, Dragomir N Neshev, and Yuri S Kivshar. Functional and nonlinear optical metasurfaces. *Laser & Photonics Reviews*, 9(2):195–213, 2015.

[284] Hongcang Guo, Na Liu, Liwei Fu, Heinz Schweizer, Stefan Kaiser, and Harald Giessen. Thickness dependence of the optical properties of split-ring resonator metamaterials. *physica status solidi (b)*, 244(4):1256–1261, 2007.

[285] Chul Chung, Young-Kwan Kim, Dolly Shin, Soo-Ryoon Ryoo, Byung Hee Hong, and Dal-Hee Min. Biomedical applications of graphene and graphene oxide. *Accounts of chemical research*, 46(10):2211–2224, 2013.

[286] Khan MF Shahil and Alexander A Balandin. Thermal properties of graphene and multilayer graphene: Applications in thermal interface materials. *Solid state communications*, 152(15):1331–1340, 2012.

[287] Houk Jang, Yong Ju Park, Xiang Chen, Tanmoy Das, Min-Seok Kim, and

Jong-Hyun Ahn. Graphene-based flexible and stretchable electronics. *Advanced Materials*, 28(22):4184–4202, 2016.

[288] Phaedon Avouris and Fengnian Xia. Graphene applications in electronics and photonics. *Mrs Bulletin*, 37(12):1225–1234, 2012.

[289] Lili Jiang, Zhiwen Shi, Bo Zeng, Sheng Wang, Ji-Hun Kang, Trinity Joshi, Chenhao Jin, Long Ju, Jonghwan Kim, Tairu Lyu, et al. Soliton-dependent plasmon reflection at bilayer graphene domain walls. *Nature materials*, 15(8):840–844, 2016.

[290] Daria A Smirnova, Roman E Noskov, Lev A Smirnov, and Yuri S Kivshar. Dissipative plasmon solitons in graphene nanodisk arrays. *Physical Review B*, 91(7):075409, 2015.

[291] Maxim L Nesterov, Jorge Bravo-Abad, Alexey Yu Nikitin, Francisco J García-Vidal, and Luis Martin-Moreno. Graphene supports the propagation of subwavelength optical solitons. *Laser & Photonics Reviews*, 7(2):L7–L11, 2013.

[292] Semih Cakmakyapan, Humeyra Caglayan, and Ekmel Ozbay. Coupling enhancement of split ring resonators on graphene. *Carbon*, 80:351–355, 2014.

[293] Borislav Vasić, Milka M Jakovljević, Goran Isić, and Radoš Gajić. Tunable metamaterials based on split ring resonators and doped graphene. *Applied Physics Letters*, 103(1):011102, 2013.

[294] Yanhong Zou, Philippe Tassin, Thomas Koschny, and Costas M Soukoulis. Interaction between graphene and metamaterials: split rings vs. wire pairs. *Optics express*, 20(11):12198–12204, 2012.

[295] Daria A Smirnova, Andrey E Miroshnichenko, Yuri S Kivshar, and Alexander B Khanikaev. Tunable nonlinear graphene metasurfaces. *Physical Review B*, 92(16):161406, 2015.

[296] Jin-Luo Cheng, Nathalie Vermeulen, and JE Sipe. Third order optical nonlinearity of graphene. *New Journal of Physics*, 16(5):053014, 2014.

[297] ZhiBo Liu, XiaoLiang Zhang, XiaoQing Yan, YongSheng Chen, and JianGuo Tian. Nonlinear optical properties of graphene-based materials. *Chinese science bulletin*, 57(23):2971–2982, 2012.

[298] Euan Hendry, Peter J Hale, Julian Moger, AK Savchenko, and Sergey A Mikhailov. Coherent nonlinear optical response of graphene. *Physical review letters*, 105(9):097401, 2010.

[299] Martti Kauranen and Anatoly V Zayats. Nonlinear plasmonics. *Nature photonics*, 6(11):737–748, 2012.

[300] Pai-Yen Chen, Christos Argyropoulos, Giuseppe D'Aguanno, and Andrea Alu. Enhanced second-harmonic generation by metasurface nanomixer and nanocavity. *Acs Photonics*, 2(8):1000–1006, 2015.

[301] AH Castro Neto, Francisco Guinea, Nuno MR Peres, Kostya S Novoselov, and Andre K Geim. The electronic properties of graphene. *Reviews of modern physics*, 81(1):109, 2009.

[302] Young-Jun Yu, Yue Zhao, Sunmin Ryu, Louis E Brus, Kwang S Kim, and Philip Kim. Tuning the graphene work function by electric field effect. *Nano letters*, 9(10):3430–3434, 2009.

[303] Joanna Hass, François Varchon, Jorge-Enrique Millan-Otoya, Michael Sprinkle, Nikhil Sharma, Walt A de Heer, Claire Berger, Phillip N First, Laurence Magaud, and Edawrd H Conrad. Why multilayer graphene on 4 h- sic (000 1) behaves like a single sheet of graphene. *Physical review letters*, 100(12):125504, 2008.

[304] LA Falkovsky and SS Pershoguba. Optical far-infrared properties of a graphene monolayer and multilayer. *Physical Review B*, 76(15):153410, 2007.

[305] Kosuke Nagashio, Tomonori Nishimura, Koji Kita, and Akira Toriumi. Mobility variations in mono-and multi-layer graphene films. *Applied physics express*, 2(2):025003, 2009.

[306] Feng Hao, Yannick Sonnefraud, Pol Van Dorpe, Stefan A Maier, Naomi J Halas, and Peter Nordlander. Symmetry breaking in plasmonic nanocavities: subradiant lspr sensing and a tunable fano resonance. *Nano letters*, 8(11):3983–3988, 2008.

[307] Boris Luk'yanchuk, Nikolay I Zheludev, Stefan A Maier, Naomi J Halas, Peter Nordlander, Harald Giessen, and Chong Tow Chong. The fano resonance in plasmonic nanostructures and metamaterials. *Nature materials*, 9(9):707–715, 2010.

[308] Mikhail F Limonov, Mikhail V Rybin, Alexander N Poddubny, and Yuri S Kivshar. Fano resonances in photonics. *Nature Photonics*, 11(9):543–554, 2017.

[309] Hugen Yan, Fengnian Xia, Zhiqiang Li, and Phaedon Avouris. Plasmonics of coupled graphene micro-structures. *New Journal of Physics*, 14(12):125001, 2012.

[310] Alexander B Khanikaev, Chihhui Wu, and Gennady Shvets. Fano-resonant metamaterials and their applications. *Nanophotonics*, 2(4):247–264, 2013.

[311] Zhichao Ruan and Shanhui Fan. Temporal coupled-mode theory for fano resonance in light scattering by a single obstacle. *The journal of physical chemistry C*, 114(16):7324–7329, 2010.

[312] Hermann A Haus and Weiping Huang. Coupled-mode theory. *Proceedings of the IEEE*, 79(10):1505–1518, 1991.

[313] Shanhui Fan, Wonjoo Suh, and John D Joannopoulos. Temporal coupled-mode theory for the fano resonance in optical resonators. *JOSA A*, 20(3):569–572, 2003.

[314] Yertay Zhiyenbayev, Yannis Kominis, Constantinos Valagiannopoulos, Vassilios Kovanis, and Anastasios Bountis. Enhanced stability, bistability, and exceptional points in saturable active photonic couplers. *Physical Review A*, 100(4):043834, 2019.

[315] Jiyong Wang, Aurelien Coillet, Olivier Demichel, Zhiqiang Wang, Davi Rego, Alexandre Bouhelier, Philippe Grelu, and Benoit Cluzel. Saturable plasmonic metasurfaces for laser mode locking. *Light: Science & Applications*, 9(1):1–9, 2020.

[316] Constantinos Valagiannopoulos and Sergei A Tretyakov. Stability of active photonic metasurface pairs. *New Journal of Physics*, 23(11):113045, 2021.

[317] Toshihiro Okamoto, Tomoya Otsuka, Shuji Sato, Tetsuya Fukuta, and Masanobu Haraguchi. Dependence of lc resonance wavelength on size of silver split-ring resonator fabricated by nanosphere lithography. *Optics express*, 20(21):24059–24067, 2012.

[318] Ming Zhou, Dianjing Liu, Samuel W Belling, Haotian Cheng, Mikhail A Kats, Shanhui Fan, Michelle L Povinelli, and Zongfu Yu. Inverse design of metasurfaces based on coupled-mode theory and adjoint optimization. *ACS Photonics*, 8(8):2265–2273, 2021.

[319] Bakytgul Yerezhep and Constantinos Valagiannopoulos. Approximate stability dynamics of concentric cylindrical metasurfaces. *IEEE Transactions on Antennas and Propagation*, 69(9):5716–5724, 2021.

[320] Mojtaba Dehmollaian, Nima Chamanara, and Christophe Caloz. Wave scattering by a cylindrical metasurface cavity of arbitrary cross section: Theory and applications. *IEEE Transactions on Antennas and Propagation*, 67(6):4059–4072, 2019.

[321] Amdad Chowdury, Wonkeun Chang, and Marco Battiato. Higher-order rogue-wave fission in the presence of self-steepening and raman self-frequency shift. *Physical Review A*, 107(5):053507, 2023.

[322] Ivan M Uzunov, Todor N Arabadzhiev, and Svetoslav G Nikolov. Self-steepening and intrapulse raman scattering in the presence of nonlinear gain and its saturation. *Optik*, 271:170137, 2022.

[323] P Mohanraj, R Sivakumar, M Vijayakumar, and Jayaprakash Kaliyamurthy. Role of self-steepening and intra-pulse raman scattering on modulation instability in three-core oppositely directed coupler. *Optik*, 271:170094, 2022.

[324] PRGDJ Graves and D Gardiner. Practical raman spectroscopy. *Springer*, 10:978–3, 1989.

[325] Masamichi Tsuboi, James M Benevides, and George J Thomas Jr. Raman tensors and their application in structural studies of biological systems. *Proceedings of the Japan Academy, Series B*, 85(3):83–97, 2009.

[326] Xiujuan Zhang and Ying Wu. Effective medium theory for anisotropic metamaterials. *Scientific reports*, 5(1):7892, 2015.

[327] Zhiyong Xu, Lu Li, Zhonghao Li, and Guosheng Zhou. Soliton interaction under the influence of higher-order effects. *Optics Communications*, 210(3-6):375–384, 2002.

[328] Jigen Chen, Zitong Luan, Qin Zhou, Abdullah Kamis Alzahrani, Anjan Biswas, and Wenjun Liu. Periodic soliton interactions for higher-order non-

linear schr¨odinger equation in optical fibers. *Nonlinear Dynamics*, 100:2817–2821, 2020.

[329] Houhui Yi, Yanli Yao, Xin Zhang, and Guoli Ma. High-order effect on the transmission of two optical solitons. *Chinese Physics B*, 32(10):100509, 2023.

[330] Chen Chen, Yuqi Pan, Jiyuan Guo, Ying Wang, Guojun Gao, and Wei Wang. Soliton dynamics for quantum systems with higher-order dispersion and nonlinear interaction. *AIP Advances*, 10(6), 2020.

[331] Angelin Vithya and MS Mani Rajan. Impact of fifth order dispersion on soliton solution for higher order nls equation with variable coefficients. *Journal of Ocean Engineering and Science*, 5(3):205–213, 2020.

[332] Lei Wang, Jian-Hui Zhang, Zi-Qi Wang, Chong Liu, Min Li, Feng-Hua Qi, and Rui Guo. Breather-to-soliton transitions, nonlinear wave interactions, and modulational instability in a higher-order generalized nonlinear schr¨odinger equation. *Physical Review E*, 93(1):012214, 2016.

[333] Muhammad Arshad, Aly R Seadawy, and Dianchen Lu. Modulation stability and optical soliton solutions of nonlinear schr¨odinger equation with higher order dispersion and nonlinear terms and its applications. *Superlattices and Microstructures*, 112:422–434, 2017.

[334] Rongcao Yang, Ruiyu Hao, Lu Li, Zhonghao Li, and Guosheng Zhou. Dark soliton solution for higher-order nonlinear schr¨odinger equation with variable coefficients. *Optics communications*, 242(1-3):285–293, 2004.

[335] Rui Guo and Hui-Qin Hao. Breathers and multi-soliton solutions for the higher-order generalized nonlinear schr¨odinger equation. *Communications in Nonlinear Science and Numerical Simulation*, 18(9):2426–2435, 2013.

[336] Hai-Ping Zhu and Hai-Yan Chen. Parameter modulation of periodic waves and solitons in metamaterials with higher-order dispersive and nonlinear effects. *Nonlinear Dynamics*, 104:1545–1554, 2021.

[337] Xuemin Min, Rongcao Yang, Jinping Tian, Wenrui Xue, and JM Christian. Exact dipole solitary wave solution in metamaterials with higher-order dispersion. *Journal of Modern Optics*, 63(sup3):S44–S50, 2016.

[338] Yuanjiang Xiang, Xiaoyu Dai, Shuangchun Wen, Jun Guo, and Dianyuan Fan. Controllable raman soliton self-frequency shift in nonlinear metamaterials. *Physical Review A*, 84(3):033815, 2011.

[339] Samudra Roy and Shyamal K Bhadra. Solving soliton perturbation problems by introducing rayleigh's dissipation function. *Journal of lightwave technology*, 26(14):2301–2322, 2008.

[340] Zhigang Chen, Mordechai Segev, and Demetrios N Christodoulides. Optical spatial solitons: historical overview and recent advances. *Reports on Progress in Physics*, 75(8):086401, 2012.

[341] Alwyn C Scott, FYF Chu, and David W McLaughlin. The soliton: a new concept in applied science. *Proceedings of the IEEE*, 61(10):1443–1483, 1973.

[342] Alwyn Scott. *Encyclopedia of nonlinear science*. Routledge, 2006.

[343] Masatoshi Suzuki, Itsuro Morita, Shu Yamamoto, Noboru Edagawa, Hidenori Taga, and Shigeyuki Akiba. Timing jitter reduction by periodic dispersion compensation in soliton transmission. In *Optical Fiber Communication Conference*, page PD20. Optica Publishing Group, 1995.

[344] K Nakkeeran. An exact soliton solution for an averaged dispersion-managed fibre system equation. *Journal of Physics A: Mathematical and General*, 34(24):5111, 2001.

[345] Sergei K Turitsyn, Brandon G Bale, and Mikhail P Fedoruk. Dispersion-managed solitons in fibre systems and lasers. *Physics reports*, 521(4):135–203, 2012.

[346] Akira Hasegawa, Yuji Kodama, and Akihiro Maruta. Recent progress in dispersion-managed soliton transmission technologies. *Optical Fiber Technology*, 3(3):197–213, 1997.

[347] Mark J Ablowitz and Ziad H Musslimani. Discrete spatial solitons in a diffraction-managed nonlinear waveguide array: a unified approach. *Physica D: Nonlinear Phenomena*, 184(1-4):276–303, 2003.

[348] Mark J Ablowitz and Ziad H Musslimani. Discrete diffraction managed spatial solitons. *Physical Review Letters*, 87(25):254102, 2001.

[349] HS Eisenberg, Yaron Silberberg, R Morandotti, and JS Aitchison. Diffraction management. *Physical Review Letters*, 85(9):1863, 2000.

[350] PA Subha, CP Jisha, and VC Kuriakose. Nonlinearity management and diffraction management for the stabilization of two-dimensional spatial solitons. *Pramana*, 69:229–239, 2007.

[351] Demetrios N Christodoulides and Eugenia D Eugenieva. Blocking and routing discrete solitons in two-dimensional networks of nonlinear waveguide arrays. *Physical Review Letters*, 87(23):233901, 2001.

[352] Bao-Lai Liang, Ying Wang, Su-Heng Zhang, Qing-Lin Guo, Shu-Fang Wang, Guang-Sheng Fu, Paul J Simmonds, and Zhao-Qi Wang. Optical image processing by using a photorefractive spatial soliton waveguide. *Physics Letters A*, 381(13):1207–1212, 2017.

[353] Andrea Fratalocchi, Gaetano Assanto, Kasia A Brzdąkiewicz, and Mirek A

Karpierz. All-optical switching and beam steering in tunable waveguide arrays. *Applied Physics Letters*, 86(5):051112, 2005.

[354] Pascal Kockaert, Philippe Tassin, Guy Van der Sande, Irina Veretennicoff, and Mustapha Tlidi. Negative diffraction pattern dynamics in nonlinear cavities with left-handed materials. *Physical Review A*, 74(3):033822, 2006.

[355] Jinggui Zhang, Yongfan Li, Zuwei Tian, and Jie Xiao. Modulation instability controlled by nonlinear diffraction in metamaterials. *Optik*, 130:1259–1265, 2017.

[356] Marios Mattheakis, Constantinos A Valagiannopoulos, and Efthimios Kaxiras. Epsilon-near-zero behavior from plasmonic dirac point: Theory and realization using two-dimensional materials. *Physical Review B*, 94(20):201404, 2016.

[357] AD Boardman, O Hess, RC Mitchell-Thomas, YG Rapoport, and L Velasco. Temporal solitons in magnetooptic and metamaterial waveguides. *Photonics and Nanostructures-Fundamentals and Applications*, 8(4):228–243, 2010.

[358] Allan D Boardman, Neil King, and Yuriy Rapoport. On the possibility of gain control and special solitons in metamaterials. In *Photonic Metamaterials*, volume 6638, pages 129–140. SPIE, 2007.

[359] AD Boardman, P Egan, RC Mitchell-Thomas, Yu G Rapoport, and NJ King. Weakly and strongly nonlinear waves in negative phase metamaterials. In *Metamaterials: Fundamentals and Applications*, volume 7029, pages 136–149. SPIE, 2008.

[360] AD Boardman, RC Mitchell-Thomas, NJ King, and YG Rapoport. Bright spatial solitons in controlled negative phase metamaterials. *Optics Communications*, 283(8):1585–1597, 2010.

[361] AD Boardman, N King, and Yu Rapoport. Metamaterials driven by gain and special configurations. In *Metamaterials II*, volume 6581, pages 55–64. SPIE, 2007.

[362] Shiyin Du, Jie You, Jun Zhang, Zilong Tao, Hao Hao, Yuhua Tang, Xin Zheng, and Tian Jiang. Expedited circular dichroism prediction and engineering in two-dimensional diffractive chiral metamaterials leveraging a powerful model-agnostic data enhancement algorithm. *Nanophotonics*, 10(3):1155–1168, 2020.

[363] Neeraj Sharma and Soumendu Jana. Dissipative soliton dynamics and switching in split ring resonator based metamaterial with multi-photon absorption and diffusion. *Physics Letters A*, 398:127261, 2021.

[364] Zilong Tao, Jun Zhang, Jie You, Hao Hao, Hao Ouyang, Qiuquan Yan, Shiyin Du, Zeyu Zhao, Qirui Yang, Xin Zheng, et al. Exploiting deep learning network in optical chirality tuning and manipulation of diffractive chiral metamaterials. *Nanophotonics*, 9(9):2945–2956, 2020.

[365] Manoj Mishra, Sandeep Kumar Kajala, Mohit Sharma, Swapan Konar, and Soumendu Jana. Energy optimization of diffraction managed accessible solitons. *JOSA B*, 39(10):2804–2812, 2022.

[366] Muthusamy Lakshmanan and Shanmuganathan Rajaseekar. *Nonlinear dynamics: integrability, chaos and patterns*. Springer Science & Business Media, 2012.

Publications

Publications from this thesis work

- *Dissipative soliton dynamics and switching in split ring resonator based metamaterial with multi-photon absorption and diffusion*,

  Neeraj Sharma, Soumendu Jana,

  Physics Letters A. 2021 May 17;398:127261.

- *Making a meta-surface soliton-ready*,

  Neeraj Sharma, Soumendu Jana,

  Zeitschrift für Naturforschung A. 2022 Sep 26;77(9):841-9.

- *Diffraction Managed Soliton in Metamaterial*,

  Neeraj Sharma, Soumendu Jana, Manoj Mishra,

  Nonlinear Dynamics (Under review).

- *Soliton Generation and Dynamics in Metamaterial with Higher Order Nonlinear Effects*,

  Neeraj Sharma, Soumendu Jana,

  Optics Communications (Submitted).

Conference publications

- *Soliton dynamics in metamaterial with higher order nonlinear phenomena*,

  Neeraj Sharma, Soumendu Jana,

  International Conference on Nonlinear Dynamics and Applications 2024, Feb 21-23, 2024 at Sikkim Manipal Institute of Technology (Accepted).

- *Diffraction Managed Dissipative Breather Soliton in Alternative Slabs of Meta-*

material and Dielectric,

Neeraj Sharma, Manoj Mishra, Soumendu Jana,

Proceedings of the DAE-BRNS National Laser Symposium (NLS-31), Dec 3-6, 2022 at IIT Kharagpur. Available: `https://www.ila.org.in/nls31/download/proceedings?folder=NLS-31%2BPapers%2Band%2BThesis%252FCP4-PDF` (CP4_930).